



A University of Sussex DPhil thesis

Available online via Sussex Research Online:

<http://sro.sussex.ac.uk/>

This thesis is protected by copyright which belongs to the author.

This thesis cannot be reproduced or quoted extensively from without first obtaining permission in writing from the Author

The content must not be changed in any way or sold commercially in any format or medium without the formal permission of the Author

When referring to this work, full bibliographic details including the author, title, awarding institution and date of the thesis must be given

Please visit Sussex Research Online for more information and further details

Chemistry of β -diketiminate Group 14 and
Group 2 complexes and macrocyclic
amines and amine ethers.

Morgan James Taylor

DPhil Chemistry

University of Sussex

May 2012

I hereby declare that this thesis has not been and will not be, submitted in whole or in part to another University for the award of any other degree.

Signed:.....Morgan J Taylor.....

Abstract

Group 14 metal(II) alkyl complexes are very rare, with few examples being studied in great detail. To this end, a series of β -diketiminate lead(II) alkyl and aryl complexes, $[\{(2,6\text{-}^i\text{Pr}_2\text{C}_6\text{H}_3)\text{NC}(\text{CH}_3)\}_2\text{CH}]\text{PbR}$ ($\text{R} = \text{Me}, ^i\text{Pr}, ^s\text{Bu}, \text{Np}, \text{Bn}, ^t\text{Bu}$ and Ph) were synthesised and a number of computational studies were performed on them to increase the understanding of the nature of these compounds. Reactivity studies on both the lead, and the analogous tin systems, showed that they could be used as precursors to generate examples of very rare two-coordinate group 14 metal cation complexes, including the first example of a β -diketiminate two-coordinate lead(II) cation, and an analogous example of a rare low-coordinate tin(II) system. These were studied in detail by computational methods, including the stabilising effects of a coordinated solvent molecule on the metal centre.

β -Diketiminato magnesium alkyl complexes were generated to investigate the +2 oxidation state metal environment without the presence of a stereochemically active lone pair, as present in the group 14 metal(II) complexes. A carbodiimide was successfully inserted into the magnesium-carbon bond, and novel magnesium phosphides were generated from the alkyl complexes. Solvent stabilisation effects on these phosphides were also studied by computational methods.

A series of macrocyclic amines and amine ethers were synthesised to investigate the hydrolysis of a phosphate diester model RNA system by lead(II) salts, monitored by UV-visible kinetics. The reaction kinetics gave no reproducible results, but the syntheses of the macrocycles are presented in detail for further citation.

Acknowledgements

My primary thanks must go to my supervisor, Dr Robin Fulton, for giving me the opportunity to study in her research group for the past four years. Even though we have sometimes had our creative differences, Robin has always provided me with excellent guidance, as well as willingness to answer any of my concerns or questions regarding my work. My thanks must also extend to other faculty; Drs Peter Hitchcock and Martyn Coles have worked wonders with my X-ray crystal structures, and Martyn has always been present – assuming there were a few Jaffa Cakes around – to offer the odd light-hearted word of “support” – it wasn’t always my fault that I kept making pink compounds! My thanks must also go to Drs Iain Day and Ian Crossley for all their assistance with NMR spectroscopy, Dr Ali Abdul-Sada for mass spectrometry, Dr Hazel Cox for assistance with computational chemistry and to EPSRC for funding.

Special thanks must go to everyone who has worked in Ar319 over the years, especially Lorenzo, Eric, Lisa, Mat and Lamin, who have made my time as a postgraduate very memorable indeed – especially lunchtimes up at the Swan, or evenings at the pub – I’m lucky to have had such good colleagues. Even though, in the end, we all belonged to the lab! Outside of university, my acknowledgements go to my friends from Brighton – Mike, Ben, Lotte, Jack, James and Tim – I might not have known you as long as I have the people in university, but I’m still going to miss you! Thanks for being there for me over the last couple of years, and for providing much needed doses of sanity every so often!

My most special thanks must go to my best friend Marisian – thank you for being there for me over the eight years we’ve been at university together, for never grumbling if I came and complained at you, for advising me on things that needed advising about... and for giving me the odd kick up the backside as and when I needed it! My time at university would have been significantly poorer, had you not been here. Also, we still need to go and see the second half of “Woman In Black”; I still want to know how that play ends!

Last, but by no means least, I would like to thank my parents, Jill and Chris, and my brother Oliver, for their love, encouragement and faith in me during my studies. Even though I may not have fully appreciated it at the time, I am truly grateful for their unconditional support.

I would like to take this opportunity to dedicate my thesis to my grandpa, Jack Laurence Moss, who sadly passed away suddenly in November 2010. I know he was very proud to have his grandson studying for a doctorate, and he always took great interest in hearing about my work and university life.

My thesis is also dedicated to the memory of my late aunty, Judith Helen Moss, who sadly passed away in May 2011.

“People become part of you; you don’t realise it until they’re gone.”

~ Snaff, *Edge of Destiny*.

Table of Contents

1. Synthesis, structure and reactivity of β-diketimate lead alkyl complexes	19
1.1 <i>β-Diketimate ligands and metal complexes</i>	20
1.1.1 The ability of β -diketimate ligands to stabilise low-coordinate metal centres	20
1.1.2 Synthesis of β -diketimate ligands	23
1.1.3 β -Diketimate metal alkyl complexes	26
1.1.4 Group 13, 14 and 15 β -diketimate complexes	31
1.2 <i>Discussion and synthesis of β-diketimate lead alkyl complexes</i>	43
1.2.1 Synthesis and characterisation of β -diketimate lead(II) methyl, LPbMe (3)	44
1.2.2 Synthesis and characterisation of β -diketimate lead(II) <i>iso</i> -propyl, LPb ⁱ Pr (4)	47
1.2.3 Synthesis and characterisation of β -diketimate lead(II) <i>sec</i> -butyl, LPb ^s Bu (5)	50
1.2.4 Synthesis and characterisation of β -diketimate lead(II) <i>neo</i> -pentyl, LPbNp (6)	52
1.2.5 Synthesis and characterisation of β -diketimate lead(II) benzyl, LPbBn (7)	55
1.2.6 Synthesis and characterisation of β -diketimate lead(II) <i>tert</i> -butyl, LPb ^t Bu (8)	58
1.2.7 Synthesis and characterisation of β -diketimate lead(II) phenyl, LPbPh (9)	60
1.3 <i>Hammett correlation studies</i>	64
1.4 <i>Reactivity studies</i>	69
1.5 <i>Computational studies</i>	72
1.5.1 Discussion of geometry optimisations	73
1.5.2 Conformational stability; <i>endo</i> - vs. <i>exo</i> -	79
1.5.3 NBO analysis and natural electron configuration	82
1.5.4 Dipole moments	87

1.5.5	TD-DFT calculations	88
1.5.6	NMR calculations.....	88
1.6	<i>Summary</i>	90
1.7	<i>Experimental details</i>	91
2.	Synthesis, structure and reactivity of β-diketimate plumbylene and stannylene complexes.....	100
2.1	<i>Low-coordinate group 14 metal complexes</i>	101
2.1.1	Low-coordinate group 14 metal systems	101
2.1.2	Group 14 metal ionic complexes.....	104
2.2	<i>Synthesis and reactivity of β-diketimate plumbylene and stannylene complexes</i> 107	
2.2.1	Synthesis and characterisation of β -diketimate plumbyl-(II)-ene <i>tris</i> -(pentafluorophenyl) (methyl) borate, $[\text{LPb}]^+ [\text{B}(\text{Me})(\text{C}_6\text{F}_5)_3]^-$ (10).....	107
2.2.2	Synthesis and characterisation of β -diketimate plumbyl-(II)-ene <i>tetrakis</i> -(pentafluorophenyl) borate, $[\text{LPb}]^+ [\text{B}(\text{C}_6\text{F}_5)_4]^-$ (11)	108
2.2.3	Synthesis and characterisation of β -diketimate stannyl-(II)-ene <i>tris</i> -(pentafluorophenyl) (methyl) borate, $[\text{LSn}]^+ [\text{B}(\text{Me})(\text{C}_6\text{F}_5)_3]^-$ (12).....	111
2.2.4	Synthesis and characterisation of β -diketimate stannyl-(II)-ene <i>tetrakis</i> -(pentafluorophenyl) borate, $[\text{LSn}]^+ [\text{B}(\text{C}_6\text{F}_5)_4]^-$ (13)	114
2.2.5	Synthesis and characterisation of β -diketimate stannyl-(II)-ene tetrachloroaluminate, $[\text{LSn}]^+ [\text{AlCl}_4]^-$ (14)	115
2.3	<i>Reactivity studies</i>	118
2.4	<i>Computational studies</i>	119
2.4.1	Discussion of geometry optimisations	120
2.4.2	Solvent stabilisation effects.....	122
2.4.3	Molecular orbitals	124
2.4.4	NBO analysis and natural electron configuration	128
2.5	<i>Summary</i>	130
2.6	<i>Experimental details</i>	131

3. Synthesis, structure and reactivity of β-diketimate magnesium complexes	135
3.1 Magnesium and other s-block β -diketimate complexes	136
3.2 Synthesis and reactivity of β -diketimate magnesium complexes.....	146
3.2.1 Synthesis of β -diketimate magnesium alkyl complexes	146
3.2.2 Reactivity studies with heterocumulenes	146
3.2.3 Synthesis and characterisation of β -diketimate magnesium N,N'- dicyclohexylethylamidinate, $\text{LMg}[(\text{NCy})_2\text{CMe}]$ (17)	147
3.2.4 Synthesis and characterisation of β -diketimate magnesium N,N'- dicyclohexylphenylethylamidinate, $\text{LMg}[(\text{NCy})_2\text{CBn}]$ (18)	150
3.2.5 Synthesis and characterisation of β -diketimate magnesium diphenylphosphide, $\text{LMgPPh}_2\cdot\text{THF}$ (19)	152
3.2.6 Synthesis and characterisation of β -diketimate magnesium dicyclohexylphosphide, $\text{LMgPCy}_2\cdot\text{THF}$ (20)	155
3.3 Computational studies.....	157
3.3.1 Discussion of geometry optimisations and structural differences	157
3.3.2 Solvent stabilisation effects.....	160
3.4 Summary.....	161
3.5 Experimental details.....	162
4. Macrocyclic amines and amine ethers.....	166
4.1 Introduction to macrocyclic chemistry.....	167
4.1.1 Metal complexes of macrocycles	167
4.1.2 Synthesis of macrocyclic amines and ethers.....	174
4.1.3 Phosphate ester hydrolysis by metal centres.....	177
4.2 Results and discussion	182
4.2.1 Synthesis of barium 2-hydroxypropyl 4-nitrophenyl phosphate (21).	182
4.2.2 Macrocycle synthesis	183
4.2.3 Macrocyclic complexes with metal centres	193
4.2.4 Studies on the hydrolysis of 2-hydroxypropyl 4-nitrophenyl phosphate	194
4.3 Summary.....	201
4.4 Experimental details.....	202

5. References	215
----------------------------	------------

Appendices

1. β -Diketimate lead (II) alkyl complexes; computational details	A223
2. β -Diketimate plumbylene and stannylene complexes; computational details .	A237
3. β -Diketimate magnesium phosphide complexes; computational details	A45
4. Publication: "Lead and Tin Cations"; Taylor, M.J.; Saunders, A.J.; Coles, M.P.; Fulton, J.R.; <i>Organometallics</i> ; 2011; 30; 1334-1339... Attached Electronically	
5. NMR data	Attached Electronically
6. X-ray crystallography files.....	Attached Electronically
7. Mass spectrometry data.....	Attached Electronically
8. Computational calculation files.....	Attached Electronically

List of figures, schemes and tables

Figure		Page
1	Neutral and anionic forms of a β -diketimine	20
2	Common bonding modes of β -diketiminato ligands	21
3	Effect of increasing steric bulk at R^2 , on the coordination site of β -diketiminato ligands	21
4	Effect of varying the bulk at the N-substituted R^3 position	22
5	Activated dinitrogen complexes utilising (BDI)Fe fragments	22
6	Product of insertion and coordination of CO to (BDI)FeR complexes	23
7	The two different conformations of a group 14 metal-BDI complex	35
8	LPbMe (3)	46
9	LPbMe (3) side-on, showing extent of <i>endo</i> - conformation	46
10	LPb ⁱ Pr (4)	49
11	LPb ⁱ Pr (4) side-on, showing extent of <i>exo</i> - conformation	49
12	LPb ^s Bu (5)	51
13	LPb ^s Bu (5) side-on, showing extent of <i>exo</i> - conformation	52
14	LPbNp (6)	54
15	LPbNp (6) side-on, showing extent of <i>exo</i> - conformation	55
16	LPbBn (7)	57
17	LPbBn (7) side-on, showing extent of <i>exo</i> - conformation	57
18	LPb ^t Bu (8)	59
19	LPb ^t Bu (8) side-on, showing extent of <i>exo</i> - conformation	60
20	LPbPh (9)	62
21	LPbPh (9) side-on, showing extent of <i>endo</i> - conformation	62
22	Correlation graph of Hammett constants, σ_{para} , against λ_{max} (nm)	66
23	Correlation graph of Hammett constants, σ_{para} , against ^{207}Pb NMR chemical shift (ppm)	67
24	Combined graph of Dubois Steric Parameter against ^{207}Pb NMR signal (ppm) and λ_{max} (nm)	68
25	Optimised <i>endo</i> - and <i>exo</i> - geometries for LPbMe 3	73
26	Optimised <i>endo</i> - and <i>exo</i> - geometries for LPb ⁱ Pr 4	74
27	Optimised <i>endo</i> - and <i>exo</i> - geometries for LPb ^s Bu 5	75

28	Optimised <i>exo</i> - geometry for LPbNp 6	76
29	Optimised <i>exo</i> - geometry for LPbBn 7 and alternate starting geometry	77
30	Optimised <i>exo</i> - geometry for LPb ^t Bu 8	78
31	Optimised <i>endo</i> - geometry for LPbPh 9 and alternate starting geometry	79
32	View of the lead-centred lone pair on an <i>endo</i> - conformer and an <i>exo</i> - conformer	83
33	View of the LUMO and HOMO of the lead methyl complex 3	86
34	View of the LUMO and HOMO of the lead <i>iso</i> -propyl complex 4	87
35	Lead and tin forms of silylamides LXII and LXIII	101
36	[LPb] ⁺ [B(C ₆ F ₅) ₄] ⁻ (11) with coordinated DCM	110
37	[LPb] ⁺ [B(C ₆ F ₅) ₄] ⁻ (11) side-on, showing position of coordinated DCM molecule	110
38	[LSn] ⁺ [B(Me)(C ₆ F ₅) ₃] ⁻ (12) with coordinated Et ₂ O	113
39	[LSn] ⁺ [B(Me)(C ₆ F ₅) ₃] ⁻ (12) side-on, showing position of coordinated Et ₂ O molecule	113
40	[(H)LAiCl ₂] ⁺ [AlCl ₄] ⁻ with coordinated DCM	116
41	[(H)LAiCl ₂] ⁺ [AlCl ₄] ⁻ side-on, showing displacement of C2 from the ligand plane	117
42	Solid state geometry and optimised geometry for solvated cation [LPb] ⁺ .DCM	120
43	Optimised geometry for solvated cation [LSn] ⁺ .Et ₂ O	122
44	Position of the DCM molecule in the output from the single basis set calculation and the mixed basis set calculation	122
45	View of the LUMO and HOMO of the lead cationic complex 11	125
46	View of the lead-centred lone pair for free cation [LPb] ⁺ and solvated cation [LPb] ⁺ .DCM	126
47	View of the LUMO of the free cation [LSn] ⁺ and solvated cation [LSn] ⁺ .Et ₂ O	127
48	View of the lead-centred lone pair for free cation [LSn] ⁺ and solvated cation [LSn] ⁺ .Et ₂ O	128
49	Monomeric, dimeric and dodecameric forms of (BDI)Li	137
50	LMg(NCy) ₂ CMe (17)	149
51	LMg(NCy) ₂ CMe (17) side-on, showing configuration around the metal centre	149

52	LMgPPh ₂ .THF (19)	154
53	LMgPPh ₂ .THF (19) side-on, showing configuration around the metal centre	154
54	Optimised geometry for solvated LMgPPh ₂ .THF and unsolvated LMgPPh ₂	158
55	Optimised geometry for solvated LMgPCy ₂ .THF and unsolvated LMgPCy ₂	159
56	A potassium macrocyclic ether and nickel macrocyclic amine	168
57	Nickel complex [Ni(3N12ane)(OH)(H ₂ O) ₂] ⁺ and copper complex [Cu(3N11ane)(NO ₃) ₂]	168
58	Geometrical isomers of [Ni(3N10ane) ₂] ²⁺	169
59	Staggered conformation of [Fe(3N9ane) ₂] ³⁺ and [Fe(3N9ane) ₂] ²⁺	169
60	Structures of [Pb(3N9ane)(ClO ₄) ₂] and [Pb(3N9ane)(NO ₃) ₂]	170
61	Adamantyl-phenoxide-substituted [U(3N9ane)]	171
62	Square pyramidal [Cu(3N9ane)Cl ₂] and trigonal bipyramidal [Cu(3N11ane)Br ₂]	173
63	4-nitrophenyl phosphate diester of propylene glycol (21)	178
64	<i>Bis</i> -(<i>tris</i> -(hydroxymethyl)aminomethane)propane spectator ligand	179
65	Concentration of <i>para</i> -nitrophenolate against time (five repetitions). Initial phosphate concentration = 2.0 x 10 ⁻³ M	195
66	Change in reaction rate, dependent upon initial phosphate concentration	198
67	Concentration of <i>para</i> -nitrophenolate against time (five repetitions). Initial phosphate concentration = 2.0 x 10 ⁻³ M	199

Scheme		Page
1	Synthesis of [{(2,6- ⁱ Pr ₂ C ₆ H ₃)NC(CH ₃) ₂ CH]H, via a double condensation reaction	24
2	Synthesis of a lithium β-diketimate with mixed groups at the R ² position	24
3	One-pot synthesis of aluminium β-diketimate complexes	25
4	Budzelaar and co-workers method of synthesis of bulky β-diketimate ligands	25
5	Synthesis of electron poor XV , with –CF ₃ groups at the R ² position	26
6	Generation of β-diketimate zirconium trialkyls	27

7	β -Diketimate gold(III) complexes	27
8	Generation of BDI erbium(III) metal alkyl complexes	28
9	Synthesis of a hexa-coordinate terbium complex, with a BDI ligand containing N-chelating substituents	28
10	BDI copper alkyl cyclopropanation catalysts	29
11	(BDI)ScX ₂ complexes, to investigate C-O bond cleavage	30
12	(BDI) rhodium(I) insertion into a C-X bond	30
13	Formation of (BDI)FePh by B-C bond cleavage	31
14	Generation of (BDI)M-C ₆ F ₅ group 12 complexes	31
15	Synthesis of an early boron-difluoride β -diketimate	32
16	Generation of <i>bis</i> -pyridyl methyl group 13 β -diketimates	32
17	Exchange of substituent groups within (BDI)Al complexes	33
18	Group 13 metal carbene analogue complexes	33
19	Synthesis of various tin β -diketimate complexes by Roesky and co-workers	34
20	Synthesis of a model tin-lactide propagating species	35
21	Synthesis of BDI tin carbamates and carbonates from carbon dioxide insertion	36
22	Synthesis of group 14 σ -complexes to iron	37
23	Synthesis of BDI group 14 terminal hydrides	37
24	Formation of BDI lead halides and subsequent amide and alkoxide complexes	38
25	Study into the insertion by heterocumulenes into the Pb-O bond	39
26	Syntheses of rare BDI lead phosphides	40
27	Stepwise synthesis of the first phosphorous β -diketimate	40
28	Generation of a N,N'-chelated phosphenium cation	41
29	Steric effects on the generation of BDI antimony complexes	41
30	Synthesis of a very rare (BDI)BiX ₂ complex, utilising a BDI ligand containing N-chelating substituents	42
31	Synthesis of lead chloride 2 from β -diketimate ligand 1	43
32	Synthesis of lead(II) alkyl complexes from lead chloride 2	43
33	Test reactions, with suggested products, for probing insertion into the Pb-C bond in methyl compound 3 by heterocumulenes	70

34	Test reactions for probing abstraction of the terminal methyl group from the lead centre in methyl 3 , resulting in the synthesis of methyl borate 10	70
35	Synthesis of low-coordinate group 14 silylamides and silylalkyls	101
36	Hypersilyl tin(II) and lead(II)	102
37	Low-coordinate lead systems with Ar*	102
38	Synthesis of multiple-bonded group 14 metal complexes	103
39	Synthesis of a one-coordinate lead cation with Ar*	103
40	Generation of tin cation $[\text{}^n\text{Pr}_2(\text{ATI})\text{Sn}]^+.[\text{OTf}]^-$	104
41	Formation of a germanium cation and germanium hydroxide with deoxygenated water	104
42	Generation of a neutral, two-coordinate BDI germylene	105
43	Reactivity of germylene LXXV	105
44	Synthesis of germylidenide and stannylidenide Cp-like ring structures	106
45	Synthesis of $[\text{LPb}]^+ [\text{B}(\text{Me})(\text{C}_6\text{F}_5)_3]^-$ (10)	107
46	Synthesis of $[\text{LPb}]^+ [\text{B}(\text{C}_6\text{F}_5)_4]^-$ (11)	108
47	Synthesis of $[\text{LSn}]^+ [\text{B}(\text{Me})(\text{C}_6\text{F}_5)_3]^-$ (12)	111
48	Synthesis of $[\text{LSn}]^+ [\text{B}(\text{C}_6\text{F}_5)_4]^-$ (13)	114
49	Synthesis of $[\text{LSn}]^+ [\text{AlCl}_4]^-$ (14)	115
50	Addition of coordinating PMe_3 to $[\text{LPb}]^+ [\text{B}(\text{Me})(\text{C}_6\text{F}_5)_3]^-$ (10)	118
51	Test reaction, with suggested product, for deprotonating one of the methyl groups to form a neutral, two-coordinate plumbylene	118
52	BDI dimerisation affected by the presence of a co-ligand	136
53	Synthesis of BDI potassium	137
54	Synthesis of solvated monomeric (BDI) MgMe species	138
55	Synthesis of $[(\text{BDI})\text{MgMe}]_2$ dimer	139
56	Effect of increasing the steric bulk of the Grignard reagent	139
57	Conversion of β -diketimate magnesium alkyl complexes to alkoxides and amides	140
58	Synthesis of <i>bis</i> - β -diketimate magnesium	140
59	Generation of β -diketimate magnesium halides	141
60	Generation of beryllium and calcium β -diketimate halides	141
61	Synthesis of Jones' (BDI) magnesium(I) dimer C	142
62	The ability of dimer C to reduce Ge(II) to Ge(0)	142

63	Synthesis of β -diketiminato magnesium hydride dimer	145
64	Hydroamination by BDI calcium amides	145
65	Synthesis of strontium β -diketiminato complexes	146
66	Barium β -diketiminato complexes	147
67	Synthesis of LMgMe (15) and LMgBn (16)	148
68	Reactivity studies for insertion with CO ₂	149
69	Synthesis of ethylamidinate complex 17	149
70	Synthesis of phenylethylamidinate complex 18	151
71	Synthesis of magnesium diphenylphosphide 19	152
72	Synthesis of magnesium dicyclohexylphosphide 20	156
73	Dimer complexes of [Mo(3N9ane)]	171
74	Hydrolysis, dissociation and transesterification of [Co(3N9ane)] ₂ complexes	172
75	Tosylation of diethyltriamine by Richman and Atkins	174
76	Cyclisation of macrocyclic amines in DMF	175
77	Detosylation of macrocyclic amines	176
78	Methylation of 4N14ane	176
79	Accepted mechanism for the stepwise lead-induced hydrolysis of RNA	177
80	Hydrolysis of phosphate diester 21	178
81	Proposed mechanism for copper-catalysed phosphate hydrolysis	180
82	Synthesis of phosphate diester 21	182
83	Generation of the isomers of phosphate diester 21	183
84	Methylation of 3N9ane 38 to produce 3N9ane-Me ₃	192
85	Attempted synthesis of Pb(3N9ane)(NO ₃) ₂	193
86	Attempted synthesis of M(3N9ane)Cl ₂	194

Table		Page
1	Bond angles (°) and bond lengths (Å) for LPbMe (3)	45
2	Bond angles (°) and bond lengths (Å) for LPb ⁱ Pr (4)	48
3	Bond angles (°) and bond lengths (Å) for LPb ^s Bu (5)	51
4	Bond angles (°) and bond lengths (Å) for LPbNp (6)	54
5	Bond angles (°) and bond lengths (Å) for LPbBn (7)	56
6	Bond angles (°) and bond lengths (Å) for LPb ^t Bu (8)	59

7	Bond angles ($^{\circ}$) and bond lengths (\AA) for LPbPh (9)	61
8	Maximum and secondary absorbencies (nm) and molar extinction coefficients ($\text{mol}^{-1} \text{ cm}^{-1}$) for compound 3 to 9	64
9	<i>Para</i> - and <i>meta</i> - Hammett constants, σ , for the substituents in the alkyl series of compounds	65
10	Energy differences between calculations for lead methyl 3	80
11	Energy differences between calculations for lead iso-propyl 4	81
12	Energy differences between calculations for lead sec-butyl 5	81
13	NBO analysis of Pb metal centre for the lead alkyl complexes. Basis set: LANL2DZ over all atoms	84
14	NBO analysis of Pb metal centre for the lead alkyl complexes. Basis set: LANL2DZ on Pb, 6-31G* on N, C and H atoms	85
15	Calculated dipole moments (Db) of lead alkyl complexes 3 – 9	88
16	Bond angles ($^{\circ}$) and bond lengths (\AA) for $[\text{LPb}]^{+} [\text{B}(\text{C}_6\text{F}_5)_4]^{-}$ (11)	109
17	Bond angles ($^{\circ}$) and bond lengths (\AA) for $[\text{LSn}]^{+} [\text{B}(\text{Me})(\text{C}_6\text{F}_5)_3]^{-}$ (12)	112
18	Energy differences between calculations for lead borate 11	123
19	Energy differences between calculations for tin methyl borate 12	124
20	NBO analysis of metal centre for the lead at tin cationic complexes	129
21	Bond angles ($^{\circ}$) and lengths (\AA) for $\text{LMg}(\text{NCy})_2\text{CMe}$ (17)	148
22	Bond angles ($^{\circ}$) and lengths (\AA) for $\text{LMgPPh}_2\cdot\text{THF}$ (19)	153
23	Energy differences between calculations for diphenylphosphide 19	160
24	Energy differences between calculations for dicyclohexylphosphide 20	160
25	Concentration ranges for metal ions showing first-order dependence	179
26	Starting materials, respective methods and tosylated products	185
27	Combinations of protected amines and activated alcohols to form cyclised products 28 – 33 .	187
28	Fast cracking of tosylated macrocycles 28 , 30 , 31 , and 33 to produce hydrochloride salts 37 – 37	190
29	Neutral macrocycles 38 , 39 , and 40 , acquired from their corresponding salts	191
30	Observed reaction rates, k_{obs} (M s^{-1}) obtained from each run for differing initial concentrations of nitrophenyl phosphate 21	198
31	Reaction rates (M s^{-1}) obtained from each run in the presence of one equivalent of 3N9ane 38	199

List of abbreviations

Ad	Adamantyl
Ar	Aryl (chemical group – specified)
ATI	Aminotroponiminato
BDI	β -Diketiminato
Bn	Benzyl
Cp	Cyclopentadienyl
Db	Debye
DCC	Dicyclohexylcarbodiimide
DCM	Dichloromethane
DMAP	Dimethylaminopyridine
DMF	N,N-Dimethylformamide
DOP	Degree of Pyramidalisation
Et	Ethyl
HEPES	N-(2-hydroxyethyl)piperazine-N'-ethanesulphonic acid
HOMO	Highest Occupied Molecular Orbital
ⁱ Pr	<i>Iso</i> -propyl
ⁿ Pr	<i>n</i> -propyl
L	Ligand ([{ ⁱ Pr ₂ C ₆ H ₃ NC(Me)} ₂ CH] ⁻ unless otherwise specified)
LP	Lone Pair
LUMO	Lowest Unoccupied Molecular Orbital
M	Metal (chemical group – specified)
Me	Methyl
NBO	Natural Bond Orbital
ⁿ Bu	<i>n</i> -butyl
nm	Nanometre
NMR	Nuclear Magnetic Resonance
Np	<i>Neo</i> -pentyl
ORTEP	Oak Ridge Thermal Ellipsoid Plot (molecular graphics)
OTf	Triflate (-OSO ₂ CF ₃)
Ph	Phenyl
R	Alkyl (chemical group – general or specified)

RNA	Ribonucleic acid
^s Bu	<i>Sec</i> -butyl
^t Bu	<i>Tert</i> -butyl
(TD) DFT	(Time Dependent) Density Functional Theory
THF	Tetrahydrofuran
tmeda	Tetramethylethylenediamine
TMS	Trimethylsilyl
Ts	Tosyl (-SO ₂ (C ₆ H ₄)CH ₃)
UV-Vis	Ultraviolet-visible (light)

**1. Synthesis, structure and reactivity of β -diketiminate
lead alkyl complexes**

1.1 *β -Diketiminato ligands and metal complexes*

1.1.1 The ability of β -diketiminato ligands to stabilise low-coordinate metal centres

β -Diketimine complexes have been extensively investigated with respect to both main group and transition metal chemistry in recent years. These ligands show great versatility, with easily tuneable steric and electronic properties, and provide an excellent bidentate ligand system. They have been labelled a “cyclopentadienyl (Cp) alternative”, due to the monoanionic nature of the ligand and the wide range of steric and electronic properties, which can be easily tuned by varying the different substituents at the R^1 , R^2 and R^3 positions.

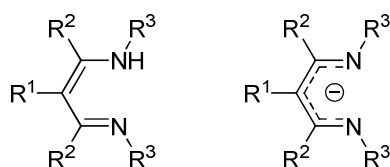


Figure 1 – neutral (left) and anionic (right) forms of a β -diketimine.

There are four main binding modes by which a β -diketiminato (BDI) ligand can bind to a metal centre.¹ Of the modes described, the most common is the situation in which the two nitrogen atoms are coordinated to the metal atom in a bidentate fashion (**I**), with the metal either lying in-plane with the backbone ring of the ligand, or lying out-of-plane due to steric or orbital interactions. Other bonding modes can be observed, however, including a rare example of a mercury complex **II** bonded to two β -diketiminato ligands through the γ -carbon of the backbone, reported by Fulton and co-workers.² A modification of this mode of γ -carbon-binding is shown in **III**, where not only is the metal centre bound to the γ -carbon, but one of the nitrogen atoms coordinates as well.³ Dimerisation has also been observed in β -diketiminato complexes, in the case of lithium complex **IV**, where the ligand is not sterically bulky enough to stabilise the monomeric form.⁴

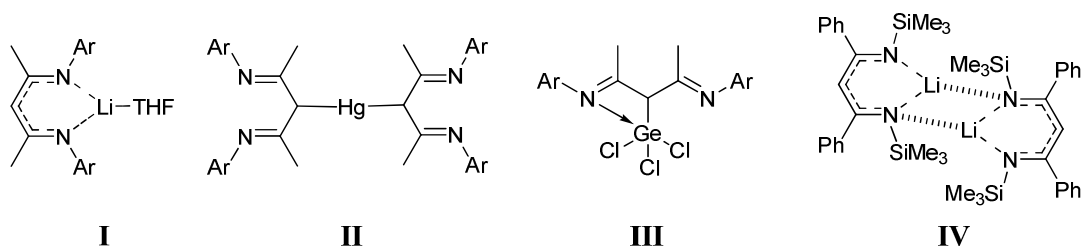


Figure 2 – Common bonding modes of β -diketiminato ligands. Ar = 2,6-diisopropylphenyl.

With over 700 entries in the Cambridge Structural Database, the most common version of the β -diketiminato (BDI) ligand is $[(2,6\text{-}i\text{Pr}_2\text{C}_6\text{H}_3)\text{NC}(\text{CH}_3)]_2\text{CH}]$ H. This contains 2,6-diisopropylphenyl groups at the R^3 position, and small methyl groups at the R^2 position. Increasing the bulk at the R^2 position imposes a larger C-N-C angle, effectively pushing the R^3 substituents closer to the coordination site. This was briefly studied by Jones and co-workers, who noted that by using methyl groups in the R^2 position, nickel complexes such as solvent-coordinated $(\text{BDI})\text{NiCl}_2\cdot\text{Li}(\text{OEt}_2)(\text{THF})$ and the dimer $[(\text{BDI})\text{NiCl}]_2$ were able to be formed. However, on changing the R^2 substituent to a tert-butyl group, it was possible to isolate the monomeric $(\text{BDI})\text{NiCl}$.⁵ As the bulk of both the R^2 groups increases, coordination of additional ligands around the metal centre becomes increasingly disfavoured – the R^3 substituents are pushed towards the metal, forcing the metal deeper into the NN binding pocket, enlarging the N-M-N bond angle but reducing the space available for other coordination to the metal centre.

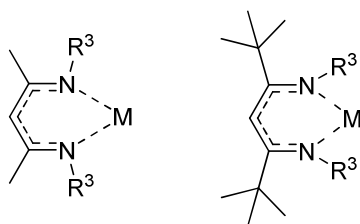


Figure 3 – Effect of increasing steric bulk at R^2 , on the coordination site of β -diketiminato ligands.

Hill varied the bulk of the aryl substituent in the R^3 position, in order to generate a series of indium(I) complexes. The composition of the complex was found to be dependent on the particular N-substituent. When a bulky 2,6-diisopropylphenyl group is utilised, a monomeric indium(I) complex is reported (V). If the bulk of the aryl ring is

decreased to a mesityl group (2,4,6-trimethylphenyl), the reaction yields an indium dimer (**VI**), and upon changing the N-substituent to a 3,5-dimethylphenyl, a remarkable hexa-indium chain complex is formed (**VII**), capped with an iodine atom at either end.⁶

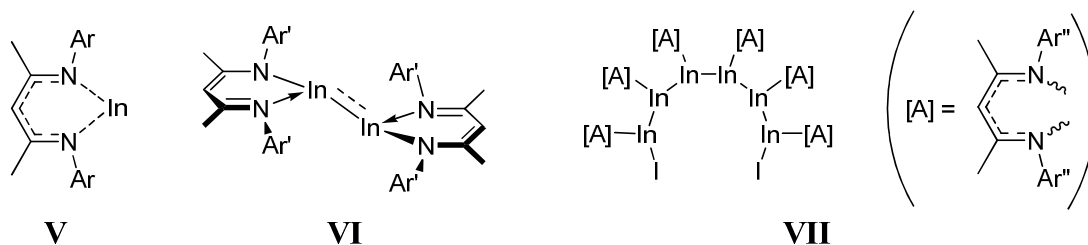


Figure 4 – Effect of varying the bulk at the N-substituted R³ position. Ar = 2,6-diisopropylphenyl. Ar' = 2,4,6-trimethylphenyl, Ar'' = 3,5-dimethylphenyl.

In other areas of low-coordinate chemistry, Holland and co-workers have produced a transition metal species shown to activate dinitrogen using iron(II) centres within a BDI ligand framework. Reduction of (BDI)FeCl in an atmosphere of dinitrogen produces compound **VIII**, described as a rare example of a three-coordinate transition-metal dinitrogen complex.⁷ Upon coordination, the N-N bond was observed to lengthen, and spectroscopic evidence showed that the iron binding had weakened the N-N bond relative to N₂. Further reaction with potassium produced the complex **IX**, where the [FeNNFe]²⁺ core of the molecule has been reduced to [FeNNFe]⁰, and the potassium ions coordinate to the N₂ fragment and the aryl rings on the BDI ligand. This acts to further reduce the strength of the N-N bond.

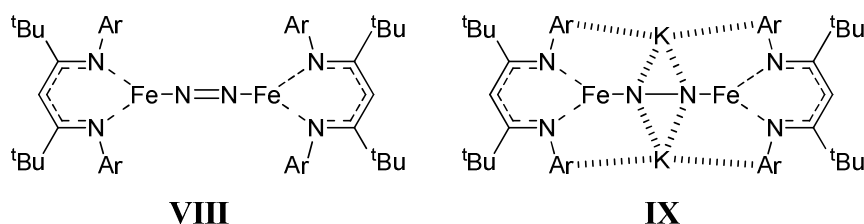


Figure 5 – Activated dinitrogen complexes utilising (BDI)Fe fragments. Ar = 2,6-diisopropylphenyl.

In addition to the activation of dinitrogen, Holland and co-workers have also shown that low-coordinate BDI iron complexes can allow insertion and activation of carbon monoxide.⁸ β -Diketimate iron(II) alkyl compounds were reacted with excess CO and

found to undergo insertion in the Fe-C bond, as well as coordination of carbonyl groups to the iron centre, forming a square pyramidal structure (**X**). This not only highlights the ability of BDI ligands to stabilise iron(II) alkyls with low coordination numbers, but also the ability to stabilise unusual geometries of reaction products.

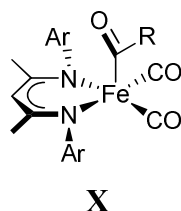


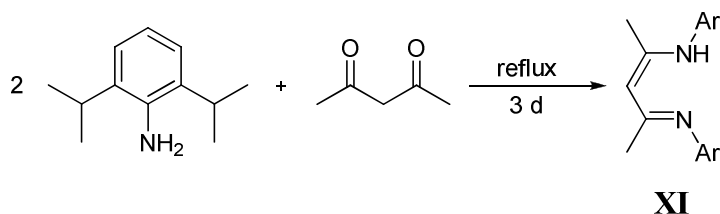
Figure 6 – Product of insertion and coordination of CO to (BDI)FeR complexes.
Ar = 2,6-diisopropylphenyl. R = Me, ⁱPr, Np.

1.1.2 Synthesis of β -diketiminato ligands

The first examples of neutral β -diketimines, synthesised by a double condensation reaction from a β -diketone and two equivalents of a suitable amine were published by Parks, Everett and Holm in the late 1960s (of the type of reaction shown in Scheme 1).^{9,10} This synthesis is suitable for many variations of amine, as well as small substituents on the diketone, and provides a convenient one-pot synthesis to neutral β -diketimines. A variation of this procedure was described by McGeachin, where the protonated versions of β -diketimines are isolated, along with a BF_4^- counterion.¹¹ A third procedure by Dorman involves converting a 1,3-diketone into a ketoacetal, and subsequent conversion into a β -diketimine.¹²

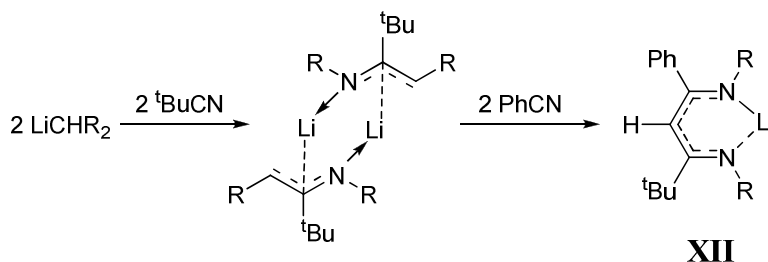
The most widely used β -diketiminato ligand, the sterically encumbered compound **XI**, $[\{(2,6\text{-}^i\text{Pr}_2\text{C}_6\text{H}_3)\text{NC}(\text{CH}_3)_2\}\text{CH}]\text{H}$, as the protonated form of the ligand, contains large diisopropylphenyl substituents in the R_3 position, which help to create a more stable site for a metal centre to coordinate to the ligand. This variant also includes small methyl groups on the backbone at the R_2 position, so as not to crowd the coordination site too much, and the ligand is easily synthesised by the Parks and Holm double condensation reaction between acetylacetone and 2,6-diisopropylaniline (Scheme 1).¹³

Scheme 1 – Synthesis of $[\{(2,6\text{-}^i\text{Pr}_2\text{C}_6\text{H}_3)\text{NC}(\text{CH}_3)_2\text{CH}\}]_2\text{H}$, via a double condensation reaction. Ar = 2,6-diisopropylphenyl.

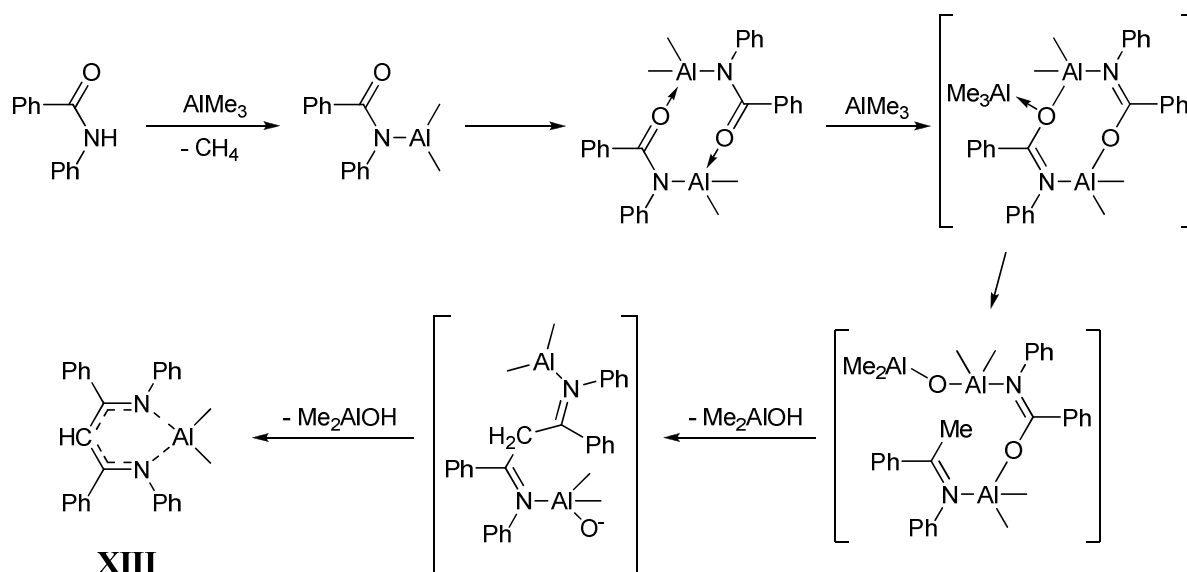


The methods of synthesising many BDI ligands depend greatly on the identity of the R groups indicated. Lappert and co-workers published a synthesis of a β -diketimine system with mixed groups in the R^2 position. In this procedure, a lithium alkyl was added to *tert*-butyl cyanide to produce a η^3 -aza-allyl compound, which was subsequently treated with phenyl cyanide to produce the desired lithium β -diketiminato **XII** (scheme 2).¹⁴ It was also observed that this complex could be easily transformed into a five-coordinate zirconium(IV) or hafnium(IV) trichloride on treatment with the corresponding metal tetrachloride reagent.

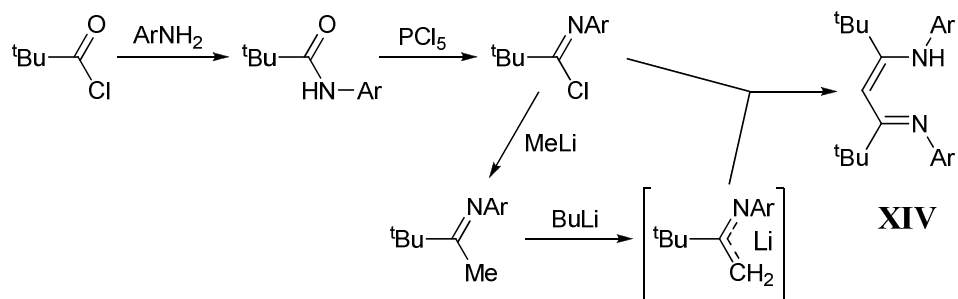
Scheme 2 – Synthesis of a lithium β -diketiminato with mixed groups at the R^2 position. R = SiMe₃.



β -Diketiminates can also be synthesised in a one-pot approach. For instance, the aluminium complexes of type **XIII**, described by Lin and co-workers, were prepared by treating two equivalents of an aluminium alkyl with one equivalent of a substituted amide.¹⁵ This produces a dialkyl aluminium β -diketiminato, with the amide substituents at the R^2 and R^3 positions. The generation of this six-membered Al-N-C-C-C-N ring occurs by coordination of one molecule of AlMe₃ to the amide, followed by dimerisation and ring contraction with the loss of Me₂AlOH to give the β -diketiminato.

Scheme 3 – One-pot synthesis of aluminium β -diketiminate complexes.

Budzelaar and co-workers reported that the Parks and Holm method was sluggish for large R^2 substituents, and so have described a stepwise synthesis of β -diketimines which have *tert*-butyl groups at the R^2 position.¹⁶ It was observed that complexes of titanium and vanadium were not able to be generated using this bulkier ligand (**XIV**) when a 2,6-diisopropylphenyl group was present in the R^3 position. Reducing the bulk of the R^3 substituent to a mesityl group allowed generation of both the titanium and vanadium complexes.¹⁶

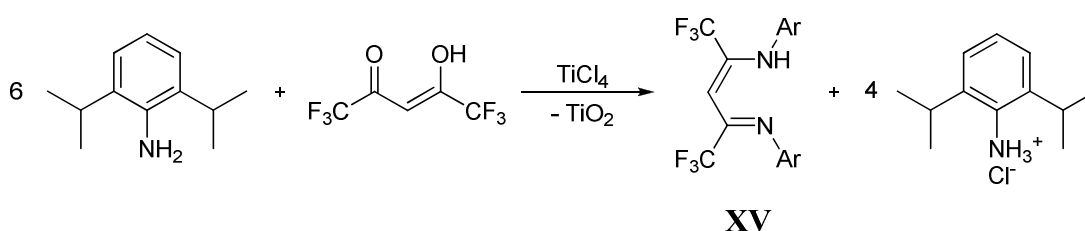
Scheme 4 – Budzelaar and co-workers method of synthesis of bulky β -diketiminate ligands. Ar = 2,6-diisopropylphenyl or 2,4,6-trimethylphenyl.

In addition to tuning the steric bulk of β -diketiminate ligands, one can also modify the electronic properties of β -diketiminate ligands. Mair, Woods and co-workers have reported the synthesis of a series of β -diketimines, including a novel hexafluoro-

variant, containing CF_3 groups in the R^2 position (**XV**).¹⁷ This synthesis required the presence of titanium tetrachloride in the condensation reaction, resulting in a compound that shows a purely monomeric state as the lithium salt. This is in contrast to lithiated non-fluorinated β -diketimines, which are oligomers in the solid state in the absence of a coordinating solvent molecule.¹³

Scheme 5 – Synthesis of electron poor **XV**, with $-\text{CF}_3$ groups at the R_2 position.

Ar = 2,6-diisopropylphenyl



The fluorination of the methyl groups at the R^2 positions also acts to halt alkylation at the central R^1 position, possibly by removing excess electron density from the NCCCN backbone, as the CF_3 units are highly electron-withdrawing.¹⁷ In addition to this, it was observed that the aryl groups at the R^3 position are pushed towards the coordinative pocket of the ligand, perhaps explaining the absence of oligomeric behaviour in the solid state.

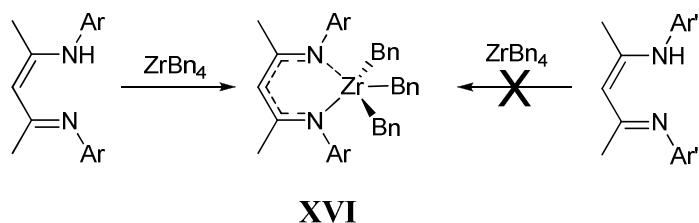
1.1.3 β -Diketimate metal alkyl complexes

There are a significant number of metal alkyl complexes supported by a β -diketimate ligand reported in the literature, with over 300 examples in the Cambridge Structural Database. The scope of β -diketimate metal alkyl complexes range across the periodic table from the *s*-block (*vide infra*), across the transition series to the *p*-block.

Treatment of a neutral β -diketimine with tetrabenzyl zirconium afforded the zirconium trialkyl in scheme 6.¹⁸ Collins and co-workers reported that, although this reaction proceeded cleanly with the elimination of toluene, attempts to use a more acidic ligand did not give an analogous product. This led to the conclusion that the electron donor

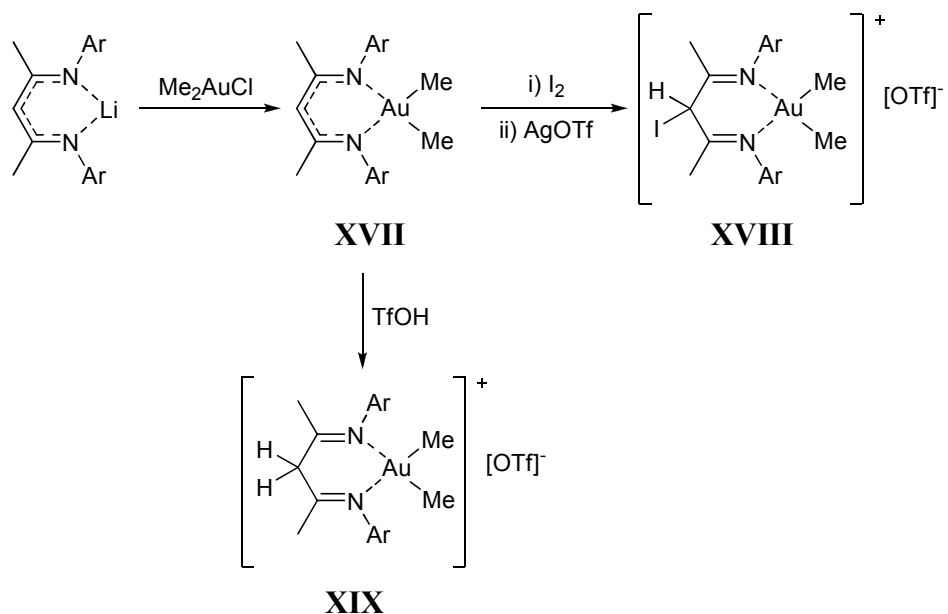
properties of the β -diketiminato ligand may be the driving force in reactions, rather than the acidity of the amine proton.

Scheme 6 – Generation of β -diketiminato zirconium trialkyls. Ar = phenyl. Ar' = para-(trifluoromethyl)-phenyl.



β -Diketiminato gold complexes have been recently investigated by Heyn and co-workers, and a rare example of a β -diketiminato gold(III) alkyl complex has been generated.¹⁹ Treatment of a lithiated BDI ligand with dimethyl gold chloride gave a complex with a square planar gold centre (**XVII**). This dimethyl complex showed reactivity towards electrophiles; however, all studies showed the site of electrophilic attack is the backbone γ -carbon on the ligand, and not the Au-C bond as anticipated.

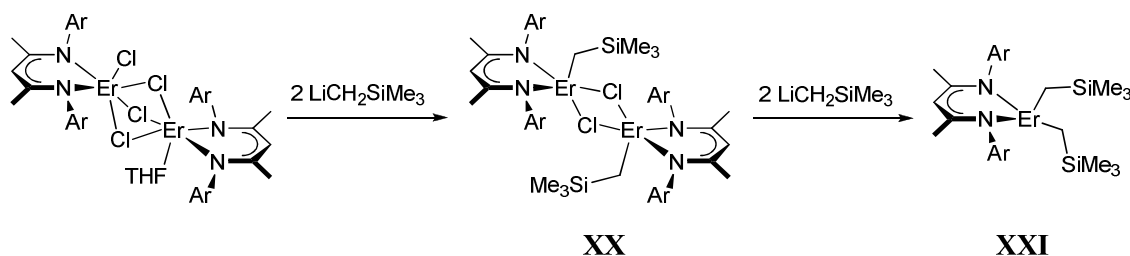
Scheme 7 – β -Diketiminato gold (III) complexes. Ar = 2,6-dimethylphenyl.



There have also been β -diketiminato metal alkyl complexes reported containing elements from the lanthanide series. Hayes and co-workers synthesised an erbium complex in the same fashion to the dimethyl gold complex above.²⁰ Erbium trichloride

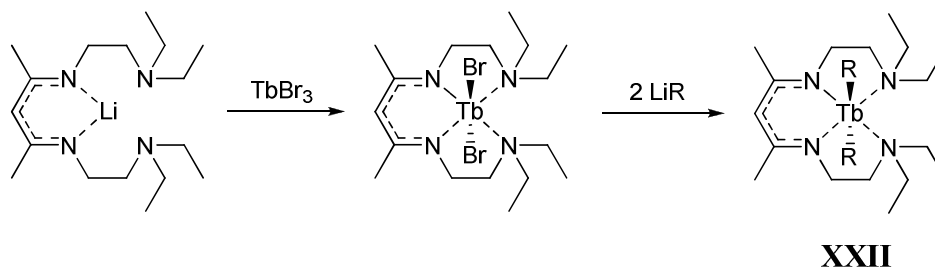
was treated with lithiated BDI to yield the metal chloride complex, which, in the case of erbium, exists as a trichloro-bridged dimer with two Er(III) centres, one with an extra coordinated chloride and the other with a coordinated THF molecule. Conversion to an alkyl complex is carried out by treatment with two equivalents of trimethylsilyl methyl lithium to yield the dimeric complex $[(\text{BDI})\text{Er}(\text{Cl})(\text{CH}_2\text{SiMe}_3)]_2$ **XX**. Addition of a further two equivalents of the lithium reagent yielded the monomeric $(\text{BDI})\text{Er}(\text{CH}_2\text{SiMe}_3)_2$ complex **XXI**.²⁰

Scheme 8 – Generation of BDI erbium(III) metal alkyl complexes. Ar = 2,6-diisopropylphenyl.



Lanthanide complexes of β -diketiminates are still fairly rare. Complexes with some of the larger, earlier f-block metals, such as the hexa-coordinate terbium complex $(\text{BDI})\text{Tb}(\text{CH}_2\text{SiMe}_3)_2$ (**XXII**) reported by Roesky and co-workers, have required extra N-chelating groups in the R^3 position on the BDI ligand structure to stabilise the metal centre.²¹

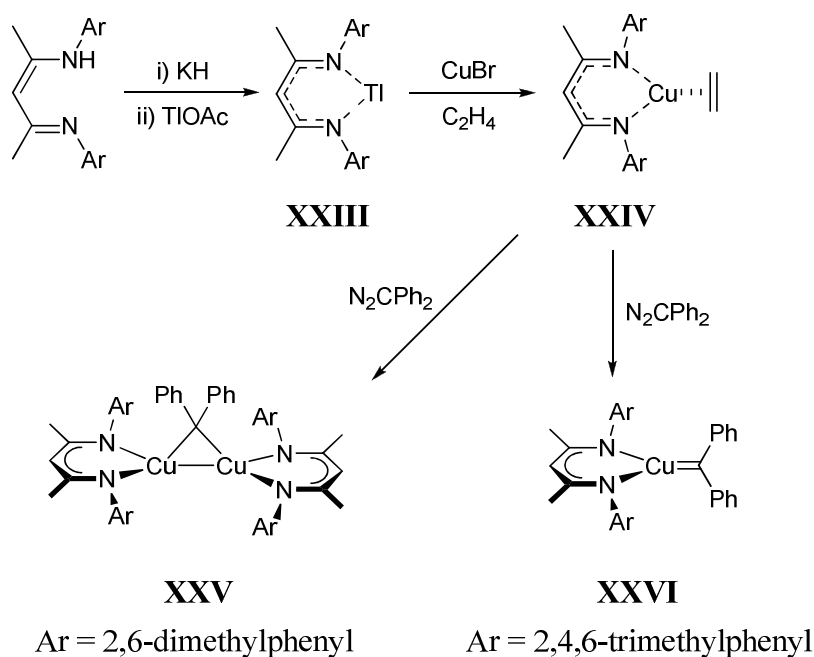
Scheme 9 – Synthesis of a hexa-coordinate terbium complex, with a BDI ligand containing N-chelating substituents. $\text{R} = \text{CH}_2\text{SiMe}_3$.



β -Diketimate copper (I) complexes have been synthesised by Warren and co-workers, and have been investigated for their catalytic reactivity for the cyclopropanation of styrene with diphenyldiazomethane (N_2CPh_2).²² The initial copper(I) ethylene

compound **XXIV** is prepared by way of a thallium(I) precursor (scheme 10).²³ Copper carbene complexes are prepared by treating the BDI copper-ethylene with equivalent amounts of N_2CPh_2 .

Scheme 10 – BDI copper alkyl cyclopropanation catalysts.

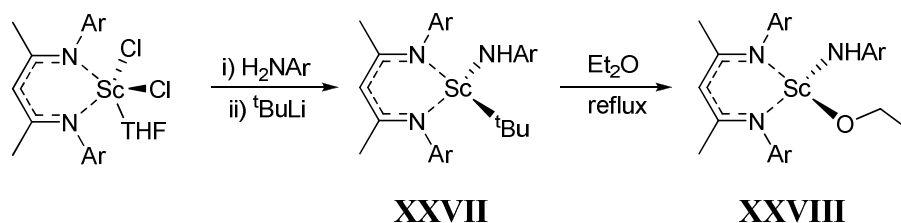


Increasing the bulk on the N-substituted aryl rings allowed generation of the complex $(\text{BDI})\text{Cu}=\text{CPh}_2$ **XXVI**, a rare example of a β -diketimate metal complex with a metal-carbon double bond between the diphenylmethyl substituent and the metal centre.²²

Another use for metal β -diketimates has been to perform C-O bond cleavage in Et_2O and THF, studied by Mindiola and co-workers.²⁴ It is shown that reaction of $(\text{BDI})\text{ScCl}_2\cdot\text{THF}$ with potassium diisopropylaniline and subsequent reaction with *tert*-butyllithium gives a scandium alkyl-amide complex **XXVII** (Scheme 11). This compound exchanges the *tert*-butyl substituent for an ethoxide ligand upon refluxing in diethyl ether, to give alkoxide-amide **XXVIII**. No expected β -hydride elimination was observed, however, which led the authors to believe the reaction occurred via the loss of a $^t\text{Bu}\bullet$ radical. This pathway was supported by the absence of isobutene (which would have formed, had the reaction taken place by β -hydride elimination), and the presence of *t*-butane in the reaction atmosphere, formed from the radical and subsequent C-H abstraction.²⁴ Attempts to heat the *tert*-butyl complex **XXVII** to force β -hydride elimination to form a scandium hydride led to neither product nor decomposition,

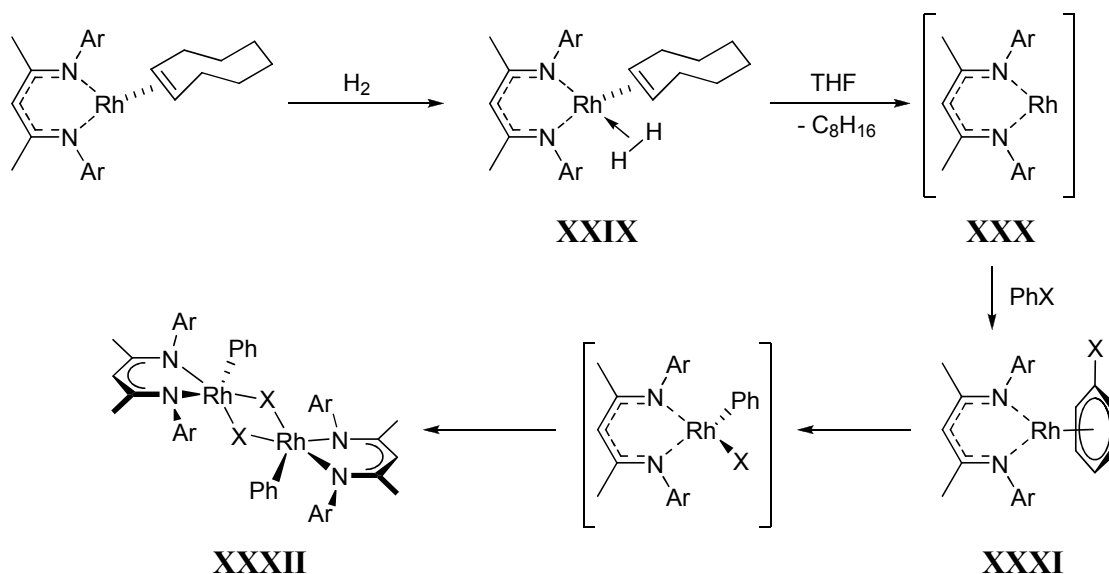
revealing that the highly congested structure acted to stabilise the compound, rather than promote loss of the substituent groups.

Scheme 11 – (BDI)ScX₂ complexes, to investigate C-O bond cleavage. Ar = 2,6-diisopropylphenyl.



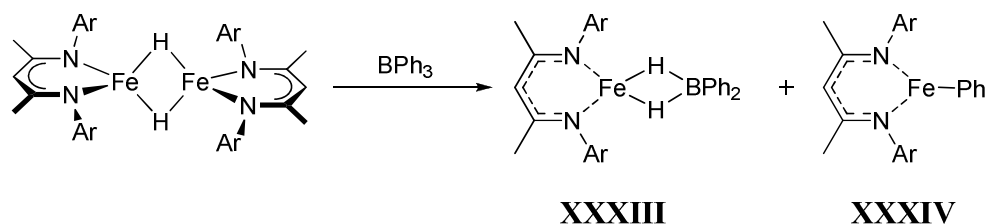
In addition to aliphatic alkyl groups present on the metal centre, a number of aryl-substituted metal β -diketiminates are known, and can exist in both the dimeric and monomeric forms. The rhodium dimer **XXXII** was synthesised by Budzelaar and co-workers, and is a result of an oxidative addition of a halogenated aryl to a rhodium(I) centre.²⁵ Mechanistic studies indicate the generation of the 12-electron rhodium(I) intermediate **XXX** is the rate-determining step, due to the increase in rate when the reaction is performed in both an atmosphere of hydrogen gas and in a coordinating solvent such as THF. This was only possible with aryl compounds, due the initial coordination required of the PhX to the Rh centre in **XXXI**.

Scheme 12 – (BDI) rhodium(I) insertion into a C-X bond. Ar = 2,6-dimethylphenyl. X = Cl, Br.



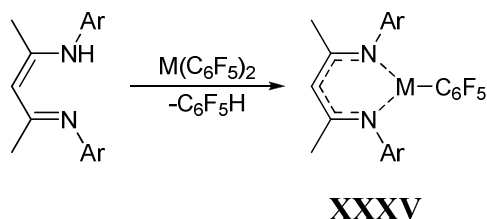
A monomeric β -diketiminate metal aryl was synthesised as a consequence of B-C bond cleavage by Holland and co-workers.²⁶ A dimeric (BDI) iron(II) hydride was used to break a B-C bond in triphenylborane, and the complexes underwent metathesis to yield a dihydridoborate iron complex **XXXIII**, and iron phenyl complex **XXXIV**.

Scheme 13 – Formation of (BDI)FePh by B-C bond cleavage. Ar = 2,6-diisopropylphenyl.



Fluorinated aryl groups have also been shown to form complexes with metal-BDI environments, although such compounds are uncommon. Tyrra and co-workers produced both zinc and cadmium complexes of BDI with a pentafluorophenyl group present on the metal centre (**XXXV**).²⁷ Synthesis of the complexes was carried out by the addition of the neutral BDI ligand to one equivalent of the bis-pentafluorophenyl metal. Although the zinc and cadmium complexes were isolated, a mixture of decomposition products was observed in the analogous mercury reaction, with no evidence of a mercury β -diketiminate complex.

Scheme 14 – Generation of (BDI)M- C_6F_5 group 12 complexes. M = Zn, Cd. Ar = 2,6-diisopropylphenyl.

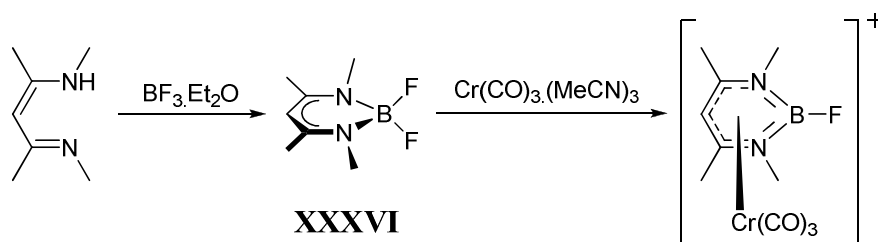


1.1.4 Group 13, 14 and 15 β -diketiminate complexes

In addition to their transition metal counterparts, many main group β -diketiminate complexes have been reported in the last three decades. The first simple group 13

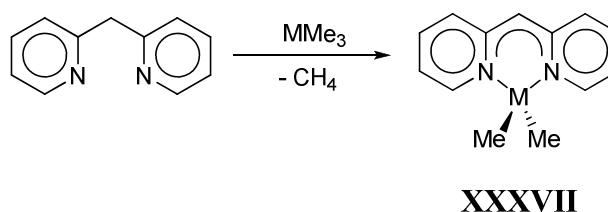
complex reported was a difluoro-boron structure by Kuhn and co-workers, prepared from a neutral β -diketimine and boron trifluoride etherate in triethylamine (**XXXVI**).²⁸ This was observed to act as a cyclohexadienide-type ligand when coordinated to a $[\text{Cr}(\text{CO})_3]$ fragment.

Scheme 15 – Synthesis of an early boron-difluoride β -diketiminate.



More common metal-containing β -diketiminate complexes in group 13 were initially reported in the early 1990s with such examples as an aluminium dichloride β -diketiminate complex, prepared in the same fashion as the boron complex above, again by Kuhn and co-workers.²⁹ A pair of simple β -diketiminate aluminium and gallium metal alkyl complexes (**XXXVII**), were reported in 1994 by Gornitzka and co-workers. These complexes utilised a deprotonated bis-pyridyl methyl system as the β -diketiminate ligand, and showed the metal atom in a pseudo-tetrahedral environment.³⁰ The addition of the respective metal trialkyl deprotonated the central backbone carbon of bis(2-pyridyl)methane, generating the recognisable β -diketiminate structure. These metal complexes are also notable for having the substituents at R^2 and R^3 tethered together.

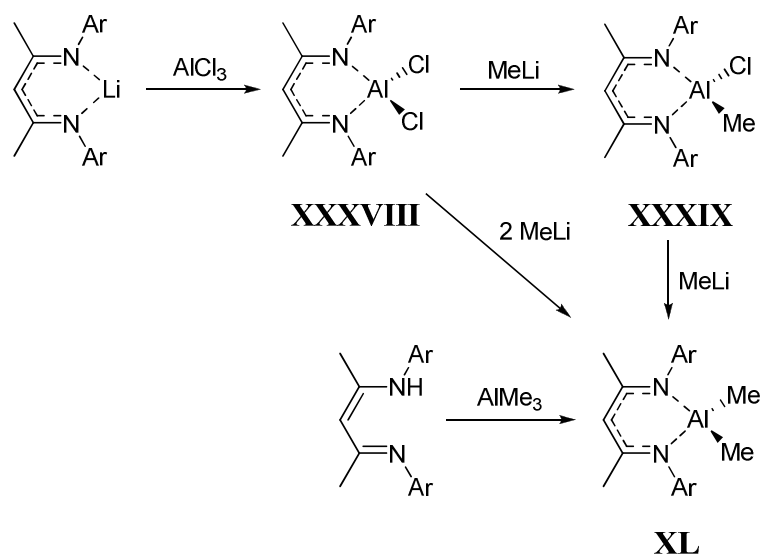
Scheme 16 – Generation of bis-pyridyl methyl group 13 β -diketimines. $\text{M} = \text{Al}, \text{Ga}$.



In 1998, Smith and co-workers published work showing the scope of the preparation and reactions of β -diketiminate aluminium complexes.³¹ It was shown that the substituents on the aluminium centre could be exchanged in a stepwise process.

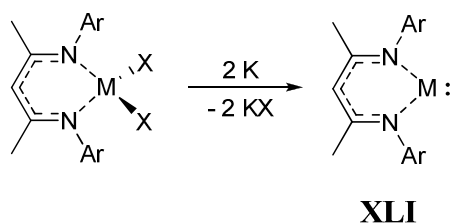
Dichloride **XXXVIII** was generated from a lithium β -diketiminate, by reaction with aluminium trichloride. One or both chlorides could be substituted by reaction with methyl lithium, to produce the aluminium chloro-methyl complex **XXXIX** or aluminium dimethyl complex **XL** respectively, with the latter able to be directly prepared from the addition of trimethyl aluminium to the neutral β -diketimine.

Scheme 17 – Exchange of substituent groups within (BDI)Al complexes. Ar = 4-methylphenyl.



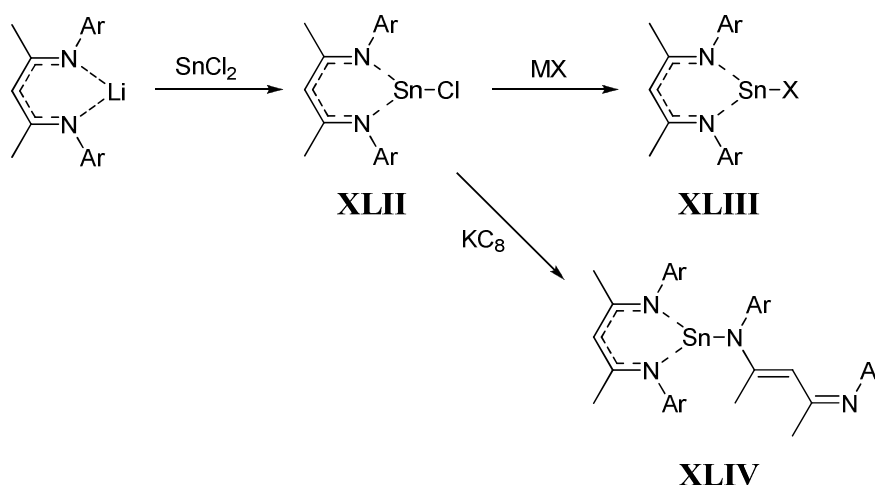
In a similar fashion to Smith's aluminium work detailed above, Power, Roesky and co-workers generated a rare example of an aluminium(I)- or gallium(I) carbene analogue.^{32,33} Lithiated BDI was treated with the respective metal trihalide (or the oligomeric "GaI", in the case of gallium) to yield the BDI metal dihalides, similar to that shown above (**XXXVIII**). The iodo-complexes of aluminium and gallium were reduced with potassium to yield the two-coordinate carbene analogues **XLI**.

Scheme 18 – Group 13 metal carbene analogue complexes. M = Al, Ga. X = I. Ar = 2,6-diisopropylphenyl.



Germanium and tin β -diketiminate complexes were reported by Power, Roesky and co-workers in 2001 as a group of monomeric, divalent complexes containing the sterically bulky 2,6-diisopropyl β -diketiminate, $[\{(2,6\text{-}^i\text{Pr}_2\text{C}_6\text{H}_3)\text{NC}(\text{CH}_3)\}_2\text{CH}]^-$.³⁴ These complexes were synthesised by addition of germanium(II) or tin(II) chloride to a solution of the lithiated BDI ligand. The generated β -diketiminate tin(II) chloride **XLII** was also used as a starting material for the generation of an alkyl, a triflate and an azide complex, showing that the substituent on the metal centre could be readily exchanged with a variety of other chemical groups (**XLIII**). Reduction of the tin(II) chloride complex with potassium graphite (KC_8) was shown to afford a β -diketiminate complex where one BDI ligand is coordinated to the metal centre in a bidentate fashion, and another BDI ligand is arranged as an amide substituent on the metal (**XLIV**).

Scheme 19 – Synthesis of various tin β -diketiminate complexes by Roesky and co-workers.³⁴ Ar = 2,6-diisopropylphenyl. (M = Na, X = N_3 ; M = Ag, X = OTf; M = Li, X = ^tBu).



The solid state geometry of most group 14 β -diketiminate complexes can take one of two different forms – a feature that is apparent in the series of β -diketiminate lead alkyl complexes synthesised in this work. When the metal centre and substituent lie on the same side of the plane comprised of the BDI backbone (the C_3N_2 plane), with the terminal substituent arranged between the two aryl groups on the ligand, this can be termed the *endo*- conformation (Figure 7). The alternate geometry is termed the *exo*- conformation, and is apparent when the metal centre lies above the C_3N_2 plane, with the terminal substituent pointing away from the metal-ligand core of the complex.³⁵

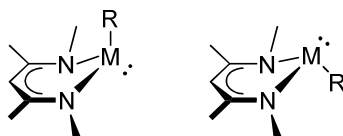
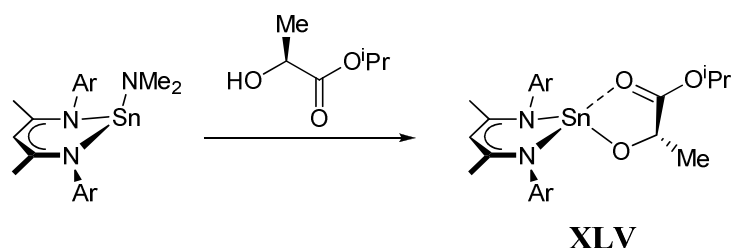


Figure 7 – The two different conformations of a group 14 metal-BDI complex; *endo*- (left), *exo*- (right).

Further tin(II) complexes have been published by Roesky with a wide variety of terminal substituents on the tin centre, including methyl, amide and other halide substituents, including an example of a very rare tin(II) fluoride.³⁶ β -Diketiminato tin(II) chloride has been shown to be useful in lactide polymerisation studies, by generating the initiators (BDI)SnOⁱPr and (BDI)SnNMe₂.³⁷ Computational studies showed that, although the first insertion of a lactide monomer into the Sn-substituent bond is straightforward, the rate-determining step is the propagation step, where a monomer unit is inserted into the metal-lactate complex. This is due to the increase in steric bulk and coordination number around the metal centre from the initiator complex (with small, less bulky substituents at the tin atom) to the first-monomer-inserted complex, with a 5-membered Sn-lactate ring. This 5-membered ring was also present in a model tin(II) lactide complex, which was synthesised to study the propagating species in the polymerisation reaction (**XLV**).

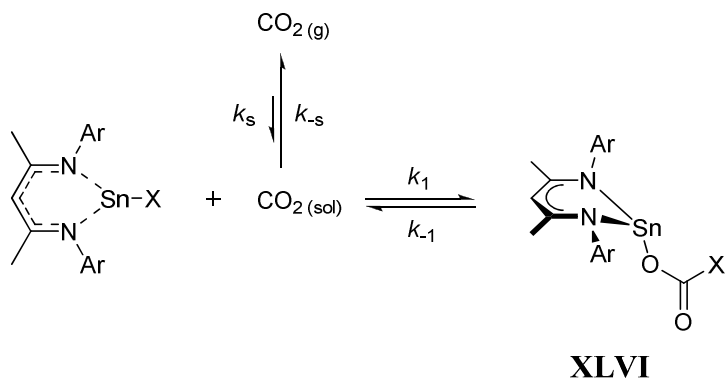
Scheme 20 – Synthesis of a model tin-lactide propagating species. Ar = 2,6-diisopropylphenyl.



In addition to examples used for lactide polymerisation, further examples of tin(II) amides and alkoxides have been reported by Fulton and co-workers.^{35,38} These tin complexes were observed to react reversibly with carbon dioxide, giving novel carbamates and carbonates respectively. Reaction kinetics were used to study the mechanism of insertion of carbon dioxide into the tin alkoxides, and the rate and reversibility of the insertion was shown to be dependent on the nature of the alkoxide

substituent, with the bulkier *tert*-butyl alkoxide displaying more sluggish reactivity than the corresponding *iso*-propyl alkoxide complex.³⁸

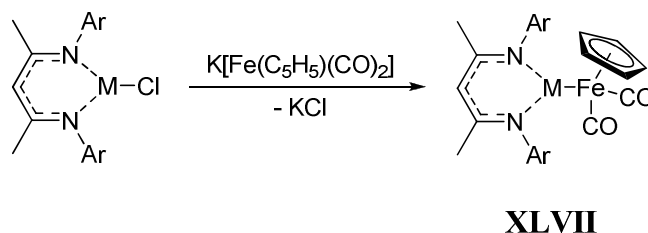
Scheme 21 – Synthesis of BDI tin carbamates and carbonates from carbon dioxide insertion. Ar = 2,6-diisopropylphenyl. (X = NR₂, NRR'),³⁵ (X = OR).³⁸



A nonafluoro-*tert*-butoxide tin complex was also synthesised to probe the electronic, as well as the steric, factors within the reactivity trends of the tin alkoxides, by changing the *tert*-butyl protons for fluorine atoms. However, the perfluorinated complex did not undergo reaction with carbon dioxide. Computational calculations were used to study the apparent mechanism in greater depth, and showed that there was a significant electronic contribution to the insertion reaction.³⁸ This acted to explain why the nonafluorinated complex did not react; the change in polarity of the molecule prohibited the reaction.

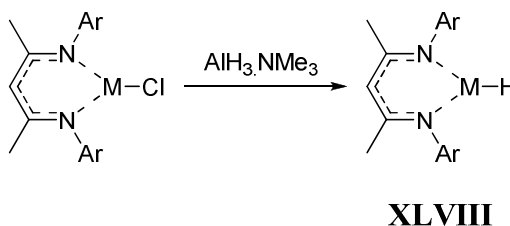
In addition to small organic groups being bound to the metal centre, it has also been observed that larger organometallic fragments can also be utilised to give novel group 14 β -diketiminate complexes. Driess and co-workers have published details of iron-germanium and iron-tin compounds, including the first example of a complex with an iron-germanium single bond ever characterised by X-ray analysis.³⁹ The BDI germanium or tin chloride was treated with one equivalent of K[Fe(η^5 -C₅H₅)(CO)₂], yielding complexes with a Ge-Fe or Sn-Fe bond respectively. Computational calculations were carried out and showed that there was no π -type bonding within the M-Fe bond, and that the bonding orbitals were highly polarised towards the iron atom, making them the first germanium and tin complexes bound by a single bond to an iron centre.

Scheme 22 – Synthesis of group 14 σ -complexes to iron.³⁹ M = Ge, Sn. Ar = 2,4,6-tri-*t*-butylphenyl.



Low valent, group 14 metal hydrides with a β -diketiminato ligand system are incredibly rare; one of the few examples of a terminal group 14 hydride to be fully characterised was $[2,6\text{-Ar}_2\text{C}_6\text{H}_3\text{Sn}(\mu\text{-H})]_2$ (Ar = 2,4,6-*i*-Pr₃C₆H₂) by Power and co-workers in 2000.⁴⁰ The first β -diketimine examples were published by Roesky and co-workers six years later (**XLVIII**), comprising both tin(II) and germanium(II) examples of these complexes.⁴¹ Reactions of the respective BDI metal chloride with common hydride sources did not yield the desired products, and so the slightly more exotic source $\text{AlH}_3\cdot\text{NMe}_3$ was used.⁴² Attempts by the Fulton group to use this source on the analogous (BDI)PbCl system were not successful.

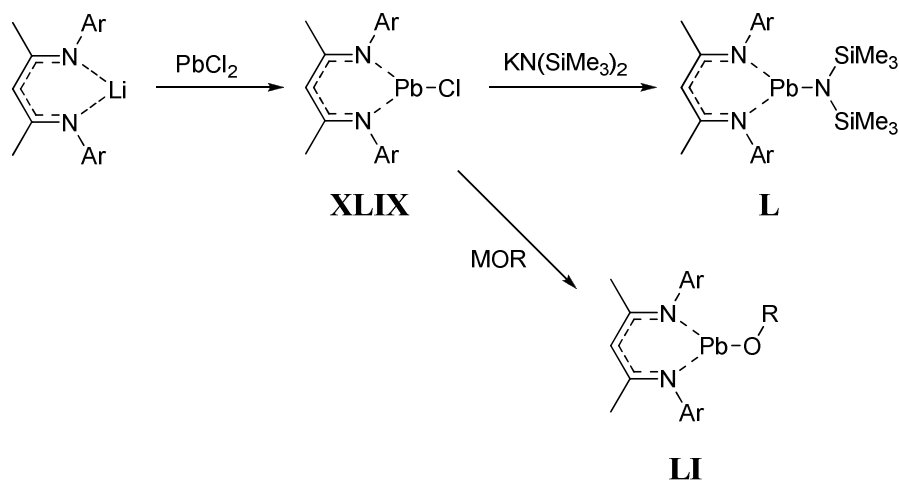
Scheme 23 – Synthesis of BDI group 14 terminal hydrides. M = Ge, Sn. Ar = 2,6-diisopropylphenyl.



Low-coordinate lead(II) complexes using β -diketiminato ligands were produced by Fulton and co-workers in 2007.⁴³ Lead halides of type **XLIX** were produced in a similar fashion to the tin and germanium analogues; by reaction of lithiated β -diketiminato ligand with one equivalent of lead dichloride. It was also shown to be possible to generate a lead amide complex, upon reaction with $\text{KN}(\text{SiMe}_3)_2$. Fulton also carried out computational studies to investigate the nature of the bonding and the role of the lone pair within the lead halide complexes, the latter of which was shown to affect the stereochemistry around the metal centre. A combination of electronic and steric factors were found to be responsible for the geometry of the molecules, and it is interesting to

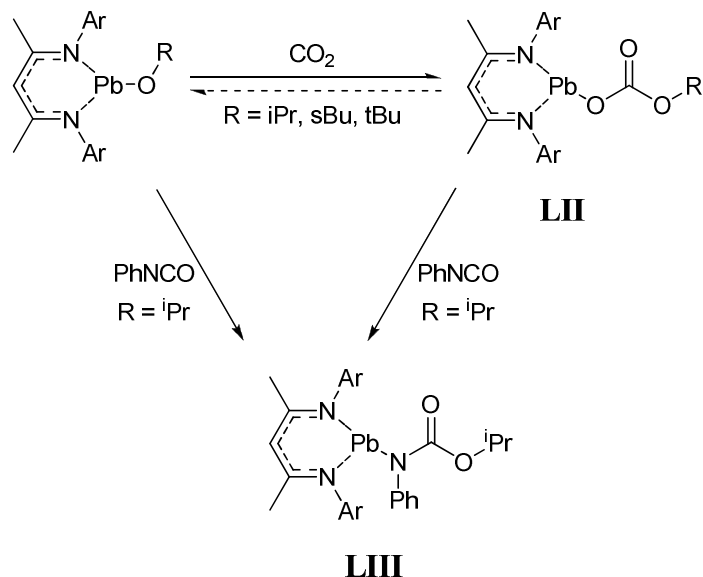
note that the lone pair in the BDI lead complexes contained very little mixing between the 6s and 6p orbitals; much less than in the isostructural tin and germanium systems.⁴³ In addition to molecules with halide substituents, Fulton has also produced complexes with alkoxide substituents, prepared from sodium or potassium alkoxides and the previously-synthesised lead halides.^{44,45}

Scheme 24 – Formation of BDI lead halides and subsequent amide and alkoxide complexes. M = Na, K. Ar = 2,6-diisopropylphenyl.



In common with the tin alkoxides described earlier, BDI lead alkoxides were observed to react favourably with heterocumulenes such as carbon dioxide and phenyl isocyanate to form carbonates and carbamates respectively.⁴⁵ It was shown that, as the bulk of the alkoxide substituent increases from *iso*-propoxide to *tert*-butoxide, the insertion of carbon dioxide becomes more easily reversible, to such a degree that the corresponding *tert*-butyl carbonate could not be characterised in the solid state due to spontaneous loss of carbon dioxide when stored at standard atmospheric pressure. The reversibility of a *sec*-butoxide/*sec*-butyl carbonate lay in between the former two complexes, demonstrating the effects of sterics upon insertion into the Pb-O bond.

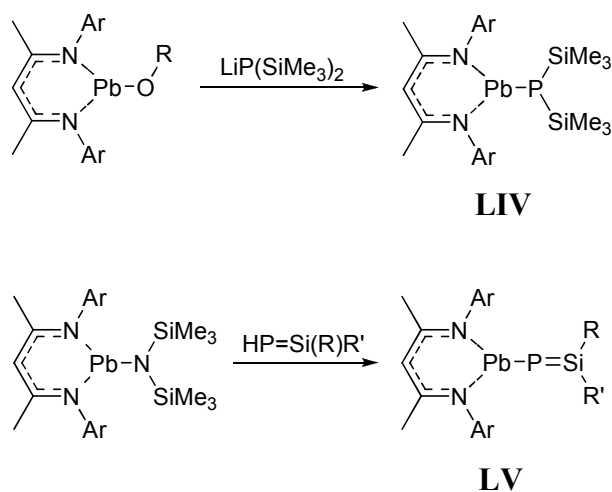
Scheme 25 – Study into the insertion by heterocumulenes into the Pb-O bond.
 Ar = 2,6-diisopropylphenyl.



The first example of a β -diketiminato lead alkyl complex was published by Roesky, concurrently with our work. Using methyl- or phenyllithium, the BDI lead chloride was able to be converted to the corresponding lead methyl or phenyl complex.⁴⁶ These compounds are very new, and no other studies have been carried out outside of our work (*vide infra*), other than the reporting of the synthesis.

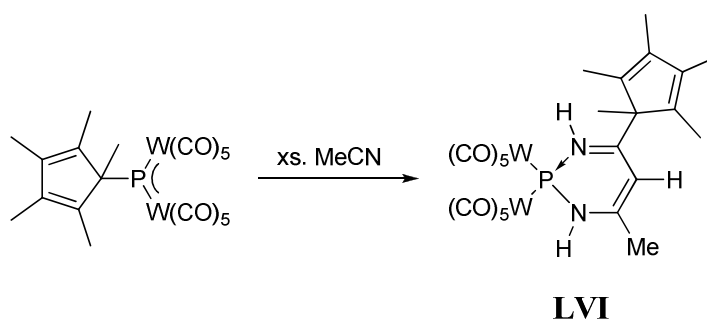
Driess and co-workers have published a very small number of terminal lead phosphides using the β -diketiminato ligand, including the first example of a lead-substituted phosphasilene, (BDI)PbP=Si(R)R' (**LV**).⁴⁷ Although these lead phosphide complexes are still fairly rare, Driess has reported that they show promise towards such applications as lactide polymerisation.

Scheme 26 – Syntheses of rare BDI lead phosphides. Ar = 2,6-diisopropylphenyl.



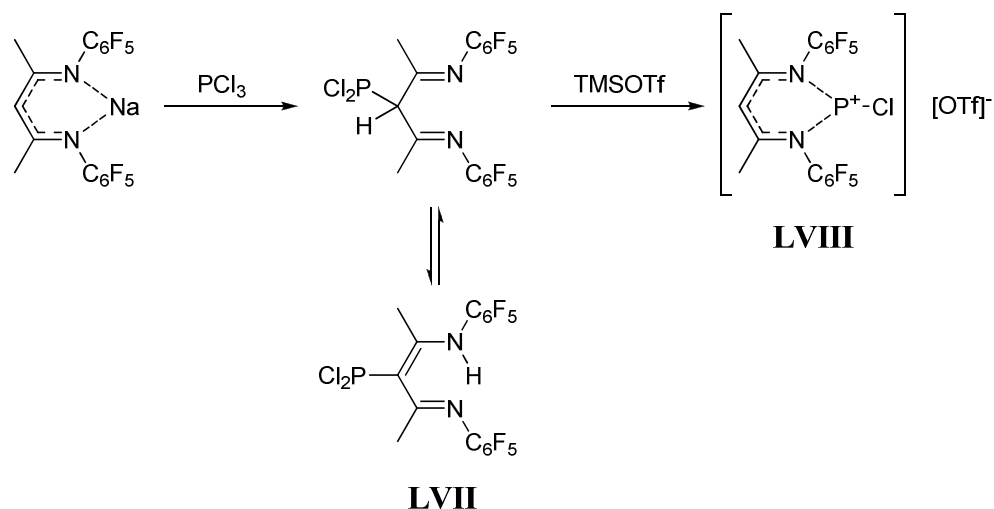
There are very few examples of group 15-coordinated β -diketiminato complexes known, with the first example of a phosphorus N,N'-chelated β -diketiminato reported by Scheer in 2001.⁴⁸ This was synthesised in a stepwise fashion, similar to early β -diketiminates, with the addition of acetonitrile to a phosphorus bridge between two tungsten centres (**LVI**). By altering the groups around the phosphorus and on the nitrile fragment, this method was billed as a convenient route to six-membered phosphorus heterocycles.

Scheme 27 – Synthesis of the first phosphorus β -diketiminato.



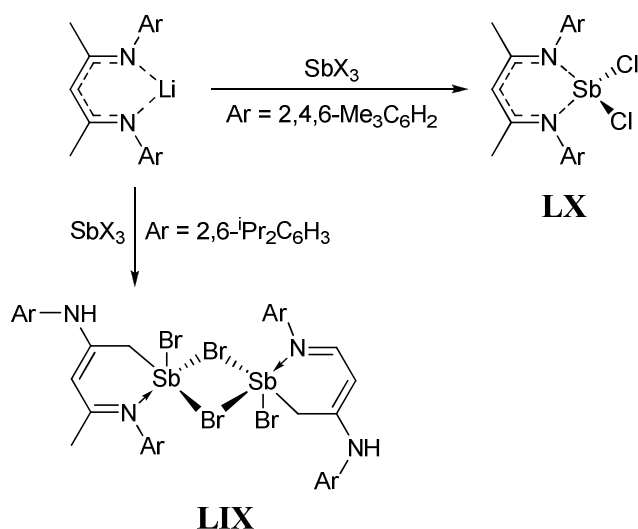
It was shown that other phosphorus-containing β -diketiminato complexes displayed a preference for addition to the backbone carbon, but some could be treated with a triflate to form N,N'-chelated phosphonium cations, such as those published by Cowley and co-workers.⁴⁹ Although the backbone-bound adduct **LVII** is in equilibrium between the diimine and ene-imine forms, the equilibration is slow enough to allow easy generation of the phosphonium cation **LVIII**.

Scheme 28 – Generation of a N,N'-chelated phosphonium cation.



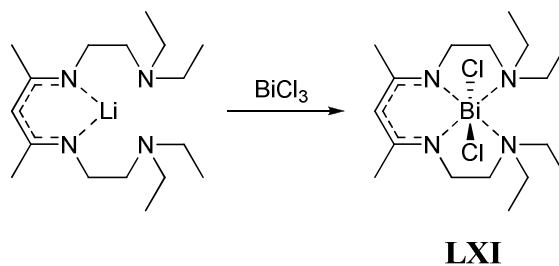
Complexes of the heavier elements of group 15 have been synthesised using the more standard synthetic procedure common with group 14 metal β -diketiminates – reaction of a lithiated β -diketimate ligand with the antimony or bismuth trichloride respectively.^{50,51} However, steric bulk is seen to play a part in the coordination number around the metal in the antimony product. Use of 2,6-diisopropylphenyl groups at the R^3 positions on the ligand (at the nitrogen) results in dimerisation, and coordination of the ligand to the antimony centre via one nitrogen and one of the backbone methyl groups (resulting in a methylene group) at the R^2 position (**LIX**). Switching this group to a mesityl group allows generation of the N,N'-coordinated monomeric BDI antimony dichloride (**LX**).⁵⁰

Scheme 29 – Steric effects on the generation of BDI antimony complexes. X = Cl, Br.



In order to avoid the dimerisation shown in **LIX**, a BDI ligand with extra coordinating groups can be used, to occupy the surplus coordination sites on the central metal atom. Roesky and co-workers have reported a bismuth complex with a BDI ligand containing (diethylamino)ethyl groups at the R³ positions.⁵¹

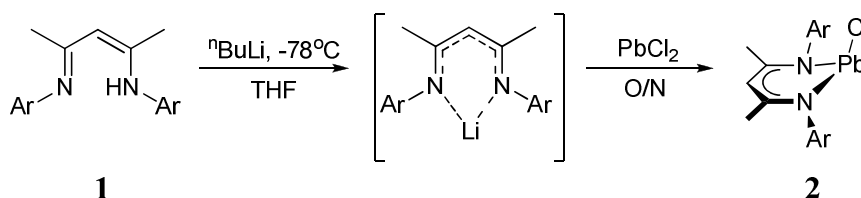
Scheme 30 – Synthesis of a very rare (BDI)BiX₂ complex, utilising a BDI ligand containing N-chelating substituents.



1.2 Discussion and synthesis of β -diketiminate lead alkyl complexes

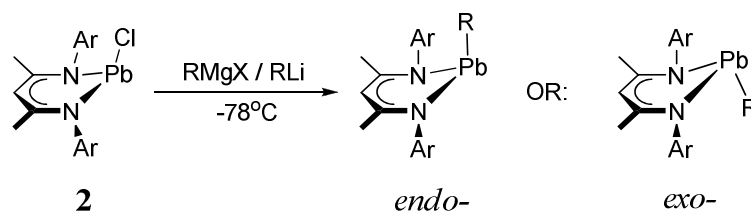
A series of β -diketiminate (BDI) lead(II) alkyl and phenyl complexes have been generated from the LPbCl precursor **2** ($L = \{[(2,6\text{-}i\text{Pr}_2\text{C}_6\text{H}_3)\text{NC}(\text{CH}_3)_2]\text{CH}\}$). This latter compound was prepared by deprotonating the β -diketiminate ligand **1**, LH, by using *n*-BuLi to generate the lithium β -diketiminate *in situ*. This lithium salt was added to a THF suspension of lead dichloride (scheme 31). After stirring overnight at room temperature, chloride compound **2** can be isolated in 70-80% yield.⁴³

Scheme 31 – Synthesis of lead chloride **2** from β -diketiminate ligand **1**. Ar = 2,6-diisopropylphenyl.



The general procedure employed in the generation of complexes of type LPbR, where R is an alkyl or phenyl group, was to treat the β -diketiminate lead (II) chloride **2** with a Grignard reagent or alkyllithium compound at low temperature and subsequently isolate the desired complex.

Scheme 32 – Synthesis of lead(II) alkyl complexes from lead chloride **2**. Ar = 2,6-diisopropylphenyl, R = alkyl or phenyl group, X = Cl, Br.



1.2.1 Synthesis and characterisation of β -diketimate lead(II) methyl, LPbMe (**3**)

Lead methyl **3** was generated from the addition of a slight excess of methylmagnesium bromide to a toluene solution of the precursor lead chloride **2**, cooled to -78°C . After complete addition, the mixture was allowed to warm to room temperature and stirred for one hour. The yellow solution was filtered through Celite®, and compound **3** was isolated in 40 % yield. Methyl complex **3** was found to be soluble in most common aliphatic and aromatic hydrocarbon solvents, mostly soluble in more polar solvents such as dichloromethane, but was found to decompose immediately in ethereal solvents such as diethyl ether and THF.

After 6-8 hours in a hydrocarbon solution at room temperature, formation of a black precipitate (presumed to be Pb(0)) was observed, and an unidentifiable mixture of other products, including evidence of some reversion to neutral β -diketimate ligand **1**, is observed by ^1H NMR spectroscopy. Methyl **3** is also light-sensitive, causing the same degradation as caused by thermal effects. Both these sensitivities necessitated strict storage conditions. Upon synthesis, the complex was stored in a -30°C freezer in an inert atmosphere glovebox, and all NMR experiments were carried out with freshly prepared samples, which were stored in foil coverings to exclude light when not inside an NMR spectrometer.

Crystals of lead methyl **3** suitable for X-ray diffraction studies were grown in a pentane solution at -30°C , and the complex was found to adopt the *endo*- conformation (figure 8). The distance between the lead centre and the plane comprised of the BDI backbone (the C_3N_2 plane) of 0.762 \AA is slightly larger than the corresponding distance in the parent chloride (0.683 \AA). The Pb-methyl bond length is $2.317(7)\text{ \AA}$, which is similar to the corresponding bond in the only other Pb(II) terminal methyl complex reported, $\text{Pb}(\text{Me})\text{C}_6\text{H}_3\text{-2,6-(2,4,6-}^i\text{Pr}_3\text{C}_6\text{H}_2)_2$, by Power and co-workers ($2.274(15)\text{ \AA}$).⁵²

The three angles around the Pb atom are used in calculating the degree of pyramidalisation (DOP) by the formula in equation 1, where the term “ $\Sigma \alpha_i$ ” denotes the sum of all angles around the metal centre.⁵³ DOP can be explained as the “sharpness” of the angles at the Pb atom, normalised to 90° . Hence, a compound where the N1-Pb-N2,

N1-Pb-C and N2-Pb-C angles are all 90° would have a DOP of 100%. Angles of less than 90° would cause a sharper DOP of more than 100%, with angles greater than 90° denoting a flatter DOP of less than 100%.

$$\text{DOP (\%)} = [360 - \sum \alpha_i] / 0.9 \quad (1)$$

The DOP in the methyl complex **3** is 109.4%, which is larger than that reported for other *endo*- type configurations, such as the lead chloride **2**.⁴³ This is potentially due to the relatively small methyl group present in the complex.

Table 1 – Bond angles (°) and bond lengths (Å) for LPbMe (**3**)

N1-Pb-C30	91.3(2)	Pb-C30	2.317(7)
N2-Pb-C30	88.6(2)	N1-Pb	2.328(5)
N1-Pb-N2	81.68(17)	N2-Pb	2.351(5)
C1-N1-C6	121.4(5)	N1-C1	1.325(8)
C1-N1-Pb	123.9(4)	C1-C2	1.415(8)
C6-N1-Pb	114.2(3)	C2-C3	1.414(8)
C3-N2-C18	123.8(5)	C3-N2	1.312(7)
C3-N2-Pb	124.5(4)		
C18-N2-Pb	111.7(3)	Pb – plane	0.762
N1-C1-C2	125.0(5)		
C1-C2-C3	129.8(6)	DOP (%)	109.36
C2-C3-N2	125.5(5)		

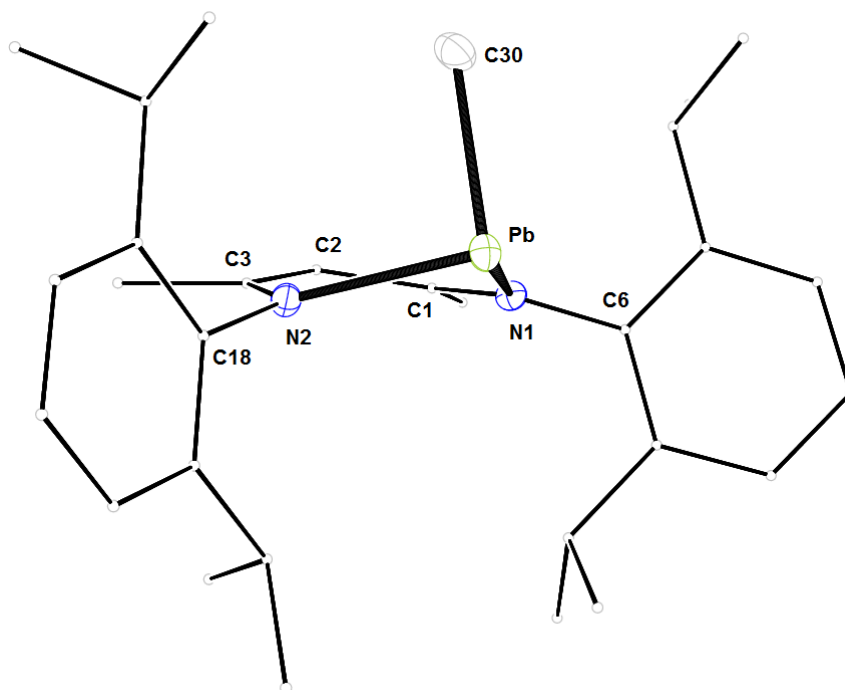


Figure 8 – LPbMe (**3**). 30% probability ORTEP ellipsoids, BDI ligand minimised and H-atoms omitted for clarity.

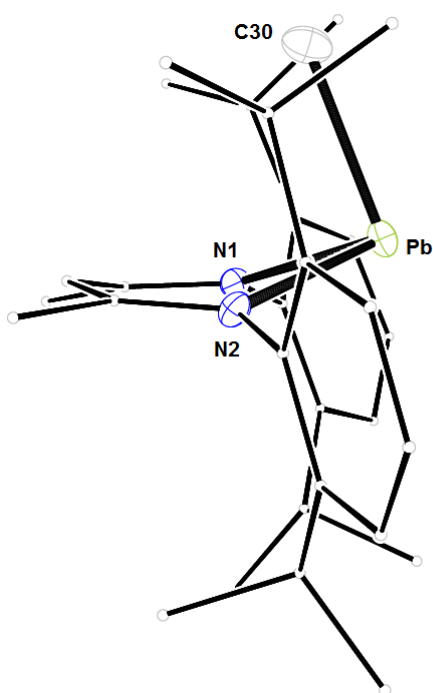


Figure 9 – LPbMe (**3**) side-on, showing extent of *endo*- conformation. 30% probability ORTEP ellipsoids, BDI ligand minimised and H-atoms omitted for clarity.

Concurrent with our synthesis of this compound, Roesky and co-workers published synthetic and structural details of this complex, synthesised using methyllithium rather than a Grignard reagent. The unit cell of our methyl complex **3**, as well as our spectroscopic data, matches with the data reported.⁴⁶

The ^1H NMR spectrum of methyl complex **3** in C_6D_6 shows a singlet peak at δ 0.56. Although no ^{207}Pb satellites are observed to indicate the methyl group coupling with the metal centre, Roesky reports a value of $^2J = 72$ Hz.⁴⁶ The non-symmetric metal centre is indicated by two environments for the N-aryl substituents, with two septets ($J = 6.9$ Hz), integrating 2 protons each, at δ 3.56 and 3.46 and four doublets ($J = 6.9$ Hz), integrating to 6 protons each between δ 1.33 and 1.22. Three of these doublets overlap with each other, with the apparent multiplet integrating to a total of 18 protons. However, this is consistent with three signals of 6 protons each. The $^{207}\text{Pb}\{^1\text{H}\}$ NMR spectrum shows a single peak at δ 3002, very similar to the signal reported by Roesky at δ 3009.⁴⁶ This signal differs greatly from the signal of the parent chloride **2**, the signal of which was reported by Roesky at δ 1413 in the same paper.⁴⁶

1.2.2 Synthesis and characterisation of β -diketimate lead(II) *iso*-propyl, LPb^iPr (**4**)

Lead *iso*-propyl **4** was synthesised in a similar fashion to methyl **3** by adding a slight excess of *iso*-propylmagnesium chloride to a toluene solution of the precursor lead chloride **2** at -78°C . After complete addition, the mixture was allowed to warm to room temperature and stirred for two hours, after which the pale orange solution was filtered through Celite®, and compound **4** isolated in 53% yield. Lead *iso*-propyl **4** was soluble in most common aliphatic and aromatic hydrocarbon solvents, whilst becoming less soluble in more polar solvents such as dichloromethane. It was found to decompose in ethereal solvents such as THF and other ethers.

In common with methyl **3**, hydrocarbon solutions of *iso*-propyl **4** is unstable if left at or above room temperature for 7-8 hours, decomposing into black $\text{Pb}(0)$ and other, unidentifiable products. Compound **4** was also observed to be light-sensitive, requiring that it be handled in a similar fashion to methyl complex **3**, to minimise exposure.

Crystals suitable for X-ray diffraction studies were slowly grown in a heptane solution at -30°C. The diffraction study showed the *iso*-propyl **4** to adopt the *exo*- conformation, shown in figures 10 and 11. This complex has the smallest alkyl group in the LPbR series that displays this *exo*- conformation. The metal atom is significantly more pyramidal than that of the methyl analogue, with a flatter DOP of 93.2%. The Pb-C30 bond distance is slightly shorter than in methyl compound **3** by around 0.01 Å. However, the metal atom is displaced from the C₃N₂ plane by just under 0.36 Å, a significantly greater distance than that in methyl **3**. The N-Pb-C30 bond angles are larger than the corresponding angles in compound **3**, with the N1-Pb-N2 bond angle slightly smaller.

Table 2 – Bond angles (°) and bond lengths (Å) for LPbⁱPr (**4**)

N1-Pb-C30	98.51(14)	Pb-C30	2.305(4)
N2-Pb-C30	97.67(14)	N1-Pb	2.327(3)
N1-Pb-N2	79.90(10)	N2-Pb	2.330(3)
C1-N1-C6	120.8(3)	N1-C1	1.323(4)
C1-N1-Pb	120.6(2)	C1-C2	1.404(5)
C6-N1-Pb	117.3(2)	C2-C3	1.404(5)
C3-N2-C18	120.6(3)	C3-N2	1.332(5)
C3-N2-Pb	120.2(2)		
C18-N2-Pb	116.7(2)	Pb – plane	1.121
N1-C1-C2	124.3(3)		
C1-C2-C3	129.4(3)	DOP (%)	93.24
C2-C3-N2	124.2(3)		

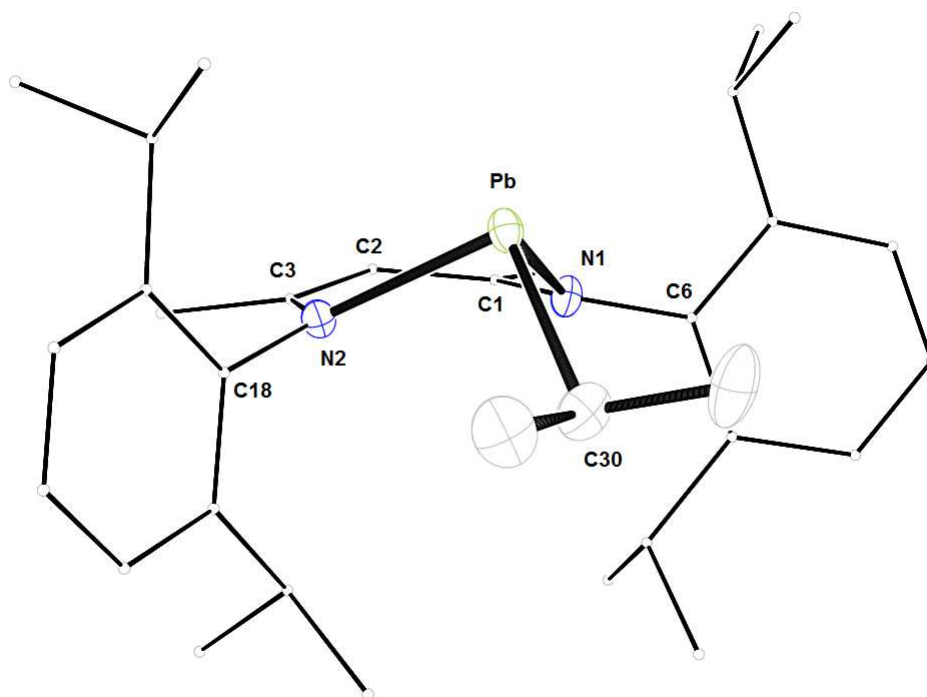


Figure 10 – LPbⁱPr (**4**). 30% probability ORTEP ellipsoids, BDI ligand minimised and H-atoms omitted for clarity.

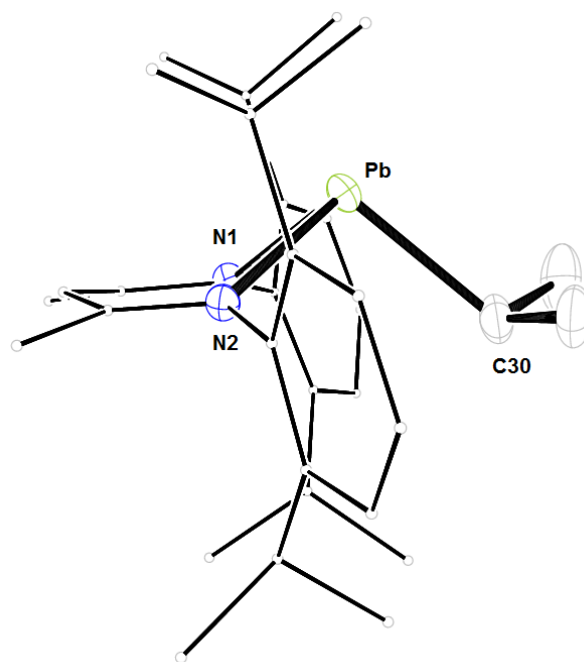


Figure 11 – LPbⁱPr (**4**) side-on, showing extent of *exo*- conformation. 30% ORTEP ellipsoids, BDI ligand minimised and H-atoms omitted for clarity.

The ^1H NMR spectrum shows a non-symmetric environment around the metal centre, with two septets ($J = 6.9$ Hz) and four doublets ($J = \sim 6.9$ Hz), assigned to the two *iso*-propyl group environments on the aromatic rings on the BDI ligand. Unlike methyl compound **3**, all four doublets are separated in the spectrum, and can be identified individually. There is a third septet at δ 3.31 ($J = 6.9$ Hz), corresponding to the *iso*-propyl methyne proton on the alkyl ligand. No $J_{\text{Pb-H}}$ coupling constant was observed, potentially due to the very close proximity of the signal to the other septets, thus obscuring any potential coupling to the Pb atom. A doublet at δ 1.54 ($J = 4.0$ Hz) is assigned to the CH_3 units of the *iso*-propyl group bonded to the metal centre. A signal at δ 3145 is observed in the $^{207}\text{Pb}\{^1\text{H}\}$ NMR spectrum, slightly more downfield than that of the methyl **3**.

1.2.3 Synthesis and characterisation of β -diketiminate lead(II) *sec*-butyl, LPb^sBu (**5**)

The first of two complexes with butyl substituents, lead *sec*-butyl **5**, was generated by addition of a slight excess of *sec*-butylmagnesium chloride to a -78°C toluene solution of lead chloride **2**. After complete addition, the solution was warmed to room temperature and stirred for two hours. The orange solution was filtered through Celite® and complex **5** was isolated in 61% yield.

Similarly with the rest of the compounds in the series, *sec*-butyl **5** was observed to be light-sensitive, and decomposed within 8 hours if stored at or above room temperature, depositing black $\text{Pb}(0)$. To alleviate this, compound **5** was stored in a foil-covered vial at -30°C in an inert atmosphere glovebox, and all NMR samples were stored in foil-covered tubes whilst not undergoing analysis.

Sec-butyl **5** showed very similar solubility to the rest of the lead alkyl series, and so crystals suitable for X-ray diffraction studies were grown in a saturated pentane solution held at -30°C . The diffraction studies showed that **5** adopted the *exo*- conformation, similarly to *iso*-propyl **4**. The DOP is 94.2%, slightly greater than that of compound **4**, indicating a slightly “sharper” environment around the metal centre in *sec*-butyl **5**. The Pb atom lies 1.215 Å from the C_3N_2 plane, just under 0.1 Å further away than that of *iso*-propyl **4**. Both these details may be due to the presence of an extra methylene group

in *sec*-butyl **5**, when compared to *iso*-propyl **4**. The Pb-C30 bond distance is 2.306(5) Å, almost the same as the Pb-C30 distance in the *iso*-propyl **4**. The bond angles around the metal centre are also very similar.

Table 3 – Bond angles (°) and bond lengths (Å) for LPb^sBu (**5**)

N1-Pb-C30	97.5(6)	Pb-C30	2.306(5)
N2-Pb-C30	98.2(7)	N1-Pb	2.3287(19)
N1-Pb-N2	79.56(10)	N2-Pb	2.3287(19)
C1-N1-C6	121.46(19)	N1-C1	1.325(3)
C1-N1-Pb	118.73(15)	C1-C2	1.406(3)
C6-N1-Pb	117.13(14)	C2-C3	1.406(3)
C3-N2-C18	121.46(19)	C3-N2	1.325(3)
C3-N2-Pb	118.73(15)		
C18-N2-Pb	117.13(14)	Pb – plane	1.215
N1-C1-C2	123.9(2)		
C1-C2-C3	129.4(3)	DOP (%)	94.16
C2-C3-N2	123.9(2)		

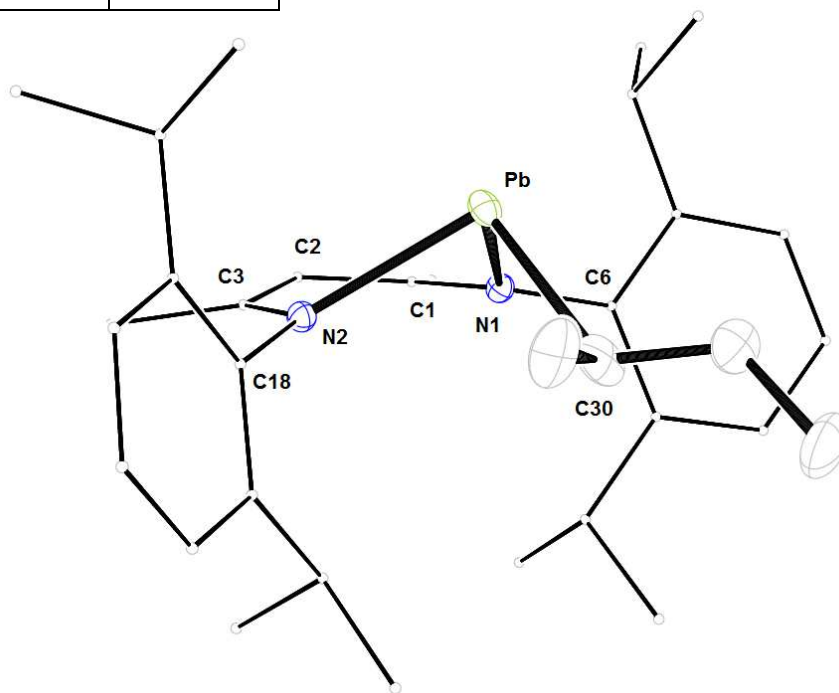


Figure 12 – LPb^sBu (**5**). 30% probability ORTEP ellipsoids, BDI ligand minimised and H-atoms omitted for clarity.

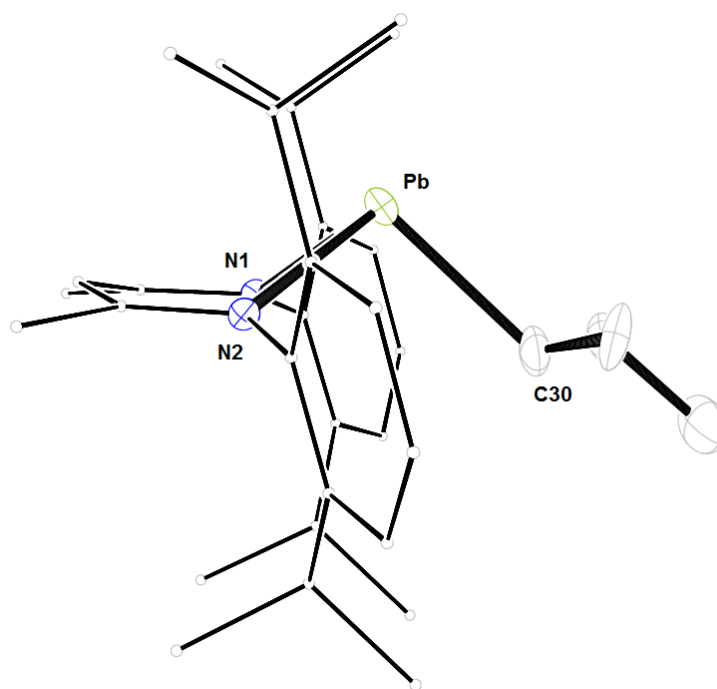


Figure 13 – LPb^sBu (**5**) side-on, showing extent of *exo*- conformation. 30% ORTEP ellipsoids, BDI ligand minimised and H-atoms omitted for clarity.

The ^1H NMR spectrum shows the iconic two septets that denote a non-symmetric environment around the metal centre ($J = \sim 6.6$ Hz), however, the corresponding doublets are crowded amongst the signals from the *sec*-butyl substituent, with some of the signals overlaid with each other. The *sec*-butyl substituent can be assigned, with clear signals of a doublet at δ 1.61, and a triplet at δ 0.80. A third signal overlaps with the two doublets from the *iso*-propyl groups on the aryl rings in a large multiplet at δ 1.25. The multiplet signal at δ 2.46 corresponds to the proton on the α -carbon of the *sec*-butyl group, but no $J_{\text{Pb-H}}$ coupling was observed in the ^1H NMR spectrum. The $^{207}\text{Pb}\{^1\text{H}\}$ NMR shift is slightly more downfield from the *iso*-propyl **4**, at δ 3262.

1.2.4 Synthesis and characterisation of β -diketiminate lead(II) *neo*-pentyl, LPbNp (**6**)

Lead *neo*-pentyl **6** was synthesised by the addition of one equivalent of *neo*-pentyllithium (NpLi) to the precursor lead chloride **2** at 0°C . Colder temperatures did not allow for complete dissolution of the NpLi reagent. After allowing to warm to room temperature, the mixture was stirred for two hours before being filtered through Celite®. An orange powder, compound **6**, was isolated in 67% yield. *Neo*-pentyl **6** was

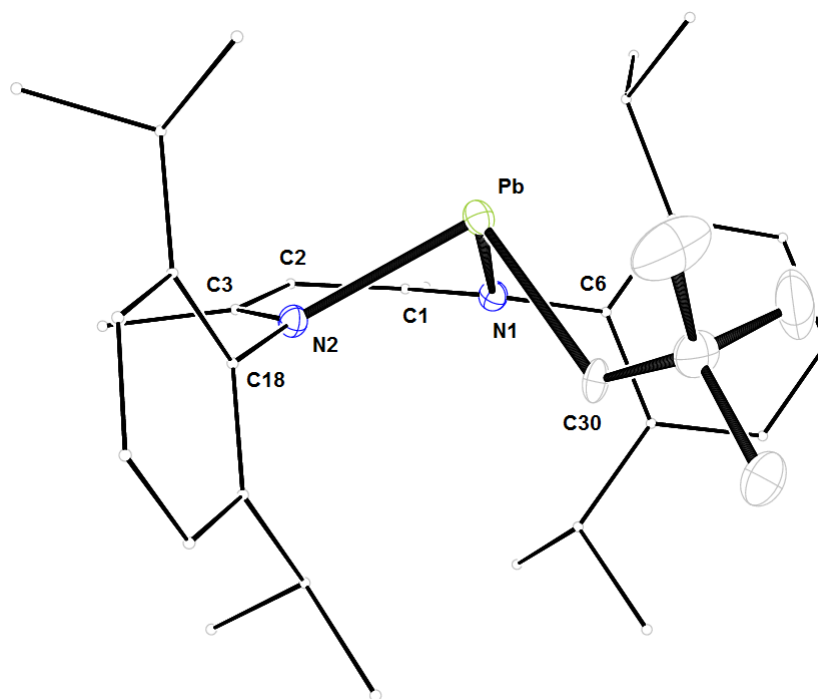
found to be soluble in common aromatic and aliphatic solvents, mostly soluble in hydrocarbon solvents, and was found to decompose in ethereal solvents.

Neo-pentyl **6** was observed to begin decomposition to black Pb(0) after 24-36 hours at room temperature, although this was accelerated by the application of higher temperatures. However, the same storage and light-exclusion principles were applied to it as to the rest of the compounds in the series; storage under foil at -30°C in inert atmosphere.

Crystals suitable for X-ray diffraction studies were grown in a saturated pentane solution at -30°C. The solid-state structure showed that the *neo*-pentyl **6** adopts the *exo*-conformation, and exhibits the second largest DOP in the *exo*- portion of the series; nearly 8 % “sharper” than *iso*-propyl **4** and *sec*-butyl **5**. The Pb-C30 bond distance is 2.293(4) Å, which is the shortest Pb-C30 distance in the LPbR series. This bond length is very close to the Pb-C bond distance reported by Power in his Pb(II) alkyl complex (2.274(15) Å).⁵² Due to the overall bulk of the alkyl group,⁵⁴ the distance between the C₃N₂ plane and the Pb atom is 1.179 Å, a distance between that observed in the *iso*-propyl **4** and *sec*-butyl **5**. The bond angles are similar to the rest of the series. However, one of the N-Pb-C30 bond angles is around 6° sharper than the other, demonstrating the asymmetry of the compound, with the result that the *neo*-pentyl group lies slightly off to one side of the central axis.

Table 4 – Bond angles (°) and bond lengths (Å) for LPbNp (**6**)

N1-Pb-C30	91.04(14)	Pb-C30	2.293(4)
N2-Pb-C30	97.54(15)	N1-Pb	2.3273(16)
N1-Pb-N2	79.64(8)	N2-Pb	2.3273(16)
C1-N1-C6	122.86(16)	N1-C1	1.324(2)
C1-N1-Pb	119.41(12)	C1-C2	1.408(2)
C6-N1-Pb	114.89(12)	C2-C3	1.408(2)
C3-N2-C18	122.86(16)	C3-N2	1.324(2)
C3-N2-Pb	119.41(12)		
C18-N2-Pb	114.89(12)	Pb – plane	1.179
N1-C1-C2	123.99(18)		
C1-C2-C3	129.5(2)	DOP (%)	101.98
C2-C3-N2	123.99(18)		

Figure 14 – LPbNp (**6**). 30% probability ORTEP ellipsoids, BDI ligand minimised and H-atoms omitted for clarity.

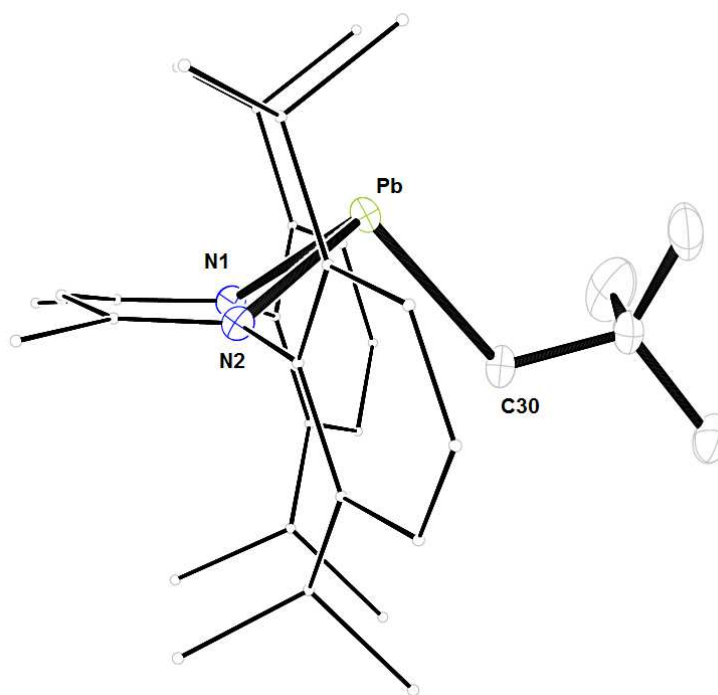


Figure 15 – LPbNp (**6**) side-on, showing extent of *exo*- conformation. 30% ORTEP ellipsoids, BDI ligand minimised and H-atoms omitted for clarity.

The solid-state asymmetry around the central axis described earlier is not evident in solution, but the ^1H NMR spectrum clearly shows the two septets ($J = \sim 6.9$ Hz) and the four doublets ($J = \sim 6.9$ Hz) common to the rest of the compounds in the LPbR series. The *neo*-pentyl group is also clearly observed, with singlets at δ 0.87 and 0.66. No $J_{\text{Pb-H}}$ coupling was able to be discerned around the CH_2 signal at δ 0.87. A signal at δ 3506 is observed in the $^{207}\text{Pb}\{^1\text{H}\}$ NMR spectrum.

1.2.5 Synthesis and characterisation of β -diketiminate lead(II) benzyl, LPbBn (**7**)

Lead benzyl **7** was synthesised from the addition of one equivalent of benzylmagnesium chloride to a toluene solution of the precursor chloride **2** at -78°C . The mixture was allowed to warm to room temperature and stirred for two hours, after which the orange solution was filtered through Celite®, and benzyl complex **7** was isolated in 40% yield. Benzyl **7** was observed to decompose after 12-18 hours at room temperature, and so similar precautions against exposure to temperature and light were taken as to the rest of the series.

Similar solubility properties to the rest of the lead alkyl series were observed for benzyl **7**, and crystals suitable for X-ray diffraction studies were grown in a saturated pentane solution at -30°C. The solid state structure exhibits the *exo*- conformation, and the metal atom has the largest DOP of those compounds within the *exo*- portion of the series, just over 1% larger than the bulky *neo*-pentyl **6**. The Pb-C30 bond length is 2.314(5) Å; longer than that of *neo*-pentyl **6**, and the Pb atom lies further away from the C₃N₂ plane, at 1.251 Å. Both these distances indicate that the benzyl group can be considered bulkier in some regards than the *neo*-pentyl group in compound **6**.

Table 5 – Bond angles (°) and bond lengths (Å) for LPbBn (**7**)

N1-Pb-C30	93.38(11)	Pb-C30	2.314(5)
N2-Pb-C30	93.38(1)	N1-Pb	2.321(2)
N1-Pb-N2	80.22(12)	N2-Pb	2.321(2)
C1-N1-C6	121.7(2)	N1-C1	1.329(4)
C1-N1-Pb	117.42(19)	C1-C2	1.406(3)
C6-N1-Pb	118.61(18)	C2-C3	1.406(3)
C3-N2-C18	121.7(2)	C3-N2	1.329(4)
C3-N2-Pb	117.42(19)		
C18-N2-Pb	118.61(18)	Pb – plane	1.251
N1-C1-C2	124.0(3)		
C1-C2-C3	129.4(4)	DOP (%)	103.36
C2-C3-N2	124.0(3)		

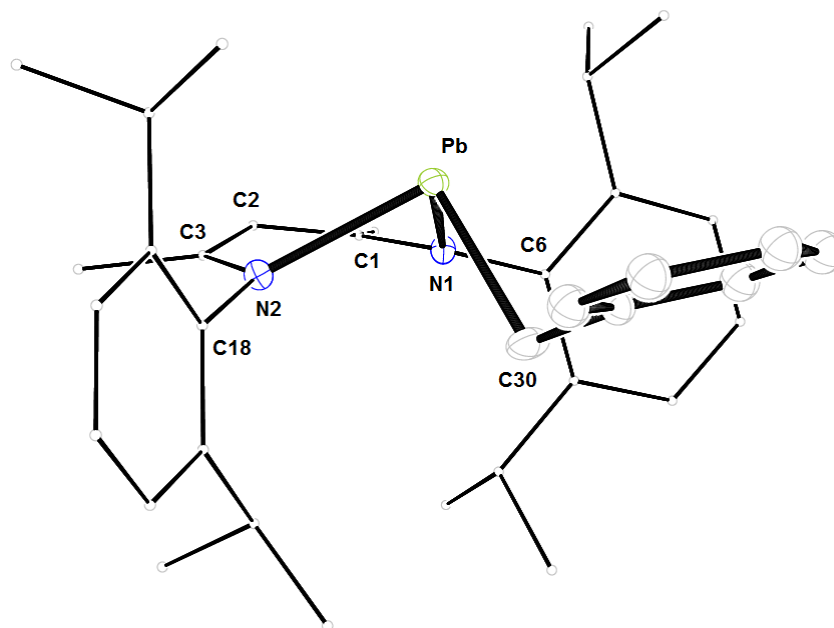


Figure 16 – LPbBn (**7**). 30% probability ORTEP ellipsoids, BDI ligand minimised and H-atoms omitted for clarity.

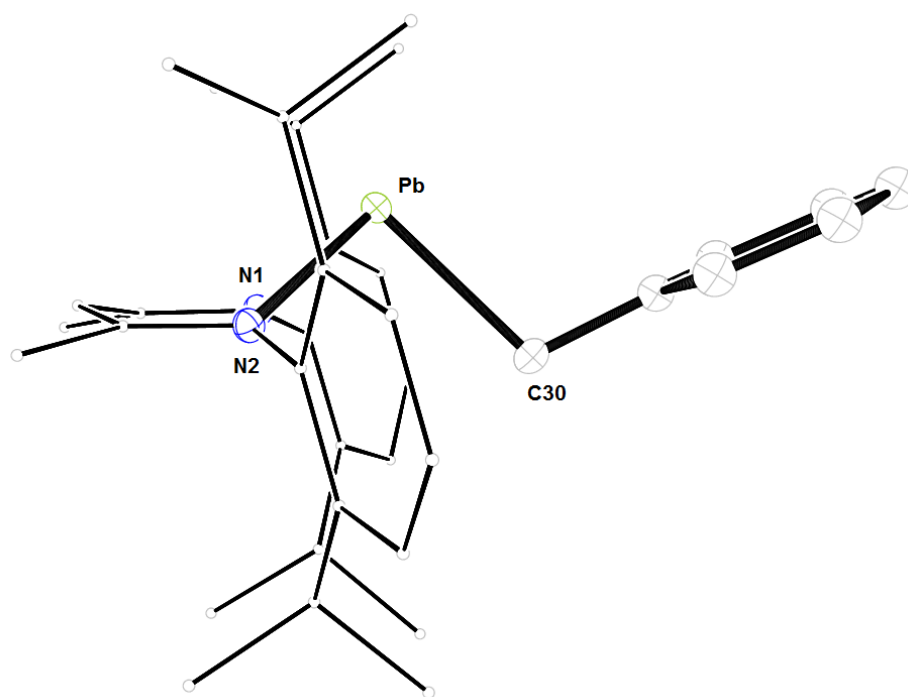


Figure 17 – LPbBn (**7**) side-on, showing extent of *exo*- conformation. 30% ORTEP ellipsoids, BDI ligand minimised and H-atoms omitted for clarity.

Both the septets ($J = \sim 6.9$ Hz) and doublets ($J = \sim 6.9$ Hz) are clearly distinguishable in the ^1H NMR spectrum, as is the signal for the α -carbon protons of the substituent, at δ 1.77. However, like many of the other compounds in the series, $J_{\text{Pb-H}}$ couplings were not observed in the NMR spectrum. The protons on the aromatic ring of the substituent can be distinctly observed in the aromatic region of the spectrum, comprising of two triplets ($J = 7.6$ Hz and 7.4 Hz) and a doublet ($J = 7.4$ Hz) of integration 2:1:2 respectively. A signal in the $^{207}\text{Pb}\{^1\text{H}\}$ NMR spectrum is observed at δ 2871, significantly upfield from the compounds with aliphatic substituents.

1.2.6 Synthesis and characterisation of β -diketiminate lead(II) *tert*-butyl, LPb^tBu (**8**)

Lead *tert*-butyl **8** was generated by addition of one equivalent of *tert*-butyllithium ($^t\text{BuLi}$) to a toluene solution of the parent chloride **2**. After allowing to warm to room temperature, the mixture was stirred overnight. The resultant red solution was filtered through Celite® and *tert*-butyl **8** was isolated in 56% yield. The increased reaction time was attributed to the steric bulk of the *tert*-butyl group effecting a slower reaction. The decomposition time was markedly increased for *tert*-butyl **8**, black Pb(0) only being observed after 24-36 hours at room temperature. However, the same storage and light-exclusion conditions as the rest of the series were applied for procedural ease, rather than the explicit need to reduce decomposition in the short term.

The solubility of *tert*-butyl **8** was found to be similar to the rest of the series, with crystals suitable for X-ray diffraction analysis grown from a concentrated pentane solution at -30°C . Two independent molecules of compound **8** were shown to crystallise in the unit cell, both exhibiting the *exo*- conformation with similar bond angles and bond lengths. The Pb-C30 bond length is very similar in both molecules, at $2.333(6)$ Å and $2.334(7)$ Å. This bond length is the longest of the type in the series, probably due to the steric bulk of the *tert*-butyl group being directly attached to the metal atom. The Pb-C30 bond is around 0.03 Å longer than the other complexes in the series. The DOP around the metal atom is an average of 83%, which is significantly less than the rest of the compounds in the LPbR series that display the *exo*- conformation.

Table 6 – Bond angles ($^{\circ}$) and bond lengths (\AA) for LPb^tBu (**8**) – both molecules in the crystal structure unit cell; (a) and (b)

	(a)	(b)		(a)	(b)
N1-Pb-C30	102.32(19)	103.1(2)	Pb-C30	2.333(6)	2.334(7)
N2-Pb-C30	104.22(18)	103.1(2)	N1-Pb	2.362(4)	2.352(4)
N1-Pb-N2	79.14(15)	78.76(15)	N2-Pb	2.362(4)	2.364(4)
C1-N1-C6	122.0(5)	122.7(5)	N1-C1	1.326(7)	1.333(7)
C1-N1-Pb	114.8(3)	113.1(4)	C1-C2	1.402(8)	1.409(8)
C6-N1-Pb	118.6(3)	119.5(3)	C2-C3	1.409(8)	1.400(8)
C3-N2-C18	121.6(5)	121.6(5)	C3-N2	1.315(7)	1.332(7)
C3-N2-Pb	114.0(3)	113.8(4)			
C18-N2-Pb	120.9(3)	120.8(3)	Pb – plane	1.383	1.441
N1-C1-C2	124.6(5)	124.3(5)			
C1-C2-C3	129.3(5)	129.5(6)	DOP (%)	82.58	83.38
C2-C3-N2	125.0(5)	123.8(5)			

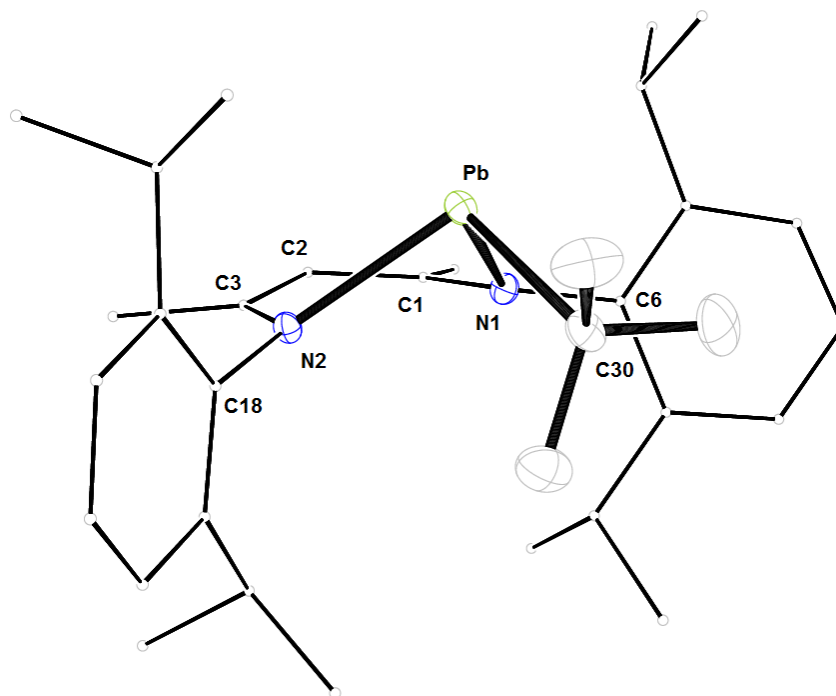


Figure 18 – LPb^tBu (**8**). 30% probability ORTEP ellipsoids, BDI ligand minimised for clarity.

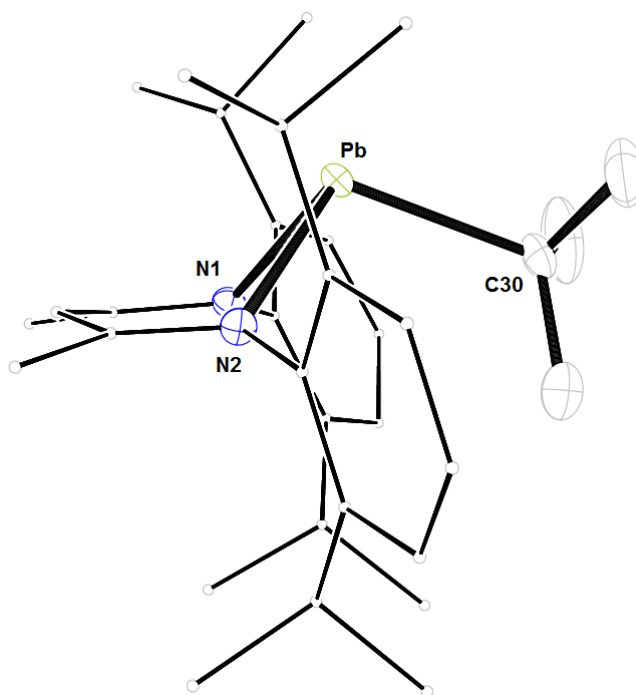


Figure 19 – LPb^tBu (**8**) side-on, showing extent of *exo*- conformation. 30% ORTEP ellipsoids, BDI ligand minimised for clarity.

As the α -carbon is quaternary, there is no signal in the ^1H NMR spectrum to observe $J_{\text{Pb-H}}$ couplings. However, the septets ($J = \sim 6.9$ Hz) and doublets ($J = \sim 6.9$ Hz) are clear and well-defined, demonstrating the asymmetry of the complex. A clear singlet at δ 2.20 is evident for the protons on the *tert*-butyl substituent. A distinct peak at δ 3684 in the $^{207}\text{Pb}\{^1\text{H}\}$ NMR spectrum indicates that the Pb atom in *tert*-butyl **8** is the most deshielded metal atom present in the series.

1.2.7 Synthesis and characterisation of β -diketiminate lead(II) phenyl, LPbPh (**9**)

Lead phenyl **9** was generated by addition of one equivalent of phenylmagnesium bromide to a toluene solution of the precursor chloride **2** at -78°C . After complete addition, the mixture was allowed to warm to room temperature and stirred for two hours. The yellow solution was filtered through Celite®, and phenyl compound **9** was isolated in 25% yield. In common with the rest of the series, lead phenyl **9** is soluble in aliphatic and aromatic hydrocarbon solvents, mostly soluble in halogenated solvents such as dichloromethane, and was observed to decompose in ethereal solvents such as THF. A pentane solution held at -30°C produced crystals suitable for X-ray diffraction

studies. Similar to other complexes in the series, phenyl compound **9** was observed to decompose when held at or above room temperature after 6 to 8 hours, and was also observed to decompose upon prolonged exposure to light. To minimise this, the complex was stored at -30°C in foil-wrapped vials in an inert atmosphere glovebox.

In the same fashion as tert-butyl **8**, phenyl compound **9** crystallises with two independent molecules within the unit cell, but similar to methyl compound **3**, the phenyl complex crystallises in the *endo*- conformation. The Pb-C30 bond distance is similar to those in the rest of the series, at an average of 2.30 Å between the two molecules in the unit cell, although a little shorter (0.02 Å) than methyl **3**, the other *endo*- structure. The DOP is about 9-10 % smaller than that of methyl **3**, indicating a flatter environment around the metal centre. The bond angles are similar to the rest of the series, both *endo*- and *exo*- structures, but with the N1-Pb-N2 angle slightly increased. The substituent aromatic ring in phenyl **9** is placed perpendicular to the C₃N₂ plane.

Table 7 – Bond angles (°) and bond lengths (Å) for LPbPh (**9**) – both molecules in the crystal structure unit cell; (a) and (b)

	(a)	(b)		(a)	(b)
N1-Pb-C30	95.57(12)	93.83(12)	Pb-C30	2.308(4)	2.290(4)
N2-Pb-C30	91.24(12)	91.33(12)	N1-Pb	2.323(3)	2.327(3)
N1-Pb-N2	82.61(10)	83.29(10)	N2-Pb	2.323(3)	2.338(3)
C1-N1-C6	120.5(3)	119.7(3)	N1-C1	1.333(5)	1.332(5)
C1-N1-Pb	125.6(2)	126.7(2)	C1-C2	1.403(5)	1.405(5)
C6-N1-Pb	113.9(2)	112.8(2)	C2-C3	1.406(5)	1.412(5)
C3-N2-C18	121.2(3)	120.1(3)	C3-N2	1.326(4)	1.316(5)
C3-N2-Pb	126.6(2)	126.3(2)			
C18-N2-Pb	112.2(2)	113.4(2)	Pb – plane	0.486	0.229
N1-C1-C2	125.6(3)	125.1(3)			
C1-C2-C3	131.1(3)	131.4(3)	DOP (%)	100.64	101.72
C2-C3-N2	124.6(3)	125.9(3)			

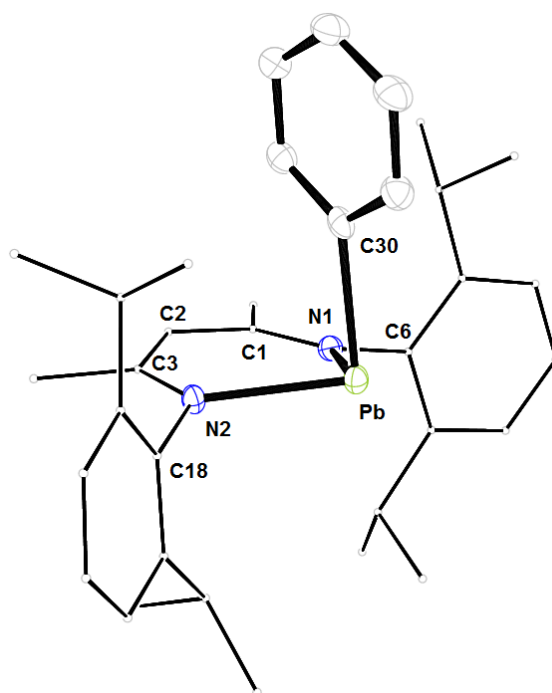


Figure 20 – LPbPh (**9**). 30% probability ORTEP ellipsoids, BDI ligand minimised and H-atoms omitted for clarity.

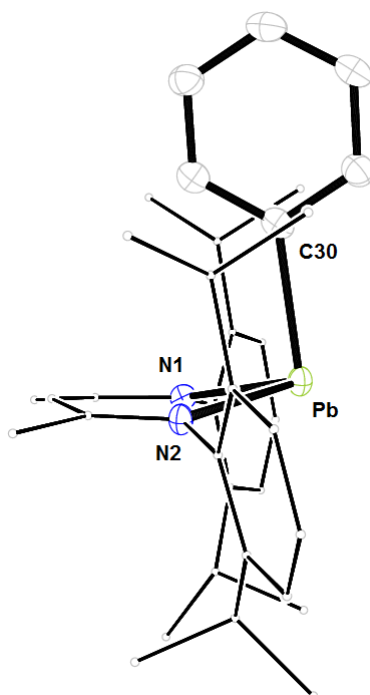


Figure 21 – LPbPh (**9**) side-on, showing extent of *endo*- conformation. 30% ORTEP ellipsoids, BDI ligand minimised and H-atoms omitted for clarity.

Concurrent with our synthesis of this compound, Roesky and co-workers published synthetic and structural details of this complex, synthesised using phenyllithium rather than a Grignard reagent. The unit cell, in addition to the spectroscopic data of our phenyl complex **9** matches with the data reported.⁴⁶

In the ^1H NMR spectrum, the signature septets ($J = \sim 6.9$ Hz) and doublets ($J = \sim 6.8$ Hz) are all distinct and not overlaid with each other. In common with benzyl **7**, the aromatic protons on the substituent can be distinguished. A doublet ($J = 6.9$ Hz) at δ 8.51, a triplet ($J = 7.6$ Hz) at δ 7.58 and a doublet of doublets ($J = 7.0, 2.2$ Hz) at δ 7.04 clearly describe the protons on the phenyl ring. The $^{207}\text{Pb}\{^1\text{H}\}$ NMR signal is observed upfield from the rest of the series at δ 2419. This agrees well with the signal reported by Roesky at δ 2424.⁴⁶

1.3 Hammett correlation studies

UV-visible spectrophotometric studies were carried out at concentrations around 10^{-5} mol l⁻¹ in dry benzene in a quartz cell under a nitrogen atmosphere. The major absorbance occurred between 300-400 nm, with a second, minor absorbance observed at 440-450 nm for some compounds in the series. Molar extinction coefficients were calculated for both major and minor absorbances, and are shown in table 8.

Table 8 – Maximum and secondary absorbencies (nm) and molar extinction coefficients (M⁻¹ cm⁻¹) for compounds **3** to **9**.

Alkyl		λ_{\max} (nm)	ϵ (M ⁻¹ cm ⁻¹)	$\lambda_{\text{secondary}}$ (nm)	ϵ (M ⁻¹ cm ⁻¹)
3	Me (<i>endo</i>)	395.02	6736.4	-	-
4	^t Pr (<i>exo</i>)	331.99	4908.6	448.01	966.27
5	^s Bu (<i>exo</i>)	299.95	3283.3	452.01	37.320
6	Np (<i>exo</i>)	343.07	2390.6	448.92	241.35
7	Bn (<i>exo</i>)	316.04	5382.5	442.94	858.99
8	^t Bu (<i>exo</i>)	374.98	3635.9	-	-
9	Ph (<i>endo</i>)	397.03	6736.4	-	-

The wavelength of maximum absorbance, λ_{\max} , was used to find a correlation across the series of compounds by being plotted against the Hammett constant, σ , for the corresponding alkyl substituent. Hammett constants are numerical values drawn from the Hammett equation in organic chemistry, used as an equivalent to pK_a measures of acidity. Hammett discovered that the change in free energy of activation is proportional to the change in Gibbs free energy for any two reactions with two aromatic reagents, only differing from each other in the type of substituent. Equation 2 describes this, where K and k are equilibrium and rate constants, respectively, for a substituted benzoic acid derivative, and K_0 and k_0 are the same constants for the equivalent compound where the substituent is a hydrogen atom. The parameter σ describes the electron-withdrawing or electron-donating nature of the substituent, and is denoted as σ_{para} and σ_{meta} , depending on the position of the substituent in either the para- or the meta-position respectively. A positive value of σ denotes a group that is electron-withdrawing

with respect to a proton at the substituent position, and increasing positivity indicates increased electron-withdrawing capability of the group. The same is true for negative values of σ , with respect to electron donating ability; the more negative a value for a given substituent is, the higher its electron-donating power.⁵⁵

The parameter ρ measures the sensitivity of the reaction to electronic effects, so therefore depends on the type of reaction being carried out, and is independent of the substituent. A positive ρ value indicates more electrons are present in the transition state or the reaction than in the starting material, whereas a negative ρ indicates fewer electrons are present in the transition state.⁵⁵

$$\log K/K_0 = \sigma.\rho \quad \text{or:} \quad \log k/k_0 = \sigma.\rho \quad (2)$$

Due to the fact that the series of β -diketiminato lead alkyl compounds only differs from one another by the type of alkyl substituent, it was speculated whether a similar correlation, based on the Hammett constants, existed for this series of complexes. This would allow a numerical value to be applied to the otherwise-similar alkyl groups in the series.

Table 9 – *Para*- and *meta*- Hammett constants, σ , for the substituents in the alkyl series of compounds.⁵⁶

Alkyl		σ_{meta}	σ_{para}
3	Me (<i>endo</i>)	-0.07	-0.17
4	^t Pr (<i>exo</i>)	-0.04	-0.15
5	^s Bu (<i>exo</i>)	-0.08	-0.12
6	Np (<i>exo</i>)	-0.05	-0.17
7	Bn (<i>exo</i>)	-0.08	-0.09
8	^t Bu (<i>exo</i>)	-0.10	-0.20
9	Ph (<i>endo</i>)	0.06	-0.01

A graph of the λ_{max} was plotted against the para-position Hammett constants, σ_{para} , shown in table 9. Figure 22 shows a broad trend in that the λ_{max} increases as the

Hammett constant decreases. There are two outlying points, at $\lambda_{\text{max}} > 390$ nm, which correspond to the methyl and phenyl compounds **3** and **9** respectively. These compounds both crystallise in the *endo*- conformation, rather than the rest of the series, which all crystallise in the *exo*- conformation. Although the NMR studies are in solution, computational studies (*vide infra*) show that the crystallised conformation is the most stable for each compound. At this point, it is unknown if the complexes exhibit definitive *endo*- or *exo*- geometries in solution, but for the purposes of this study, they were assumed to, based on the computational evidence. This can explain the position on the graph of the two *endo*- complexes, and they can be ascribed differing absorbance properties to the *exo*- compounds. The point at 316 nm, whilst still contributing to the correlation, is the furthest from the trend line. This point corresponds to benzyl compound **7**, which contains both an aliphatic α -carbon to the metal atom and an aromatic ring as part of the substituent. This appears to make the λ_{max} of the complex deviate slightly from the trendline.

The exact excitation that is causing this absorbance is unknown. Driess and co-workers synthesised a series of germane-, stannane- and plumbanediyls with remarkable electronic structures, and attributed their excitations to either a HOMO – LUMO transition, or a HOMO-1 – LUMO transition.⁵⁷ In order to investigate our transitions, time-dependant DFT (TD-DFT) computational calculations were run (*vide infra*).

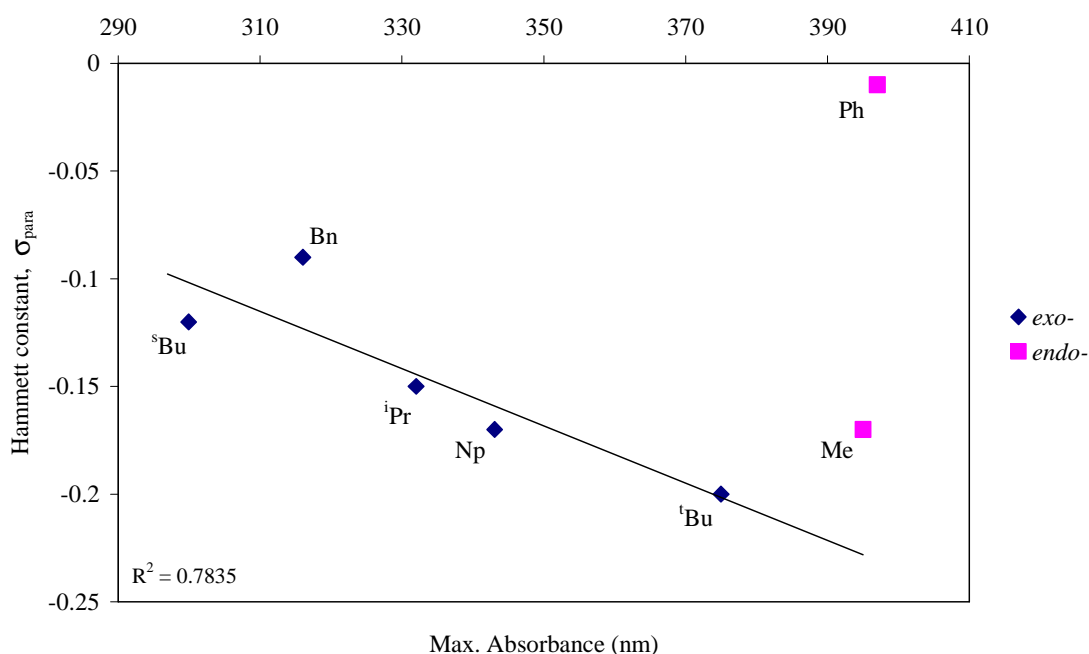


Figure 22 – Correlation graph of Hammett constants, σ_{para} , against λ_{max} (nm).

It was also decided to investigate the correlation between σ_{para} and the ^{207}Pb NMR chemical shift of the complexes, as shown in figure 23. The correlation is shown for the *exo*- configured complexes, with the *endo*- configured methyl and phenyl compounds **3** and **9** discounted. However, although we can observe methyl **3** at δ 3001.7 ppm as an outlying point, phenyl complex **9**, at δ 2419.0 ppm, appears to fit to the correlation. This may be due to these compounds exhibiting the *endo*- conformation, whereas all the others exhibit the *exo*- structure. Methyl compound **3** is also the only complex to have a primary carbon atom bonded to the metal centre; all the other complexes have a larger substituent group, containing other carbon atoms.

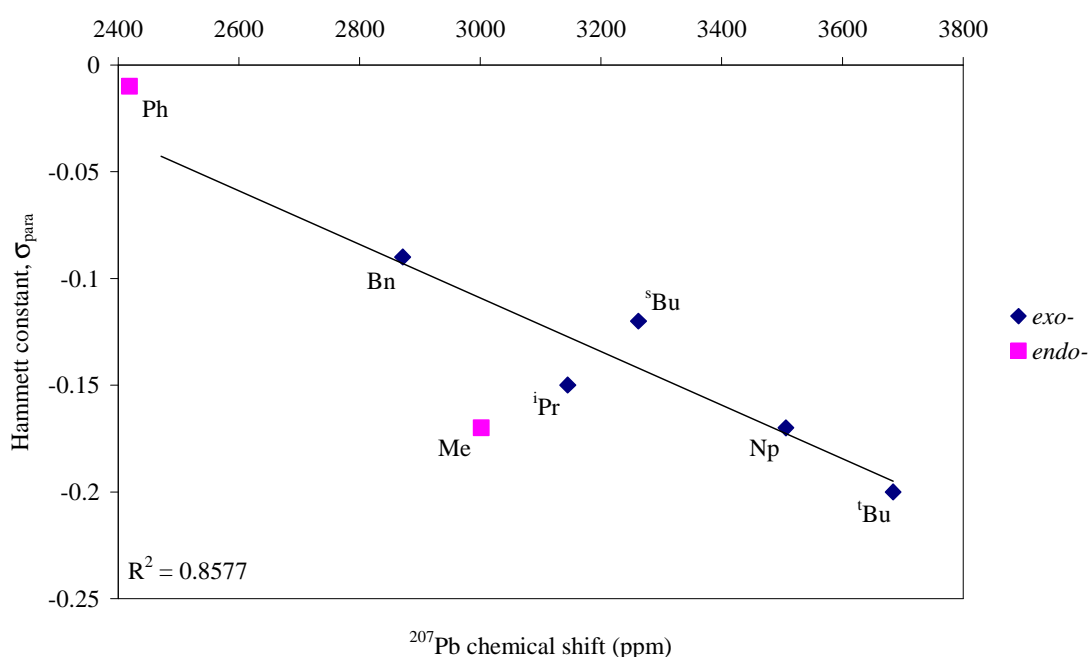


Figure 23 – Correlation graph of Hammett constants, σ_{para} , against ^{207}Pb NMR signal (ppm).

Although the correlations between chemical shift, λ_{max} and the Hammett constant for each substituent are not exact, they do show a broad agreement, indicating some form of relationship between the complexes as the alkyl substituent is changed. However, it should be noted that the trend is opposite to what would be expected, based on conventional understanding of the shielding and deshielding of nuclei. That is, more electron-rich substituents are generally more shielding, and the metal centre to which they are coordinated has a lower chemical shift, although this trend would be specifically influenced by the precise orbitals involved in the shielding process. The

trend that we observe is opposite – the metal centres with the more electron-donating groups appear to be more deshielded, and possess a higher chemical shift. The reasoning for this is unclear, but may be affected by the high percentage of s-orbital character shown by the lone pair within the complexes.

The steric bulk of an alkyl substituent can be described numerically by Dubois' steric parameter, E'_s . The steric effects of various alkyl substituents present in cobalamins was studied by Datta and co-workers, but poor correlations were observed in their studies.⁵⁴ The Dubois parameter was used in place of the Hammett function to generate the graph in figure 24, in order to describe the trend with relation to steric and not electronic effects. However, very little correlation was observed with either the maximum absorbance or the ^{207}Pb NMR signal.

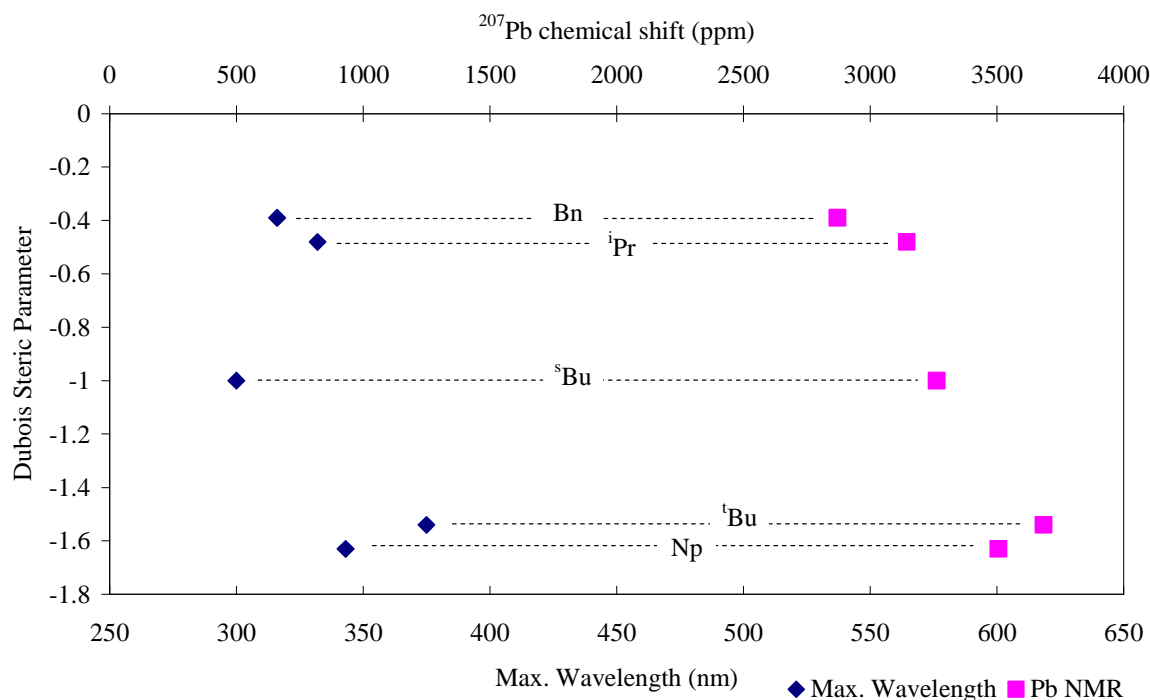


Figure 24 – Combined graph of Dubois Steric Parameters against ^{207}Pb NMR signal (ppm) and λ_{max} (nm). Only *exo*- conformations are shown for clarity.

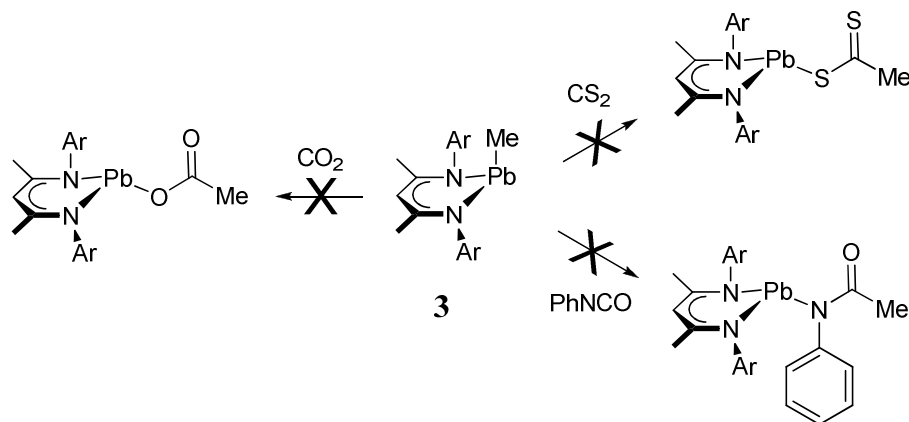
1.4 Reactivity studies

Lead methyl **3** was chosen as the parent compound to perform reactivity studies on, due to its ease of synthesis and the small, more open-to-reaction substituent. A number of test reactions were carried out, where a reagent was added to one equivalent of methyl **3** in an NMR tube, and the reactivity observed by ^1H NMR spectroscopy. Due to the thermal instability of the methyl complex, on heating to higher than 30°C the material within the NMR tube decomposed into a mixture of unidentifiable products and a precipitate of black powder, assumed to be lead(0). As a result, all reactions were carried out at or below room temperature, and no heat was applied to raise the temperature above 30°C .

The affinity of the lead alkyl complexes towards insertion in the M-C30 bond was studied using various heterocumulenes. Carbon dioxide has been shown to insert into the metal-oxygen bond of β -diketiminato lead(II) and tin(II) alkoxides to form metal carbonates.^{38,45} It was decided to test the reaction of the lead (II) alkyls with the addition of CO_2 to attempt the formation of esters.

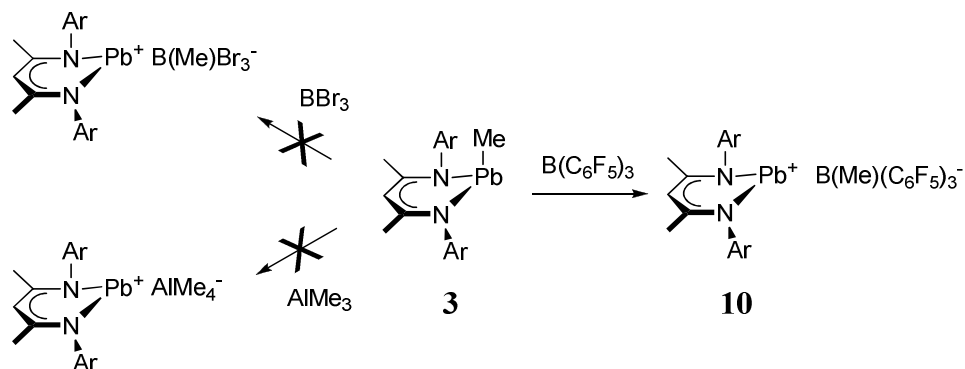
Methyl complex **3** was dissolved in deuterated benzene, and cooled to freezing with dry ice to allow evacuation of the nitrogen atmosphere in the NMR tube before addition of one equivalent of gaseous CO_2 . When this addition failed to produce a reaction, excess CO_2 was added to flood the tube with one atmosphere pressure, with no reaction observed by ^1H NMR spectroscopy. Reactions with carbon disulphide and phenyl isocyanate were also carried out, to attempt synthesis of their respective insertion products. However, in both cases, no reaction was observed. The test reactions were left to react for a few days without heating, to avoid accelerated decomposition. However the reactions were abandoned when the decomposition products made observing any reactivity products difficult.

Scheme 33 – Test reactions, with suggested products, for probing insertion into the Pb-C bond in methyl compound **3** by heterocumulenes. Ar = 2,6-diisopropylphenyl.



Reaction of one equivalent of methyl **3** with tribromoborane resulted in immediate formation of a thick, insoluble cream-coloured substance that was unable to be identified. *Tris*-pentafluorophenylborane was added to methyl **3** at room temperature, resulting in a vivid colour change from lemon yellow to orange-red, and produced a very clean conversion to a borate salt of a lead cation **10**, studied later in greater detail in chapter 2 (*vide infra*). Extending this methodology, a reaction was carried out between methyl **3** and trimethyl aluminium, to try and generate an aluminium analogue of the borate salt **10**. However, no reaction was observed until decomposition of the methyl compound began after a few days at room temperature.

Scheme 34 – Test reactions for probing abstraction of the terminal methyl group from the lead centre in methyl **3**, resulting in the synthesis of methyl borate **10**. Ar = 2,6-diisopropylphenyl.



Reactions of methyl **3** with phenyl acetylene, methyl iodide and 2,6-*tert*-butyl-4-methylphenol to investigate substitution of the alkyl substituent produced no reaction before decomposition of the methyl compound was observed. The addition of methyl triflate to lead methyl **3** resulted in an immediate precipitation of black material, assumed to be Pb(0). The ^1H NMR spectrum showed a complex mixture of inseparable products, as well as the presence of reprotonated ligand **1**.

A test reaction of methyl **3** with benzaldehyde, to investigate nucleophilic attack on the carbonyl group by the metal alkyl was carried out, however, no change was observed in the ^1H NMR until natural thermal decomposition of the methyl compound began.

An effort was made to deprotonate methyl **3**, by reacting with one equivalent of methyllithium to generate methane and a lithium salt of the complex. The aim was to either deprotonate the terminal methyl substituent to form a double bond to the lead atom, or deprotonate at the backbone proton, assuming that it was sufficiently acidic enough to undergo deprotonation. However, upon reaction, large amounts of black material were quickly deposited, assumed to be Pb(0). Study of the resultant mixture of products in the ^1H NMR spectra revealed the presence of the lithium salt of β -diketimine ligand **1**, as well as an array of unidentifiable side-products.

1.5 Computational studies

Computational calculations were carried out on all the lead alkyl complexes using Gaussian G03W and Gaussview v4.1. Calculations were performed on all lead alkyl structures using the B3LYP function with the LANL2DZ basis set, in addition to a second set of calculations using the 6-31G* basis set (with LANL2DZ still used on the lead atom, due to the large number of electrons present on the metal). The calculations were carried out using the crystal structure as a starting point where possible, and optimisation/frequency calculations were carried out to determine optimum geometries and molecular orbital shapes and energies. As the calculations show these molecules in the gas phase, comparisons were able to be made between the optimised structure and the solid-state information gained from the crystal structure. Additional calculations of the opposite geometry (*endo*- or *exo*-) to that from the crystal structure were also run, using both the single and mixed basis sets. Some complexes showed conversion from one conformation to the other, indicating the crystal structure was more likely a global minimum, and some did not convert, indicating only local minima. Only three compounds showed a minimum for both *endo*- and *exo*- conformations. For those that did not convert, the conformation shown in the crystal structure was always the lower energy conformation.

In addition to geometry optimisations, the calculations were also performed to obtain the energy levels associated with the highest-occupied, lowest-unoccupied and lone pair (HOMO, LUMO and LP respectively) molecular orbitals. The orbital assigned to the LP was also noted, as was the dipole moment of the optimised molecule, measured in Debyes, a measure of charge along the displacement vector separating the areas of charge within the molecule.

Data tables can be found in appendix 1 (bond lengths, bond angles and molecular orbital energy levels).

1.5.1 Discussion of geometry optimisations

β -diketiminate lead (II) methyl, LPbMe, 3

From the results of both the single (LANL2DZ only) and mixed (6-31G* and LANL2DZ) basis set optimisation calculations, there can be seen to be a symmetrical environment around the lead centre in the *endo*- conformations of lead methyl **3**, with both N-Pb-C30 angles and both N-Pb bond lengths identical to each other. The N-Pb-C30 angles compare favourably with the corresponding angles found in the solid state, although they are not identical. This can be attributed to crystal packing effects in the solid state, versus the gas phase that is considered in the calculations. The *exo*- conformation shows a very slight deviation between the two N-Pb-C30 angles ($\sim 0.09^\circ$), although this conformation is not displayed in the solid state. However, due to the position of the alkyl substituent relative to the ligand in the *exo*-calculation, the N-Pb-C30 angles are around 5° larger than in the *endo*- version. The bond distances calculated from both the single and mixed basis set calculations are comparable to each other, with the Pb-C30 distances in the *endo*- calculations found to be slightly longer ($\sim 0.1 \text{ \AA}$) than those from the *exo*- calculations. The corresponding Pb-C30 bond length found from the solid state structure is around $0.3\text{-}0.4 \text{ \AA}$ longer than that calculated. The DOP found for the *endo*- structures is larger than that found for the *exo*- structures by 10-12%, but is 8-9% smaller than the DOP of the metal centre in the solid state. The distance of the metal atom from the C_3N_2 plane in the *endo*- structures is slightly smaller than that in the solid state ($\sim 0.14 \text{ \AA}$), whereas the corresponding distance in the *exo*-calculations is slightly larger ($\sim 0.6 \text{ \AA}$).

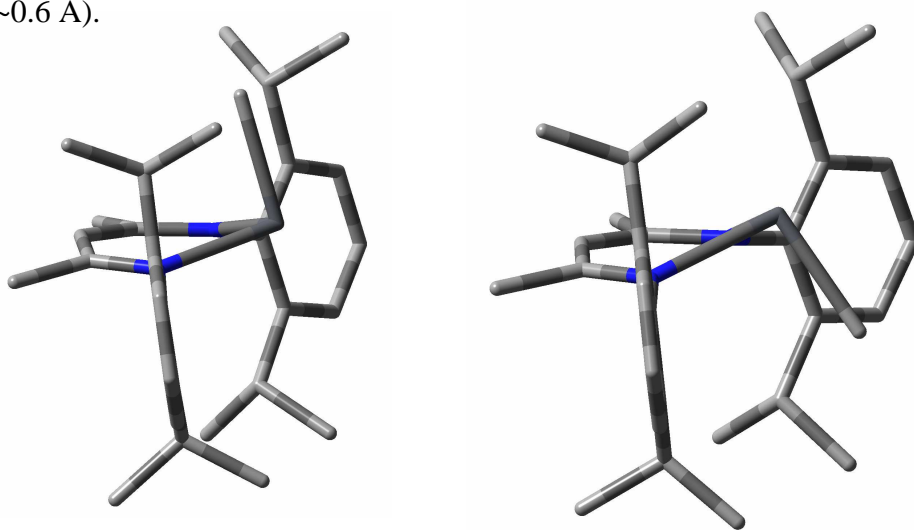


Figure 25 – Optimised *endo*- (left) and *exo*- (right) geometries for LPbMe **3**.

β -diketiminato lead (II) iso-propyl, LPbⁱPr, 4

A symmetrical environment around the lead atom is evident in both the *exo*-calculations on lead iso-propyl **4**, although the calculated N-Pb-C30 angles are slightly larger than those shown from the solid state ($\sim 2\text{-}3^\circ$ larger in the single basis set calculation, and $\sim 1\text{-}2^\circ$ larger in the mixed basis set calculation). The calculated DOP of the metal centre is 5-7% smaller in the *exo*- calculations than in the *endo*- calculations for the iso-propyl **4**. Although the calculated DOP in the *exo*- structures is much smaller than that in the solid state, the distance of the lead atom to the C_3N_2 plane is only slightly smaller ($0.1\text{-}0.2\text{ \AA}$) than that shown in the solid state. The Pb-C30 bond lengths calculated in the iso-propyl **4** calculations do not differ greatly from the bond length in the solid state, with all Pb-C30 distances lying around 2.3 \AA . In accordance with the crystal structure, the *exo*- calculations show the iso-propyl substituent lies perpendicular to the Pb-C30 bond, with the terminal carbon atoms pointing away from the C_3N_2 backbone. In contrast, however, both *endo*- calculations have the iso-propyl group rotated along to the Pb-C30 bond (figure 26). As a result of this, one N-Pb-C30 angle is around 9° larger than the other N-Pb-C30 angle in both *endo*- calculations. The Pb-C30 bond distances calculated in the *endo*- calculations are around 0.02 \AA longer than the distances in the *exo*- calculations, possibly due to steric repulsion between the iso-propyl group on the metal atom and the iso-propyl substituents on the aromatic rings of the ligand, forcing the slight lengthening of the Pb-C30 bond.

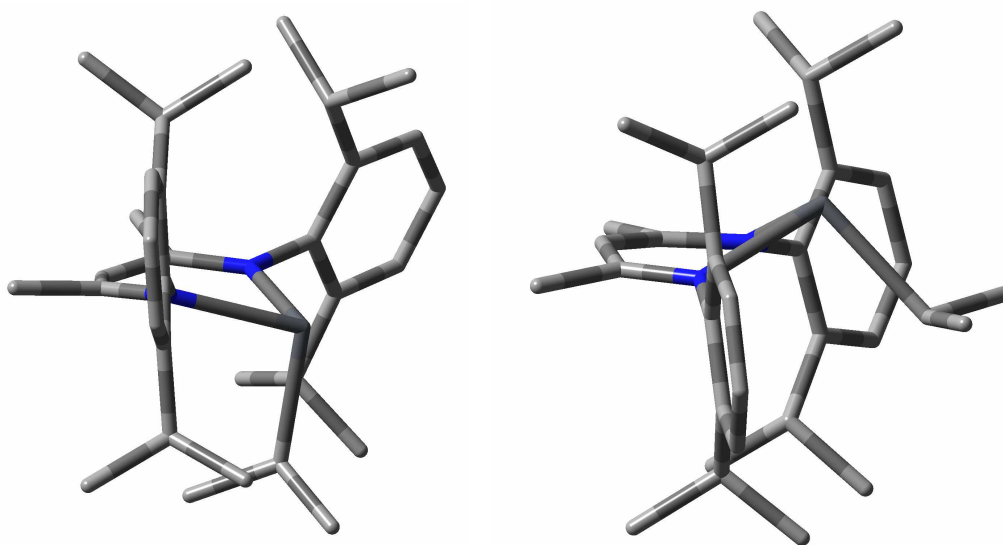


Figure 26 – Optimised *endo*- (left) and *exo*- (right) geometries for LPbⁱPr **4**.

β -diketiminate lead (II) sec-butyl, LPb^sBu, 5

Lead sec-butyl **5** has a chiral alkyl substituent on the lead centre, which leads to an unsymmetrical environment around the metal atom in all calculations, with N-Pb-C30 angles that are slightly larger ($\sim 2\text{--}3^\circ$) than the angles shown in the solid state. The calculated DOP of the metal centre in the *exo*- calculations is around 10-11 % smaller than that found in the solid state, but the calculated distance between the lead atom and the C₃N₂ plane is only slightly shorter (~ 0.2 Å). The Pb-C30 bond distances derived by the calculations are within ~ 0.04 Å of one another, with the bond distance in the solid state lying on the bottom edge of this range, at 2.306(5) Å. In common with iso-propyl **4**, the *endo*- calculation for sec-butyl **5** rotates the substituent around the Pb-C30 bond, to avoid steric clashing with the iso-propyl groups on the aromatic rings of the BDI ligand. As a result of this, the difference in the N-Pb-C30 angles in the *exo*- calculations are much smaller ($\sim 0.5^\circ$) than in the *endo*- calculations ($\sim 8\text{--}9^\circ$). The solid state structure shows a slightly unsymmetrical metal centre environment, in agreement with the related *exo*-calculations, rather than a more extreme unsymmetrical environment, indicated by the *endo*- calculations.

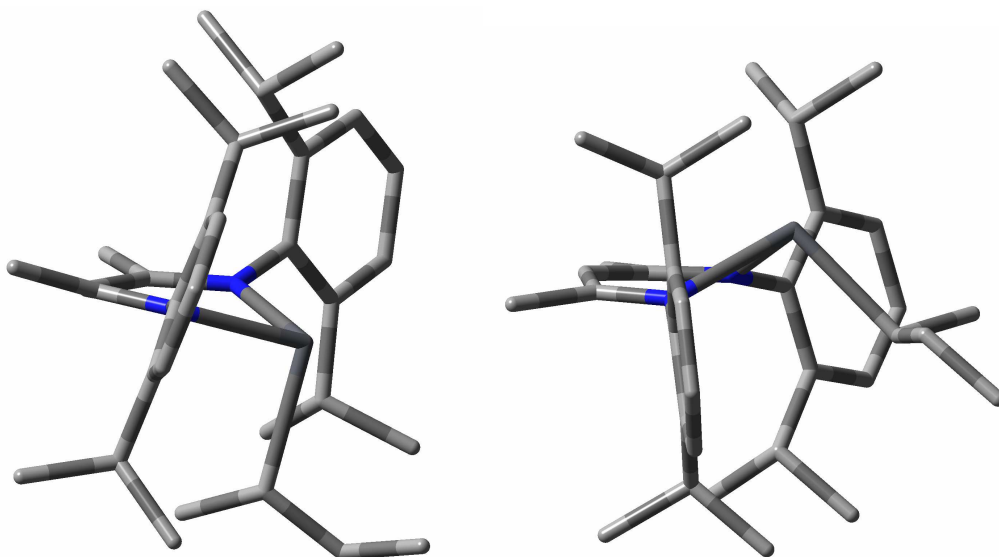


Figure 27 – Optimised *endo*- (left) and *exo*- (right) geometries for LPb^sBu **5**.

β -diketiminate lead (II) neo-pentyl, LPbNp, 6

Lead neo-pentyl **6** converts from the *endo*- conformation during the course of a calculation, to produce a structure in the same conformation as that found in the solid state. As such, only comparisons between the mixed and single basis set calculations with the crystal structure were carried out. Neo-pentyl **6** exhibits the *exo*- conformation upon completion of the calculations, with a non-symmetric environment around the metal centre. The single basis set calculation shows a difference in the N-Pb-C30 bond angles of $\sim 0.4^\circ$, much smaller than the $\sim 2^\circ$ difference shown in the mixed set calculation. However, these degrees of asymmetry are still smaller than that shown in the solid state, with a difference in bond angles of $\sim 6.5^\circ$. The DOP calculated in the mixed set calculation is around 2 % larger than that in the single set calculation, but still far smaller ($\sim 7\%$) than the DOP evident in the solid state. Similarly, both calculations display a shorter distance between the lead atom and the C_3N_2 plane (~ 0.10 - 0.16 Å) than that shown in the solid-state structure, with the single basis set calculation giving a shorter distance (~ 0.06 Å) than the mixed set calculation.

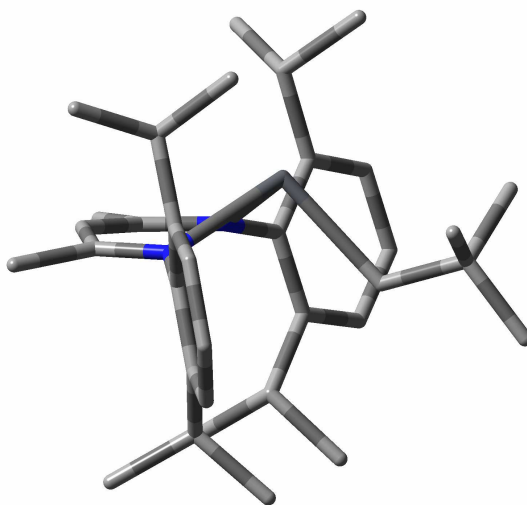


Figure 28 – Optimised *exo*- geometry for LPbNp **6**.

 β -diketiminate lead (II) benzyl, LPbBn, 7

In common with neo-pentyl **6**, any attempt to run a calculation in the *endo*- conformation for lead benzyl **7** resulted in the conversion to the *exo*- geometry, attributed to the bulk of the substituent on the metal centre. Lead benzyl **7** contains an

aromatic ring as part of the alkyl substituent, as well as an aliphatic CH₂ unit α - to the lead metal atom. The solid state structure shows a symmetric environment around the metal centre, with both N-Pb-C30 angles the same. This is not the case in either of the computational calculations, which both show a very slight deviation from symmetry. The single basis set calculation shows a smaller deviation ($\sim 0.11^\circ$) than the mixed set calculation ($\sim 0.29^\circ$) in the N-Pb-C30 angles. Both calculations also give larger values ($\sim 4.2^\circ$) than those angles found in the crystal structure. The DOP evident in the crystal structure is much larger than that found in both the single set ($\sim 12.3\%$) and the mixed set ($\sim 11.2\%$) calculations. This is likely due to the arrangement in space of the aromatic ring in the benzyl group, which is situated in the same plane as the backbone, perpendicular to the aromatic rings on the BDI ligand. Calculations begun from a conformation where the benzyl ring was perpendicular to the backbone showed a rotation along the C30-C31 bond as the calculation proceeded, to bring the ring into the position observed in the solid state (figure 29). The arrangement of the aromatic ring in the solid state also acts to move the metal atom further from the C₃N₂ plane than is evident in the gas phase, with the single basis set calculation giving a distance $\sim 0.28\text{ \AA}$ shorter, and the mixed set giving a distance $\sim 0.21\text{ \AA}$ shorter than the solid-state distance. This smaller distance between the lead atom and the C₃N₂ plane in either calculation does not affect the Pb-C30 bond length, as the calculated length is in agreement with that found in the solid state.

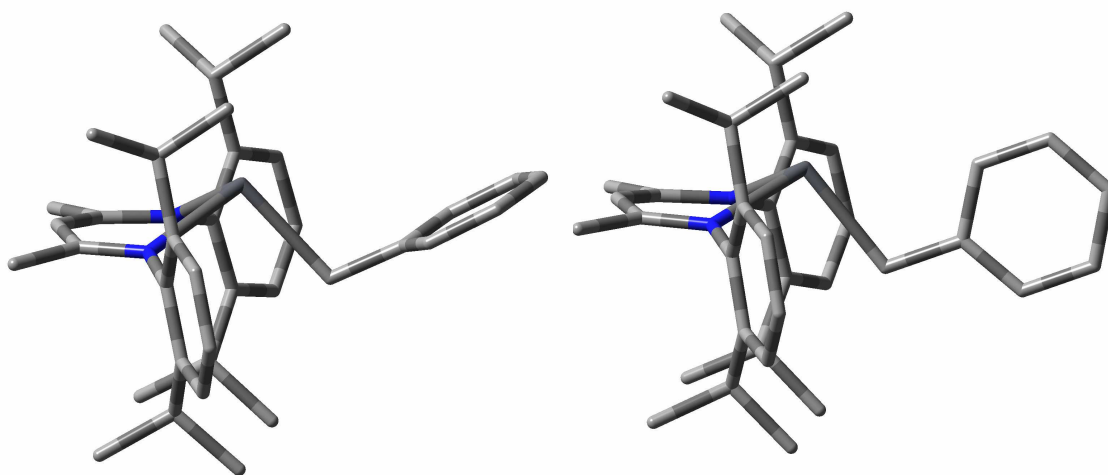


Figure 29 – Optimised *exo*- geometry for LPbBn **7** (left) and alternate starting geometry (right).

β -diketiminato lead (II) tert-butyl, LPb^tBu, 8

The results of the calculations of lead tert-butyl **8** show a small deviation in symmetry around the metal centre, with a difference of $\sim 0.4^\circ$ for the N-Pb-C30 angles. This is in between the differences in the corresponding angles in the two different molecular units found in the unit cell of the crystal structure, where one molecule has equal N-Pb-C30 angles, and the other has a difference in angles of $\sim 1.9^\circ$. The angles found in the solid state structure are slightly smaller than those found by calculation ($\sim 2^\circ$). The DOP of the metal centre in the calculations is ~ 7 -8 % sharper than that in the crystal structure, showing the effects of crystal packing on the molecules in the unit cell. The effect of being in the solid state also pushes the metal atom further from the C₃N₂ plane. However, this effect does not affect the Pb-C30 bond distance, with both calculations giving a bond length in agreement with both molecules in the unit cell.

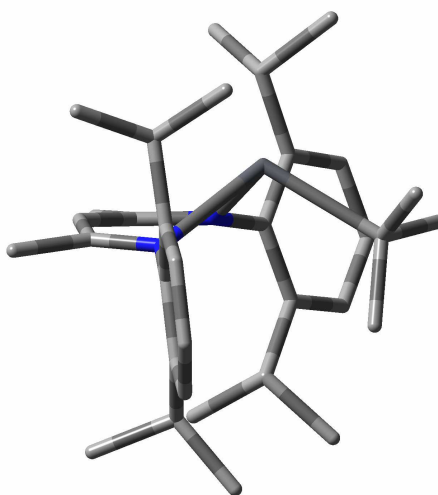


Figure 30 – Optimised *exo*- geometry for LPb^tBu **8**.

β -diketiminato lead (II) phenyl, LPbPh, 9

Similar to tert-butyl **8**, lead phenyl **9** crystallises with two molecules in the unit cell. Both of these molecules show a much less symmetrical environment around the metal centre than that found in either calculation, with the single basis set showing a difference in N-Pb-C30 angles of $\sim 0.25^\circ$, and the corresponding angles in the mixed set calculation almost identical to one another. This is in contrast to the solid state structure, which shows a larger difference in angles ($> 2.5^\circ$), showing that the symmetry around

the metal atom decreases as the molecule moves from the gaseous phase into the solid phase, to be influenced by crystal packing effects. The DOP calculated from the solid state structure shows a flatter environment ($\sim 6\%$) than those calculated in the gas phase. The mixed basis set calculation reveals a very slightly sharper DOP than that found from the single set calculation, but the agreement is still very good, showing the structural effect of packing the molecule into the solid state. However, both calculations show a distance between the lead atom and the C_3N_2 plane only in agreement with molecule (**a**) in the unit cell. The Pb-C30 bond distance is almost identical to that found in the solid state structure, with a difference from the calculations of ~ 0.02 Å. In common with lead benzyl **7**, calculations were begun from a conformation where the phenyl ring was at 90° to that found in the solid state. A rotation along the Pb-C30 bond was observed, to bring the ring into the position perpendicular to the backbone, as observed in both the optimised structure and the solid state (figure 31).

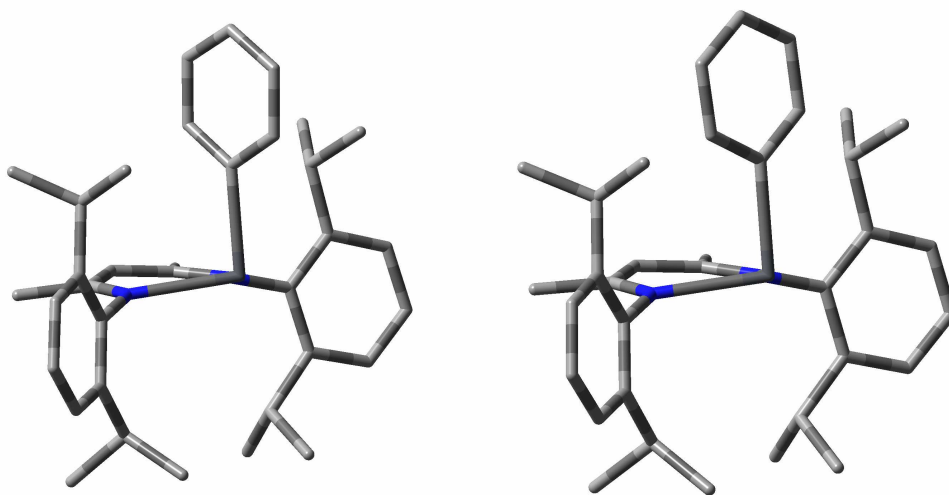
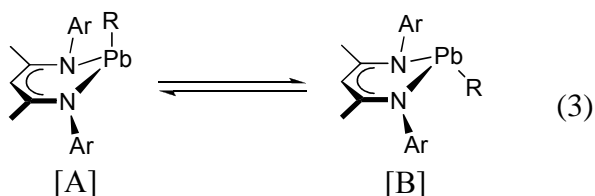


Figure 31 – Optimised *endo*- geometry for LPbPh **9** (left) and alternate starting geometry (right), with a 90° difference in orientation of the phenyl group.

1.5.2 Conformational stability; *endo*- vs. *exo*-

Computational calculations provided three energy readings that were used to help explain the stability of the *endo*- and *exo*- conformations found in the solid state. E, the sum of the electronic and zero-point energies in the molecule, H, the sum of the electronic and thermal enthalpies, and G, the sum of the electronic and thermal free

energies within the molecule give very large numerical values for each calculation, as they are a sum of all the appropriate energies within the molecule. The most practical use for these, therefore, is to find the difference between them for the change in stability between the *endo*- and *exo*- conformations of each of the structures. This can assist in the understanding as to why one form dominates over the other in the solid state.



[A]: R = Me, Ph. [B]: R = ⁱPr, ^sBu, Np, Bn, ^tBu.

Ar = 2,6-diisopropylphenyl.

When using the single basis set to study lead methyl **3**, the *endo*- structure is lower in electronic energy (ΔE), enthalpy (ΔH) and free energy (ΔG) than the *exo*- counterparts. These lower-energy readings are in agreement with the dominance of the *endo*- form in the solid state. Similarly, in the mixed basis set calculations, the *endo*- form is lower in ΔE and ΔH , but is higher in terms of ΔG . This on its own does not negate the support for the *endo*- over the *exo*- conformation, but instead demonstrates that no computational model is a perfect analogue of what can be observed experimentally. The negative ΔG is also explained by the fact that the stabilisation energy is very small, and so, even a small deviation in the calculation can produce an anomalous result; it is small enough not to be hailed as important.

Table 10 – Energy differences between calculations for lead methyl **3**. Values are the stability of *endo*- vs. *exo*- conformations.

Basis set	ΔE (kcal mol ⁻¹)	ΔH (kcal mol ⁻¹)	ΔG (kcal mol ⁻¹)	ΔS (cal K ⁻¹ mol ⁻¹)
Single	1.42	1.52	1.04	1.61
Mixed	1.26	2.00	-1.38	11.3

In both the single and mixed basis set calculations, the stabilisation energies for lead *iso*-propyl **4** are slightly larger than those for lead methyl **3**, but all indicate that the *exo*-

conformation is 2-3 kcal mol⁻¹ more stable than the *endo*- conformation. The single set calculation shows a very slightly greater stability, but only of the order of ~ 0.5 kcal mol⁻¹.

Table 11 – Energy differences between calculations for lead *iso*-propyl **4**. Values are the stability of *endo*- vs. *exo*- conformations.

Basis set	ΔE (kcal mol ⁻¹)	ΔH (kcal mol ⁻¹)	ΔG (kcal mol ⁻¹)	ΔS (cal K ⁻¹ mol ⁻¹)
Single	-2.61	-2.35	-3.73	4.61
Mixed	-2.31	-2.19	-3.04	2.88

Similar to lead *iso*-propyl **4**, the *exo*- conformation of lead *sec*-butyl **5** is shown to have lower energy values than its *endo*- counterpart in both types of calculation, showing the preference for the conformation observed in the solid state. The ΔG value for the mixed basis set calculation is slightly smaller than that within the single set calculation. However, the energy readings in the mixed set calculation still portray the lower energy conformation to be that which is observed in the solid state.

Table 12 – Energy differences between calculations for lead *sec*-butyl **5**. Values are the stability of *endo*- vs. *exo*- conformations.

Basis set	ΔE (kcal mol ⁻¹)	ΔH (kcal mol ⁻¹)	ΔG (kcal mol ⁻¹)	ΔS (cal K ⁻¹ mol ⁻¹)
Single	-2.36	-2.05	-3.89	6.19
Mixed	-2.49	-3.31	-0.67	-8.85

The computational calculations give insight into the preference of a molecule for either the *endo*- or the *exo*- conformation. A large part of the preference seems to be the steric bulk and shape of the substituent on the lead centre. Small substituents that can fit within the space between the aryl rings on the BDI ligand appear to adopt the *endo*- conformation, whereas bulkier substituents are pushed away from the coordination site in the *exo*- conformation. This is supported by calculations that begin from an

environment deliberately containing increased steric crowding, which exhibit a reversion to a less-sterically-crowded environment.

1.5.3 NBO analysis and natural electron configuration

The natural electron configuration of the lead atom always showed around two electrons in the $6s$ orbital and around one electron in the $6p$ orbitals for all complexes, which indicates a covalent bond to the substituent from the $6p$ shell. From the Natural Bond Orbital (NBO) analysis, the occupancy and the s - and p -orbital contributions to the lone pair could be determined. These were compared to the data from the parent chloride compound **2**. In all cases, the lone pair of chloride **2** was seen to have a greater s -character (91.79%) than the corresponding orbital in any of the lead alkyl complexes.⁴³ Comparisons were made between the lead chloride **2** and the alkyl complexes using the single basis set calculation, as calculations were performed using only LANL2DZ on chloride **2** in previous literature.⁴³

In common with the lead chloride **2**, lead methyl **3** has a large percentage of s -character to its lone pair orbital. In the *endo*- calculations, the single basis set describes the lone pair as being 87.14% s -character, with the remainder of the contributions coming from the p -orbitals. The lone pair in *iso*-propyl **4** shows an s -orbital contribution to the lone pair of 87.86%, and *sec*-butyl **5** contains an s -orbital contribution of 87.72%. These values show that, although the conformation and substituent have changed from methyl **3** to *iso*-propyl **4** to *sec*-butyl **5**, this has little effect upon the contribution to the lone pair orbital. This pattern of very little change is continued in *neo*-pentyl **6**, where the contribution to the lone pair by the s -orbital is 87.78%. Benzyl **7** and *tert*-butyl **8** show a slightly higher contribution of 88.74% and 88.17% respectively, but this extra contribution is still small. The s -orbital contribution in phenyl **9** returns to the ~ 87% mark, at 87.07%, with the remaining contribution to the lone pair orbital originating from the corresponding p -orbitals.

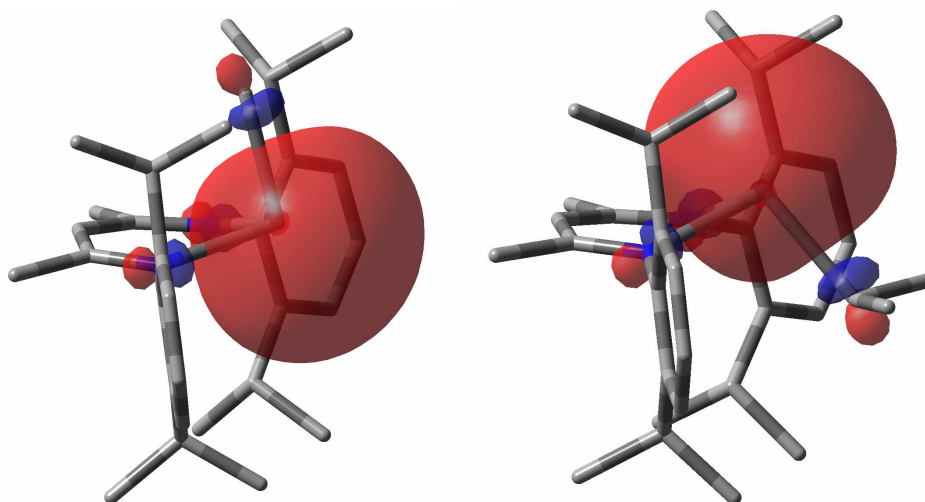


Figure 32 – View of the lead-centred lone pair on an *endo*-conformer (LPbMe **3**; left) and an *exo*-conformer (LPbⁱPr, **4**; right).

The same pattern is evident in the mixed set calculations, where the *s*-orbital contribution to the lone pair does not change very much throughout the series. However, it is worth noting that the *s*-orbital contributions in the mixed set calculations are around 1-2% higher than those in the single set calculations, with values around 88-89%. In common with the single set calculations, benzyl **7** and *tert*-butyl **8** show *s*-orbital contributions slightly higher than the rest of the series. Tables 13 and 14 show the NBO analyses for the Pb centre, from both the single basis set and mixed basis set calculations.

Table 13 – NBO analysis of Pb metal centre for the lead alkyl complexes. Basis set: LANL2DZ over all atoms.

Compound	Natural electron configuration (Pb)	Lone pair NBO on Pb	Lone pair occupancy
LPbMe (3) <i>endo</i>	6s (1.78), 6p (0.99)	s[87.14%] p 0.15 [12.86%]	1.980
LPbMe (3) <i>exo</i>	6s (1.77), 6p (0.97)	s[87.12%] p 0.15 (12.88%)	1.973
LPb ⁱ Pr (4) <i>endo</i>	6s (1.78), 6p (0.98)	s[87.29%] p 0.15 [12.71%]	1.975
LPb ⁱ Pr (4) <i>exo</i>	6s (1.78), 6p (0.95), 7p (0.01)	s[87.86%] p 0.14 [12.14%]	1.971
LPb ^s Bu (5) <i>endo</i>	6s (1.79), 6p (0.97)	s[87.65%] p 0.14 [12.35%]	1.975
LPb ^s Bu (5) <i>exo</i>	6s (1.78), 6p (0.94), 7p (0.01)	s[87.72%] p 0.14 [12.28%]	1.970
LPbNp (6)	6s (1.78), 6p (0.95), 7p (0.01)	s[87.78%] p 0.14 [12.22%]	1.970
LPbBn (7)	6s (1.80), 6p (0.89)	s[88.74%] p 0.13 [11.26%]	1.973
LPb ^t Bu (8)	6s (1.79), 6p (0.92), 7p (0.01)	s[88.19%] p 0.13 [11.81%]	1.964
LPbPh (9)	6s (1.77), 6p (0.95)	s[87.07%] p 0.15 [12.93%]	1.974

Table 14 – NBO analysis of Pb metal centre for the lead alkyl complexes. Basis sets: LANL2DZ on Pb; 6-31G* on N, C and H atoms.

Compound	Natural electron configuration (Pb)	Lone pair NBO on Pb	Lone pair occupancy
LPbMe (3) <i>endo</i>	6s (1.81), 6p (1.01)	s[88.66%] p 0.13 [11.34%]	1.987
LPbMe (3) <i>exo</i>	6s (1.81), 6p (0.99)	s[88.80%] p 0.13 [11.20%]	1.979
LPb ⁱ Pr (4) <i>endo</i>	6s (1.82), 6p (1.00)	s[89.37%] p 0.12 [10.63%]	1.985
LPb ⁱ Pr (4) <i>exo</i>	6s (1.82), 6p (0.97)	s[89.79%] p 0.11 [10.21%]	1.978
LPb ^s Bu (5) <i>endo</i>	6s (1.82), 6p (1.00)	s[89.48%] p 0.12 [10.52%]	1.984
LPb ^s Bu (5) <i>exo</i>	6s (1.82), 6p (0.96), 7p (0.01)	s[89.58%] p 0.12 [10.42%]	1.978
LPbNp (6)	6s (1.82), 6p (0.97)	s[89.55%] p 0.12 [10.45%]	1.977
LPbBn (7)	6s (1.83), 6p (0.92), 7p (0.01)	s[90.23%] p 0.11 [9.77%]	1.979
LPb ^t Bu (8)	6s (1.83), 6p (0.95), 7p (0.01)	s[90.21%] p 0.11 [9.79%]	1.976
LPbPh (9)	6s (1.81), 6p (0.98)	s[88.89%] p 0.12 [11.11%]	1.984

When considering the frontier molecular orbitals of the complexes, the Lowest Unoccupied Molecular Orbital (LUMO) of the lead methyl complex **3** displays a dumbbell-shape of an empty *p*-orbital on the metal centre (Figure 33), and so would suggest affinity for reaction with nucleophiles. However, the orbital is arranged at right angles to the Pb-C30 bond; pointing towards the aryl groups on the BDI ligand, and it is possible that these groups act to sterically prohibit attack at the metal centre. The Highest Occupied Molecular Orbital (HOMO) on the methyl complex **3** (also shown in

figure 33) is the lone pair on one of the nitrogen atoms in the C_3N_2Pb ring of the complex, and is most likely shielded from reaction with electrophiles in much the same way as the LUMO; the close proximity to the bulky aryl groups of the BDI ligand.

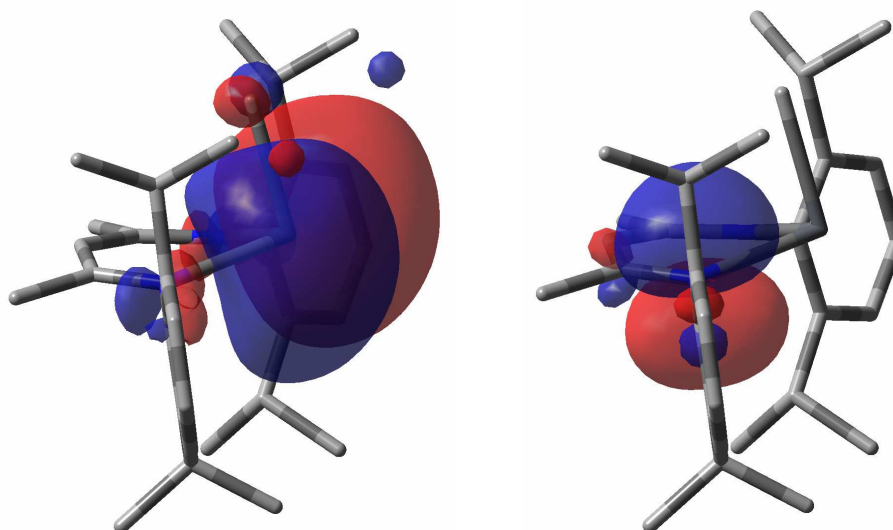


Figure 33 – View of the LUMO (left) and HOMO (right) of the lead methyl complex **3**.

These orbitals are also present as the LUMO and HOMO respectively in most of the other complexes in the β -diketiminate lead alkyl series. The LUMO and HOMO orbitals of *neo*-pentyl **6**, benzyl **7**, *tert*-butyl **8** and phenyl **9** all agree with the same orbital shapes as contained within lead methyl **3**.

In the case of the lead *iso*-propyl complex **4**, the LUMO and HOMO of the complex are not the same orbitals as found in methyl **3**. Instead, the LUMO of *iso*-propyl complex **4** is now an empty *p*-orbital on one of the carbon atoms on the C_3N_2 backbone of the BDI ligand (Figure 34), and the HOMO is now centred on the α -carbon of the *iso*-propyl terminal substituent (also shown in figure 34). However, it is worth noting that the LUMO+1 and HOMO-1 orbitals of lead *iso*-propyl **4** are of the same nature as the LUMO and HOMO of lead methyl **3**, respectively. That is, the LUMO+1 orbital of lead *iso*-propyl **4** is an empty *p*-orbital on the metal centre, and the HOMO-1 is the lone pair of one of the nitrogen atoms in the BDI ligand. In addition to the LUMO+1 orbital of *iso*-propyl **4**, the LUMO+1 orbital of lead *sec*-butyl **5** also displays the same shape as an empty *p*-orbital on the metal centre, although the HOMO orbital agrees with the rest of the series, and is shown as a lone pair on a nitrogen atom.

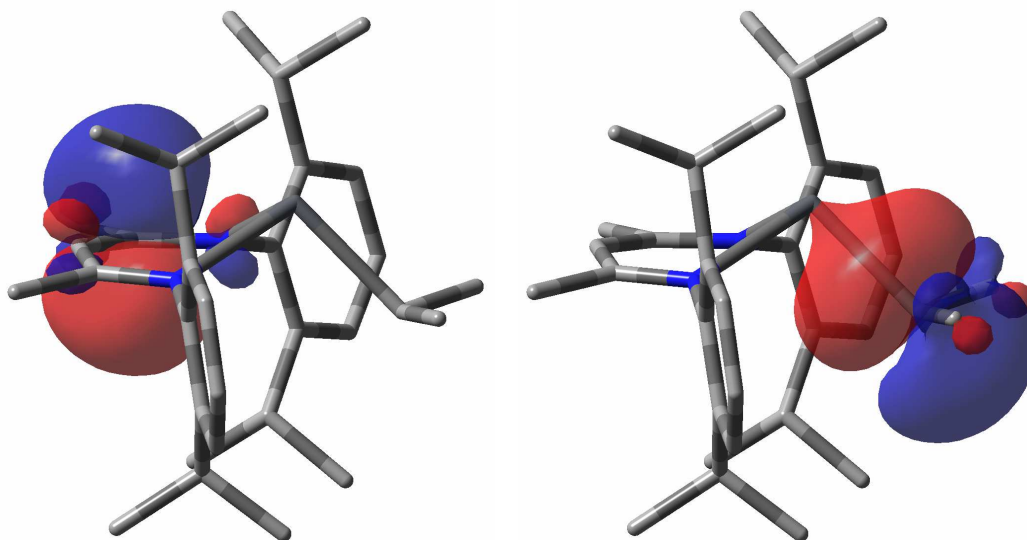


Figure 34 - View of the LUMO (left) and HOMO (right) of the lead *iso*-propyl complex **4**. The LUMO+1 and HOMO-1 appear as the orbitals in figure 33.

1.5.4 Dipole moments

For lead methyl **3**, the single basis set calculations produce an optimised structure with a slightly larger dipole moment (0.3-0.5 Db) than the structure produced from the mixed set calculations, with both *endo*-calculations producing structures with smaller dipole moments (~0.35 Db) than the corresponding *exo*- structures. The opposite is true for *iso*-propyl **4**. Although the structures produced by the single basis set calculations show a higher dipole moment (~0.29 Db) than the structures from the mixed set calculations, in this case both *endo*- structures show a very slightly larger dipole (~0.05 Db) than the corresponding *exo*- structures. The single set calculations for *sec*-butyl **5** reveal a slightly higher dipole moment (~0.28 Db) than in the mixed set calculations, however, in this case there is very little spread between conformations. The single set *endo*-calculation and the mixed set *exo*- calculation give very slightly higher dipole moments, 0.02 and 0.06 Db respectively, than their partner calculations, the single set *exo*- and mixed set *endo*-.

No difference between conformations can be determined for *neo*-pentyl **6**, benzyl **7**, *tert*-butyl **8** or phenyl **9**, due to the single minimum output from the calculations, but it can be seen that the mixed set calculations provide a dipole moment smaller than that of

the single set calculations. Benzyl **7** and *tert*-butyl **8** exhibit the largest dipole moments in the series, with the values for the benzyl > 1.0 Db larger than the moment of the *tert*-butyl in both calculations.

Table 15 – Calculated dipole moments (Db) of lead alkyl complexes **3** – **9**.

	LANL2DZ (All atoms)		LANL2DZ (Pb), 6-31G* (N, C, H)	
	<i>endo</i> -	<i>exo</i> -	<i>endo</i> -	<i>exo</i> -
LPbMe (3)	1.722	2.107	1.349	1.610
LPb ⁱ Pr (4)	2.158	2.111	1.866	1.816
LPb ^s Bu (5)	2.115	2.095	1.793	1.853
LPbNp (6)	-	2.166	-	1.820
LPbBn (7)	-	3.866	-	3.116
LPb ^t Bu (8)	-	2.217	-	2.034
LPbPh (9)	2.132	-	1.853	-

1.5.5 TD-DFT calculations

Time-dependent DFT calculations were attempted, in order to calculate the electronic transitions that give rise to the wavelengths of maximum absorbance of the compounds in the LPbR series. Calculations were run using the mixed basis set LANL2DZ and 6-31G* as above, at both the B3LYP and TPSSSTPSS functional levels. Although other TD-DFT calculations have been shown to have good agreement with the corresponding experimental results in previous works,⁵⁸ our calculated transitions showed nonsensical values, leading us to believe that we were not providing the correct input to the calculations.

1.5.6 NMR calculations

The NMR chemical shift of lead atoms within complexes have been shown to be able to be calculated accurately using computational calculations.^{59,60} Initial calculations on our LPbR systems at the B3LYP level of theory produced results for the ²⁰⁷Pb chemical

shift that bore no relation to the experimental data. In much the same fashion as the TD-DFT calculations described above, we believed we believed that we were not performing the calculations in the correct fashion. Due to time and operational limits, both the TD-DFT and NMR calculations were not able to be completed, prior to submission of this thesis, although calculations are currently being performed using the Amsterdam Density Functional package (ADF) in collaboration with Dr Hazel Cox at Sussex.

1.6 Summary

We have synthesised and fully characterised a number of low-coordinate β -diketiminato lead alkyl and aryl complexes. Depending upon the alkyl or aryl substituent on the metal centre, a complex can exhibit either the *endo*- or *exo*- conformation in the solid state. Density Functional Theory calculations have been carried out to investigate this dependency, and have shown that the conformation exhibited in the solid state is the lowest energy minimum. For complexes with small, less bulky substituents, there exists a second energy minimum, although this is at a higher energy. Reactivity studies were carried out on the lead alkyl complexes, and they were found to be fairly sensitive to both heat and light, which encouraged decomposition of the complex. Other than this sensitivity, the complexes were found to be mostly unreactive, although some promising reactivity was found with respect to boranes.

1.7 Experimental details

General considerations (all sections):

All air-sensitive manipulations were carried out under an atmosphere of dry nitrogen gas using standard Schlenk line techniques, or inside an inert atmosphere glovebox. Hydrocarbon and ethereal solvents were dried over sodium metal, and halogenated solvents were dried over calcium hydride. All solvent were distilled, degassed and stored over 4 Å molecular sieves in ampoules containing an inert nitrogen atmosphere. Reagents were purchased from Acros Organics or Sigma-Aldrich, or freshly distilled (liquids) or recrystallised (solids) from existing stocks and stored under inert atmosphere. Solid *neo*-pentyl lithium was kindly donated by Prof. Geoff Cloke's research group. LSnCl and LSnMe were used from previously synthesised stocks from Amy Saunders.

^1H , $^{13}\text{C}\{^1\text{H}\}$, ^{19}F , $^{27}\text{Al}\{^1\text{H}\}$, $^{31}\text{P}\{^1\text{H}\}$, $^{119}\text{Sn}\{^1\text{H}\}$ and $^{207}\text{Pb}\{^1\text{H}\}$ NMR spectra were recorded on Varian VNMR 400 (^1H 399.5, ^{13}C 100.46, ^{19}F 375.9, ^{27}Al 104.1, ^{31}P 161.7, ^{119}Sn 149.0, ^{207}Pb 83.6 MHz), 500 (^1H 499.91, ^{13}C 125.7 MHz) or 600 (^{119}Sn 223.6, ^{207}Pb 125.4 MHz) spectrometers, equipped with X $\{^1\text{H}\}$ broadband-observe probes. The ^1H and ^{13}C NMR chemical shifts were externally referenced to TMS, the ^{19}F signals were externally referenced to CFCl_3 , the ^{27}Al signals were externally referenced to aqueous $\text{Al}(\text{NO}_3)_3$, the ^{31}P signals were externally referenced to H_3PO_4 , the ^{119}Sn signals were externally referenced to SnMe_4 and the ^{207}Pb signals were externally referenced to PbMe_4 . The NMR samples were prepared in deuterated solutions of benzene (C_6D_6), chloroform (CDCl_3) or dichloromethane (CD_2Cl_2), and the spectra collected at 303 K (VNMR 400 and 500) or 298 K (VNMR 600).

The data for the X-ray structures of the complexes were collected at 173 K on a Nonius Kappa CCD diffractometer ($\lambda(\text{Mo K}\alpha) = 0.71073 \text{ \AA}$) and refined using the SHELXL-97 software package. The data for the X-ray structure of magnesium diphenylphosphide **19** (Chapter 3) was collected by the UK National Crystallographic Service (NCS) at the University of Southampton, on a Bruker-Nonius Roper CCD diffractometer and refined

using the SHELXL-97 software package. Manipulation for presentation was carried out with ORTEP 3v2 software.

UV-visible spectra were recorded on a Varian Cary 50 instrument equipped with a water-cooled Peltier system. UV-visible samples were prepared in an inert-atmosphere quartz cell in solutions of benzene, with a baseline spectrum of pure benzene being run before each acquisition to provide a 'blank'. Data was collected at 298 K, unless otherwise specified.

Elemental Analyses were carried out by Steven Boyer at the London Metropolitan University's Elemental Analysis Service.

Starting materials:*Synthesis of 2,6-diisopropyl β -diketimine; LH (1)*

2,6-Diisopropylaniline (58.4 ml, 0.309 mol) and 2,4-pentandione (14.0 ml, 0.136 mol) were added to ethanol (~600 ml) in a round-bottomed flask equipped with a magnetic stirrer. Reagent-grade hydrochloric acid (12 M, ~12 ml) was added, evolving a large quantity of white gas. The mixture was refluxed for three days (~72 hrs) under air, after which a thick pink/white slurry was observed. The solvent was removed *in vacuo*, and the residue washed with saturated sodium hydrogen carbonate solution (~150 ml) and extracted with dichloromethane (~ 1000-1500 ml). The red solution was dried with magnesium sulphate, filtered and the solvent removed *in vacuo*, giving a pale orange residue. This was washed to remove all traces of colouring with copious amounts of methanol, giving a bright white solid, which was dried under vacuum and used without further purification. Yield: 37.2 g (65.4%).

^1H NMR (499.91 MHz, C_6D_6 , 30°C): δ 12.46 (s, 1H, NH), 7.18 (m, 6H, H_{aryl}), 4.89 (s, 1H, middle-CH), 3.32 (sept, 4H, CHMe_2), 1.67 (s, 6H, NCMe), 1.22 (d, 12H, CHMe_2), 1.17 (d, 12H, CHMe_2).

Literature ^1H NMR (CDCl_3 , 25°C): δ 12.12 (br, 1H, NH), 7.12 (m, 6H, H_{aryl}), 4.84 (s, 1H, middle-CH), 3.10 (m, 4H, CHMe_2), 1.72 (s, 6H, NCMe), 1.22 (d, 12H, CHMe_2), 1.12 (d, 12H, CHMe_2).⁶¹

Synthesis of β -diketiminato lead chloride; LPbCl (2)

Neutral β -diketimine **1** (2.0 g, 4.78 mmol) was dissolved in ~20 ml of THF in a Schlenk tube, to which was added $^n\text{BuLi}$ (2.35 M, 2.1 ml, 4.93 mmol). The mixture was stirred for ~30 minutes at room temperature, and then added dropwise to a slurry of PbCl_2 (1.33 g, 4.78 mmol) in ~10 ml of THF in another Schlenk tube. The pale yellow mixture was stirred overnight at room temperature, after which an orange solution was observed. The solvent was removed *in vacuo*, and toluene was added. The solution was filtered through Celite®, and reduced to dryness, giving a lemon yellow powder. The powder was carefully washed with pentane, dried and used without further purification. Yield: 2.04 g (64.8%).

^1H NMR (499.91 MHz, C_6D_6 , 30°C): δ 7.08 (m, 6H, H_{aryl}), 4.87 (s, 1H, middle-CH), 3.96 (sept, 2H, CHMe_2), 3.05 (sept, 2H, CHMe_2), 1.68 (s, 6H, NCMe), 1.51 (d, 6H, CHMe_2), 1.24 (d, 6H, CHMe_2), 1.16 (d, 6H, CHMe_2), 1.08 (d, 6H, CHMe_2).

Literature ^1H NMR (500 MHz, C_6D_6 , 20°C): δ 7.23 (d, $J = 7.5$ Hz, 2H, $m\text{-H}_{\text{aryl}}$), 7.18 (t, $J = 7.5$ Hz, 2H, $p\text{-H}_{\text{aryl}}$), 7.10 (d, $J = 7.5$ Hz, 2H, $m\text{-H}_{\text{aryl}}$), 4.91 (s, 1H, middle CH), 3.99 (sept, $J = 6.8$ Hz, 2H, CHMe_2), 3.08 (sept, $J = 6.8$ Hz, 2H, CHMe_2), 1.71 (s, 6H, NCMe), 1.54 (d, $J = 6.7$ Hz, 6H, CHMe_2), 1.27 (d, $J = 6.8$ Hz, 6H, CHMe_2), 1.19 (d, $J = 6.9$ Hz, 6H, CHMe_2), 1.12 (d, $J = 6.8$ Hz, 6H, CHMe_2).⁴³

Alkyls:

Synthesis of β -diketiminato lead methyl; LPbMe (3)

Lead chloride **2** (300 mg, 0.45 mmol) was dissolved in ~10 ml of toluene in a Schlenck tube, and cooled to -78°C . MeMgBr (1.6 M, 330 μl , 0.45 mmol, THF) was mixed with ~5 ml of toluene in another Schlenk tube, and was added dropwise to the yellow solution of **2**. The mixture was left to stir for one hour, after which the solvent was removed *in vacuo*, pentane was added, and the lemon yellow solution filtered through Celite®. The solution was concentrated and the product left to crystallise in the freezer at -30°C , giving bright yellow crystals. Yield: 115 mg (39.6%).

^1H NMR (499.91 MHz, C_6D_6 , 30°C): δ 7.13 (m, 6H, H_{aryl}), 4.79 (s, 1H, middle CH), 3.56 (sept, $J = 6.9$ Hz, 2H, CHMe_2), 3.46 (sept, $J = 6.9$ Hz, 2H, CHMe_2), 1.72 (s, 6H, NCMe), 1.33 (d, $J = 6.9$ Hz, 6H, CHMe_2), 1.22 (m, 18H, CHMe_2), 0.56 (s, $J_{\text{Me-Pb}} = 39.5$ Hz, 3H, PbMe).

$^{13}\text{C}\{^1\text{H}\}$ NMR (100.5 MHz, C_6D_6 , 30°C): δ 164.2 (NCMe), 144.0, 142.4, 125.6, 123.8 (C_{aryl}), 99.3 (middle CH), 76.4 (Pb-CH_3), 28.3 (CHMe_2), 27.1 (CHMe_2), 26.8 (CHMe_2), 24.5 (CHMe_2), 24.4 (CHMe_2), 23.8 (CHMe_2), 23.6 (NCMe).

$^{207}\text{Pb}\{^1\text{H}\}$ NMR (125.4 MHz, C_6D_6 , 30°C): δ 3001.7

Elemental Analysis for $\text{C}_{30}\text{H}_{44}\text{N}_2\text{Pb}$: Calc.: C, 56.32; H, 6.88; N, 4.38. Found: C, 56.34; H, 6.75; N, 4.29.

UV-vis (C_6H_6 , 25°C): λ_{max} 395.0 nm, $\epsilon = 6736 \text{ mol}^{-1} \text{ cm}^{-1}$.

Synthesis of β -diketiminate lead iso-propyl; LPbⁱPr (4)

Lead chloride **2** (300 mg, 0.45 mmol) was dissolved in ~10 ml of toluene in a Schlenk tube, and cooled to -78°C. ⁱPrMgCl (2.0 M, 230 μ l, 0.45 mmol, THF) was mixed with ~5 ml of toluene in another Schlenk tube, and was added dropwise to the cold solution of **2**. The mixture was left to stir for two hours, after which the toluene was removed *in vacuo*. Pentane was then added and the orange solution filtered through Celite®. The solution was concentrated and placed at -30°C for crystallisation. Orange crystals suitable for x-ray diffraction were grown from a heptane solution, also held at -30°C.

Yield: 161 mg (53.1%)

¹H NMR (399.5 MHz, C₆D₆, 30°C): δ 7.07 (m, 6H, H_{aryl}), 4.62 (s, 1H, middle CH), 3.79 (sept, J = 6.9 Hz, 2H, CHMe₂), 3.32 (sept, J = 6.9 Hz, 2H, CHMe₂), 3.31 (sept, J = 6.9 Hz, 1H, PbCHMe₂) 1.72 (s, 6H, NCM_e), 1.54 (d, J = 4.0 Hz, 6H, PbCHMe₂), 1.42 (d, J = 6.9 Hz, 6H, CHMe₂), 1.25 (d, J = 6.9 Hz, 6H, CHMe₂), 1.23 (d, J = 6.9 Hz, 6H, CHMe₂), 1.19 (d, J = 6.8 Hz, 6H, CHMe₂).

¹³C{¹H} NMR (100.5 MHz, C₆D₆, 30°C): δ 165.9 (NCMe), 143.7, 143.3, 142.5, 126.6, 125.4, 124.0, 123.6, 123.2 (C_{aryl}), 101.7 (Pb-CHMe₂), 97.5 (middle CH), 28.2 (CHMe₂), 27.6 (CHMe₂), 24.7 (CHMe₂), 24.3 (CHMe₂), 24.2 (CHMe₂), 24.1 (CHMe₂), 23.0 (NCMe), 17.2 (PbCMe₂).

²⁰⁷Pb{¹H} NMR (125.4 MHz, C₆D₆, 30°C): δ 3144.9

Elemental Analysis for C₃₂H₄₈N₂Pb: Calc.: C, 57.55; H, 7.19; N, 4.20. Found: C, 57.49; H, 7.27; N, 4.15.

UV-vis (C₆H₆, 25°C): λ_{max} 332.0 nm, $\lambda_{\text{secondary}}$ 448.0 nm.

Synthesis of β -diketiminate lead sec-butyl; LPb^sBu (5)

Lead chloride **2** (300 mg, 0.45 mmol) was dissolved in ~10 ml of toluene in a Schlenk tube, and cooled to -78°C. ^sBuMgCl (1.9 M, 260 μ l, 0.5 mmol) was mixed with ~5 ml of toluene in another Schlenk tube, and was added dropwise to the cold solution of **2**. The mixture was left to stir at -78°C for two hours, after which the toluene was evaporated, replaced with pentane and the orange solution filtered through Celite®. The solution was placed at -30°C and small, dark orange crystals were observed after a few days. Yield: 186 mg (60.7%).

^1H NMR (399.5 MHz, C_6D_6 , 30°C): δ 7.06 (m, 6H, H_{aryl}), 4.63 (s, 1H, middle CH), 3.80 (sept, $J = 6.8$ Hz, 2H, CHMe_2), 3.32 (sept, $J = 6.5$ Hz, 2H, CHMe_2), 2.46 (m, 1H, $\text{PbCH}(\text{Me})\text{CH}_2\text{Me}$), 1.73 (s, 6H, NCMe), 1.61 (d, $J = 7.3$ Hz, 3H, $\text{PbCH}(\text{Me})\text{CH}_2\text{Me}$), 1.45 (d, $J = 6.7$ Hz, 6H, CHMe_2), 1.25 (m, 14H, $\text{PbCH}(\text{Me})\text{CH}_2\text{Me}$, CHMe_2), 1.18 (d, $J = 6.7$ Hz, 6H, CHMe_2), 0.80 (t, $J = 7.3$ Hz, 3H, $\text{PbCH}(\text{Me})\text{CH}_2\text{Me}$).

$^{13}\text{C}\{^1\text{H}\}$ NMR (100.5 MHz, C_6D_6 , 30°C): δ 169.5, 166.1 (NCMe), 143.9, 143.3, 142.5, 131.8, 125.4, 124.0, 123.6 (C_{aryl}), 108.7 ($\text{PbCH}(\text{Me})\text{CH}_2\text{Me}$), 97.5 (middle CH), 28.3, 28.2 (CHMe_2), 27.7 ($\text{PbCH}(\text{Me})\text{CH}_2\text{Me}$), 26.9, 26.8 (CHMe_2), 25.0, 24.7, 24.3, 24.2, 24.1 (CHMe_2), 23.1, 23.0 (NCMe), 15.6 ($\text{PbCH}(\text{Me})\text{CH}_2\text{Me}$), 13.0 ($\text{PbCH}(\text{Me})\text{CH}_2\text{Me}$).

$^{207}\text{Pb}\{^1\text{H}\}$ NMR (125.4 MHz, C_6D_6 , 30°C): δ 3262.2

Elemental Analysis for $\text{C}_{33}\text{H}_{50}\text{N}_2\text{Pb}$: Calc.: C, 58.13; H, 7.34; N, 4.11. Found: C, 57.03; H, 7.29; N, 4.02.

UV-vis (C_6H_6 , 25°C): λ_{max} 300.0 nm, $\lambda_{\text{secondary}}$ 452.0 nm.

Synthesis of β -diketiminato lead neo-pentyl; LPbNp (6)

Lead chloride **2** (300 mg, 0.45 mmol) was dissolved in ~10 ml of toluene in a Schlenk tube, and cooled to 0°C . NpLi (35 mg, 0.45 mmol) was mixed with ~5 ml of toluene in another Schlenk tube, and was added dropwise to the cold solution of **2**. The mixture was left to stir for two hours, after which the toluene was removed *in vacuo*. Pentane was then added and the orange solution filtered through Celite®. The solution was concentrated and placed at -30°C . After a week, orange crystals suitable for X-ray analysis were observed. Yield: 209 mg (66.8%).

^1H NMR (399.5 MHz, C_6D_6 , 30°C): δ 7.03 (m, 6H, H_{aryl}), 4.60 (s, 1H, middle CH), 3.76 (sept, $J = 6.9$ Hz, 2H, CHMe_2), 3.28 (sept, $J = 6.8$ Hz, 2H, CHMe_2), 1.71 (s, 6H, NCMe), 1.49 (d, $J = 6.9$ Hz, 6H, CHMe_2), 1.23 (d, $J = 6.9$ Hz, 6H, CHMe_2), 1.21 (d, $J = 6.8$ Hz, 6H, CHMe_2), 1.16 (d, $J = 6.8$ Hz, 6H, CHMe_2), 0.87 (s, 2H, PbCH_2^tBu), 0.66 (s, 9H, PbCH_2^tBu).

$^{13}\text{C}\{^1\text{H}\}$ NMR (100.5 MHz, C_6D_6 , 30°C): δ 166.2 (NCMe), 143.4, 143.3, 142.8, 125.4, 123.9, 123.6 (C_{aryl}), 114.0 ($\text{PbCH}_2\text{CMe}_3$), 97.3 (middle CH), 36.6 ($\text{PbCH}_2\text{CMe}_3$), 28.3 (CHMe_2), 27.7 (CHMe_2), 26.6 (CHMe_2), 24.8 (CHMe_2), 24.6 (CHMe_2), 24.4 (CHMe_2), 22.9 (NCMe).

$^{207}\text{Pb}\{^1\text{H}\}$ NMR (125.4 MHz, C_6D_6 , 30°C): δ 3506.3

Elemental Analysis for $C_{34}H_{52}N_2Pb$: Calc.: C, 58.69; H, 7.48; N, 4.03. Found: C, 58.64; H, 7.56; N, 3.98.

UV-vis (C_6H_6 , 25°C): λ_{max} 343.0 nm, $\lambda_{secondary}$ 449.0 nm.

Synthesis of β -diketiminate lead benzyl; LPbBn (7)

Lead chloride **2** (300 mg, 0.45 mmol) was dissolved in ~10 ml of toluene in a Schlenk tube, and cooled to -78°C. BnMgCl (20% wt., 343 mg, 0.45 mmol, THF) was mixed with ~5 ml of toluene in another Schlenk tube, and was added dropwise to the solution of **2**. The mixture was left to stir for two hours, after which the toluene was removed *in vacuo*, pentane was added, and the orange solution filtered through Celite®. The solution was concentrated and the product left to crystallise at -30°C, yielding pale orange crystals. Yield: 126 mg (39.2%).

1H NMR (400 MHz, C_6D_6 , 30°C): δ 7.03 (m, 6H, H_{aryl}), 7.01 (t, J = 7.6 Hz, 2H, m- H_{Ph}), 6.60 (t, J = 7.4 Hz, 1H, p- H_{Ph}), 5.97 (d, J = 7.4 Hz, 2H, o- H_{Ph}), 4.67 (s, 1H, middle CH), 3.77 (sept, J = 6.9 Hz, 2H, $CHMe_2$), 3.21 (sept, J = 6.8 Hz, 2H, $CHMe_2$), 1.77 (s, 2H, $PbCH_2$), 1.72 (s, 6H, $NCMe$), 1.46 (d, J = 6.9 Hz, 6H, $CHMe_2$), 1.27 (d, J = 6.8 Hz, 6H, $CHMe_2$), 1.18 (d, J = 6.8 Hz, 6H, $CHMe_2$), 1.07 (d, J = 6.9 Hz, 6H, $CHMe_2$).

$^{13}C\{^1H\}$ NMR (100.5 MHz, C_6D_6 , 30°C): δ 165.5 ($NCMe$), 143.4, 143.2, 142.7, 141.9, 127.2, 125.7, 124.2, 124.0, 122.4 (C_{aryl}), 98.2 (middle CH), 94.6 ($Pb-CH_2$), 28.3 ($CHMe_2$), 27.6 ($CHMe_2$), 26.5 ($CHMe_2$), 24.7 ($CHMe_2$), 24.6 ($CHMe_2$), 24.2 ($CHMe_2$), 23.0 ($NCMe$).

$^{207}Pb\{^1H\}$ NMR (83.6 MHz, C_6D_6 , 30°C): δ 2871.5

Elemental Analysis for $C_{36}H_{46}N_2Pb$: Calc.: C, 60.40; H, 6.71; N, 3.91. Found: C, 60.45; H, 6.79; N, 3.87.

UV-vis (C_6H_6 , 25°C): λ_{max} 316.0 nm, $\lambda_{secondary}$ 442.9 nm.

Synthesis of β -diketiminate lead tert-butyl; LPb^tBu (8)

Lead chloride **2** (300 mg, 0.45 mmol) was dissolved in ~10 ml of toluene in a Schlenk tube, and cooled to -78°C. ^tBuLi (1.89 M, 240 μ l, 0.45 mmol) was mixed with ~5 ml of toluene in another Schlenk tube, and was added dropwise to the cold solution of **2**. The mixture was left to stir at -78°C overnight, after which the toluene was removed *in vacuo*, replaced with pentane and the bright orange solution filtered through Celite®.

Large, red crystals, suitable for x-ray analysis, were obtained from a concentrated pentane solution at -30°C . Yield: 174 mg (56.0%)

^1H NMR (400 MHz, C_6D_6 , 30°C): δ 7.06 (m, 6H, H_{aryl}), 4.67 (s, 1H, middle CH), 3.85 (sept, $J = 6.9$ Hz, 2H, CHMe_2), 3.22 (sept, $J = 6.8$ Hz, 2H, CHMe_2), 2.20 (s, 9H, CMe_3), 1.75 (s, 6H, NCMe), 1.44 (d, $J = 6.9$ Hz, 6H, CHMe_2), 1.26 (d, $J = 6.9$ Hz, 6H, CHMe_2), 1.21 (d, $J = 6.8$ Hz, 6H, CHMe_2), 1.18 (d, $J = 6.8$ Hz, 6H, CHMe_2).

$^{13}\text{C}\{^1\text{H}\}$ NMR (100.5 MHz, C_6D_6 , 30°C): δ 167.9 (NCMe), 144.6, 143.3, 142.3, 125.3, 123.8, 123.6 (C_{aryl}), 123.2 (PbCMe_3), 97.7 (middle CH), 28.6 (CHMe_2), 28.0 (CHMe_2), 26.9 (CHMe_2), 26.6 (CHMe_2), 25.0 (CHMe_2), 24.6 (CHMe_2), 24.1 (PbCMe_3), 23.5 (NCMe), 23.0 (PbCMe_3).

$^{207}\text{Pb}\{^1\text{H}\}$ NMR (125.4 MHz, C_6D_6 , 30°C): δ 3684.2

Elemental Analysis for $\text{C}_{33}\text{H}_{50}\text{N}_2\text{Pb}$: Calc.: C, 58.13; H, 7.34; N, 4.11. Found: C, 58.06; H, 7.28; N, 4.03.

UV-vis (C_6H_6 , 25°C): λ_{max} 375.0 nm.

Synthesis of β -diketiminate lead phenyl; LPbPh (9)

Lead chloride **2** (300 mg, 0.45 mmol) was dissolved in ~ 10 ml of toluene in a Schlenk tube, and cooled to -78°C . PhMgBr (3.0 M, 150 μl , 0.45 mmol) was mixed with ~ 5 ml of toluene in another Schlenk tube, and was added dropwise to the solution of **2**. The mixture was left to stir for two hours, after which the toluene was removed *in vacuo*, pentane was added, and the yellow solution filtered through Celite®. The solution was concentrated and the product crystallised at -30°C , giving cubic yellow crystals. Yield: 80 mg (25.4%).

^1H NMR (500 MHz, C_6D_6 , 30°C): δ 8.51 (d, $J = 6.9$ Hz, 2H, o- H_{Ph}), 7.58 (t, $J = 7.6$ Hz, 2H, m- H_{Ph}), 7.12 (m, 6H, H_{aryl}), 7.04 (m, 1H, p- H_{Ph}), 4.80 (s, 1H, middle CH), 3.58 (sept, $J = 6.9$ Hz, 2H, CHMe_2), 3.22 (sept, $J = 6.8$ Hz, 2H, CHMe_2), 1.77 (s, 6H, NCMe), 1.38 (d, $J = 6.9$ Hz, 6H, CHMe_2), 1.25 (d, $J = 6.9$ Hz, 6H, CHMe_2), 1.07 (d, $J = 6.9$ Hz, 6H, CHMe_2), 0.52 (d, $J = 6.7$ Hz, 6H, CHMe_2).

$^{13}\text{C}\{^1\text{H}\}$ NMR (100.5 MHz, C_6D_6 , 30°C): δ 164.1 (NCMe) 144.8, 143.6, 142.0, 137.5, 130.0, 126.8, 125.9, 124.3, 123.7 (C_{aryl}), 98.3 (middle CH), 28.3 (CHMe_2), 27.3 (CHMe_2), 25.0 (CHMe_2), 24.4 (CHMe_2), 24.2 (CHMe_2), 24.0 (CHMe_2), 23.5 (NCMe).

$^{207}\text{Pb}\{^1\text{H}\}$ NMR (125.4 MHz, C_6D_6 , 30°C): δ 2419.0

Elemental Analysis for $C_{35}H_{44}N_2Pb$: Calc.: C, 59.90; H, 6.56; N, 3.99. Found: C, 60.00; H, 6.49; N, 4.10.

UV-vis (C_6H_6 , $25^\circ C$): λ_{max} 397.0 nm.

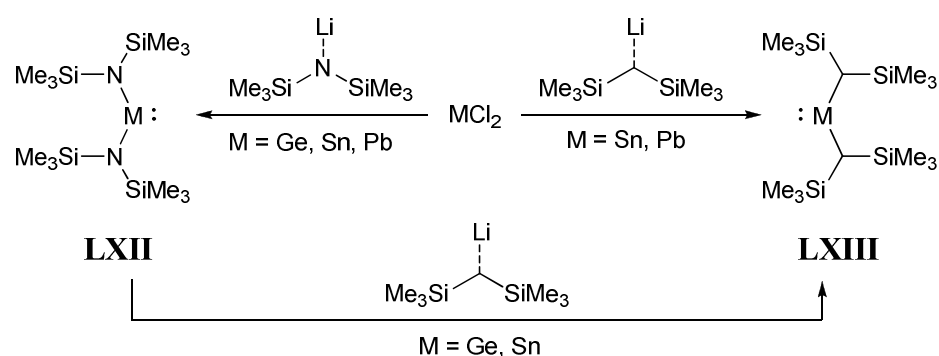
2. Synthesis, structure and reactivity of β -diketiminato plumbylene and stannylene complexes

2.1 Low-coordinate group 14 metal complexes

2.1.1 Low-coordinate group 14 metal systems

Complexes containing group 14 metals with a low coordination number are relatively rare, although they can be synthesised by addition of large, sterically encumbering groups to surround the metal centre and prevent oligomerisation. In the 1970's Lappert and co-workers synthesised some of the very first examples of a group 14 heavy element in a low-coordination environment, with the preparation of divalent germanium, tin and lead silylamides and silylalkyl complexes.^{62,63} Whereas the tin and lead dialkyl species **LXIII** could be synthesised directly from the metal dichloride, the germanium species could only be synthesised from the *bis*(trimethylsilyl) amide **LXII**, to avoid the appearance of $R_3Ge\cdot$ radical species.⁶⁴

Scheme 35 – Synthesis of low-coordinate group 14 silylamides and silylalkyls.



Whilst the lead compounds have both been reported as monomeric in nature,^{62,63} the tin complexes of both the amide and alkyl substituents have been shown to exhibit dimerisation in both solution and the solid state.^{63,65}

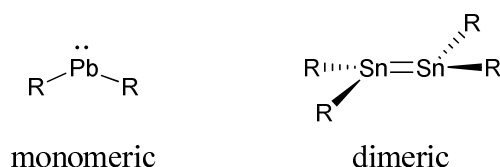
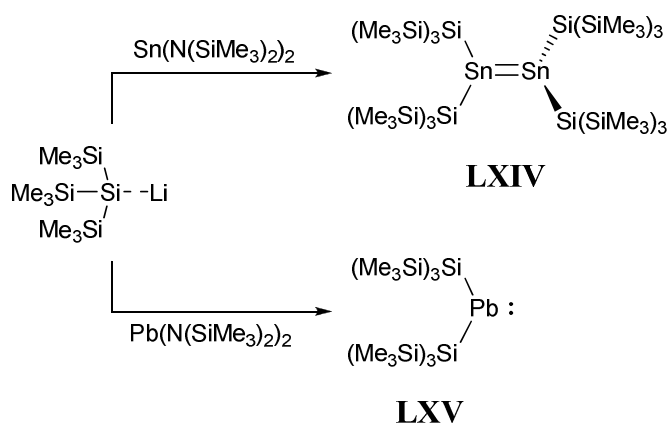


Figure 35 – Lead and tin forms of silylamides **LXII** ($R = N(\text{SiMe}_3)_2$) and silylalkyls **LXIII** ($R = \text{CH}(\text{SiMe}_3)_2$).

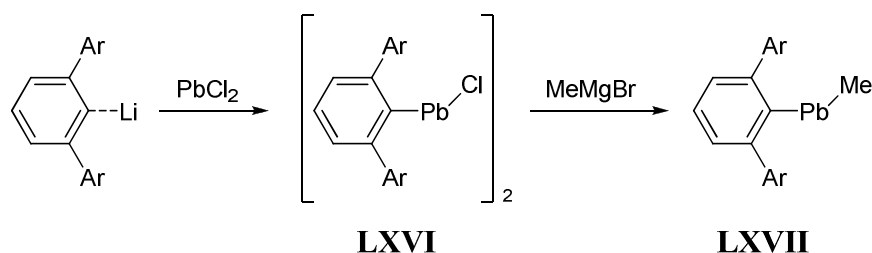
Heavily silylated ligands such as those present in **LXII** and **LXIII** have been widely used to isolate examples of group 14 metals in low coordination numbers. Most examples tend to contain electronegative substituent groups, such as those based on carbon and nitrogen. A hypersilyl ligand (*tris*-(trimethylsilyl)silyl, $[\text{Si}(\text{SiMe}_3)_3]^-$) has been used by Klinkhammer and co-workers to generate rare examples of tin and lead as electron-rich carbene analogues.⁶⁶ Synthesised by a metathesis reaction between the alkali metal salt of the hypersilyl ligand, and the group 14 metal amides of type **LXII**, the tin and lead compounds **LXIV** and **LXV** were the first examples of bis-silyl substituted stannyl- and plumbylenes.

Scheme 36 – Hypersilyl tin(II) and lead(II).



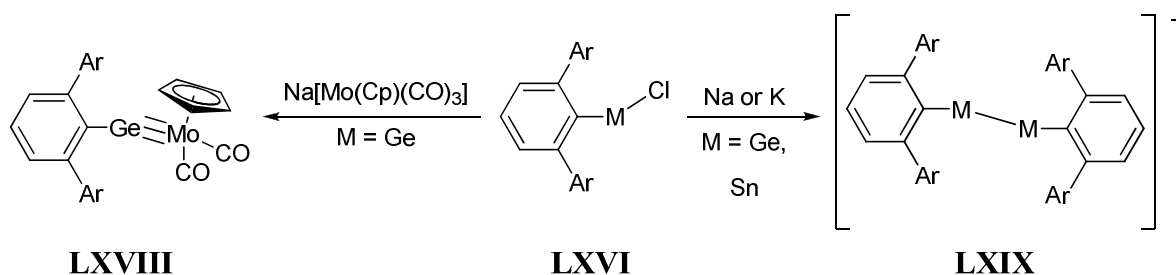
Power and co-workers produced details of low-coordinate lead complexes with a variety of small, terminal organic groups using a very bulky terphenyl ligand system, $[\text{C}_6\text{H}_3\text{-}2,6\text{-(}2,4,6\text{-}^i\text{Pr}_3\text{C}_6\text{H}_2)_2]^-$ (Ar^*).⁵² Those complexes with alkyl and aryl substituents were observed to be monomeric, and those with halides were observed to dimerise, albeit by long-range interactions.

Scheme 37 – Low-coordinate lead systems with Ar^* . $\text{Ar} = 2,4,6\text{-triisopropylphenyl}$.



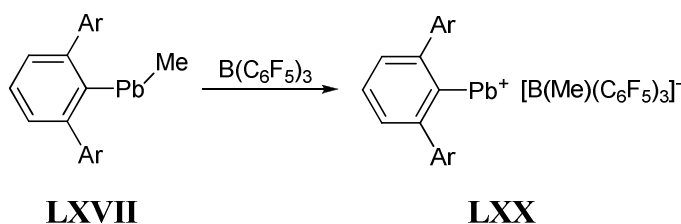
Large aryl substituents have also been used to stabilise multiple bonding to heavy group 14 metal atoms. In 1996, Power and co-workers generated the first example of a triple bond to a heavy group 14 element, in the synthesis of **LXVIII**, a two-coordinate germanium compound bound to molybdenum.⁶⁷ Multiple bonds between group 14 elements can be obtained by the corresponding reduction of the metal halide with an alkali metal (**LXIX**), with the quantity of alkali metal directly affecting the resultant metal-metal bond order – one equivalent results in a metal-metal single bond, two equivalents result in a metal-metal double bond, and so on.⁶⁸ The lead analogue of **LXIX** can be generated with LiAlH_4 instead of the pure alkali metal.

Scheme 38 – Synthesis of multiple-bonded group 14 metal complexes. Ar = 2,4,6-triisopropylphenyl.



When considering cationic metal complexes, a downside to a terphenyl ligand system is that they would produce a one-coordinate species, which would be less stable than a two-coordinate species. Upon reaction with *tris*-pentafluorophenyl borane, Ar^*PbMe **LXVII** was observed to have the terminal methyl group abstracted to give a quasi-one-coordinate lead cation, with toluene coordinated to the metal centre in the solid state.⁶⁹ However, this is a very rare example of a one-coordinate group 14 metal cation, and highlights the difficulty in isolating low-coordinate lead complexes.

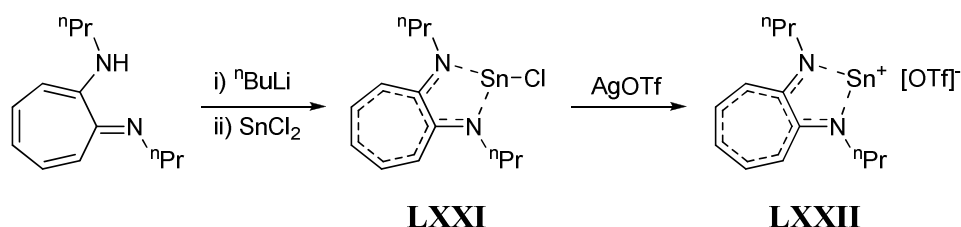
Scheme 39 – Synthesis of a one-coordinate lead cation with Ar^* . Ar = 2,4,6-triisopropylphenyl.



2.1.2 Group 14 metal ionic complexes

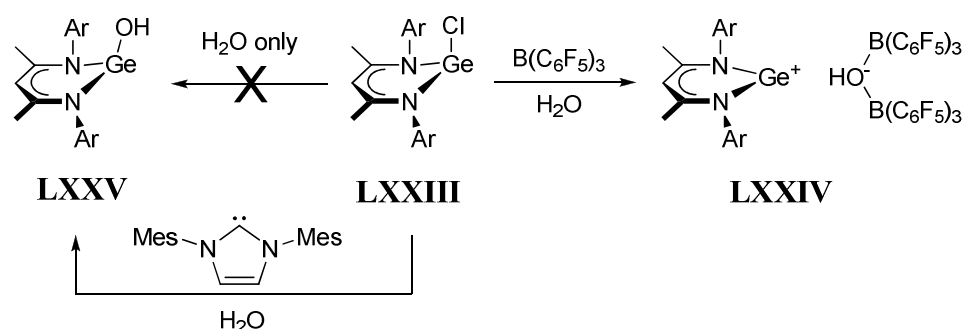
There are very few examples of two- or three-coordinate group 14 metal cationic complexes in the literature. No examples of two-coordinate lead(II) cations can be found, other than the work presented in this chapter, published in our group's paper (appendix 4).⁷⁰ Only one example of a tin(II) cation has been reported in the literature (scheme 40), stabilised by long range interactions with a triflate anion (**LXXII**).⁷¹

Scheme 40 – Generation of tin cation $[\text{}^n\text{Pr}_2(\text{ATI})\text{Sn}]^+.[\text{OTf}]^-$ (ATI = aminotroponiminato, 1,2-N,N'-C₇H₅)



The first example of a two-coordinate β -diketiminato group 14 cationic complex was isolated by Power and co-workers, and contains a germanium centre, with a very bulky $[\text{HO}\{\text{B}(\text{C}_6\text{F}_5)_3\}_2]$ anion.⁷² The closest distance between the cationic and the anionic fragments was observed to be a Ge-F distance of 3.01 Å, a distance close to that of the sum of the respective van der Waals radii (3.47 Å). The procedure to synthesise germanium cation **LXXIV** involved treating the parent chloride with a mixture of *tris*-pentafluorophenyl borane and deoxygenated water, to form a borate-type species, prior to the removal of the chloride. Simple reaction of parent chloride **LXXIII** with deoxygenated water did not produce a reaction, although Roesky showed that, if carried out in the presence of an N-heterocyclic carbene, it was possible to form the terminal germanium hydroxide.⁷³

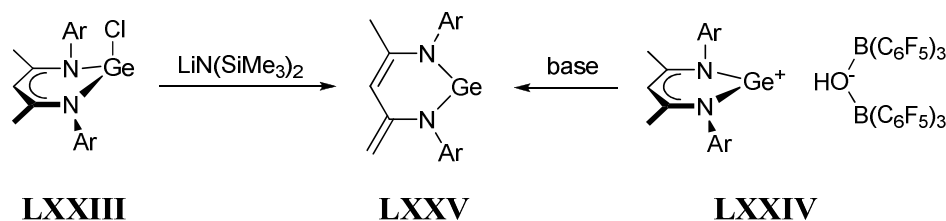
Scheme 41 – Formation of a germanium cation and germanium hydroxide with deoxygenated water. Ar = 2,6-diisopropylphenyl.



Attempts by our group to duplicate these results for tin(II) and lead(II) β -diketimines failed, as the BDI tin and lead chlorides reacted directly with deoxygenated water.

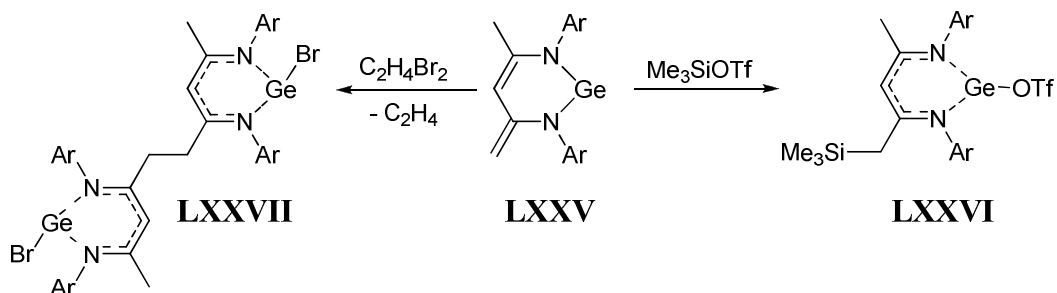
The germanium cation **LXXIV** has been studied in some detail by Driess and co-workers, and they have succeeded in forming a neutral, two-coordinate germylene complex.⁷⁴ A strong base was used to deprotonate one of the methyl groups on the backbone of the β -diketiminato ligand, to produce a diene-type structure, thus removing aromaticity from the C_3N_2Ge ring and forming the germanium species **LXXV**. Driess also made use of lithium *bis*-(trimethylsilyl)amide to form the neutral, two-coordinate germylene from the parent chloride in higher yields. However, for heavier group 14 metals such as lead, this route results in the synthesis of the corresponding lead amide, **L** (*vide supra*).⁴³

Scheme 42 – Generation of a neutral, two-coordinate BDI germylene. Ar = 2,6-diisopropylphenyl.



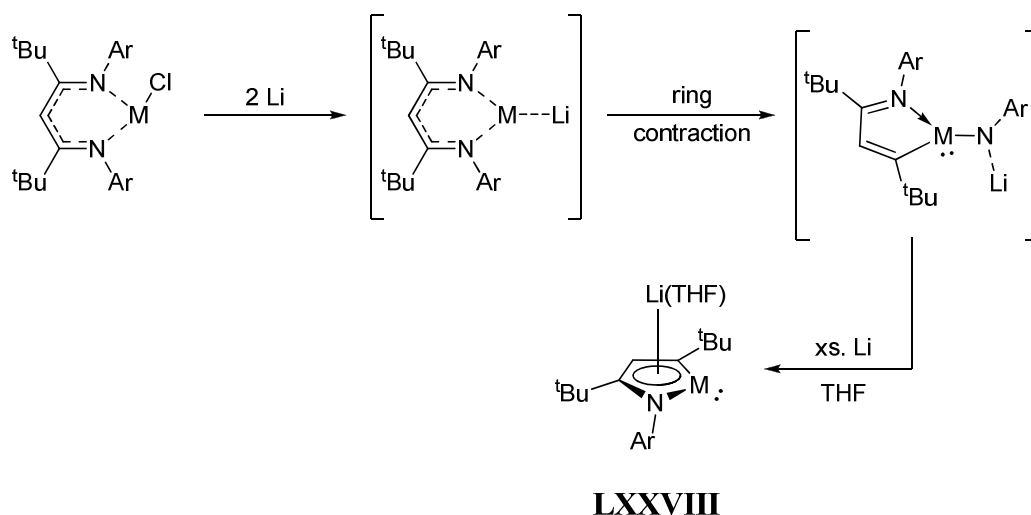
Germylene **LXXV** shows novel reactivity at the backbone methyl groups at the R^2 position; not a usual site for reactivity in a β -diketiminato-type complex. Reaction with trimethylsilyl triflate results in a TMS-methylene-substituted BDI germanium triflate, and reaction with 1,2-dibromoethane adds a bromide to the germanium centre and binds two BDI units together via the methylene groups at the R^2 position, with the elimination of ethane (scheme 43).

Scheme 43 – Reactivity of germylene **LXXV**. Ar = 2,6-diisopropylphenyl.



Recently, Jones and co-workers have published work in which BDI germanium and tin chloride are reduced with elemental lithium, and are observed to undergo a ring contraction to form a five-membered cyclopentadienide analogue.⁷⁵ A very bulky β -diketiminate ligand was used, with *tert*-butyl groups at the R² position (^tBuBDI), instead of the more common methyl groups. Reaction of the ^tBuBDI metal chloride with excess lithium in THF afforded a Cp-like anionic structure, with an η^5 -bound lithium for both germanium and tin β -diketiminate (LXXVIII). However, attempts to prepare the lead counterpart of (^tBuBDI)GeCl and (^tBuBDI)SnCl produced no identifiable products.⁷⁵

Scheme 44 – Synthesis of germylidenide and stannylidenide Cp-like ring structures. M = Ge, Sn. Ar = 2,6-diisopropylphenyl.

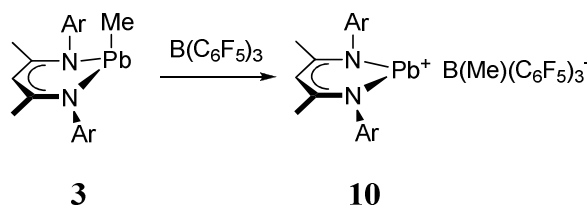


2.2 Synthesis and reactivity of β -diketiminate plumbylene and stannylene complexes

2.2.1 Synthesis and characterisation of β -diketiminate plumbyl-(II)-ene tris-(pentafluorophenyl) (methyl) borate, $[\text{LPb}]^+ [\text{B}(\text{Me})(\text{C}_6\text{F}_5)_3]^-$ (**10**)

Addition of one equivalent of the bulky neutral borane $\text{B}(\text{C}_6\text{F}_5)_3$ to the lead methyl complex **3** at -10°C resulted in complete conversion of the yellow alkyl complex to a red compound within one hour. Methyl borate **10** was isolated in 66% yield, and was found to only be soluble in polar solvents such as dichloromethane. Complex **10** was also observed to be very stable towards temperature and light, unlike its parent complex, lead methyl **3**.

Scheme 45 – Synthesis of $[\text{LPb}]^+ [\text{B}(\text{Me})(\text{C}_6\text{F}_5)_3]^-$ (**10**). Ar = 2,6-diisopropylphenyl.



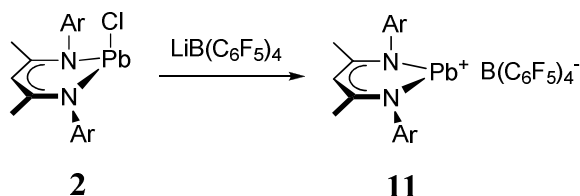
Despite repeated attempts at crystallisation in a number of solvents, no crystals suitable for X-ray diffraction were able to be grown. However, evidence from the ^1H NMR spectrum shows only one septet for the *iso*-propyl methyne protons on the ligand at δ 2.77 ($J = 6.8$ Hz), indicating a symmetrical environment around the metal centre. The abstraction of the methyl group from the lead atom is further supported by a shift in the ^1H NMR spectrum of the resonance corresponding to the methyl substituent to δ 0.45, from δ 0.56 in the parent methyl **3**. Despite repeated attempts, in increments from δ 0 – 10,000, no ^{207}Pb NMR spectroscopic signal was able to be detected for methyl borate **10**, potentially due to a short relaxation time of the lead nucleus.⁷⁰ The ^{19}F NMR spectrum shows only three fluorine environments, as one would expect from a non-coordinating pentafluorophenyl compound. Horton and co-workers have reported that the difference in chemical shift between *meta*- and *para*-positioned fluorine atoms in a $[\text{RB}(\text{C}_6\text{F}_5)_3]^-$ group (where R = Me, Bn) is a good indication of how strongly the anion

is coordinating to the cation.⁷⁶ $\Delta\delta(m,p\text{-F})$ values of 3 – 6 ppm were observed to indicate coordination, whereas values less than 3 ppm indicated noncoordination. The $\Delta\delta(m,p\text{-F})$ value observed for methyl borate **10** was 2.6 ppm, consistent with a noncoordinating anion.

2.2.2 Synthesis and characterisation of β -diketiminate plumbyl-(II)-ene *tetrakis*-(pentafluorophenyl) borate, $[\text{LPb}]^+ [\text{B}(\text{C}_6\text{F}_5)_4]^-$ (**11**)

Lead borate **11** was generated by addition of one equivalent of lithium *tetrakis*-(pentafluorophenyl) borate to a toluene solution of lead chloride **2** at -78°C . After warming to room temperature and stirring for thirty minutes, the solution was filtered through Celite® and borate **11** was isolated in 33% yield. Similar to methyl borate **10**, borate **11** was observed to be stable for long periods at room temperature, and did not decompose on exposure to light sources. Borate **11** was found to be only soluble in halogenated solvents such as dichloromethane, and decomposed to a complex mixture of products in the presence of ethereal solvents, such as THF.

Scheme 46 – Synthesis of $[\text{LPb}]^+ [\text{B}(\text{C}_6\text{F}_5)_4]^-$ (**11**). Ar = 2,6-diisopropylphenyl.



The complex was crystallised from a slow condensation of pentane into a concentrated solution in dichloromethane. The X-ray crystal structure revealed a coordinated DCM molecule. Potentially due to the presence of this DCM molecule, the metal centre is moved out of the plane of the ligand backbone by 0.480 Å, and the Pb-Cl1 distance is significantly longer in borate **11** than in the parent lead chloride **2**, as expected.⁴³ A long-range interaction is also observed between the metal centre and a fluorine from the $[\text{B}(\text{C}_6\text{F}_5)_4]^-$ anion, with Pb-F3 distance of 3.319(4) Å, just within the sum of the Pb-F van der Waals radii of 3.49 Å. This interaction may not even be present in the solution phase, evident from the ^{19}F NMR spectrum. The Pb-N bond distances (average 2.23 Å) are shorter than those reported for the electrostatically-bound $\text{LPb}(\text{OTf})$ (average 2.28 Å) reported by Roesky and co-workers,⁴⁶ as well as the parent lead chloride **2** (average 2.29 Å),⁴³ indicating a more electropositive metal centre. The N1-Pb-N2 bond angle of

84.34(16)° is slightly wider than the chloride **2** (82.77(7)°),⁴³ and the lead alkyl complexes, most likely due to the reduction of steric bulk around the metal centre.

Table 16 – Bond angles (°) and lengths (Å) for [LPb]⁺ [B(C₆F₅)₄][−] (**11**) with coordinated DCM.

N1-Pb-N2	84.34(16)	N1-Pb	2.239(4)
C1-N1-C6	121.5(4)	N2-Pb	2.226(4)
C1-N1-Pb	125.8(4)	Pb-Cl1	3.208(6)
C6-N1-Pb	112.7(3)	Pb-F3	3.319(4)
C3-N2-C18	121.3(4)	C _{DCM} -Cl1	1.769(14)
C3-N2-Pb	126.8(4)	C _{DCM} -Cl2	1.738(13)
C18-N2-Pb	111.9(3)	N1-C1	1.346(7)
N1-C1-C2	124.4(5)	C1-C2	1.396(8)
C1-C2-C3	130.4(5)	C2-C3	1.399(8)
C2-C3-N2	124.0(5)	C3-N2	1.335(7)
		Pb – plane	0.480

The ¹H NMR spectrum in deuterated DCM, shows one septet corresponding to the *iso*-propyl methyne protons on the ligand at δ 2.76 (*J* = 6.9 Hz), indicating a symmetrical environment around the metal centre, similar to that seen in the ¹H NMR spectrum of methyl borate **10**. This is in contrast to the structure seen in the solid state, and could be due to a truly symmetrical environment around the C₃N₂ plane being present when the complex is in the solution phase, or to a rapid inversion, in which the DCM molecule moves in and out of the coordination sphere of the lead atom, resulting in an average spectrum being observed in solution. Crystal packing forces could also contribute to the movement out of the plane of the lead atom when the complex is in the solid state, due to the presence of the coordinating DCM molecule. This was explored further in computational studies (*vide infra*). The ¹⁹F NMR spectrum shows three signals which are in very close agreement to the corresponding signals in methyl borate **10**, indicating the presence of a noncoordinating pentafluorophenyl borate compound. A ²⁰⁷Pb{¹H} NMR signal was observed at δ -951, significantly upfield from the alkyl complexes (average δ ~3000 ppm).

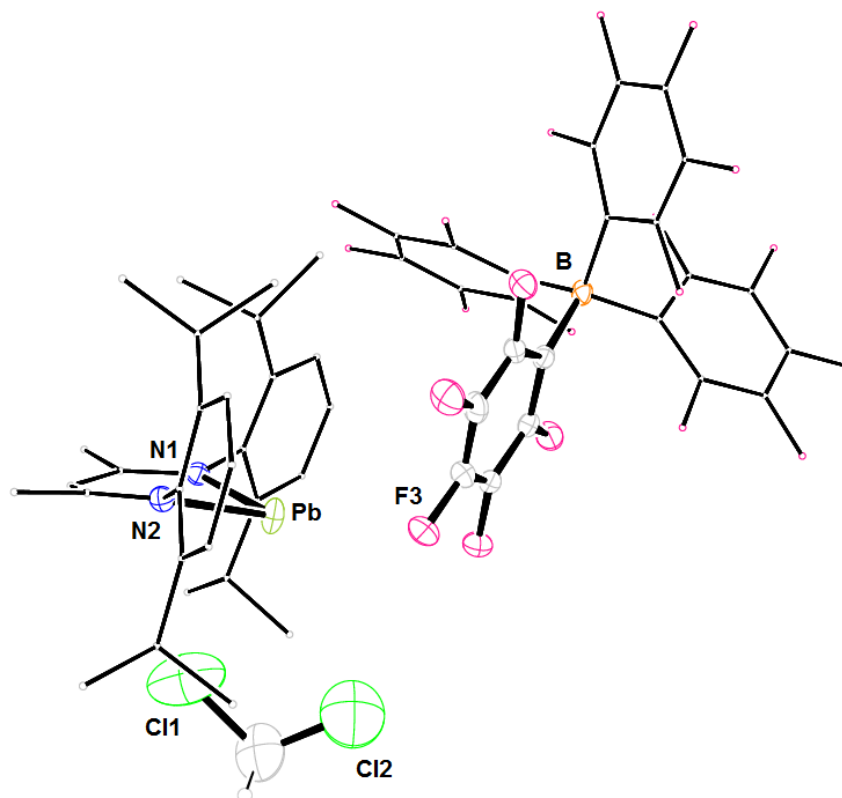


Figure 36 – $[\text{LPb}]^+ [\text{B}(\text{C}_6\text{F}_5)_4]^-$ (**11**) with coordinated DCM. 30% probability ORTEP ellipsoids, BDI ligand and three C_6F_5 rings minimised, and H-atoms omitted for clarity.

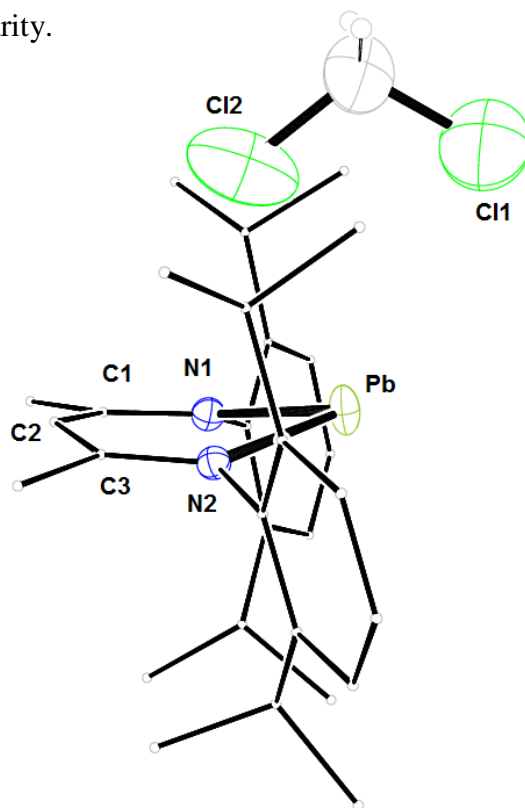
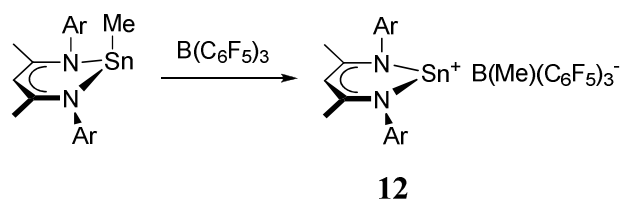


Figure 37 – $[\text{LPb}]^+ [\text{B}(\text{C}_6\text{F}_5)_4]^-$ (**11**) side-on, showing position of coordinated DCM molecule. 30% probability ORTEP ellipsoids, BDI ligand minimised and $[\text{B}(\text{C}_6\text{F}_5)_4]^-$ anion and H-atoms omitted for clarity.

2.2.3 Synthesis and characterisation of β -diketiminate stannyl-(II)-ene tris-(pentafluorophenyl) (methyl) borate, $[\text{LSn}]^+ [\text{B}(\text{Me})(\text{C}_6\text{F}_5)_3]^-$ (**12**)

In the same fashion as the lead complexes **10** and **11**, tin methyl borate **12** was synthesised by addition of *tris*-pentafluorophenyl borane to a dichloromethane solution of β -diketiminate tin(II) methyl at -10°C . After warming to room temperature, and stirring for two hours, the solvent was removed and pale yellow methyl borate **12** was isolated in 38% yield. The tin complex was observed to be insoluble in aliphatic and aromatic hydrocarbon solvents, but was soluble in halogenated and ethereal solvents such as dichloromethane and diethyl ether. The compound was also observed to be very stable at room temperature, and did not show evidence of degradation upon exposure to light sources.

Scheme 47 – Synthesis of $[\text{LSn}]^+ [\text{B}(\text{Me})(\text{C}_6\text{F}_5)_3]^-$ (**12**). Ar = 2,6-diisopropylphenyl.



Attempts to crystallise a sample of methyl borate **12** in non-coordinating solvents were unsuccessful. However, on cooling a concentrated diethyl ether solution of the complex to -30°C , crystals were obtained suitable for X-ray diffraction studies. The solid-state structure has a diethyl ether molecule bound to the metal centre, where the Sn-O distance is 0.133 \AA longer than that in the triflate, LSnOTf ,³⁴ and $0.364\text{--}0.382 \text{ \AA}$ longer than in the tin alkoxide complexes, LSnOR ($\text{R} = {}^i\text{Pr}, {}^s\text{Bu}, {}^t\text{Bu}$).³⁸ Due to the presence of this coordinated Et_2O molecule, the tin atom is displaced from the C_3N_2 plane by 0.473 \AA . This is 0.334 \AA and 0.177 \AA smaller than the displacement in the parent LSnMe and the triflate, LSnOTf , respectively.^{34,36} The Sn-N bond distances are shorter than those of the parent LSnMe (by $\sim 0.07 \text{ \AA}$) and of LSnCl (by $\sim 0.04 \text{ \AA}$), but very similar to those of LSnOTf .^{34,36} This indicates a more electropositive metal centre, and supports the evidence for the presence of a cationic tin species. In common with lead borate **11**, the N1-Sn-N2 bond angle of $86.61(7)^\circ$ is wider than the parent LSnMe ($84.69(7)^\circ$),³⁶ potentially due to the decrease in steric bulk at the metal centre.

The DOP around the tin atom is 98.13%, which is 6.54% smaller than that reported for the tin triflate.³⁴ However, the DOP around the oxygen is 2.86%, showing that the oxygen atom is very close to planarity, and three-coordinate.

Table 17 – Bond angles (°) and lengths (Å) for [LSn]⁺ [B(Me)(C₆F₅)₃][−] (**12**) with coordinated diethyl ether.

N1-Sn-N2	86.61(7)	N1-Sn	2.1342(17)
C1-N1-C6	117.97(17)	N2-Sn	2.1480(17)
C1-N1-Sn	124.86(14)	Sn-O	2.3872(17)
C6-N1-Sn	117.16(13)	B-C52	1.633(4)
C3-N2-C18	120.44(18)	O-C30	1.445(4)
C3-N2-Sn	126.51(15)	O-C32	1.447(4)
C18-N2-Sn	112.29(12)	N1-C1	1.347(3)
N1-C1-C2	124.5(2)	C1-C2	1.392(3)
C1-C2-C3	128.7(2)	C2-C3	1.395(3)
C2-C3-N2	123.6(2)	C3-N2	1.332(3)
Sn – plane	0.473	DOP _{tin} (%)	98.13
		DOP _{oxygen} (%)	2.86

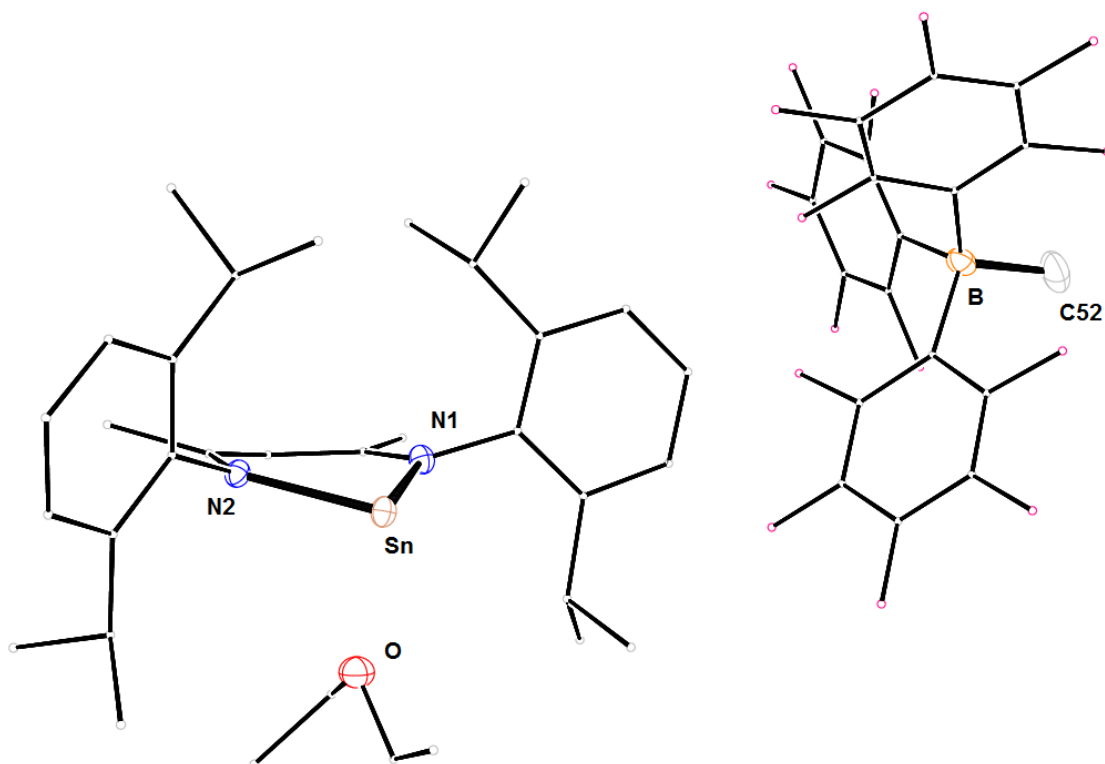


Figure 38 – $[\text{LSn}]^+ [\text{B}(\text{Me})(\text{C}_6\text{F}_5)_3]^-$ (**12**) with coordinated Et_2O . 30% probability ORTEP ellipsoids, BDI ligand, ethyl groups and C_6F_5 rings minimised, and H-atoms omitted for clarity.

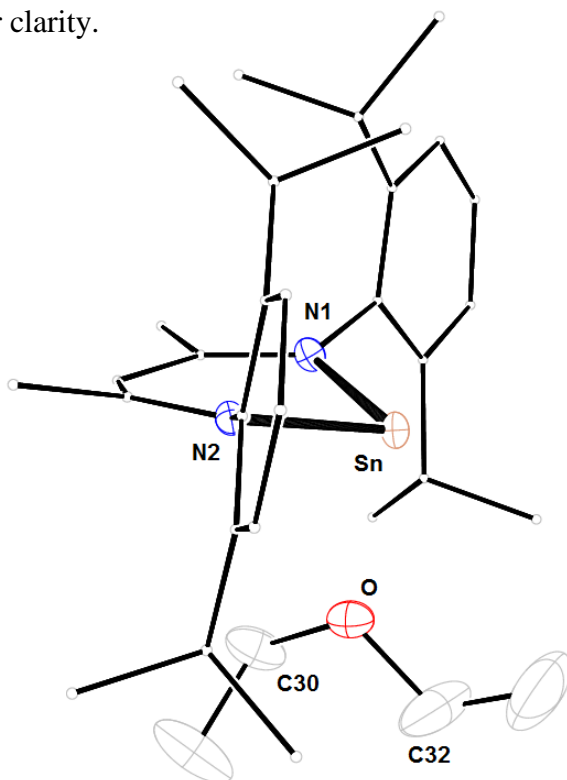


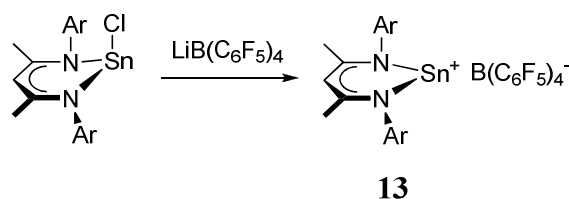
Figure 39 – $[\text{LSn}]^+ [\text{B}(\text{Me})(\text{C}_6\text{F}_5)_3]^-$ (**12**) side-on, showing position of coordinated Et_2O molecule. 30% probability ORTEP ellipsoids, BDI ligand minimised and $[\text{B}(\text{Me})(\text{C}_6\text{F}_5)_3]^-$ anion and H-atoms omitted for clarity.

In the ^1H NMR spectrum (CD_2Cl_2), only one environment is observed for the *iso*-propyl methyne protons on the ligand, at δ 2.71 ($J = 6.8$ Hz), leading to the same conclusion as for lead borate **11**; the environment in solution allows the ether molecule to rapidly move in and out of the coordination sphere of the metal, or the metal centre is displaced from the C_3N_2 plane in the solid state due to the coordination of diethyl ether. A $^{119}\text{Sn}\{^1\text{H}\}$ NMR signal was observed at δ -139.5, significantly upfield from that of the parent LSnMe , at δ 192.7.³⁶

2.2.4 Synthesis and characterisation of β -diketiminato stannyl-(II)-ene tetrakis-(pentafluorophenyl) borate, $[\text{LSn}]^+ [\text{B}(\text{C}_6\text{F}_5)_4]^-$ (**13**)

Similar to the case with the corresponding lead system, borate **11**, treatment of LSnCl with one equivalent of $\text{Li}[\text{B}(\text{C}_6\text{F}_5)_4]$ at -78°C results in the formation of stannylene $[\text{LSn}]^+ [\text{B}(\text{C}_6\text{F}_5)_4]^-$ after two hours of stirring at room temperature. After filtration through Celite®, tin borate **13** was isolated in 42% yield. In addition to being soluble in halogenated solvents such as dichloromethane, borate **13** is also stable in ethereal solvents such as diethyl ether. However, despite repeated attempts, no crystals suitable for X-ray diffraction studies were able to be grown.

Scheme 48 – Synthesis of $[\text{LSn}]^+ [\text{B}(\text{C}_6\text{F}_5)_4]^-$ (**13**). Ar = 2,6-diisopropylphenyl.

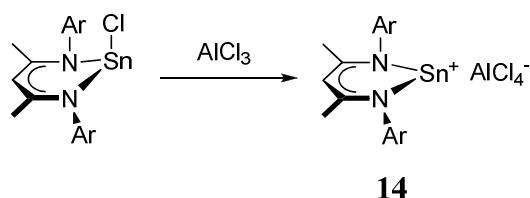


The ^1H NMR spectrum shows one environment for the *iso*-propyl methyne protons on the ligand at δ 2.95 ($J = 6.8$ Hz), indicating a solution-phase symmetric environment around the metal centre, similar to the rest of the series. Three distinct environments are present in the ^{19}F NMR, with a $\Delta\delta(m,p\text{-F})$ value of 2.6 ppm, indicating a non-coordinating anion. A $^{119}\text{Sn}\{^1\text{H}\}$ NMR signal was observed at δ 197.0, significantly downfield from that of the parent tin chloride, LSnCl , at δ -224.³⁴ Despite multiple attempts, a satisfactory elemental analysis for this compound was unable to be obtained.

2.2.5 Synthesis and characterisation of β -diketiminate stannyl-(II)-ene tetrachloroaluminate, $[\text{LSn}]^+ [\text{AlCl}_4]^-$ (**14**)

By the addition of AlCl_3 to the tin chloride, LSnCl , the chloride group was abstracted in a similar fashion to the methyl group in the lead complex **10** and the tin complex **12**. A dichloromethane solution of aluminium trichloride held at -78°C was treated with one equivalent of β -diketiminate tin(II) chloride and allowed to warm to room temperature. After stirring for two hours, tin tetrachloroaluminate **14** was isolated in 33% yield. The complex was found to be only soluble in halogenated solvents such as dichloromethane, and did not show any evidence of decomposition on exposure to light sources.

Scheme 49 – Synthesis of $[\text{LSn}]^+ [\text{AlCl}_4]^-$ (**14**). Ar = 2,6-diisopropylphenyl.



The solution-phase ^1H NMR spectrum in deuterated DCM showed one environment for the *iso*-propyl methyne protons on the ligand, with a septet at δ 3.26 ($J = 6.7$ Hz), indicating a symmetrical environment around the metal centre, in similar fashion to the rest of the plumbyl and stannyl complexes in the series. A $^{119}\text{Sn}\{^1\text{H}\}$ NMR signal was observed at δ 626.6, significantly more downfield from the other stannylene complexes in the series, as well as the parent tin chloride. A sharp $^{27}\text{Al}\{^1\text{H}\}$ NMR signal was observed at δ 99.7, indicative of an $[\text{AlCl}_4]^-$ anion.⁷⁷

However, when placed in a concentrated dichloromethane solution at -30°C to crystallise, the compound decomposed and crystallised as a compound in which the BDI ligand is protonated at the γ -carbon, and coordinated to a cationic aluminium centre. (figure 40). This compound has not been previously characterised, and does not appear in the Cambridge Structural Database. However, despite our attempts, the complex is unable to be reproduced, due to the exact conditions for formation being unknown; the BDI-Al complex $[(\text{H})\text{LAlCl}_2]^+ [\text{AlCl}_4]^-$ was generated by accident. Searches of the Cambridge Structural Database do not reveal any other complexes with a similar ligand.

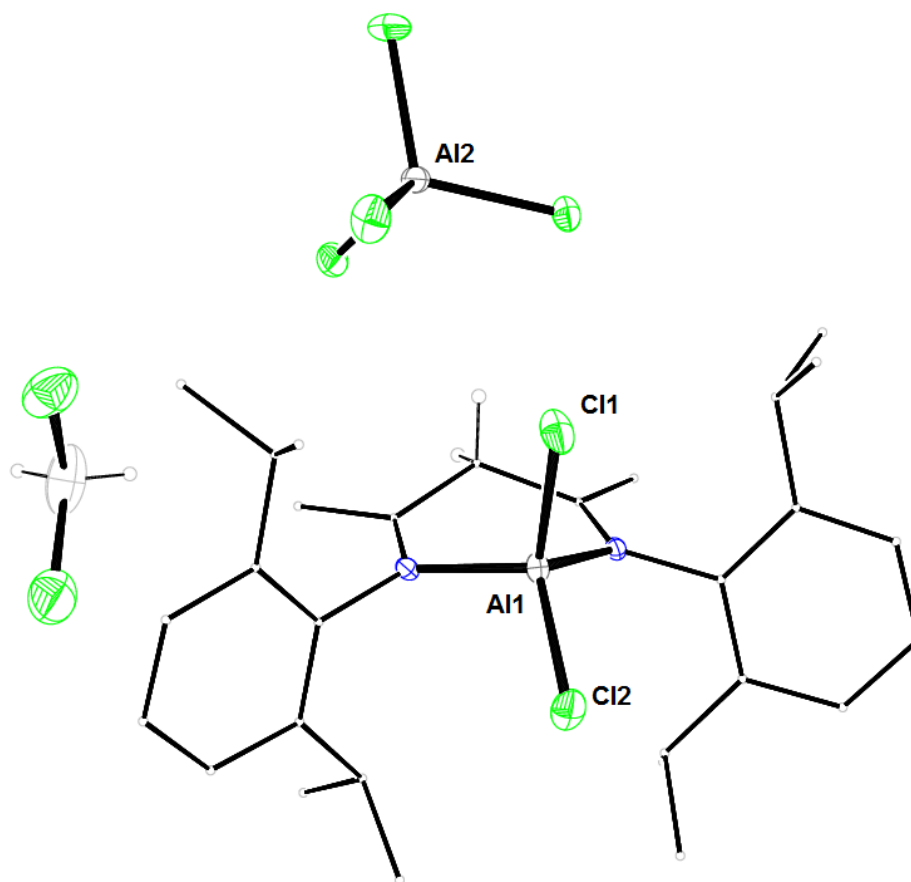


Figure 40 – $[(H)LAICl_2]^+ [AlCl_4]^-$ with coordinated DCM. 30% probability ORTEP ellipsoids, BDI ligand minimised and H-atoms omitted for clarity.

This aluminium complex has a tetrahedral carbon in the γ -position in the backbone, which is pushed out of the plane of the ligand in a similar way to the metal atom (figure 41). The crystal adopts a boat-type configuration, with the aluminium atom displaced out of the $N1-C1-C3-N2$ plane of the ligand by 0.546 Å. The γ -carbon, C2, is displaced by a smaller amount from this plane (0.370 Å). A non-coordinating dichloromethane molecule is also observed in the crystal structure, with $Al-Cl_{(DCM)}$ distances upwards of 5.79 Å, far outside the van der Waals radii for an Al-Cl interaction.

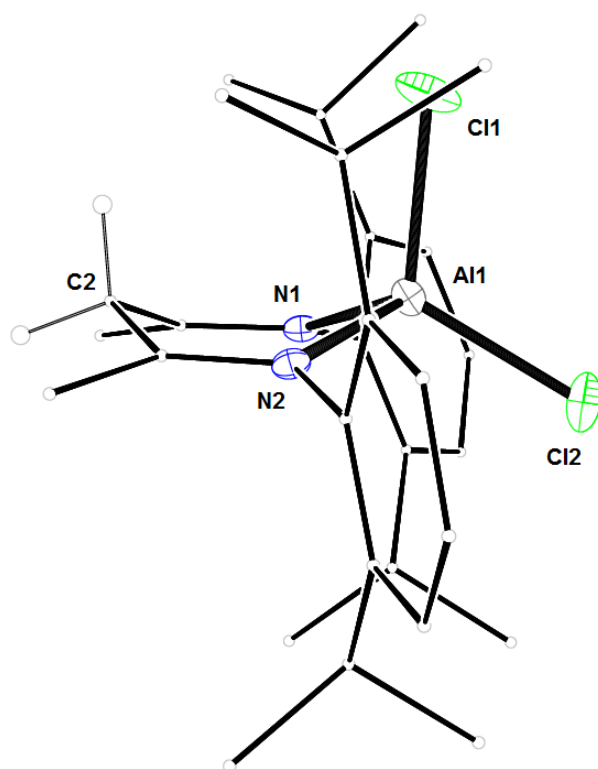
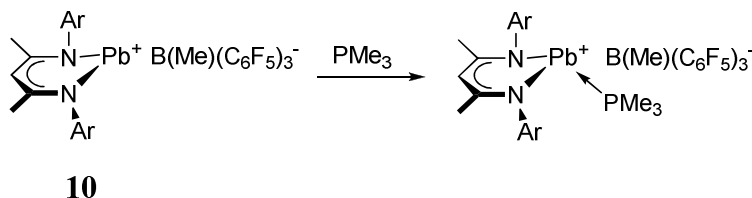


Figure 41 – $[(H)LAICl_2]^+ [AlCl_4]^-$ side-on, showing displacement of C2 from the ligand plane. 30% probability ORTEP ellipsoids, BDI ligand minimised and H-atoms, coordinated DCM molecule and $[AlCl_4]^-$ anion omitted for clarity.

2.3 Reactivity studies

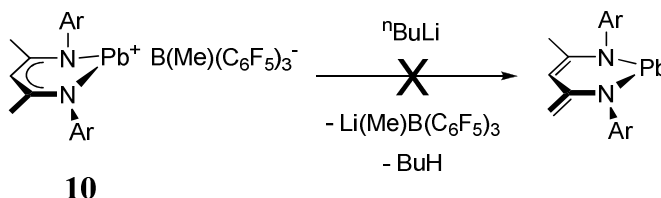
A neutral phosphine was added to one equivalent of methyl borate **10** in an attempt to generate a coordination complex in scheme 50. Upon addition, a colour change from red to yellow was observed, and a new peak was present in the ^{31}P NMR spectrum. The reaction was seen to decompose after a few days at room temperature into an unidentifiable mixture of products. However, this reactivity was unable to be duplicated when the reaction was scaled up.

Scheme 50 – Addition of coordinating PMe_3 to $[\text{LPb}]^+ [\text{B}(\text{Me})(\text{C}_6\text{F}_5)_3]^-$ (**10**). Ar = 2,6-diisopropylphenyl.



In an attempt to form a neutral lead (II) species, analogies were drawn with the germanium equivalent studied by Dreiss and co-workers.⁷⁴ One equivalent of butyl lithium was added to methyl borate **10** (scheme 51). However, this resulted in an immediate precipitation of black powder, assumed to be $\text{Pb}(0)$. The ^1H NMR spectrum showed a complex mixture of products that were unable to be isolated.

Scheme 51 – Test reaction, with suggested product, for deprotonating one of the methyl groups to form a neutral, two-coordinate plumbylene. Ar = 2,6-diisopropylphenyl.



2.4 Computational studies

Using the same methodology (B3LYP) as with the alkyl complexes, lead borate **11** and tin methyl borate **12** were studied using Gaussian G03W and Gaussview v9.0. Combined optimisation/frequency calculations using only the LANL2DZ basis set were carried out over both complexes, using the solid state structure as a starting point. A second set of calculations was carried out with a mixed basis set of LANL2DZ over the metal centre, to account for the large number of electrons, with 6-31G* used over all other atoms. The compounds were treated as ionic in nature, and the anions were omitted from the calculations to reduce processing time. The charge defined in all calculations is +1. Any coordinating solvent molecules were still included, and the stabilisation effect due to the solvent interactions were calculated by performing calculations on the lone solvent molecules, and combining the energies derived from these with the energies from the free cation calculations, then finding the energy difference. However, where two or more fragments of a molecule interact, their basis functions overlap during the course of a calculation and improve the calculation of derived properties such as energy. Therefore, the energy of the system of interacting fragments does not equal the sum of the energy of each individual fragment, when added to the stabilisation energy. This mismatch is referred to as basis set superposition error (BSSE). The calculations carried out on lead complex **11** and tin complex **12** are not corrected for this.⁷⁰ BSSE can be calculated by using Counterpoise Correction calculations, but our attempts at this failed.

The HOMO, LUMO and lone pair energy levels were obtained from the NBO analysis of the calculations, and the number of energy levels between the lone pair and the HOMO was noted. In common with the lead alkyl complexes, the natural electron configuration was noted, comprising measurements such as the occupancy and *s*- and *p*-orbital contributions to the lone pair.

Data tables can be found in appendix 2 (bond lengths, bond angles and molecular orbital energy levels).

2.4.1 Discussion of geometry optimisations

For the lead pentafluorophenyl borate $[\text{LPb}]^+ [\text{B}(\text{C}_6\text{F}_5)_4]^-$ **11**, computational calculations were performed on the free cation, $[\text{LPb}]^+$, and on the dichloromethane-solvated cation, $[\text{LPb}]^+.\text{DCM}$. The metal centre is shown to lie within the C_3N_2 plane in the free cation, but is moved out of the plane in the dichloromethane-coordinated compound by 0.05 Å in the single basis set calculation, and by ~ 0.02 Å in the mixed set calculation. This is much less than in the solid state structure, but somewhat expected, as the calculations omit the bulky anion which would have played a large role in the packing of the molecules within the crystal. The internal N1-Pb-N2 angles are slightly larger (~2-4°) than those in the lead alkyl complexes, most likely due to the absence of a substituent on the metal centre, which is now two-coordinate, as opposed to three-coordinate. Although the solid state structure was used as the starting geometry, the dichloromethane molecule was shown to change position relative to the lead centre over the course of the calculation (figure 42). This change of position moves the solvent molecule so that the Pb-Cl distance increases from 3.208(6) Å in the solid state to an average of 4.857 Å in the calculations, accounting for the two different calculations. This computed distance lies outside of the Pb-Cl van der Waals radii of 3.77 Å, indicating that the metal centre is indeed two-coordinate in the gas phase.

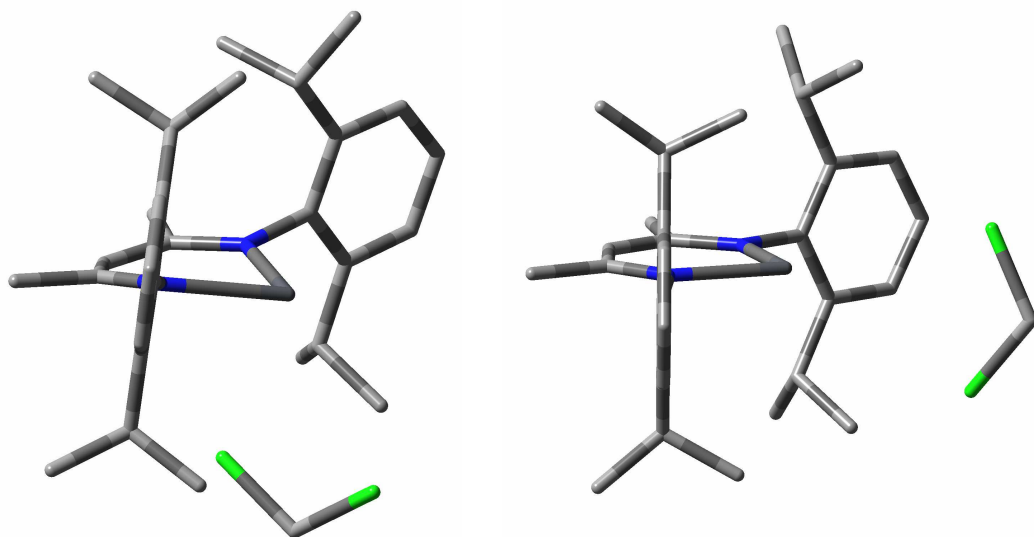


Figure 42 – Solid state (starting) geometry (left), and optimised geometry (right) for solvated cation $[\text{LPb}]^+.\text{DCM}$.

In a similar fashion to lead borate **11**, calculations were performed on both the free cation and the solvent-coordinated cation of tin methyl borate $[\text{LSn}]^+ [\text{B}(\text{Me})(\text{C}_6\text{F}_5)_3]^-$ **12**, with both the single and mixed basis sets. Coordination of diethyl ether to the metal centre moves the tin atom out of the C_3N_2 plane of the ligand by a very similar amount in both the single and mixed basis set calculations, around 0.373 Å. This is far greater than the displacement of the metal centre in the previous lead cationic complex, possibly due to the greater interaction from the solvent molecule. The distance between the tin atom and the C_3N_2 plane of the ligand is ~ 0.1 Å smaller than is evident in the solid state, allowing an indication of the effects of solid-state as opposed to gas-phase structure, as well as the added presence of the anion, omitted in the computational calculations. The Sn-O distance is ~ 2.435 Å, having been lengthened by ~ 0.5 Å from that found in the solid state. However, this distance lies well within the Sn-O van der Waals radii of 3.69 Å, indicating a coordination interaction between the two fragments. The internal N1-Sn-N2 angle is an average of 88.37° , which is $\sim 0.5^\circ$ larger than the internal angle in the reported LSnOTf ,³⁴ and $\sim 5^\circ$ larger than those reported in the tin alkoxides.³⁸

The diethyl ether molecule in tin methyl borate **12** lies in an *endo*- position, on the same side of the C_3N_2 plane as the metal atom, with a very low DOP around the oxygen of 0.48% for the single set calculation, and 0.91% for the mixed set calculation. These values indicate the environment around the oxygen atom is very close to planarity, perpendicular to the C_3N_2 ring. The DOP of the oxygen in the crystal structure is around 2% larger than that found by computation. The DOP of the tin atom from the calculations is $\sim 94\%$. This is $\sim 4\%$ smaller than that observed in the solid state and around 3-6% smaller than that observed in the tin alkoxide crystal structures.³⁸

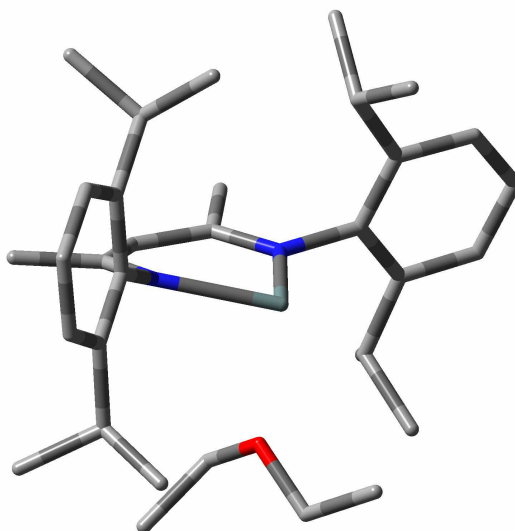


Figure 43 – Optimised geometry for solvated cation $[\text{LSn}]^+ \cdot \text{Et}_2\text{O}$.

2.4.2 Solvent stabilisation effects

Although the close proximity of the dichloromethane molecule stabilises the lead cation by $3.16 \text{ kcal mol}^{-1}$, this stabilisation is not due to any direct bonding between the metal centre and the solvent. The electronic energies (E), thermal enthalpies (H) and thermal free energies (G) for the single basis set calculation were very high due to the final position of the coordinated dichloromethane molecule in the output (figure 44).

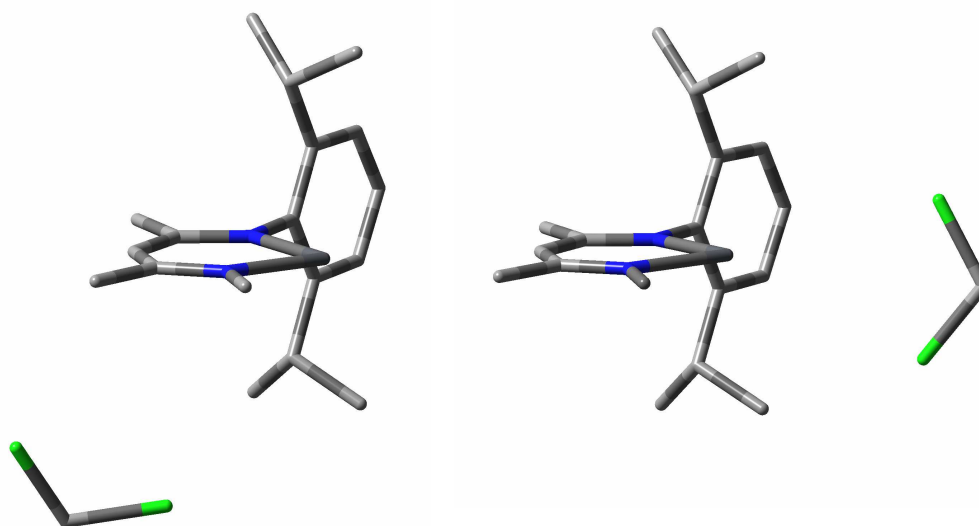


Figure 44 – Position of the DCM molecule in the output from the single basis set calculation (left) and the mixed basis set calculation (right). An N-aryl ring is omitted for clarity, but was present in the calculations.

The dichloromethane lies further away from the lead centre by 1.432 Å in the single set calculation than in the mixed set calculation, so this produces values of ΔE , ΔH and ΔG that are much closer to that of a free cation. Therefore, the energy difference between this calculation and the sum of the true free cation and dichloromethane is very large. Repeat calculations produced the same positioning of the solvent molecule, and so the result was assumed to be an inherent cause of using the LANL2DZ basis set over all of the atoms. The mixed basis set calculations produced far more plausible results, indicating that the solvated cation is $\sim 3.2 \text{ kcal mol}^{-1}$ more stable than the free cation.

Table 18 – Energy differences between calculations for lead borate **11**. Values are the stability of the solvated cation vs. free cation + dichloromethane.

Basis set	ΔE (kcal mol ⁻¹)	ΔH (kcal mol ⁻¹)	ΔG (kcal mol ⁻¹)	ΔS (cal K ⁻¹ mol ⁻¹)
Single	-558,000	-558,000	-558,000	24.5
Mixed	3.16	2.61	-4.55	24.0

In addition to the above stabilities, the strength of solvent interaction with the metal centre can also be supplied from the calculations. As the position of the DCM molecule differs between the single basis set and the mixed basis set calculations, this affects the strength of the interaction. The single basis set calculation shows little to no interaction between the DCM and metal centre ($< 0.5 \text{ kcal mol}^{-1}$), whereas the mixed set shows a small interaction of 1.0 – 1.2 kcal mol⁻¹. This supports the conclusion that the DCM molecule is weakly-coordinating.

Using the single basis set on the tin methyl borate **12**, the coordinated tin cation appears to be $\sim 8.1 \text{ kcal mol}^{-1}$ less stable than the combination of the free cation and solvent molecule. However, the mixed basis set calculation shows that the coordinated cation is $\sim 4.2 \text{ kcal mol}^{-1}$ more stable. Using the same reasoning as with the lead compound **11**, the use of the LANL2DZ basis set over all atoms produces higher values for ΔE , ΔH and ΔG than the calculation where LANL2DZ is used in conjunction with the 6-31G* basis set. As the mixed basis set produced more credible results in the calculations for lead borate **11**, it is logical to extend this plausibility to the mixed set calculation for the tin complex **12**, and place less importance upon the values derived from the single basis

set calculation. As such, we can see that the mixed set calculation shows that the coordinated cation is more stable than the free cation; which is what is observed in the solid state.

Table 19 – Energy differences between calculations for tin methyl borate **12**. Values are the stability of coordinated cation vs. free cation + diethyl ether.

Basis set	ΔE (kcal mol ⁻¹)	ΔH (kcal mol ⁻¹)	ΔG (kcal mol ⁻¹)	ΔS (cal K ⁻¹ mol ⁻¹)
Single	-8.09	-8.15	-22.0	46.4
Mixed	4.17	4.11	-9.95	47.2

It is worth noting that the ΔG term for both the tin and lead compounds is negative, as the entropy term is increased for the two distinct molecules of the free cation and solvent, against the single coordinated complex. This outweighs any thermodynamic stabilisation effects from the coordination of the solvent to the cation.

When regarding the energy of solvent interaction to the metal centre, a larger value is expected for the tin complex, compared to the lead complex, as the coordinating ether molecule is much closer to the metal centre. The single basis set calculation gives this energy as 24.5 kcal mol⁻¹, whereas the mixed set calculation provides a slightly lower value of 22.2 kcal mol⁻¹. These values are much higher than the solvent interaction energy of the lead complex, and so support the picture of a more-strongly-coordinating solvent molecule in the tin complex.

2.4.3 Molecular orbitals

Both calculations for the lead cationic complex **11** assign very similar energies (within 1-2 kcal mol⁻¹) to the HOMO and LUMO in each calculation. The HOMO-LUMO gap is ~ 95 kcal mol⁻¹, around 35 kcal mol⁻¹ smaller than the majority of the lead alkyl complexes. In common with the lead alkyl complexes, the LUMO of the lead cationic complex **11** is a dumbbell shape of an empty *p*-orbital, centred on the lead atom. This shows that the positive charge of the complex (i.e. a lack of electrons) can be formally

placed on the metal centre. However, in contrast to the lead alkyl complexes, the empty *p*-orbital in the cationic complex is aligned with the aryl groups on the BDI ligand, with the lobes of the orbital facing away from the aromatic rings (figure 45), consistent with the abstraction of a terminal substituent from the metal atom. This positioning of the orbital indicates that the cationic complex may be more reactive than its precursors in the lead alkyl series, as electrons can now be donated, unhindered, into the empty *p*-orbital. The HOMO of lead cationic complex **11** is located on one of the aryl rings of the BDI ligand (also figure 45) and is one of the aromatic C-C bonding orbitals. The orbital shapes of both the HOMO and LUMO did not change between the solvated cation and free cation calculations, and so the shape of the LUMO also demonstrates that there is no solvent coordination to the metal centre.

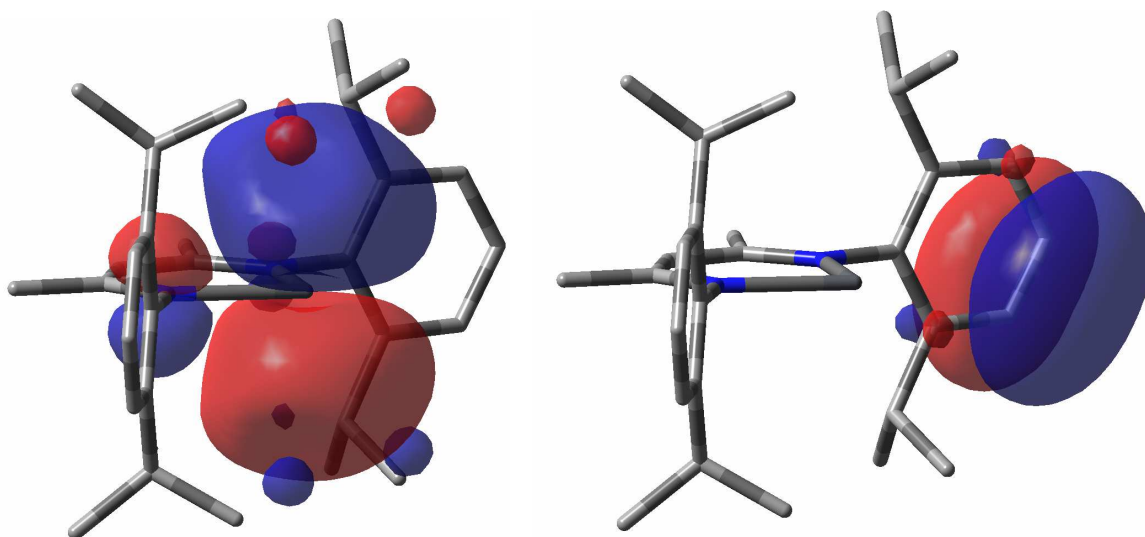


Figure 45 – View of the LUMO (left) and HOMO (right) of the lead cationic complex **11**. DCM molecule excluded for clarity; the presence of which does not affect the shape of the orbitals.

The lead-centred lone pair is found at the HOMO-15 level in the solvated calculation, and at HOMO-11 in the free cation calculation. These orbitals have similar energy to each other, at around $-340 \text{ kcal mol}^{-1}$. This is lower in energy than the lone pair orbital in the lead alkyl complexes, possibly due to the absence of another substituent and its associated molecular orbitals on the lead atom.

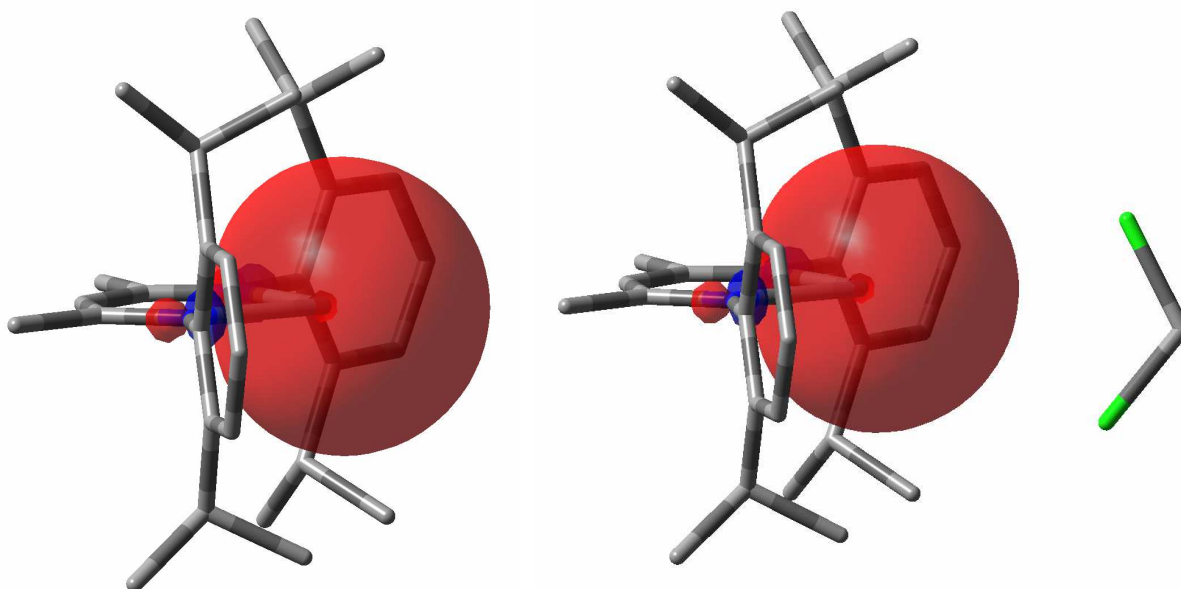


Figure 46 – View of the lead-centred lone pair for free cation $[\text{LPb}]^+$ (left, HOMO-11) and solvated cation $[\text{LPb}]^+.\text{DCM}$ (right, HOMO-15).

The HOMO-LUMO gap in the ether-coordinated tin methyl borate complex **12** differs between the two calculations, but both assign very similar energies to the HOMO energy level. The single set calculation indicates a HOMO-LUMO gap of $\sim 64 \text{ kcal mol}^{-1}$, whereas the mixed set calculation indicates a gap of nearly double this energy, at $\sim 104 \text{ kcal mol}^{-1}$. For the free cation, both calculations reveal the HOMO-LUMO gap to be $\sim 93 \text{ kcal mol}^{-1}$. In contrast to the lead cationic complex **11**, where the solvent molecule is non-coordinating, the inclusion of the coordinating ether molecule in tin complex **12** alters the orbital assigned as the LUMO of the complex. In the free cation calculations, where there is no coordinating solvent molecule present, the LUMO of the complex is an empty p -orbital (figure 47), in much the same manner as in the lead complex **11**. This is to be expected, as the central tin atom is two-coordinate, with no terminal substituent present. However, in the solvated cation calculation, when the diethyl ether molecule is included, the LUMO of the complex is no longer an empty p -orbital on the tin centre, but is now located on one of the carbon atoms on the C_3N_2 backbone of the BDI ligand (also figure 47). The movement of the LUMO can be attributed to the oxygen atom of the ether molecule donating electrons into the p -orbital on the metal centre, as this is the lowest-energy unoccupied orbital on the free cation, as described above. The presence or absence of the coordinating diethyl ether molecule does not affect the position of the HOMO, and in both the free- and solvated cation

calculations, the HOMO is located on an aryl ring of the BDI ligand, in a very similar fashion to the lead complex **11** (*vide supra*, figure 45).

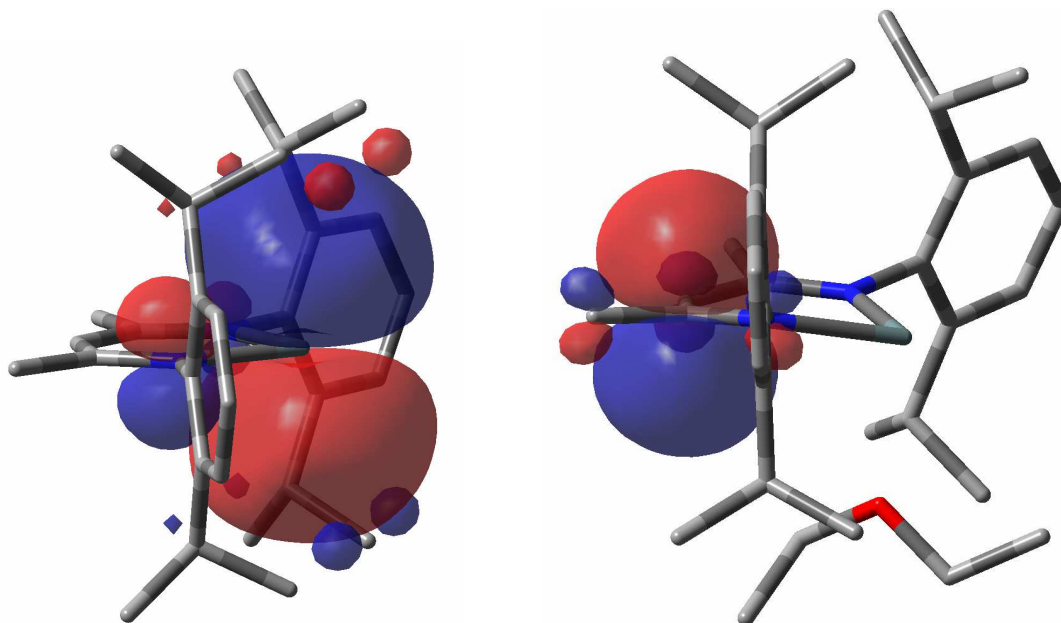


Figure 47 – View of the LUMO of the free cation $[\text{LSn}]^+$ (left) and solvated cation $[\text{LSn}]^+ \cdot \text{Et}_2\text{O}$ (right).

For both the free and solvated cation, the lone pair was recorded at the HOMO-9 level, with both calculations reporting very similar energy for the lone pair in the free cation, at $\sim 299 \text{ kcal mol}^{-1}$. In the solvated cation, the lone pair was found to be higher in energy, probably due to the coordination of a solvent molecule to the tin centre. The single set calculation reported the tin lone pair to be $\sim 10 \text{ kcal mol}^{-1}$ lower in energy than the corresponding orbital from the mixed set calculation.

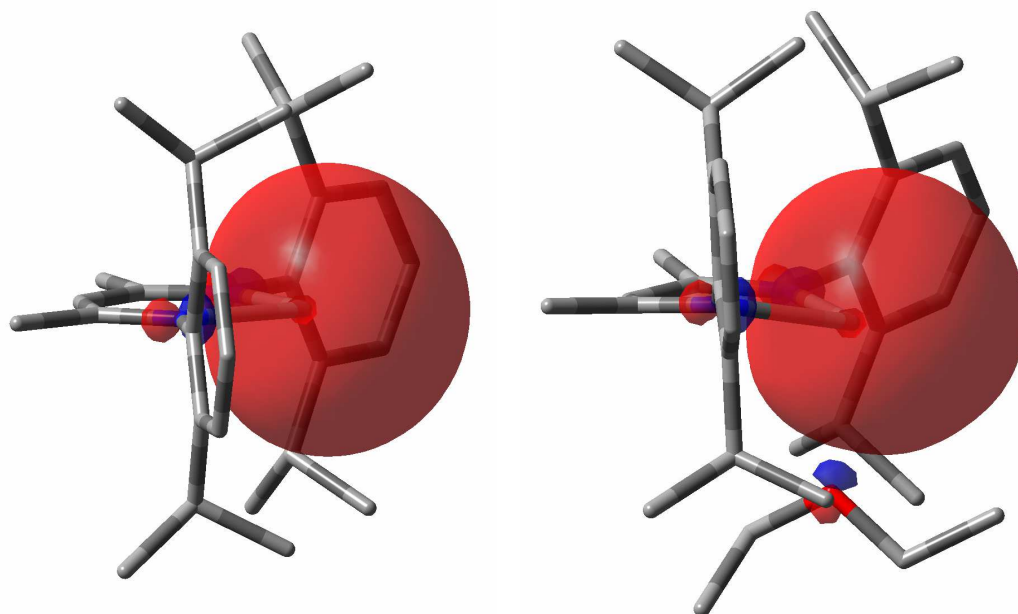


Figure 48 – View of the tin-centred lone pair for free cation $[\text{LSn}]^+$ (left) and solvated cation $[\text{LSn}]^+.\text{Et}_2\text{O}$ (right).

2.4.4 NBO analysis and natural electron configuration

From the NBO analysis, the occupancy and contribution to the lone pair from the *s*- and *p*-orbitals could be recorded. The lead cation calculations showed a higher *s*-orbital contribution to the lone pair by around 2.2% when compared to the parent lead chloride **2**, and a much higher *s*-orbital contribution, of around 6.5%, than the lead alkyl complexes. The free cation contributed a very slightly higher amount than the coordinated cation ($\sim 0.1\%$). The tin complexes also showed a higher *s*-orbital contribution to the lone pair than was present in the tin chloride, with the solvated complex giving a $\sim 2\%$ higher contribution, and the free cation giving a $\sim 4\%$ higher contribution. Comparisons were made with the single set calculations only, as this was the same level of theory used on the halide systems.⁴³ The increase in *s*-character from a halide, to an alkyl, to a solvated cation, to a free cation corresponds with an increase in the population of the 5*s* orbital (6*s* in the case of lead), and is consistent with the strength of the metal-substituent interaction – the weaker the interaction, the less *s/p* mixing is observed in the lone pair, leading to greater contribution from the *s*-orbital.

Table 20 – NBO analysis of metal centre for the lead and tin cationic complexes.

Compound	Natural electron configuration (Pb/Sn)	Lone pair NBO on Pb/Sn	Lone pair occupancy
LANL2DZ on all atoms.			
[LPb] ⁺ . [DCM]	6s (1.87), 6p (0.65)	s[94.00%] p 0.06 [6.00%]	1.979
[LPb] ⁺	6s (1.87), 6p (0.64)	s[94.09%] p 0.06 [5.91%]	1.979
[LSn] ⁺ . [Et ₂ O]	5s (1.77), 5p (0.72), 6p (0.01)	s[88.64%] p 0.13 [11.36%]	1.963
[LSn] ⁺	5s (1.81), 5p (0.72)	s[90.52%] p 0.10 [9.48%]	1.973
LANL2DZ on Pb; 6-31G* on all other atoms.			
[LPb] ⁺ . [DCM]	6s (1.91), 6p (0.66), 7p (0.01)	s[95.57%] p 0.05 [4.43%]	1.986
[LPb] ⁺	6s (1.89), 6p (0.69)	s[94.74%] p 0.06 [5.26%]	1.986
[LSn] ⁺ . [Et ₂ O]	5s (1.77), 5p (0.72), 6p (0.01)	s[88.64%] p 0.13 [11.36%]	1.963
[LSn] ⁺	5s (1.83), 5p (0.76)	s[91.32%] p 0.10 [8.68%]	1.981

2.5 *Summary*

We have synthesised a series of low-coordinate lead and tin cationic complexes. Initial reactions were carried out from lead methyl **3**, as the methyl substituent was observed to be able to be abstracted by a bulky borane species. The methodology was extended to the parent chloride **2** and the analogous tin complexes, LSnCl and LSnMe , which were found to form ionic tin complexes of similar form to the lead analogues. Aluminium trichloride was also able to be employed to abstract the chloride substituent from the parent tin chloride compound, LSnCl . This was unable to be carried out successfully with the equivalent lead complex. In solution, all the cations appear as symmetrical, but in the solid state some are observed to coordinate to solvent molecules. Computational calculations have revealed that the solvated complexes are slightly more stable than their free cationic analogues. Whilst the tin cation is observed to coordinate to a molecule of diethyl ether, the lead cation shows a minimal stabilisation effect from a very weakly coordinated DCM molecule.

2.6 Experimental details

*Synthesis of β -diketiminato lead tris-(pentafluorophenyl) methyl borate; $[LPb]^+$ $[B(Me)(C_6F_5)_3]^-$ (**10**)*

Lead methyl **3** (100 mg, 0.15 mmol) was dissolved in ~ 10 ml of dichloromethane in a Schlenk tube, and cooled to -10°C . To this was added a solution of $B(C_6F_5)_3$ (80 mg, 0.15 mmol) in ~10 ml of dichloromethane from another Schlenk tube, dropwise. The bright orange-red solution was left to stir for thirty minutes, then the dichloromethane solution concentrated and stored at -30°C to encourage crystallisation. Yield: 120 mg (66.7%).

^1H NMR (399.5 MHz, CD_2Cl_2 , 30°C): δ 7.43 (m, 6H, H_{aryl}), 5.50 (s, 1H, middle CH), 2.77 (sept, $J = 6.8$ Hz, 4H, CHMe_2), 2.02 (s, 6H, NCMe), 1.27 (d, $J = 6.8$ Hz, 12H, CHMe_2), 1.23 (d, $J = 6.9$ Hz, 12H, CHMe_2), 0.45 (s, 3H, Me).

$^{13}\text{C}\{^1\text{H}\}$ NMR (125.7 MHz, CD_2Cl_2 , 30°C): δ 167.5 (NCMe), 142.9, 137.4, 129.5, 125.1 (C_{aryl}), 115.9 (middle CH), 28.0 (CHMe_2), 26.6 (CHMe_2), 26.3 (NCMe), 23.0 (Ar_3BMe).

^{19}F NMR (375.9 MHz, CD_2Cl_2 , 30°C): δ -133.0 (d, $J = 19.7$ Hz, 6F, o -F), -165.3 (t, $J = 20.4$ Hz, 3F, p -F), -167.9 (td, $J = 23.5, 6.1$ Hz, 6F, m -F).

Elemental Analysis for $\text{C}_{48}\text{H}_{44}\text{N}_2\text{F}_{15}\text{BPb}$: Calc.: C, 50.04; H, 3.82; N, 2.43. Found: C, 50.13; H, 3.77; N, 2.36.

IR (KBr, nujol) / cm^{-1} : 1641.18 (s), 1510.62 (s), 1261.00 (s), 1087.11 (br), 1019.90 (br), 799.79 (s).

*Synthesis of β -diketiminato lead tetrakis-(pentafluorophenyl) borate; $[LPb]^+$ $[B(C_6F_5)_4]^-$ (**11**)*

Lead chloride **2** (150 mg, 0.22 mmol) was dissolved in ~ 10 ml of toluene in a Schlenk tube, and cooled to -78°C . $\text{Li}[B(C_6F_5)_4]$ (200 mg, 0.29 mmol) was mixed with ~10 ml of toluene in another Schlenk tube, and added dropwise to the cold solution of **2**. The mixture was allowed to stir for thirty minutes, after which the toluene was removed *in vacuo*, and dichloromethane was added. The bright red-orange solution was filtered by filter cannula to remove the white by-product, and then concentrated to encourage

crystallisation. Crystals were grown from slow diffusion of pentane into a concentrated dichloromethane solution of the compound at -30°C. Yield: 95 mg (33.1%).

^1H NMR (499.91 MHz, CD_2Cl_2 , 30°C): δ 7.44 (m, 6H, H_{aryl}), 5.48 (s, 1H, middle CH), 2.76 (sept, J = 6.9 Hz), 4H, CHMe_2), 2.02 (s, 6H, NCMe), 1.28 (d, J = 6.8 Hz, 12H, CHMe_2), 1.23 (d, J = 6.9 Hz, 12H, CHMe_2).

$^{13}\text{C}\{^1\text{H}\}$ NMR (100.5 MHz, CD_2Cl_2 , 30°C): δ 171.2 (NCMe), 144.2, 142.2, 130.0, 128.8, 124.5, 123.9, 114.5 (C_{aryl}), 91.8 (middle CH), 27.9, 27.4, 25.9, 25.6 (CHMe_2), 23.3, 23.2, 23.0, 22.9, 22.4 (CHMe_2), 21.5 (NCMe).

^{19}F NMR (375.9 MHz, CD_2Cl_2 , 30°C): δ -131.3 (m, 6F, o -F), -162.0 (t, J = 20.3 Hz, 3F, p -F), -165.9 (m, 6F, m -F).

^{207}Pb NMR (83.6 MHz, CD_2Cl_2 , 30°C): δ -951.2

Elemental Analysis for $\text{C}_{53}\text{H}_{41}\text{N}_2\text{F}_{20}\text{BPb}$: Calc.: C, 48.81; H, 3.15; N, 2.15. Found: C, 49.30; H, 3.47; N, 1.92.

IR (KBr, nujol) / cm^{-1} : 1644.57 (s), 1261.30 (s), 1089.65 (br), 1021.09 (br), 800.81 (s), 722.87 (s).

Synthesis of β -diketiminato tin tris-(pentafluorophenyl) methyl borate; $[\text{LSn}]^+ [\text{B}(\text{Me})(\text{C}_6\text{F}_5)_3]^-$ (12)

LSnMe (200 mg, 0.35 mmol) was dissolved in ~ 10 ml of dichloromethane in a Schlenk tube, and cooled to -10°C. $\text{B}(\text{C}_6\text{F}_5)_3$ (186 mg, 0.35 mmol) was mixed with ~10 ml of dichloromethane in another Schlenk tube, and added dropwise to the yellow solution. The solution was left to stir for two hours, then the mixture was filtered, and the dichloromethane removed *in vacuo*. A pale yellow solid was isolated. Yield: 130 mg (37.5%).

^1H NMR (499.91 MHz, CD_2Cl_2 , 20°C): δ 7.48 (m, 6H, H_{aryl}), 6.18 (s, 1H, middle CH), 2.71 (sept, J = 6.8 Hz, 4H, CHMe_2), 2.13 (s, 6H, NCMe), 1.29 (d, J = 6.8 Hz, 12H, CHMe_2), 1.20 (d, J = 6.9 Hz, 12H, CHMe_2), 0.46 (s, 3H, Me).

$^{13}\text{C}\{^1\text{H}\}$ NMR (100.5 MHz, CD_2Cl_2 , 20°C): δ 170.1 (NCMe), 142.9, 136.8, 129.9, 125.3 (C_{aryl}), 108.9 (middle CH), 28.6 (CHMe_2), 26.1, 24.1 (CHMe_2), 23.0 (NCMe), 21.1 (Ar_3BMe).

^{119}Sn NMR (223.6 MHz, CD_2Cl_2 , 30°C): δ -139.5

Elemental Analysis for $\text{C}_{48}\text{H}_{44}\text{N}_2\text{F}_{15}\text{BSn}$: Calc.: C, 54.21; H, 4.14; N, 2.64. Found: C, 54.30; H, 4.23; N, 2.56.

IR (KBr, nujol) / cm^{-1} : 1957.41 (s), 1642.55 (m), 1595.40 (m), 1510.57 (s), 1268.11 (m), 1168.34 (br), 1022.08 (m), 952.04 (br), 848.95 (br), 801.10 (s), 753.43 (s), 694.09 (s).

*Synthesis of β -diketiminate tin tetrakis-(pentafluorophenyl) borate; $[\text{LSn}]^+ [\text{B}(\text{C}_6\text{F}_5)_4]^-$ (**13**)*

LSnCl (100 mg, 0.17 mmol) was dissolved in ~ 10 ml of dichloromethane in a Schlenk tube, and cooled to -78°C . $\text{Li}[\text{B}(\text{C}_6\text{F}_5)_4]$ (117 mg, 0.17 mmol) was mixed with ~10 ml of dichloromethane in another Schlenk tube, and added dropwise to the cold LSnCl solution. The mixture was allowed to stir for two hours, after which the pale yellow solution was filtered to remove the white by-product, and then concentrated to encourage crystallisation. Yield: 87 mg (42.0%).

^1H NMR (499.91 MHz, CD_2Cl_2 , 30°C): δ 7.36 (m, 6H, H_{aryl}), 5.88 (s, 1H, middle CH), 2.97 (m, 4H, CHMe_2), 2.03 (s, 6H, NCMe), 1.25 (d, 12H, CHMe_2), 1.23 (d, 12H, CHMe_2).

$^{13}\text{C}\{^1\text{H}\}$ NMR (100.5 MHz, CD_2Cl_2 , 30°C): δ 168.5 (NCMe), 143.5, 138.2, 128.9, 125.0 (C_{aryl}), 105.7 (middle CH), 28.6 (CHMe_2), 26.1, 24.1 (CHMe_2), 23.5 (NCMe).

^{19}F NMR (375.9 MHz, CD_2Cl_2 , 30°C): δ -133.1 (d, J = 19.2 Hz, 6F, o -F), -165.3 (t, J = 20.3 Hz, 3F, p -F), -167.9 (td, J = 23.3, 6.2 Hz, 6F, m -F)

^{119}Sn NMR (223.6 MHz, CD_2Cl_2 , 30°C): δ 197.0

IR (KBr, nujol) / cm^{-1} : 1642.05 (s), 1511.13 (s), 1259.16 (m), 1167.82 (m), 978.33 (m), 798.67 (s), 773.24 (s), 755.10 (s), 694.10 (s), 659.01 (s).

*Synthesis of β -diketiminate tin tetrachloroaluminate; $[\text{LSn}]^+ [\text{AlCl}_4]^-$ (**14**)*

AlCl_3 (47 mg, 0.35 mmol) was mixed with ~10 ml of dichloromethane in a Schlenk tube, and cooled to -78°C . LSnCl (200 mg, 0.35 mmol) was dissolved in ~ 10 ml of dichloromethane in another Schlenk tube, and the added dropwise to the cold AlCl_3 solution. The mixture was allowed to stir for two hours, after which the pale yellow solution was filtered, and then concentrated to encourage crystallisation. Yield: 82 mg (33.2%).

^1H NMR (499.91 MHz, CD_2Cl_2 , 30°C): δ 7.43 (m, 6H, H_{aryl}), 5.35 (s, 1H, middle CH), 2.83 (sept, 4H, CHMe_2), 2.21 (s, 6H, NCMe), 1.30 (d, 12H, CHMe_2), 1.28 (d, 12H, CHMe_2).

$^{13}\text{C}\{^1\text{H}\}$ NMR (100.5 MHz, CD_2Cl_2 , 30°C): δ 159.3 (NCMe), 140.6, 139.0, 123.6, 121.3 (C_{aryl}), 92.1 (middle CH), 26.4 (CHMe_2), 22.3, 21.2 (CHMe_2), 18.5 (NCMe).

^{27}Al NMR (104.1 MHz, C_6D_6 , 20°C) : δ 99.7

^{119}Sn NMR (149.0 MHz, C_6D_6 , 20°C) : δ 626.7

Elemental Analysis for $\text{C}_{29}\text{H}_{41}\text{N}_2\text{Cl}_4\text{AlSn}$: Calc.: C, 49.24; H, 5.80; N, 3.96. Found: C, 49.35; H, 5.96; N, 3.92.

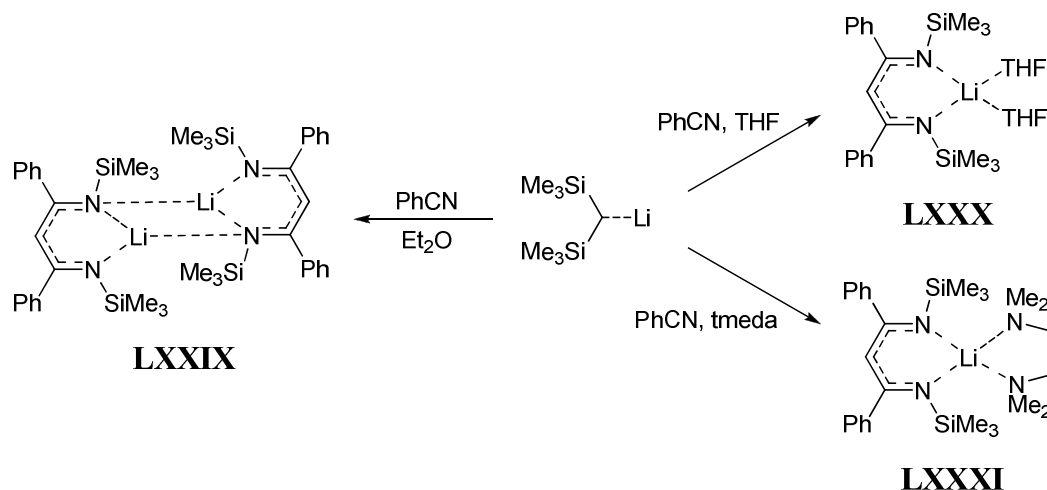
IR (KBr, nujol) / cm^{-1} : 1169.34 (br), 1020.68 (m), 966.06 (m), 891.35 (s).

3. Synthesis, structure and reactivity of β -diketiminate magnesium complexes

3.1 Magnesium and other *s*-block β -diketiminate complexes

The chemistry of *s*-block β -diketiminate complexes is very varied. Whilst many can be used as intermediates to generate more complex compounds, *s*-block complexes themselves are nevertheless very interesting. The first example of a fully characterised, crystalline, alkali metal β -diketiminate was produced by Lappert in 1994, obtained from a lithium alkyl and phenyl cyanide, as described above (**XII**).¹⁴ Lappert has used the same methodology to generate a large number of lithium β -diketimines, by varying the reagents and conditions, in addition to the presence or absence of a coordinating co-ligand, such as THF or tmeda.⁷⁸ In the absence of such a co-ligand, the resulting complex was observed to dimerise (**LXXIX**), to fill out the coordination environment around the lithium atom. However, the presence of a co-ligand allowed monomeric forms of lithiated β -diketimines to be isolated, with the co-ligand coordinating *in lieu* of a second β -diketiminate unit.

Scheme 52 – BDI dimerisation affected by the presence of a co-ligand.



The majority of lithium β -diketimines are formed by lithiation of the neutral β -diketimine by reagents such as methyl- or butyllithium. The compound $\text{Li}[\{(2,6\text{-}^i\text{Pr}_2\text{C}_6\text{H}_3)\text{NC}(\text{CH}_3)_2\text{CH}\}]$ was obtained in this fashion, in a monomeric solvated form, a dimeric form and a dodecameric form.¹³ The presence of a coordinating solvent yields the monomeric form, by coordination of a solvent molecule with the lithium metal centre. The absence of a coordinating solvent allows the compound to crystallise in two

associated forms. The dimeric form exists where the lithium atom is coordinated to the diisopropylphenyl ring on the ligand of a second molecule. The dodecameric form exists where this coordination extends along a chain of six (BDI)Li units, which are then duplicated by an inversion centre.

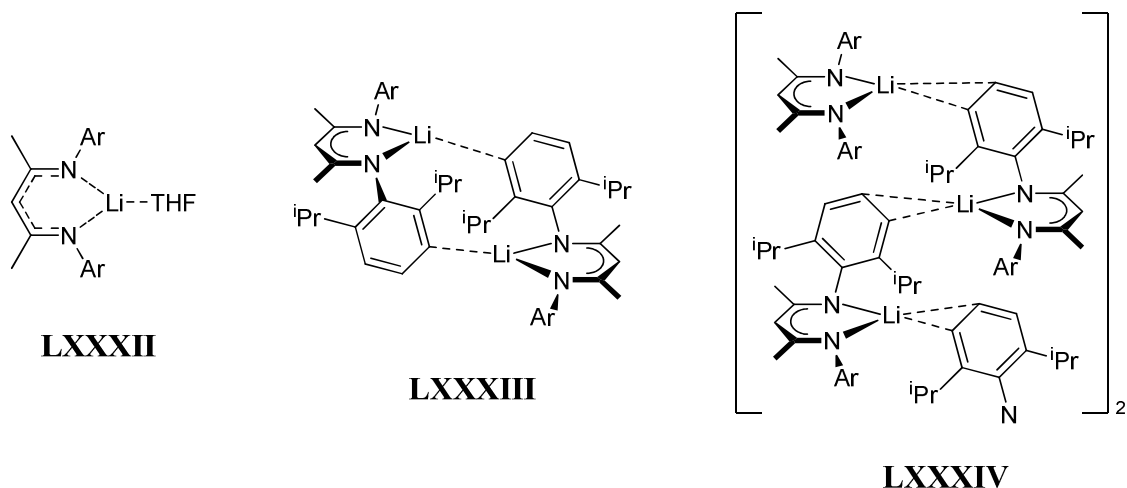
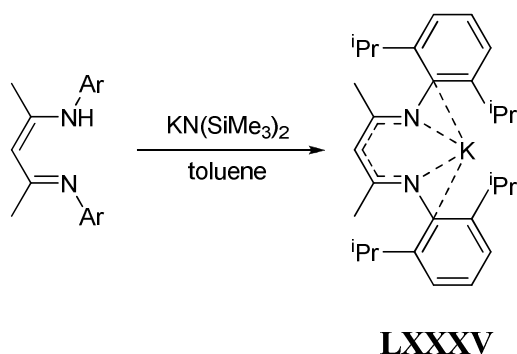


Figure 49 – Monomeric (left), dimeric (centre) and dodecameric (right) forms of (BDI)Li. Ar = 2,6-diisopropylphenyl.

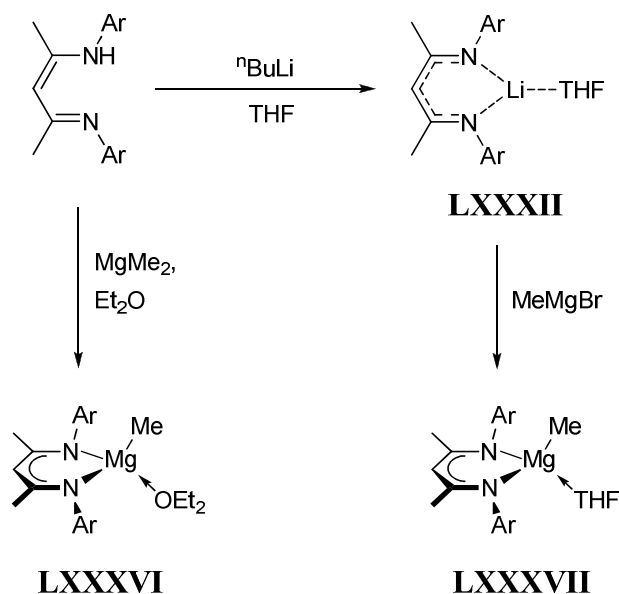
A potassium β -diketiminate salt has been isolated by Clegg and coworkers, where the BDI ligand has been observed to coordinate in a η^4 -fashion to the potassium centre.⁷⁹ This is presumably due to the larger ionic radius of the potassium ion, making it more difficult to fit into the coordination site of the BDI ligand, when compared to the smaller lithium ion. The compound also shows a tendency to polymerise by a η^5 -coordination from the metal atom to the aryl ring on a neighbouring molecule in the solid state, which is assumed to be replaced with an interaction to toluene when dissolved in solution.

Scheme 53 – Synthesis of BDI potassium. Ar = 2,6-diisopropylphenyl.



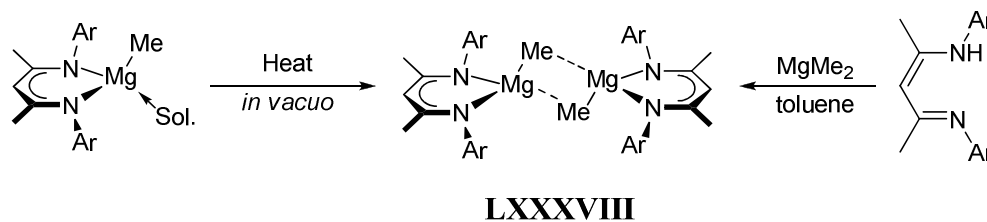
When using a β -diketiminate ligand around an alkaline earth metal centre, the second coordination site on the metal allows a wide variety of small organic groups to be substituted, and there are many examples of group two β -diketiminate complexes in the literature. One of the simplest examples is a magnesium methyl complex, commonly synthesised by one of two methods. Gibson and co-workers reported the synthesis of $\text{MeMg}[\{(2,6\text{-}^i\text{Pr}_2\text{C}_6\text{H}_3)\text{NC}(\text{CH}_3)_2\text{CH}\}.\text{OEt}_2]$ (**LXXXVI**) from the neutral β -diketimine and dimethylmagnesium, in the presence of diethyl ether,⁸⁰ whereas Bailey and co-workers have produced the THF equivalent (**LXXXVII**) from a two-stage process via the lithium salt (**LXXXII**), and then subsequent reaction with a methyl Grignard.⁸¹

Scheme 54 – Synthesis of solvated monomeric (BDI)MgMe species. Ar = 2,6-diisopropylphenyl.



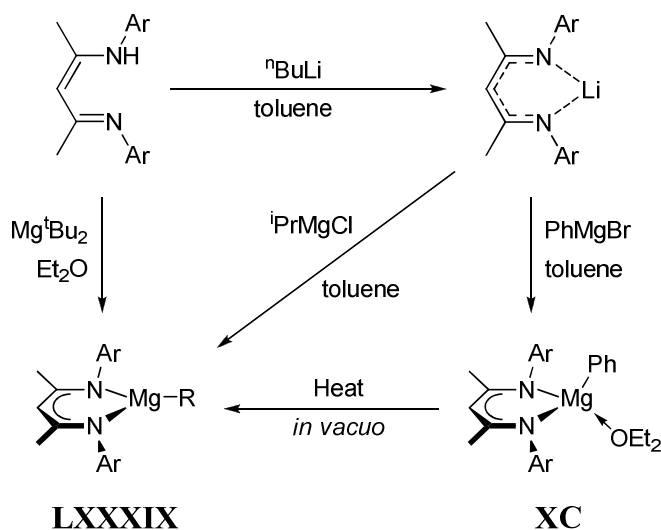
If the synthesis of a β -diketiminate magnesium alkyl complex is carried out in a polar solvent, such as diethyl ether or THF (scheme 54), then a solvent molecule is observed to coordinate to the metal centre. Upon removal of the coordinated solvent, both Bailey and Gibson observed the molecule to dimerise, with bridging methyl groups between the two magnesium centres (**LXXXVIII**).^{81,82} The dimer can also be synthesised in one step, by treating the neutral BDI ligand with dimethylmagnesium in a non-polar solvent such as toluene (scheme 55).⁸²

Scheme 55 – Synthesis of [(BDI)MgMe]₂ dimer. Ar = 2,6-diisopropylphenyl.
Sol. = Et₂O, THF



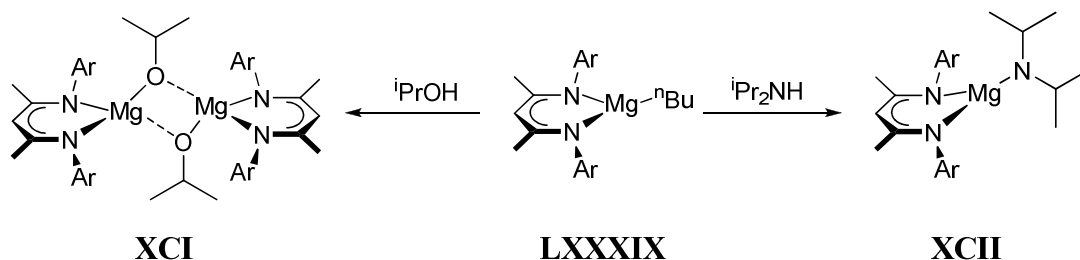
Gibson's work also shows the influence of steric effects – when a similar reaction is carried out with a bulky *tert*-butylmagnesium alkyl in a polar solvent, the monomeric structure is obtained (**LXXXIX**).⁸² This monomeric structure without solvent coordination can also be obtained from some Grignard reagents, but even if carried out in a non-polar solvent, the residual ether present in a Grignard reagent solution can be seen to coordinate to some complexes (**XC**).

Scheme 56 – Effect of increasing the steric bulk of the Grignard reagent. Ar = 2,6-disopropylphenyl. R = ^tBu, ⁱPr, Ph.



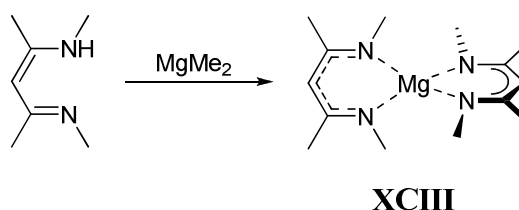
Gibson and co-workers have shown that these alkyls are effective precursors to β -diketiminato magnesium alkoxides or amides upon addition of one equivalent of a corresponding alcohol or amine, respectively.⁸² Synthesised in a “one-pot” procedure, the alkoxide structures displayed a dimeric form, with bridging alkoxide units between two magnesium centres. The amides generated by the same procedure were found to be monomeric in nature, probably due to the increase in steric bulk from a two- to three-coordinate substituent on the metal atom.⁸²

Scheme 57– Conversion of β -diketiminate magnesium alkyl complexes to alkoxides and amides.



Using a sterically uncrowded β -diketiminate ligand, a monometallic, *bis*- β -diketiminate compound can be synthesised, which can be formed using the dialkylmagnesium pathway in scheme 55. In this compound, the substituents at the R^3 positions, normally occupied by large aryl rings, are instead methyl groups, allowing space for two β -diketiminate fragments to coordinate to the same metal centre.⁸³

Scheme 58 – Synthesis of *bis*- β -diketiminate magnesium.

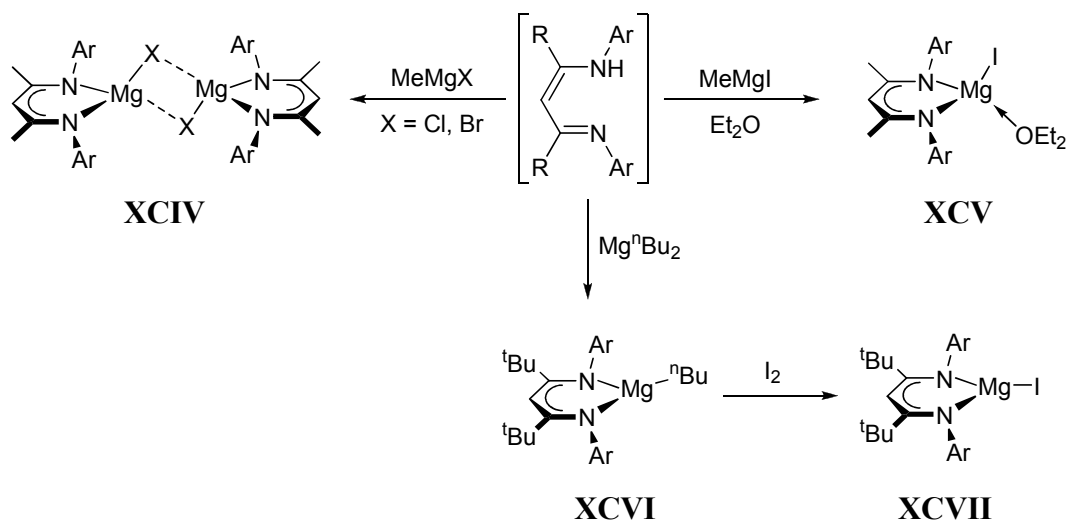


Bis- β -diketiminate magnesium complexes were also explored by Lappert and co-workers, using slightly bulkier substituents in the R^2 and R^3 positions, to form $\text{Mg}\{[(\text{Me}_3\text{Si})\text{NC}(\text{Ph})_2\text{CH}]_2\}$ (similar to **XCIII**). The steric constraints of this molecule force the central magnesium atom in a distorted tetrahedral environment, with the β -diketiminate ligands almost orthogonal to each other.⁸⁴

Group two β -diketiminate halide complexes can be obtained by reaction of a neutral β -diketimine directly with a Grignard reagent, but Gibson has shown that this leads to a dimeric magnesium halide structure, similar to the alkyl and alkoxide structures **LXXXVIII** and **XCI** respectively.⁸² Synthesis of a monomeric BDI magnesium halide has been carried out by Jones and co-workers using an iodo-Grignard in a polar solvent (**XCIV**).⁸⁵ However, the presence of a coordinating solvent yields the solvated compound. To overcome this, and generate an unsolvated, monomeric BDI magnesium halide, Jones employs a *tert*-butyl group at the R^2 position on the BDI ligand. This

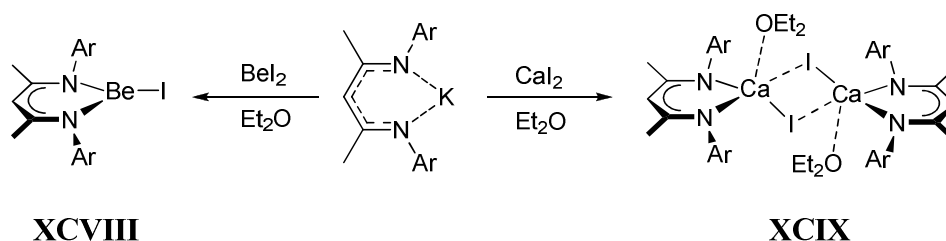
provides sufficient steric bulk to prevent both dimerisation and the coordination of solvent.

Scheme 59 – Generation of β -diketiminate magnesium halides. R = Me, ^tBu. Ar = 2,6-diisopropylphenyl.



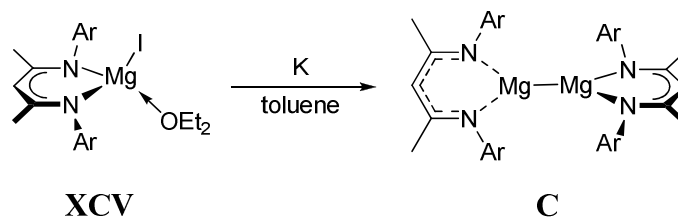
Jones and co-workers have also expanded their work to the rest of group 2, and have published the only known structure of a β -diketiminate beryllium halide, generated from the potassium β -diketiminate and beryllium diiodide.⁸⁵ A calcium analogue was also synthesised using the same procedure, but showed a similar tendency to dimerise as the magnesium compound.

Scheme 60 – Generation of beryllium and calcium β -diketiminate halides. Ar = 2,4,6-trimethylphenyl (**XCVIII**), 2,6-diisopropylphenyl (**XCIX**).



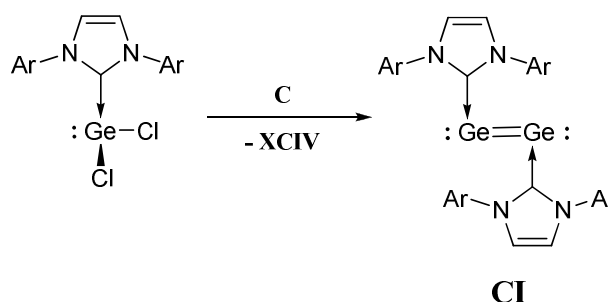
Reducing the solvated magnesium iodide β -diketiminate complex **XCV** with potassium metal, Jones synthesised the novel β -diketiminate magnesium dimer $[\text{Mg}\{(2,6\text{-}^i\text{Pr}_2\text{C}_6\text{H}_3)\text{NC}(\text{CH}_3)_2\text{CH}\}_2]_2$ (**C**). This (BDI)₂MgMg(BDI) complex is reported as the first example of a β -diketiminate magnesium(I) compound.⁸⁶

Scheme 61 – Synthesis of Jones' (BDI) magnesium(I) dimer **C**. Ar = 2,6-diisopropylphenyl.



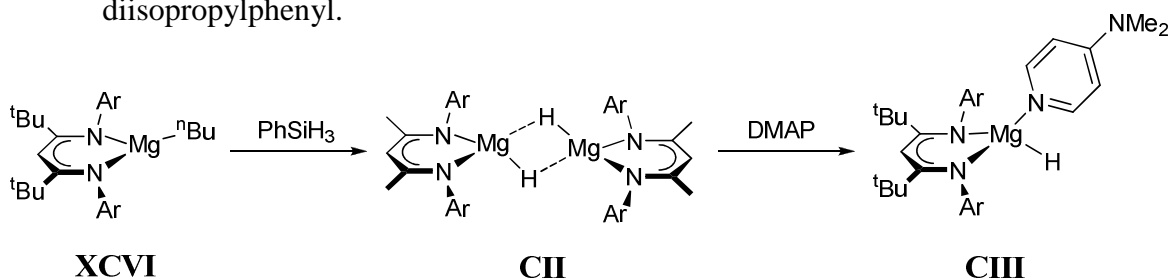
In 2009, Jones reported a potential application of this dimer as a reducing agent, in order to generate a rare example of digermanium(0), stabilised by an N-heterocyclic carbene.⁸⁷ The magnesium dimer **C** was converted to the bridged chloride dimer **XCIV**, described earlier.

Scheme 62 – The ability of dimer **C** to reduce Ge(II) to Ge(0). Ar = 2,6-diisopropylphenyl.



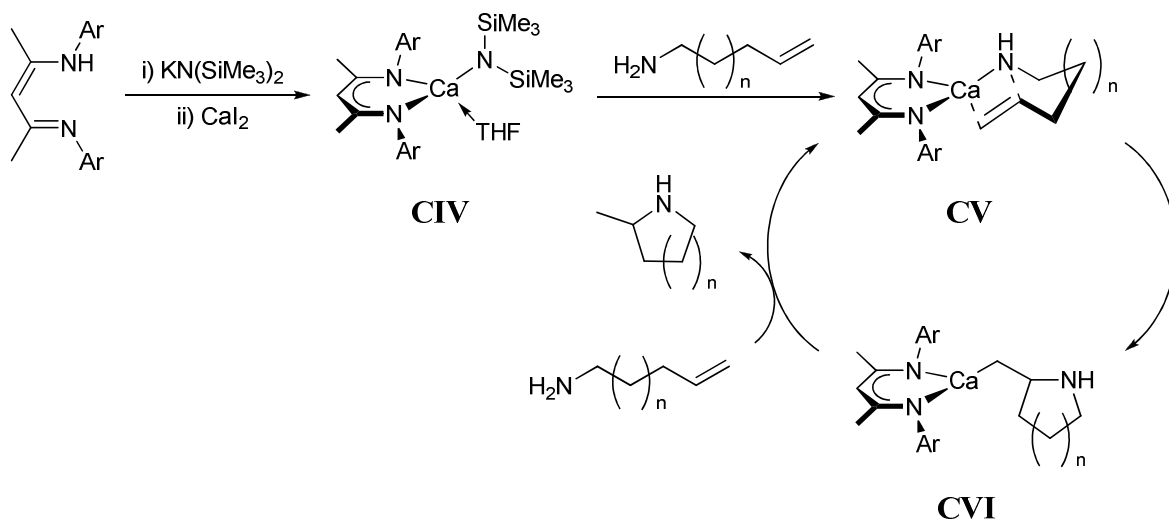
The bulky *tert*-butyl β -diketiminate magnesium butyl (**XCVI**) has been used by Jones and co-workers to produce the dimeric magnesium hydride complex **CII**, with the hydrides bridging the two metal centres (scheme 63).⁸⁵ The bulky *tert*-butyl groups at the R² positions are required to presumably better enclose the hydride atoms in the coordination site of the metal, and prevent decomposition of the product. Subsequent treatment with N,N-dimethylaminopyridine (DMAP) gives a monomer, with coordination of a DMAP molecule to the magnesium centre (**CIII**).⁸⁵

Scheme 63 – Synthesis of β -diketiminate magnesium hydride dimer. Ar = 2,6-diisopropylphenyl.



Calcium-containing BDI complexes have been shown by Hill and co-workers to catalyse the intramolecular hydroamination of aminoalkenes, and were the first examples that showed that calcium could be used as a hydroamination catalyst.⁸⁸ A β -diketiminate calcium amide precatalyst **CIV** is prepared from the neutral β -diketimine, potassium *bis*-(trimethylsilyl) amide and calcium iodide.⁸⁹ This precatalyst is initiated with a primary amine, after which the insertion of an alkene into the Ca-N bond occurs as the rate-determining step to yield the calcium alkyl **CVI**. A further equivalent of primary amine liberates the product, and regenerates the active catalyst **CV**.⁹⁰

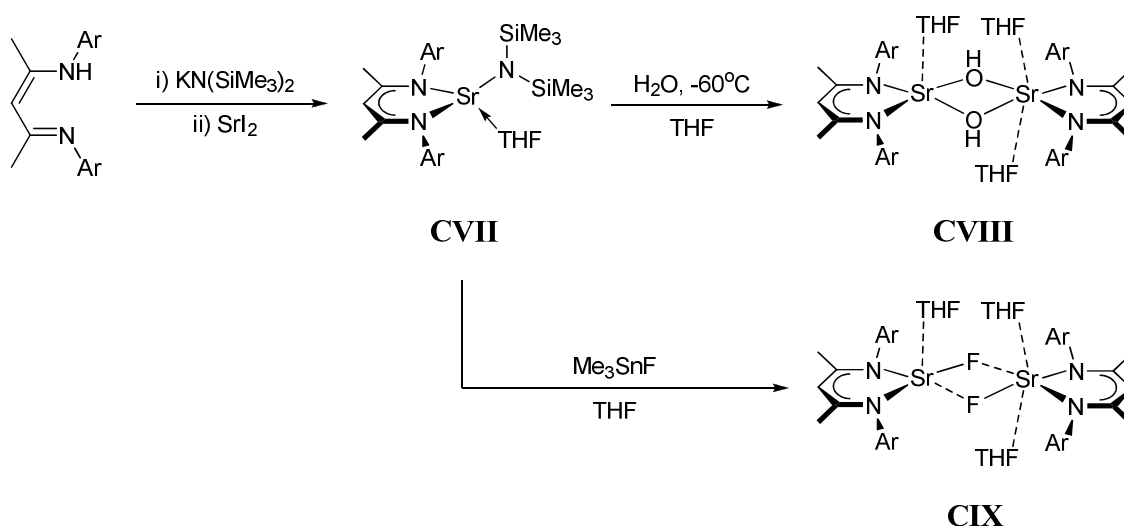
Scheme 64 – Hydroamination by BDI calcium amides. Ar = 2,6-diisopropylphenyl.



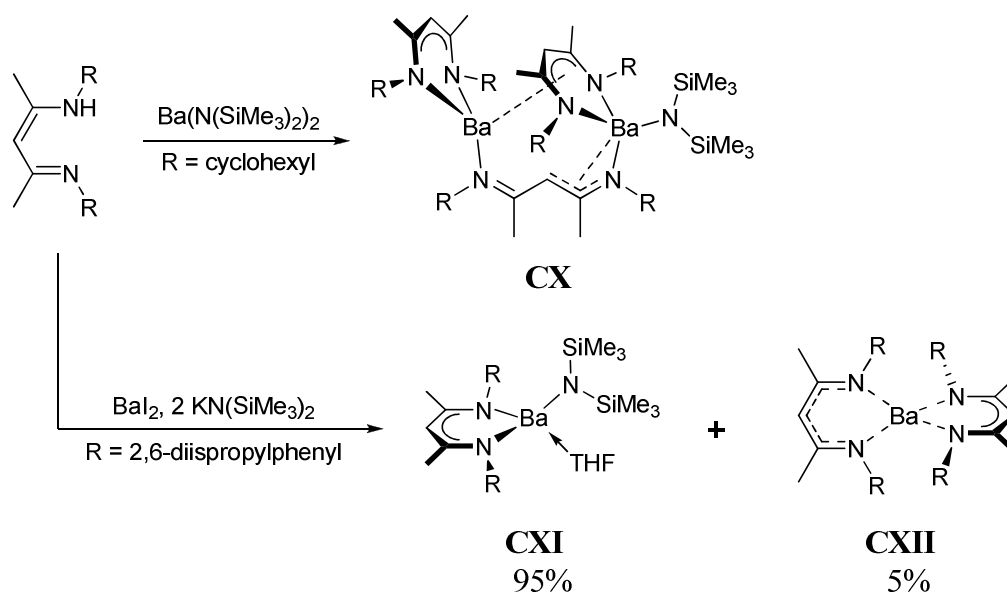
Complexes of the heavier group two metals are far less common than those of magnesium and calcium, but a few examples of β -diketiminate strontium and barium complexes have been synthesised. Roesky and co-workers have published an example of a monomeric strontium amide complex, and its subsequent hydrolysis into a dimeric strontium hydroxide (scheme 65).⁹¹ Subsequent work has also shown the halogenation

of the amide complex can produce dimeric fluoride or chloride complexes, showing the first examples of halogenated strontium β -diketiminates.⁹² Interestingly, in both the hydroxide and the halide dimers **CVIII** and **CIX**, the two metal atoms exhibit different coordination environments to each other, even though both strontium atoms are coordinated to one BDI ligand and both bridging hydroxide groups. One metal atom is coordinated to one molecule of THF, giving a distorted trigonal bipyramidal environment, whereas the other is coordinated to two molecules of THF, in a distorted octahedral environment. This is in contrast to the magnesium (**XCIV**) and calcium (**XCIX**) dimers, in which both metal atoms have the same coordination geometry.

Scheme 65 – Synthesis of strontium β -diketimate complexes



A very small number of barium complexes have been synthesised, with Mair and co-workers publishing a novel *tris*- β -diketimate-dibarium complex (**CX**) in 1998, using cyclohexyl groups in the R^3 position on the ligand (scheme 66).⁹³ When replaced with the more rigid 2,6-diisopropylphenyl groups, barium complexes analogous to those described above can be synthesised, such as a bis-trimethylsilylamide (**CXI**) and a monometallic, bis- β -diketimate (**CXII**), as reported by Hill and co-workers.⁹⁴ The monometallic, bis-BDI **CXII** is likely to be able to be synthesised with a bulkier ligand than the magnesium analogue **XCIII**, due to the increase in ionic radius from magnesium to barium, allowing larger ligands to be accommodated around the metal centre.

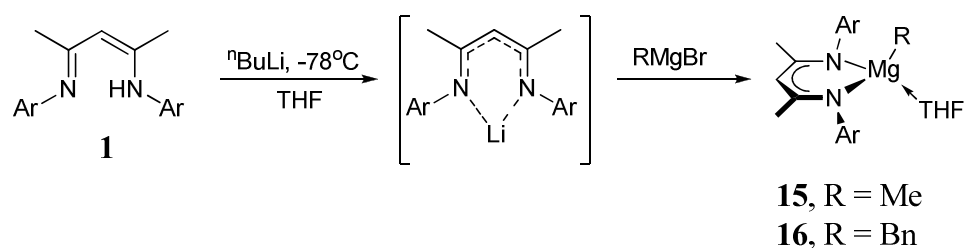
Scheme 66 – Barium β -diketiminato complexes

3.2 Synthesis and reactivity of β -diketiminate magnesium complexes

3.2.1 Synthesis of β -diketiminate magnesium alkyl complexes

β -Diketimate magnesium methyl and benzyl complexes **15** and **16** are known complexes, both synthesised by Bailey and co-workers during the last decade.^{81,95} Their approach was followed and involved using an excess of n BuLi to deprotonate the neutral ligand **1** and generate the lithiated BDI *in situ*. Addition of methyl- or benzylmagnesium bromide produced a bright pink solution after stirring overnight. After filtration to remove the lithium bromide by-product, pale pink crystals were isolated in good yield, with ^1H NMR data matching that of the literature compounds. The origin of the pink colour is unknown, and was not referred to by Bailey in the original synthesis of these compounds.

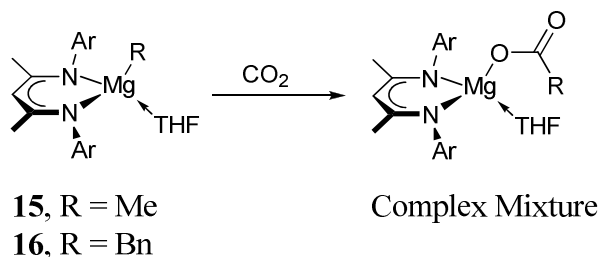
Scheme 67 – Synthesis of LMgMe (**15**) and LMgBn (**16**). Ar = 2,6-diisopropylphenyl.



3.2.2 Reactivity studies with heterocumulenes

Initial studies on an NMR scale showed that carbon dioxide reacted readily with benzene solutions of both methyl **15** and benzyl **16**, although in the case of the benzyl complex, reaction times were increased from one to two hours to overnight. However, reactions with both one equivalent and one atmosphere pressure of carbon dioxide resulted in a very complex mixture of products, unidentifiable by ^1H NMR.

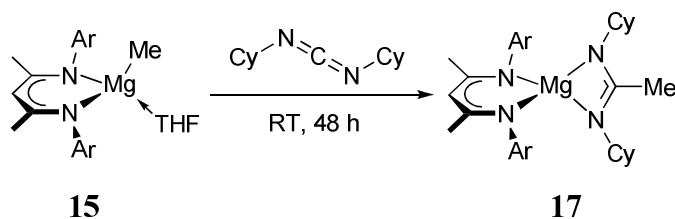
Scheme 68 – Reactivity studies for insertion with CO₂. Ar = 2,6-diisopropylphenyl.



3.2.3 Synthesis and characterisation of β -diketiminato magnesium N,N'-dicyclohexylethylamidinate, $\text{LMg}[(\text{NCy})_2\text{CMe}]$ (**17**)

Addition of one equivalent of dicyclohexylcarbodiimide (DCC) to a hexane solution of magnesium methyl **15** produced the DCC-inserted product **17** in 41% yield after stirring at room temperature for two days. The pale yellow complex was observed to be soluble in aliphatic and aromatic hydrocarbon solvents, halogenated solvents such as dichloromethane and ethereal solvents such as diethyl ether.

Scheme 69 – Synthesis of ethylamidinate complex **17**. Ar = 2,6-diisopropylphenyl.



Crystals suitable for X-ray diffraction were able to be grown in a concentrated solution of toluene, layered with hexane. The solid-state structure shows the magnesium atom in a pseudo-tetrahedral environment, with the magnesium atom bound to four nitrogen atoms. The Mg-N bond lengths are very similar to each other, around 2.05 Å. This is very similar to the Mg-N bond lengths reported by Winter and co-workers in other magnesium monoamidinates.⁹⁶ The presence of the bidentate amidinate ligand moves the magnesium atom out of the plane of the BDI ligand by 0.973 Å, with the NCN spine of the amidinate perpendicular to the C₃N₂ backbone of the β -diketiminato. The internal N3-Mg-N4 and N3-C30-N4 bond angles of the amidinate are around 66° and 113.6°

respectively, and are consistent with the corresponding angles in Winter's compound.⁹⁶ Despite multiple attempts, a satisfactory elemental analysis for this compound was unable to be obtained.

Table 21 – Bond angles (°) and lengths (Å) for LMg(NCy)₂CMe (**17**).

N1-Mg-N2	94.33(6)	N1-C1-C2	123.88(16)
N1-Mg-N3	121.81(7)	C1-C2-C3	130.14(16)
N1-Mg-N4	120.49(6)	C2-C3-N2	123.44(16)
N2-Mg-N3	129.85(6)	N1-Mg	2.0394(15)
N2-Mg-N4	126.45(6)	N2-Mg	2.0348(15)
N3-Mg-N4	66.09(6)	N3-Mg	2.0233(15)
C1-N1-C6	120.33(15)	N4-Mg	2.0805(15)
C1-N1-Mg	114.41(12)	N3-C30	1.340(2)
C6-N1-Mg	124.55(11)	N4-C30	1.336(2)
C3-N2-C18	117.33(14)	N1-C1	1.329(2)
C3-N2-Mg	114.03(11)	C1-C2	1.412(3)
C18-N2-Mg	128.29(11)	C2-C3	1.404(3)
C30-N3-Mg	91.27(10)	C3-N2	1.337(2)
C30-N4-Mg	88.94(10)		
N3-C30-N4	113.56(15)	Mg – plane	0.973

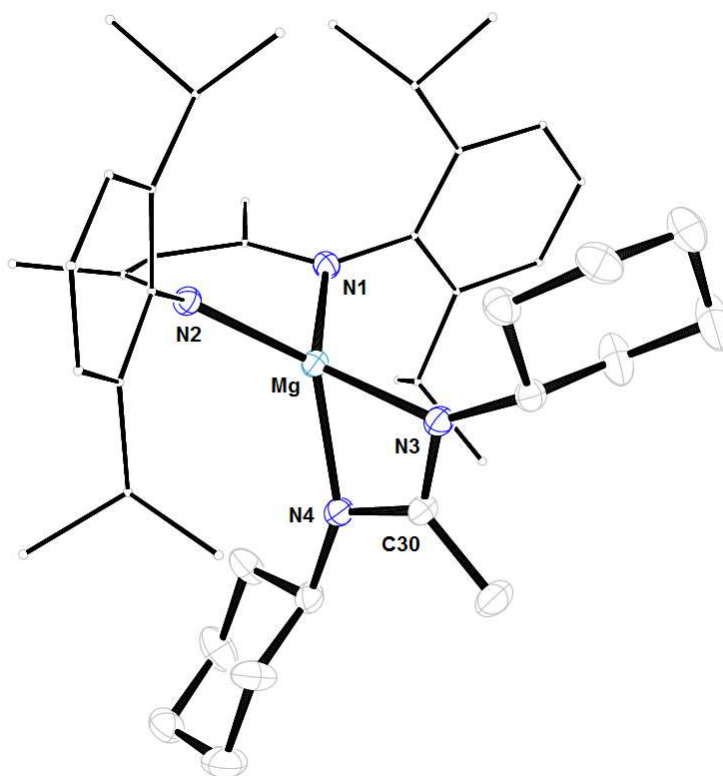


Figure 50 - LMg(NCy)₂CMe (**17**). 30% probability ORTEP ellipsoids, BDI ligand minimised and H-atoms omitted for clarity

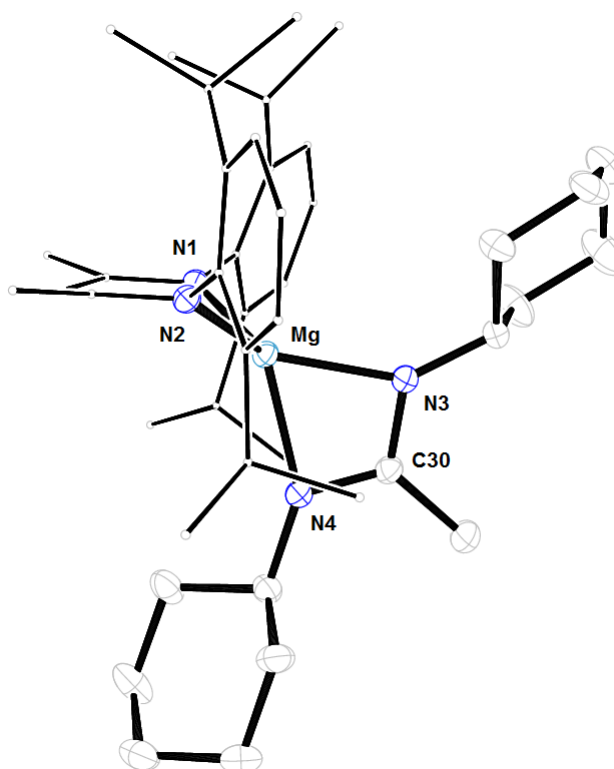


Figure 51 – LMg(NCy)₂CMe (**17**) side-on, showing configuration around the metal centre. 30% probability ORTEP ellipsoids, BDI ligand minimised and H-atoms omitted for clarity.

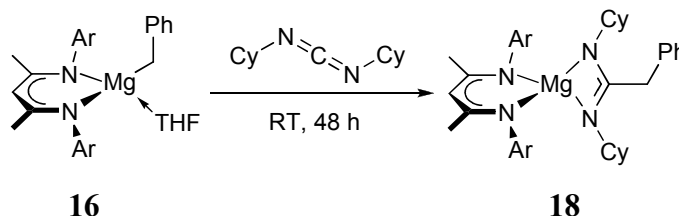
The ^1H NMR spectrum of DCC shows a characteristic signal at δ 3.12, assigned to the two protons on the N-bonded carbon atoms of the cyclohexyl rings. This signal is clearly identifiable, as it has no other peaks near it in the spectrum. In the ^1H NMR spectrum of the DCC-inserted methyl complex **17**, a shift in this signal to δ 2.84 is observed. The presence of cyclohexyl groups clutters the spectra around δ 1.0 – 2.0, but the distinct doublets assigned to the *iso*-propyl protons on the ligand are still visible at δ 1.30 and δ 1.29, although they overlap slightly with each other. The septet corresponding to the two methyne protons of the same *iso*-propyl groups is clearly visible at δ 3.49. This single signal demonstrates that there is no unsymmetrical environment around the metal centre, unlike in the lead alkyl complexes, where this signal is split. The signal assigned to the methyl substituent at δ -1.25 in the magnesium methyl **15** is no longer present, but a new singlet, integrating to 3 protons is observed at δ 1.65 in the product **17**. The chemical shift for the amidinate central carbon atom C30 is observed at δ 172.8, as the carbon unit is sandwiched between two nitrogen atoms. This shift is in agreement with other metal-coordinated amidinate complexes, such as those reported by Jordan and co-workers (NCN δ ~168),⁹⁷ and by Otero and co-workers (NCN δ ~157).⁹⁸ The peak corresponding to the backbone proton on the BDI ligand has shifted slightly from δ 4.83 in the precursor **15**, to δ 4.89 in the insertion product **17**. A coordinated THF molecule was not observed in any of the NMR spectroscopic data, unlike in the precursor complex **15**. This lack is most likely due to the interaction between the magnesium and the nitrogen atoms within the amidinate structure not allowing coordination of a solvent molecule.

3.2.4 Synthesis and characterisation of β -diketiminato magnesium N,N'-dicyclohexylphenylethylamidinate, $\text{LMg}[(\text{NCy})_2\text{CBn}]$ (**18**)

Analogous to the DCC-inserted methyl **17**, magnesium DCC-inserted benzyl **18** was synthesised by addition of one equivalent of DCC to a toluene solution of benzyl precursor **16**. After stirring overnight, the pale yellow insertion product **18** was isolated in 50% yield. Attempts to obtain crystals suitable for X-ray diffraction of complex **18** were unsuccessful, despite attempting to do so with a range of solvents and conditions. The product was observed to be soluble in ethereal solvents, as well as most aliphatic

and aromatic hydrocarbon solvents. Despite multiple attempts, a satisfactory elemental analysis for this compound was unable to be obtained.

Scheme 70 – Synthesis of phenylethylamidinate complex **18**. Ar = 2,6-diisopropylphenyl.

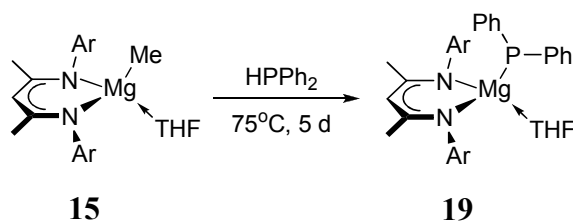


The characteristic signal of the DCC reagent has shifted in the ^1H NMR spectrum of **18**, and is observed at δ 2.84. The signal assigned to the CH_2 unit in the benzyl group, present at δ 1.47 in the magnesium benzyl **16**, has shifted to δ 3.60 in the insertion product **18**, significantly more downfield due to a C-C bond having been formed α -to the benzyl group. The amidinate central carbon atom has a very high chemical shift in the $^{13}\text{C}\{^1\text{H}\}$ NMR spectrum, at δ 173.2, which is comparable to other amidinate $^{13}\text{C}\{^1\text{H}\}$ shifts, as mentioned previously.^{97,98} The aromatic protons on the benzyl group can still be individually identified, with all three signals having moved downfield in the product. Similar to the methyl insertion product **17**, the BDI ligand backbone proton signal has shifted only slightly, from δ 4.78 in the benzyl precursor **16** to δ 4.85 in the benzyl product **18**. The signals corresponding to the methyl protons on the *iso*-propyl groups on the aromatic rings of the ligand are clearly visible at δ 1.24 and δ 1.36, though they are surrounded by many multiplets from the cyclohexyl group protons between δ 0.85 to δ 1.45. The methyne protons on the same *iso*-propyl groups show their distinctive septet at δ 3.50. Analogous to the methyl insertion complex **17**, the environment around the metal centre in the benzyl product **18** is shown to be symmetrical in solution. Unlike the parent benzyl complex **16**, no molecule of THF is present in the insertion complex **18**, as no evidence for coordination is seen in the ^1H NMR spectra. This is most likely due to the increase in steric bulk around the metal centre, removing the THF molecule from the coordination sphere, in a similar fashion to that in the methyl insertion complex **17**.

3.2.5 Synthesis and characterisation of β -diketimate magnesium diphenylphosphide, $\text{LMgPPh}_2\cdot\text{THF}$ (**19**)

Magnesium diphenylphosphide **19** was synthesised from the addition of one equivalent of diphenylphosphine to a toluene solution of the methyl precursor **15**. After addition, the solution was stirred at 75°C for five days, and the desired phosphide **19** was isolated in 59% yield. Diphenylphosphide **19** was observed to be soluble in most aliphatic and aromatic hydrocarbon solvents, as well as ethereal solvents such as diethyl ether and THF.

Scheme 71 – Synthesis of magnesium diphenylphosphide **19**. Ar = 2,6-diisopropylphenyl.



Crystals suitable for an X-ray diffraction study were grown from a layered mixture of toluene and hexane, and the solid-state structure shows that diphenylphosphide **19** retains the coordinated THF molecule from the starting parent methyl **15**. The magnesium atom is displaced 0.551 Å from the C_3N_2 plane, with the phosphide substituent arranged in the *exo*- position. To avoid the phosphorus lone pair clashing with the coordinated THF molecule, the diphenylphosphide group is orientated so that the phenyl substituents are on the same side of the Mg-P bond as the THF molecule (as shown in figure 53). The phosphorus atom has a DOP of ~ 45 %, which is considerably smaller than both the calcium analogue reported by Barrett and Hill ($\text{DOP}_\text{P} = 84.3 \%$),⁹⁰ and the simpler lithium diphenylphosphide, LiPPh_2 ($\text{DOP}_\text{P} = 61.4 \%$) produced by Mulvey and co-workers.⁹⁹ This trend of increasing DOPs is in common with the increase in van der Waals radii from magnesium (1.73) to lithium (1.82) to calcium (2.00), and may help to explain the change in DOP of the phosphorus, especially between the two β -diketimate complexes.

Very few magnesium – phosphorus bonds have been reported. The Mg-P bond distance in diphenylphosphide **19** is 2.5309(11) Å. This is very similar to the Mg-P bond distance in the magnesium phenylphosphide complex $\text{Mg}(\text{PPh})_2(\text{tmeda})$, reported by Raston (Mg-P = ~ 2.59 Å),¹⁰⁰ the novel phospho-Grignard $\{\text{Mg}[\text{P}(\text{SiMe}_3)_2]\text{Br}.\text{THF}\}_2$, reported by Coles (Mg-P = ~ 2.56 Å)¹⁰¹ and the disubstituted magnesium phosphide $\text{Mg}[\text{P}(\text{SiMe}_3)_2]_2.(\text{THF})_2$ reported by Westerhausen (Mg-P = 2.50 Å).¹⁰² The THF molecule in diphenylphosphide **19** is coordinated to the metal centre, with a Mg-O distance of 2.017(2) Å. This is similar to the corresponding Mg-O distance in the THF-coordinated complex $\text{Mg}[\text{P}(\text{SiMe}_3)_2]_2.(\text{THF})_2$ (Mg-O = 2.06 Å).¹⁰² Despite multiple attempts, a satisfactory elemental analysis for compound **19** was unable to be obtained.

Table 22 – Bond angles (°) and lengths (Å) for $\text{LMgPPh}_2.\text{THF}$ (**19**).

N1-Mg-P	122.46(8)	N1-Mg-O	104.02(9)
N2-Mg-P	120.22(7)	N2-Mg-O	103.95(9)
N1-Mg-N2	93.49(9)	O-Mg-P	109.96(7)
C1-N1-C6	119.1(2)	Mg-P	2.5309(11)
C1-N1-Mg	120.86(18)	N1-Mg	2.063(2)
C6-N1-Mg	120.02(17)	N2-Mg	2.057(2)
C3-N2-C18	120.1(2)	Mg-O	2.017(2)
C3-N2-Mg	120.87(18)	P-C30	1.837(3)
C18-N2-Mg	118.99(17)	P-C36	1.836(3)
N1-C1-C2	124.2(2)	N1-C1	1.327(4)
C1-C2-C3	129.9(3)	C1-C2	1.410(4)
C2-C3-N2	123.9(3)	C2-C3	1.414(4)
Mg-P-C30	111.19(10)	C3-N2	1.327(3)
Mg-P-C36	104.31(9)	Mg – plane	0.551
C30-P-C36	103.98(13)	DOP _(P) (%)	45.03
		DOP _(Mg-THF) (%)	26.48

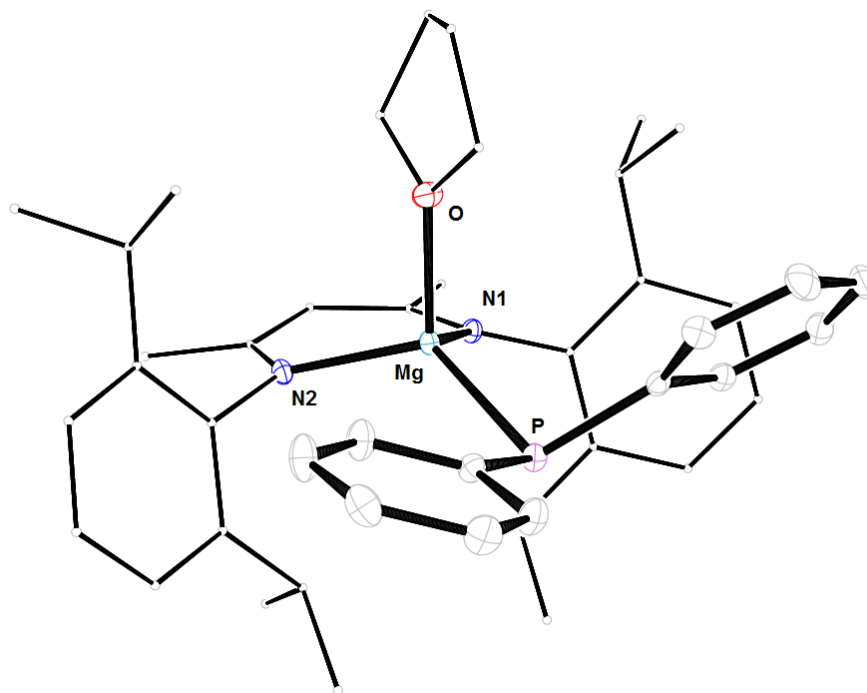


Figure 52 – LMgPPh₂.THF (**19**). 30% probability ORTEP ellipsoids, BDI ligand minimised and H-atoms omitted for clarity.

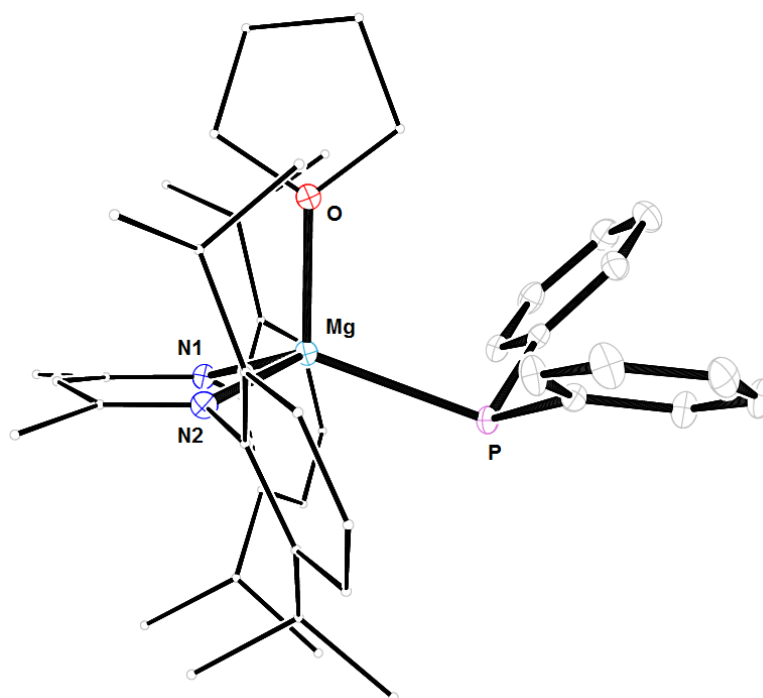


Figure 53 – LMgPPh₂.THF (**19**) side-on, showing configuration around the metal centre. 30% probability ORTEP ellipsoids, BDI ligand minimised and H-atoms omitted for clarity.

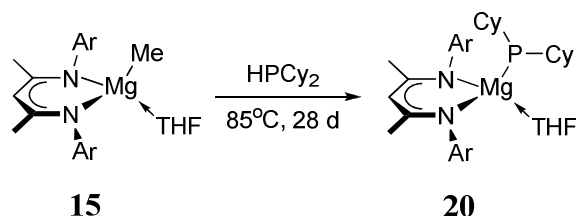
The ^1H NMR spectrum of diphenylphosphide **19** in deuterated benzene shows resonances at δ 3.56 and δ 1.10, indicating the presence of a coordinated THF molecule. There is a broad signal visible at δ 2.88, which corresponds to a methyne resonance, and is associated with the two broad methyl peaks at δ 1.43 and δ 0.84. These peaks combine to represent two of the four *iso*-propyl groups on the aromatic rings of the BDI ligand, and the broadness of the peaks indicate they may be subject to restricted motion, and possibly exchanging close to the slow exchange limit. The other two *iso*-propyl groups show a doublet at δ 1.16 ($J = 6.2$ Hz), which corresponds to the remaining methyl protons, and a methyne resonance overlaid with the THF signal at δ 3.56. These sharp signals indicate these *iso*-propyl groups are exchanging at the faster exchange limit, and are fully equilibrated. The doublet could possibly be due to through-space interaction between the methyl groups and the phosphorus lone pair, suggesting that these signals correspond to the *iso*-propyl groups further away from the central metal atom (the “lower” pair of *iso*-propyl groups, if consulting figure 53, for example). However, without further, 2-D NMR experiments, this is merely speculation. The protons on the phenyl groups of the phosphide can also be observed clearly in the ^1H NMR spectra, with the *meta*-protons observed at δ 6.89 ($J = 7.7, 1.6$ Hz) and a multiplet corresponding to the *ortho*- and *para*- protons at δ 6.77. There is one sharp signal in the $^{31}\text{P}\{^1\text{H}\}$ NMR spectra at δ -46.7, indicating one single phosphorus environment in the molecule, slightly upfield from that of the neutral phosphine, HPPH_2 , at δ -40.7.

3.2.6 Synthesis and characterisation of β -diketimate magnesium dicyclohexylphosphide, $\text{LMgPCy}_2\cdot\text{THF}$ (**20**)

Magnesium dicyclohexylphosphide complex **20** was generated from the addition of one equivalent of dicyclohexylphosphine to a toluene solution of the methyl precursor **15**. The solution was heated with stirring at 85°C for 28 days, after which time the solution was filtered through Celite®, and phosphide **20** isolated in 69% yield. Dicyclohexylphosphide **20** was observed to be mostly soluble in aliphatic hydrocarbon solvents, and was found to be very soluble in aromatic hydrocarbon and ethereal solvents such as toluene or THF. Despite repeated attempts in a number of solvent conditions, no crystals suitable for X-ray diffraction analysis could be grown. In

addition to this, despite repeated attempts, a satisfactory elemental analysis for this compound was unable to be obtained.

Scheme 72 - Synthesis of magnesium dicyclohexylphosphide **20**. Ar = 2,6-diisopropylphenyl.



The ^1H NMR spectrum of dicyclohexylphosphide **20** is similar to that of the diphenylphosphide complex **19**. The presence of a coordinated THF molecule is observed, with broad peaks at δ 3.89 and δ 1.79. The methyne *iso*-propyl protons on the BDI ligand are determined as a broad peak at δ 3.27. The methyl protons on the *iso*-propyl groups, however, show as only one doublet at δ 1.22, illustrating that the dicyclohexyl complex **20** is likely to be symmetrical in solution. The cyclohexyl ring protons show as a number of multiplets from δ 0.85 to δ 1.45. There is a very slight shift in the $^{31}\text{P}\{^1\text{H}\}$ NMR signals from reagent to product, with dicyclohexylphosphine displaying a signal at δ 28.1, and the dicyclohexylphosphide product **20** displaying a signal at δ 28.8.

3.3 Computational studies

In common with the computational studies on the lead alkyls and cationic complexes, studies were carried out on the magnesium phosphide complexes using Gaussian G03W and Gaussview v9.0. The B3LYP function and 6-31G* basis set were used to study the all atoms in the molecules, negating the need for any mixed basis set calculations, as was the case in the lead and tin calculations (*vide supra*). The calculations were carried out using the crystal structure as starting point for diphenylphosphide **19**, and then manually changing the phenyl groups for cyclohexyl groups in the calculation for dicyclohexylphosphide **20**. As no crystal structure was acquired for **20**, comparisons were only able to be made in the calculations, to see the effect of removing aromaticity from the substituent. Calculations were also performed with the THF molecule removed, in order to study the effect of a coordinated solvent molecule, and the ΔE , ΔH and ΔG values used to quantify any stabilisation effects.

Data tables can be found in appendix 3 (bond lengths, bond angles and molecular orbital energy levels).

3.3.1 Discussion of geometry optimisations and structural differences

*β -diketiminato magnesium diphenylphosphide, LMgPPh₂.THF, **19***

A slightly asymmetric environment around the metal centre in magnesium diphenylphosphide **19** is evident from the calculations, with one N-Mg-P angle being around 4° larger than the other, but both are in good agreement with the solid state structure. The *exo*- conformation between the metal and the phosphide substituent is still present, with the magnesium atom roughly the same distance from the C₃N₂ plane (~ 0.55 Å). The DOP of the phosphorus atom is 4% smaller in the calculation than in the solid state, but this may be due to the slight movement of the phenyl rings as the structure moves from the solid phase in the crystal to the gas phase in the calculation. This slight change can also be noted in the DOP of the magnesium, with the coordinated THF molecule on the 4th vertex of the metal atom, otherwise occupied by the lone pair

in the lead and tin calculations. The calculation shows a DOP $\sim 1\%$ less than in the solid state, which accounts for the slight lengthening of the Mg-O bond by 0.1 \AA . The Mg-P bond length shows good agreement with the solid state structure.

A larger structural change is apparent in the solvent-free calculation, with a rotation along the Mg-P bond of $\sim 24^\circ$, due to the steric freedom afforded by the removal of the THF molecule. This extra freedom increases the DOP of the phosphorus by $\sim 3\%$, and shortens the Mg-P bond by $\sim 0.05 \text{ \AA}$. In addition to this, the N-Mg-P bond angles increase, flattening the environment around the metal centre, reducing the DOP of the magnesium atom to $< 1\%$. The distance between the magnesium atom and the C_3N_2 plane is also greatly decreased by $\sim 0.4 \text{ \AA}$.

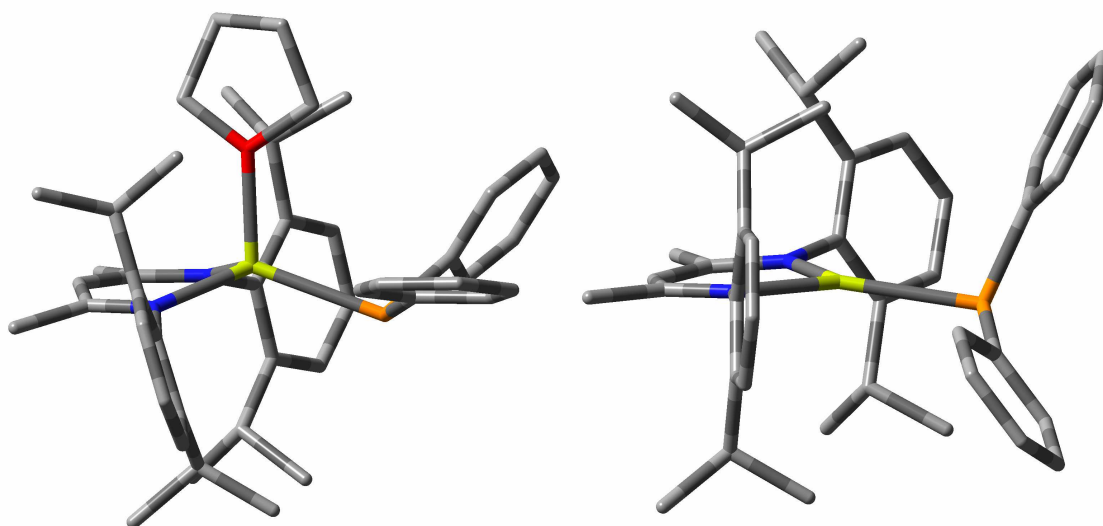


Figure 54 – Optimised geometry for solvated $\text{LMgPPh}_2\cdot\text{THF}$ (left) and unsolvated LMgPPh_2 (right).

*β -diketiminate magnesium dicyclohexylphosphide, $\text{LMgPCy}_2\cdot\text{THF}$, **20***

Due to the absence of a crystal structure for magnesium dicyclohexylphosphide **20**, no comparisons can be made to the solid state. However, using the structure and calculation results for diphenylphosphide **19**, the phenyl rings on the substituent were replaced with cyclohexyl rings, in order to briefly study any differences within the calculations. This would provide some understanding of the material in the solid state, as it is observed that the computational calculations provide good agreement with the solid state structural data for all of the calculations undertaken in this work.

The environment around the metal atom in the THF-adduct calculation for dicyclohexylphosphide **20** is still slightly unsymmetric, with one N-Mg-P angle slightly larger ($\sim 4^\circ$) than the other. The complex displays an *exo*- configuration with regard to the phosphide substituent, with the magnesium atom roughly the same distance from the C_3N_2 plane as in the calculation for diphenylphosphide **19**. The DOP of the magnesium has increased from the diphenyl **19** calculation to 31.5%, an increase of $\sim 6\%$, most likely due to the greater degrees of freedom afforded to the cyclohexyl substituents over the phenyl rings in the previous complex. The DOP on the phosphorus atom, however, has decreased by $\sim 14\%$, indicating a flattening of the environment around the substituent as the Mg-P-C and C-P-C angles increase. The Mg-O bond is increased by around 0.05 \AA from the diphenyl compound **19**, with the Mg-P bond decreased by a comparable amount.

The solvent-free calculation displays a similar structural geometry to the solvated calculation. However, there is a rotation about the Mg-P bond, as one cyclohexyl unit was observed to rotate by $\sim 102^\circ$, with the other rotating through 70° . This acts to decrease the bond angles around the phosphorus atom, and results in a sharpening of the DOP of the phosphorus by $\sim 16.6\%$. Unlike the case of the diphenyl **19**, removing the coordinated THF molecule in dicyclohexyl **20** does not shorten the Mg-P bond by a great amount, and the desolvation flattens the environment around the metal centre, reducing the DOP of the magnesium atom to $< 1\%$. Along with this, the magnesium atom is observed to move closer to the C_3N_2 plane by $\sim 0.26 \text{ \AA}$ from the solvated state.

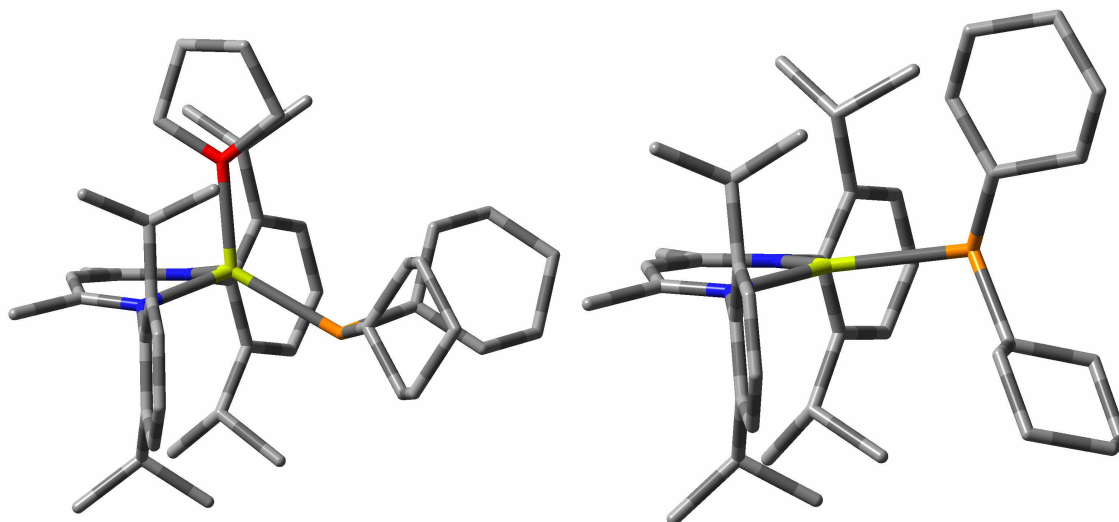


Figure 55 – Optimised geometry for solvated LMgPCy₂·THF (left) and unsolvated LMgPCy₂ (right).

3.3.2 Solvent stabilisation effects

The presence of the coordinated THF molecule can be seen to stabilise the diphenylphosphide complex **19** by 13.4 kcal mol⁻¹. This stabilisation effect explains why a coordinated THF molecule is present in the solid state. The ΔG energy term is negative, indicating the coordinated complex is less stable than the sum of the free complex and THF. This can be attributed to entropic effects from moving from a single, coordinated species to two separate molecules. None of these values are corrected for basis set superposition error.⁷⁰

Table 23 – Energy differences between calculations for diphenyl phosphide **19**. Values are the stability of coordinated complex vs. free complex + THF.

ΔE (kcal mol ⁻¹)	ΔH (kcal mol ⁻¹)	ΔG (kcal mol ⁻¹)	ΔS (cal K ⁻¹ mol ⁻¹)
13.4	12.9	-1.16	47.0

A similar stabilisation can be seen with the dicyclohexyl phosphide **20**, with the presence of the coordinated THF molecule stabilising the structure by 10.3 kcal mol⁻¹. Although no crystal structure was obtained for dicyclohexyl **20**, it is reasonable to assume that the solid state structure would contain a coordinated molecule. As with the diphenyl complex **19**, the ΔG term is negative, and can be attributed to entropic effects.

Table 24 – Energy differences between calculations for dicyclohexyl phosphide **20**. Values are the stability of coordinated complex vs. free complex + THF.

ΔE (kcal mol ⁻¹)	ΔH (kcal mol ⁻¹)	ΔG (kcal mol ⁻¹)	ΔS (cal K ⁻¹ mol ⁻¹)
10.3	9.63	-2.71	41.4

3.4 *Summary*

The insertion of heterocumulenes into the Mg-C bond of β -diketiminate magnesium alkyl complexes was investigated. Although carbon dioxide was found to yield a complex mixture of products, insertion of DCC allowed generation of two amidinate structures. Addition of phosphines to the magnesium alkyl complexes yielded two new BDI magnesium structures with terminal phosphide ligands. The generation of the phosphides proved to be a slow process, which could have been accelerated by reaction of BDI magnesium chloride and a lithiated phosphide to yield the same magnesium phosphide complexes. Computational calculations were carried out on the magnesium phosphide complexes to investigate the effect of solvent stabilisation on the molecule. The presence of a coordinating solvent was found by calculation to carry a positive effect with regard to the stabilisation energy.

3.5 Experimental details

Synthesis of β -diketiminate magnesium methyl; LMgMe (15)

β -Diketimine **1** (2.0 g, 4.78 mmol) was dissolved in ~20 ml of THF in a Schlenk tube, to which was added $^n\text{BuLi}$ (2.37 M, 2.1 ml, 4.97 mmol). The mixture was allowed to stir for ~30 minutes at room temperature, after which MeMgBr (1.4 M, 4.3 ml, 6.02 mmol) was added dropwise to the dark yellow solution. The mixture was left to stir overnight whilst heating at 30°C, after which the solution had taken on a deep orange hue. The THF was removed *in vacuo*, hexane was added and the bright pink solution filtered through Celite®. The hexane was removed under reduced pressure and the intense pink powder used without further purification. Yield: 1.88 g (86.1%).

^1H NMR (499.91 MHz, C_6D_6 , 30°C): δ 7.16 (m, 6H, H_{aryl}), 4.83 (1H, middle CH), 3.53 (t, J = 6.4 Hz, 4H, THF), 3.36 (sept, J = 6.5 Hz, 4H, CHMe_2), 1.67 (s, 6H, NCMe), 1.28 (d, J = 6.8 Hz, 12H, CHMe_2), 1.24 (d, J = 6.9 Hz, 12H, CHMe_2), -1.25 (s, 3H, Mg-Me). Literature ^1H NMR (250 MHz, CDCl_3): δ 7.2 – 6.8 (m, 6H, H_{aryl}), 4.71 (s, 1H, middle CH), 3.71 (t, 4H, THF), 3.11 (sept, J = 7.0 Hz, 4H, CHMe_2), 1.82 (t, 4H, THF), 1.60 (s, 6H, NCMe), 1.10 (d, J = 6.0 Hz, 24H, CHMe_2), -2.00 (s, 3H, Mg-Me).⁸¹

Synthesis of β -diketiminate magnesium benzyl; LMgBn (16)

β -Diketimine **1** (2.0 g, 4.78 mmol) was dissolved in ~20 ml of THF in a Schlenk tube, to which was added $^n\text{BuLi}$ (2.37 M, 2.1 ml, 4.97 mmol). After stirring for ~30 minutes at room temperature, BnMgCl (1.5 M, 4.0 ml, 6.0 mmol) was added dropwise, and the pale yellow mixture was allowed to stir overnight at 40°C. The THF was removed *in vacuo*, hexane was added, and the solution filtered through Celite®. The hexane was removed under reduced pressure and the bright pink solid used without further purification. Yield: 1.32 g (52.0%).

^1H NMR (499.91 MHz, C_6D_6 , 30°C): δ 7.21 (m, 6H, H_{aryl}), 6.89 (t, J = 7.6 Hz, 2H, $m\text{-H}_{\text{Ph}}$), 6.60 (t, J = 7.2 Hz, 1H, $p\text{-H}_{\text{Ph}}$), 6.42 (d, J = 7.0 Hz, 2H, $o\text{-H}_{\text{Ph}}$), 4.78 (1H, middle CH), 3.53 (br, 4H, THF), 3.22 (br, 4H, CHMe_2), 1.65 (s, 6H, NCMe), 1.47 (s, 2H, MgCH_2), 1.21 (d, J = 6.8 Hz, 24H, CHMe_2).

Literature ^1H NMR (250 MHz, C_6D_6): δ 7.34 (s, 5H, toluene), 7.15 – 7.33 (m, 6H, H_{aryl}), 7.01 (t, $J = 7.65$ Hz, 2H, $m\text{-H}_{\text{Ph}}$), 6.72 (t, $J = 7.46$ Hz, 1H, $p\text{-H}_{\text{Ph}}$), 6.54 (d, $J = 7.02$ Hz, 2H, $o\text{-H}_{\text{Ph}}$), 4.90 (s, 1H, middle CH), 3.66 (t, 4H, THF), 3.10 – 3.48 (m, 4H, CHMe_2), 2.24 (s, 3H, toluene), 1.77 (s, 6H, NCMe), 1.60 (s, 4H, THF), 1.34 (d, $J = 6.86$ Hz, 24H, CHMe_2).⁹⁵

*Synthesis of β -diketiminate magnesium dicyclohexylethylamidinate; $\text{LMg}[(\text{NCy})_2\text{CMe}]$ (**17**)*

Methyl compound **15** (150 mg, 0.33 mmol) was dissolved in ~10 ml of hexane in a Schlenk tube. Dicyclohexylcarbodiimide (68 mg, 0.33 mmol) was dissolved in ~5 ml of hexane and added to the pink solution of **15** at room temperature. The mixture was stirred for 48 hours, after which the pale yellow solution was concentrated and cooled to -30°C to encourage crystallisation without any further purification. Yield: 89.5 mg (40.9%).

^1H NMR (499.91 MHz, C_6D_6 , 30°C): δ 7.17 (m, 6H, H_{aryl}), 4.89 (s, 1H, middle CH), 3.49 (sept, $J = 6.8$ Hz, 4H, CHMe_2), 2.83 (m, 2H, $\text{NC}_{\text{Cy}}\text{H}$), 1.69 (s, 6H, NCMe), 1.65 (s, 3H, $\text{NC}(\text{Me})\text{N}$), 1.59 (m, 8H, NCy), 1.30 (d, $J = 6.8$ Hz, 12H, CHMe_2), 1.29 (d, $J = 6.9$ Hz, 12H, CHMe_2), 1.09 (m, 12H, NCy).

$^{13}\text{C}\{^1\text{H}\}$ NMR (125.7 MHz, C_6D_6 , 30°C): δ 172.8 ($\text{NC}(\text{Me})\text{N}$), 168.9 (NCMe), 145.2, 142.3, 137.4, 128.9, 128.1, 125.2, 124.7, 123.4 (C_{aryl}), 94.1 (middle CH), 53.8 (NC_{Cy}), 36.7 (Cy), 35.0 (CHMe_2), 27.9, 26.1, 25.5 (Cy), 24.9, 24.2, 23.8 (CHMe_2), 21.0 (NCMe), 11.8 ($\text{NC}(\text{Me})\text{N}$).

*Synthesis of β -diketiminate magnesium dicyclohexylphenylethylamidinate; $\text{LMg}(\text{NCy})_2\text{CBn}$ (**18**)*

Benzyl compound **16** (113 mg, 0.21 mmol) was dissolved in ~10 ml of toluene in a Schlenk tube. Dicyclohexylcarbodiimide (43 mg, 0.21 mmol) was dissolved in ~5 ml of toluene and added to the pale pink solution of **16** at room temperature. The mixture was stirred for 48 hours, after which the toluene was removed *in vacuo*. Hexane was added, and the pale yellow solution cooled to -30°C to encourage crystallisation without any further purification. Yield: 77 mg (49.7%).

^1H NMR (499.91 MHz, C_6D_6 , 30°C): δ 7.17 (m, 6H, H_{aryl}), 7.08 (d, $J = 7.3$ Hz, 2H, $o\text{-H}_{\text{Ph}}$), 7.03 (t, $J = 7.6$ Hz, 2H, $m\text{-H}_{\text{Ph}}$), 6.94 (t, $J = 7.2$ Hz, 1H, $p\text{-H}_{\text{Ph}}$), 4.85 (s, 1H, middle CH), 3.60 (s, 2H, PhCH_2), 3.50 (sept, $J = 6.8$ Hz, 4H, CHMe_2), 2.84 (m, 2H, $\text{NC}_{\text{Cy}}\text{H}$), 1.66 (s, 6H, NCMe), 1.47 (s, 2H, NCy), 1.34 (d, $J = 6.8$ Hz, 12H, CHMe_2), 1.26 (d, $J = 6.8$ Hz, 12H, CHMe_2), 0.92 (m, 18H, NCy).

$^{13}\text{C}\{^1\text{H}\}$ NMR (125.7 MHz, C_6D_6 , 30°C): δ 173.2 ($\text{NC}(\text{Me})\text{N}$), 169.1 (NCMe), 145.6, 142.2, 137.3, 128.2, 128.1, 125.9, 124.9, 123.4 (C_{aryl}), 94.4 (middle CH), 54.0 (NC_{Cy}), 37.1 (Cy), 32.9 (CHMe_2), 28.1 (PhCH_2), 26.0, 25.6 (CHMe_2), 25.1, 24.2, 24.0 (Cy), 21.0 (NCMe).

*Synthesis of β -diketiminato magnesium diphenylphosphide; LMgPPh_2 (**19**)*

Magnesium methyl **15** (105.8 mg, 0.232 mmol) was dissolved in ~10 ml of toluene in a small ampoule, and Ph_2PH (40 μl , 0.232 mmol) was added. The ampoule was sealed and the pink solution was heated, with stirring, at 75°C for five days (~120 hrs). The toluene was removed *in vacuo*, and the pale orange material was placed at -30°C in a mixture of toluene layered with a small amount of hexane. Crystals suitable for X-ray diffraction analysis were observed after a week. Yield: 86 mg (59.3%)

^1H NMR (499.91 MHz, C_6D_6 , 30°C): δ 7.10 (m, 6H, H_{aryl}), 6.89 (td, $J = 7.7$, 1.6 Hz, 4H, $m\text{-H}_{\text{Ph}}$), 6.77 (m, 6H, $o\text{-}/p\text{-H}_{\text{Ph}}$), 4.75 (1H, middle CH), 3.56 (t, $J = 6.6$ Hz, 6H, THF/ CHMe_2), 2.88 (br, 2H, CHMe_2), 1.62 (s, 6H, NCMe), 1.43 (br, 6H, CHMe_2), 1.16 (d, $J = 6.2$ Hz, 12H, CHMe_2), 1.10 (m, 4H, THF), 0.84 (br, 6H, CHMe_2).

$^{13}\text{C}\{^1\text{H}\}$ NMR (125.7 MHz, C_6D_6 , 30°C): δ 168.6 (NCMe), 145.3, 132.1, 131.9, 125.4, 122.5 (C_{aryl}), 94.3 (middle CH), 70.3 (PC_{Ph}), 24.9, 24.4 (CHMe_2), 24.1, 23.9 (CHMe_2), 21.0 (NCMe).

$^{31}\text{P}\{^1\text{H}\}$ NMR (161.7 MHz, C_6D_6 , 30°C): δ -46.7

*Synthesis of β -diketiminato magnesium dicyclohexylphosphide; LMgPCy_2 (**20**)*

Magnesium methyl **15** (225.5 mg, 0.494 mmol) was dissolved in ~10 ml of toluene in a small ampoule, and Cy_2PH (100 μl , 0.494 mmol) was added. The ampoule was sealed and the pink solution was heated, with stirring, at 85°C for 28 days. After this time, the toluene was removed *in vacuo*, and the pale yellow material placed at -30°C in a

mixture of toluene layered with a small amount of hexane to encourage crystallisation. .

Yield: 216 mg (68.6%)

^1H NMR (499.91 MHz, C_6D_6 , 30°C): δ 7.17 (m, 6H, H_{aryl}), 4.81 (1H, middle CH), 3.89 (br, 4H, THF), 3.27 (br, 4H, CHMe_2), 1.79 (br, 4H, THF), 1.67 (s, 6H, NCMe), 1.41 (m, 16H, PCy_2), 1.22 (d, $J = 6.8$ Hz, 24H, CHMe_2), 0.92 (m, 6H, PCy_2).

$^{13}\text{C}\{^1\text{H}\}$ NMR (125.7 MHz, C_6D_6 , 30°C) : δ 163.0 (NCMe), 141.0, 137.6, 120.1, 118.8 (C_{aryl}), 89.6 (middle CH), 64.3 (PCy_2), 23.2, 23.1 (CHMe_2), 20.4, 20.3 (CHMe_2), 20.1 (NCMe), 19.5, 19.3 (PCy_2)

$^{31}\text{P}\{^1\text{H}\}$ NMR (161.7 MHz, C_6D_6 , 30°C) : δ -28.8

4. Macrocyclic amines and amine ethers

4.1 *Introduction to macrocyclic chemistry*

4.1.1 Metal complexes of macrocycles

Macrocyclic ethers have been known for many years, with the 1987 Nobel Prize in Chemistry being awarded to Charles Pedersen for the synthesis of 18-crown-6 and other large crown ethers. From the outset, it was noted that these compounds can form stable complexes with many metal salts, formed by coordination of the oxygen atoms to the metal cation. Pedersen also noted that the coordination is independent of valence, with a 1:1 stoichiometry of polyether : metal ion in the compounds he studied.¹⁰³ Aspects influencing the stability of these crown complexes include physical factors such as the size difference between the ion and the ring, steric hindrance and the placement of the oxygen atoms within the ring, as well as electronic effects, such as the electrical charge on the ion, as well as the tendency of the ion to coordinate to solvent molecules, hindering coordination to the macrocycle. Macrocyclic amines are analogous to macrocyclic ethers, but with a substituent present on each nitrogen, allowing the possibility for functionalisation. Curtis presents a review on the coordination chemistry of metal-amine complexes and describes the creation of transition metal complexes of tetradentate amines.¹⁰⁴

In terms of nomenclature, Pedersen referred to cyclic ethers as “crowns”, as they mimicked the crown of a monarch when coordinating to a metal centre.¹⁰³ The prefix states the size of the ring, and the suffix states the number of oxygen atoms within in the ring. Hence, “18-crown-6” describes an 18-membered polyether with six oxygen atoms within it. For cyclic amines, the term “N-ane” is common. For the cyclic amines in this work, the number prefixing the “N” will describe the number of nitrogen atoms present, and the number prefixing “-ane” will describe the ring size. Hence, “3N9ane” describes a nine-membered ring containing three nitrogen atoms – the systematic name would be triazacyclononane. This terminology can be similarly extended to larger and more complex cycles.

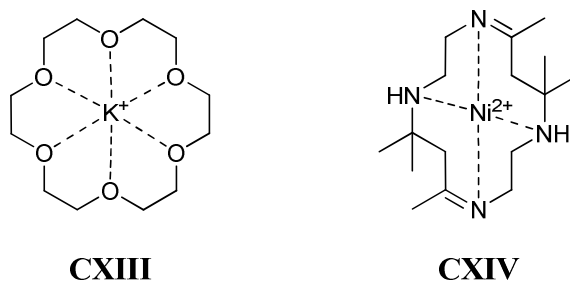


Figure 56 – A potassium macrocyclic ether (18-crown-6, left) and nickel macrocyclic amine (hexamethyl-4N14ane, right).

Nickel, copper and zinc complexes were investigated by Zompa and co-workers, and potentiometric titrations were carried out to investigate the stability of complexes containing macrocycles of various ring sizes.^{105,106} Complexes of nine-, ten-, eleven- and twelve-membered triamines were synthesised both for spectroscopic measurements, and also as a result of studying the acid dissociation constants for the hydrochloric salts of the amines. For most metal complexes, the pH of the solution was found to rise as the ring size of the ligand increased. This means that copper triazacyclononane has a lower pK_a than copper triazacyclododecane, and it is shown that deprotonation of a coordinated water molecule is more facile in a complex that contains a smaller macrocyclic ring. Zompa suggested this could be due to a smaller macrocycle binding closer to the metal centre, and so forcing the water molecules to bind further out in the coordination sphere, and so, be more accessible to deprotonation.¹⁰⁶

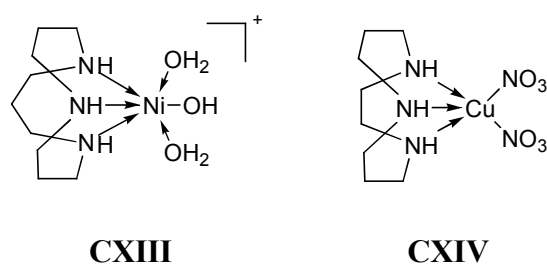


Figure 57 – Nickel complex $[\text{Ni}(\text{3N12ane})(\text{OH})(\text{H}_2\text{O})_2]^+$ (left) and copper complex $[\text{Cu}(\text{3N11ane})(\text{NO}_3)_2]$ (right).

The pH is also observed to be higher as the metal changes from copper to zinc. Calculation of formation constants for the larger macrocycles, such as 3N11ane and 3N12ane, indicated that the copper complexes were the most stable and the zinc

complexes the least stable, although this order of stability was reversed for the complexes of triazacyclononane.^{105,106} In addition to complexes containing one equivalent of macrocycle per metal atom, *bis*-complexes were also synthesised, and Zompa noted that they contained distorted octahedral geometries. For copper bis-macrocycles, it was reported that only one of the cycles was fully coordinated in solution, probably due to the other cycle undergoing exchange with water molecules.¹⁰⁵ *Bis*-complexes of nickel were observed to exhibit geometrical isomerism, as shown in figure 58.¹⁰⁶

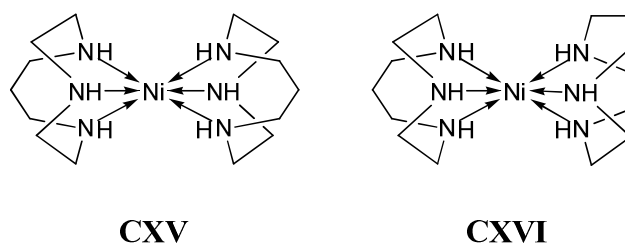


Figure 58 – Geometrical isomers of $[\text{Ni}(\text{3N10ane})_2]^{2+}$. Staggered geometry (left), and off-eclipsed (right).

Other *bis*-macrocycle complexes have been synthesised by Wieghardt and co-workers, in an attempt to study low-spin iron centres.¹⁰⁷ Two macrocycles in a *bis*-complex have been shown to exhibit a ligand field strength almost as high as that of 2,2'-bipyridine, which has previously yielded low-spin complexes of both Fe^{2+} and Fe^{3+} .¹⁰⁸ Both cationic species $[\text{Fe}(\text{3N9ane})_2]^{3+}$ and $[\text{Fe}(\text{3N9ane})_2]^{2+}$ crystallise in a staggered structure, very similar to that of the nickel complex **CXV** described above. It is observed that although Fe^{2+} and Fe^{3+} are very small ions, the Fe-N bond lengths are stretched within the complexes, most likely due to van der Waals repulsion between the 3N9ane ligands.

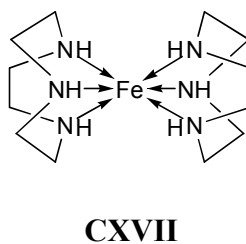


Figure 59 – Staggered conformation of $[\text{Fe}(\text{3N9ane})_2]^{3+}$ and $[\text{Fe}(\text{3N9ane})_2]^{2+}$.

Using lead, a significantly larger metal ion than either Fe^{2+} or Fe^{3+} , Wieghardt and co-workers have managed to isolate some examples of *mono*-macrocycle compounds, specifically $[\text{Pb}(\text{3N9ane})(\text{ClO}_4)_2]$ **CXVIII** and $[\text{Pb}(\text{3N9ane})(\text{NO}_3)_2]$ **CXIX**.¹⁰⁹

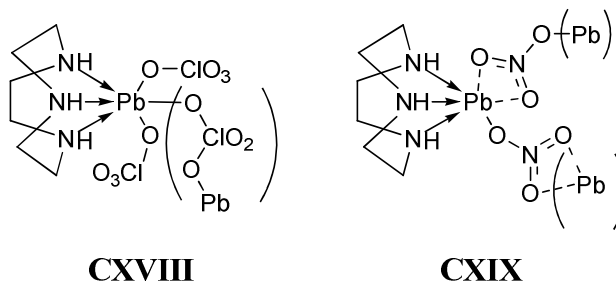


Figure 60 – Structures of $[\text{Pb}(\text{3N9ane})(\text{ClO}_4)_2]$ and $[\text{Pb}(\text{3N9ane})(\text{NO}_3)_2]$.

The complexes contain one macrocycle that lies on one side of the metal centre. In both complexes, the perchlorate or nitrate ligands bridge to other lead-macrocycle units in the solid state, giving an oligomeric structure. In both complexes, the bound oxygen atoms form a three-membered plane below the lead atom, parallel to the plane defined by the nitrogen atoms. The lead lone pair is seen to be stereochemically active, pointing outwards through the centre of this oxygen plane.¹⁰⁹

In order to prevent oligomerisation, sterically bulky substituents can be bound to the nitrogen atoms on the 3N9ane ring. Meyer and co-workers have bound very large adamantyl-phenoxide groups to 3N9ane, and have generated a uranium complex, which has been shown to undergo coordination from CO_2 in the very elusive linear binding mode, $\text{O}^- - \text{C} = \text{O}$.¹¹⁰ The bond lengths and vibrational frequencies observed in the infra-red spectrum suggest a metal-centred one-electron oxidation upon coordination of CO_2 . The binding site on the uranium centre is created by the adamantyl groups pointing in the same direction, forming a thin, cylindrical cavity, which provides access to an incoming ligand but acts to prevent the complex from dimerising at the metal atom. In addition to CO_2 , the complex has also shown similar reactivity towards trimethylsilylazide, yielding a linear U-NNN structure.¹¹⁰

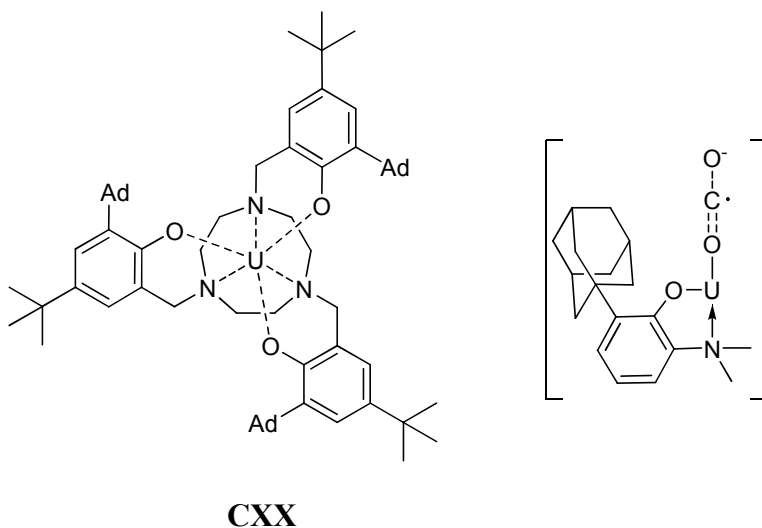
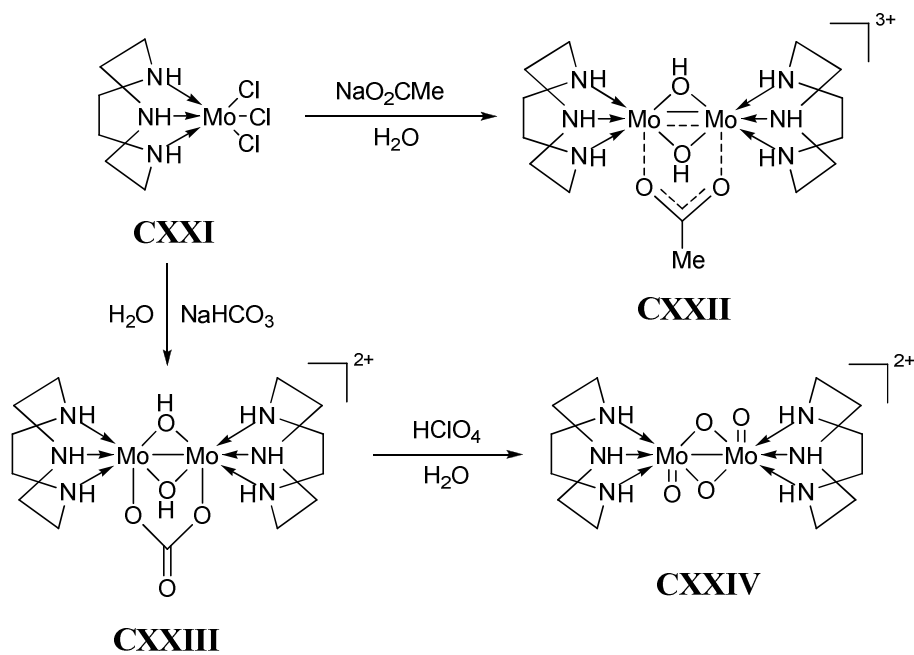


Figure 61 – Adamantyl-phenoxide-substituted [U(3N9ane)] (left; top-down view) and cylindrical binding mode of CO₂ (right; side-on view). Ad = adamantyl.

However, dimerisation can be desirable, when probing intramolecular reactivity of complexes. Wieghardt hydrolysed the mononuclear complex [Mo(3N9ane)Cl₃] **CXXI** in aqueous solution to yield the hydroxide-bridged binuclear complexes, shown in scheme 73.¹¹¹

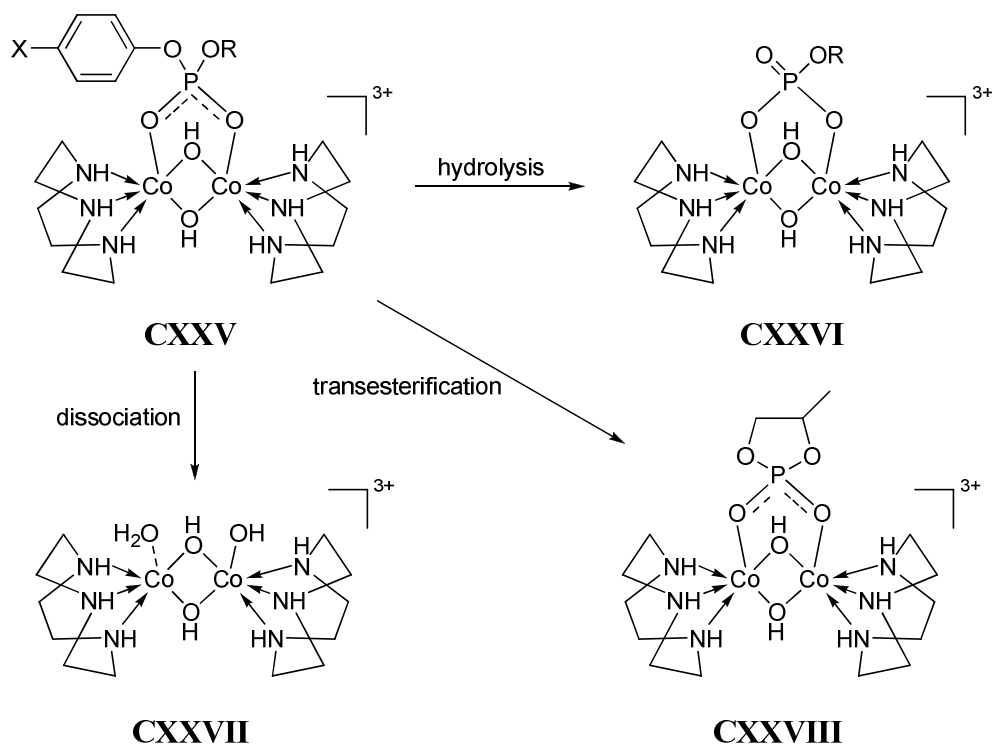
Scheme 73 – Dimer complexes of [Mo(3N9ane)].



In the presence of sodium acetate, a bridging acetate **CXXII** is formed. In the presence of sodium hydrogen carbonate, bridging carbonate **CXXIII** is formed. Treatment of carbonate **CXXIII** with perchloric acid yielded a novel molybdenum (V) dimer, with two bridging oxygen atoms, and a Mo-Mo bond. Each molybdenum centre was also doubly-bound to an additional oxygen atom (**CXXIV**).¹¹¹

Dinuclear cobalt complexes with a bridging phenylphosphate diester ligand were investigated by Williams and co-workers.¹¹² Both methyl and 2-hydroxypropyl phosphate complexes were reported, and were observed to undergo both hydrolysis and dissociation to form hydroxide-bridged complexes. The 2-hydroxypropyl phosphate complex also exhibited affinity for undergoing transesterification (scheme 74).

Scheme 74 – Hydrolysis, dissociation and transesterification of $[\text{Co}(\text{3N9ane})_2]$ complexes. $\text{X} = p\text{-NO}_2$, H . Hydrolysis and Dissociation; $\text{R} = \text{CH}_3$, $\text{CH}_2\text{CH}(\text{OH})\text{CH}_3$. Transesterification; $\text{R} = \text{CH}_2\text{CH}(\text{OH})\text{CH}_3$.



The rate of dissociation was found to be very slow for the methyl – *para*-nitrophenyl diesters ($\text{R} = \text{CH}_3$, $\text{X} = p\text{-NO}_2$), with the hydrolysis pathway favoured. The reverse is true for the unsubstituted phenyl ester ($\text{X} = \text{H}$), where the rate of hydrolysis is found to

be very slow. Although this pattern is repeated for the 2-hydroxypropyl ester ($R = \text{CH}_2\text{CH}(\text{OH})\text{CH}_3$), the transesterification pathway is favoured as well, independent of the X group.¹¹²

Burstyn and co-workers have synthesised a series of copper-macrocyclic complexes, specifically to catalyse the hydrolysis of a phosphate diester (*vide infra*).¹¹³ Copper dichloride and dibromide adducts of 3N9ane, 3N10ane and 3N11ane were synthesised from treatment of aqueous solutions of the metal salt with the hydrochloric salt of the macrocycle, followed by subsequent neutralisation with base. There was shown to be a shift in geometry from square pyramidal to trigonal bipyramidal as the ring size increased, with a corresponding decrease in the distance between the copper atom and the plane defined by the three nitrogen atoms.

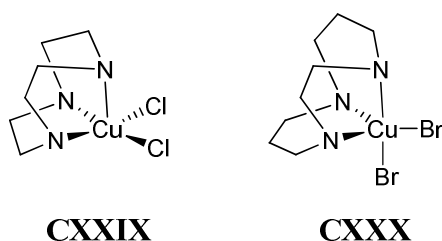


Figure 62 – Square pyramidal $[\text{Cu}(\text{3N9ane})\text{Cl}_2]$ (left) and trigonal bipyramidal $[\text{Cu}(\text{3N11ane})\text{Br}_2]$ (right).

However, despite the differences in configuration in the solid state, all of the copper complexes exhibit a square planar geometry in solution, with evidence such as high energy *d-d* electronic transitions, rather than low energy transitions, which are more indicative of trigonal bipyramidal structures.^{113,114} Another reason for the square pyramidal geometry in solution could be the coordination of water molecules to the copper centre. Coordinated water has been shown to be important when using these complexes in the hydrolysis of phosphate esters.¹¹³

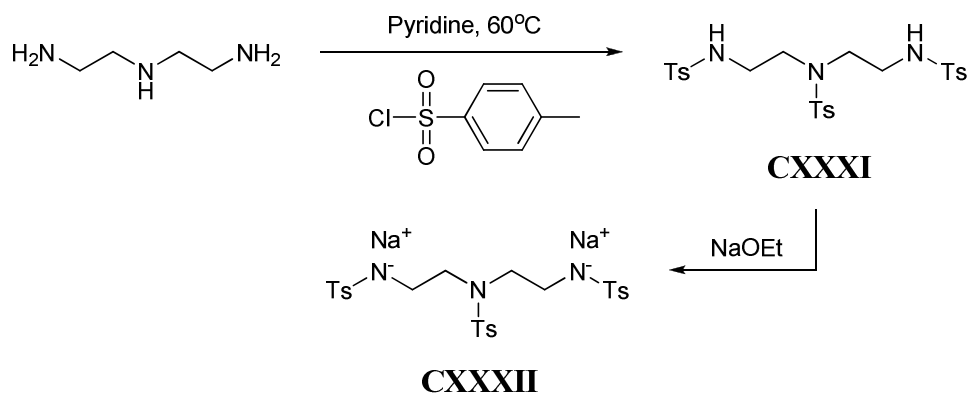
4.1.2 Synthesis of macrocyclic amines and ethers

The most common method toward synthesising cyclic amine structures was first popularised by Richman and Atkins in 1974.¹¹⁵ The synthesis they report involves three main steps. The first is the tosylation of a linear amine or alcohol to protect the nitrogen atoms, and activate the oxygens. In the second step, cyclisation with another tosylated reagent is carried out. The resulting macrocycle is then heated in strongly acidic conditions in the third step to remove the tosylate groups, and subsequently treated with sodium hydroxide to yield the final macrocycle.¹¹⁶

Step 1 – Tosylation

Richman and Atkins report the tosylation of diethylenetriamine in pyridine, followed by aqueous workup.¹¹⁶ It is this method that is referred to as “Method A” in our synthetic procedure detailed below (*vide infra*), with minor modifications. Pyridine acts as both the solvent and base, to deprotonate the initial amine.

Scheme 75 – Tosylation of diethyltriamine by Richman and Atkins.



The sodium salt **CXXXII** was found to easily crystallise from hot ethanolic solutions of tosylated amine **CXXXI**. Although isolation of the sodium salt was carried out in many synthetic procedures,^{116–118} it could also be generated *in situ* for the purpose of the next step.^{119,120}

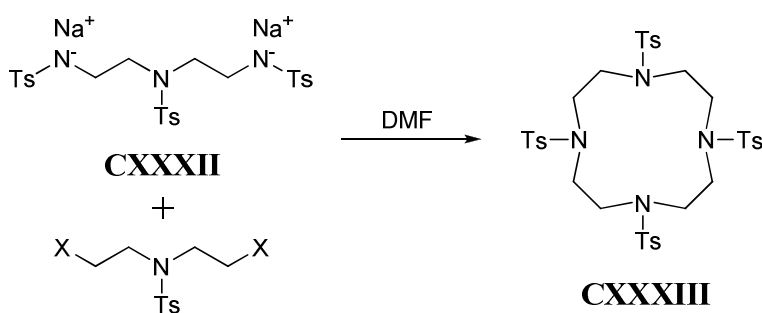
As a variation of this tosylation procedure, Paoletti and Micheloni reported that triethylamine could be used instead of pyridine for the tosylation of diethanolamine.¹²¹ An earlier paper by Mertes and co-workers reported using triethylamine as the base in

the tosylation step, but carried out the reaction in dichloromethane as a solvent.¹²² To avoid using large quantities of triethylamine, the Mertes method was preferred by us over the Paoletti method, and it was designated as “Method B” in our syntheses (*vide infra*). A variation on the Mertes procedure (Method B) was reported by Jenneskens and co-workers, simply by changing the base to powdered potassium hydroxide for the tosylation reaction.¹²³ Using this instead of triethylamine is referred to as “Method C” in our synthetic procedures.

Step 2 – Cyclisation

Richman and Atkins generate their macrocyclic complexes by treating the disodium salt **CXXXII** with another tosylated compound in N,N-dimethylformamide (DMF).¹¹⁵ This procedure is very common, and few variations exist. It was also found that, aside from a tosylated compound, disodium salt **CXXXII** could also react with dihalide complexes in the same fashion, to produce the same cyclised compounds.^{115,120}

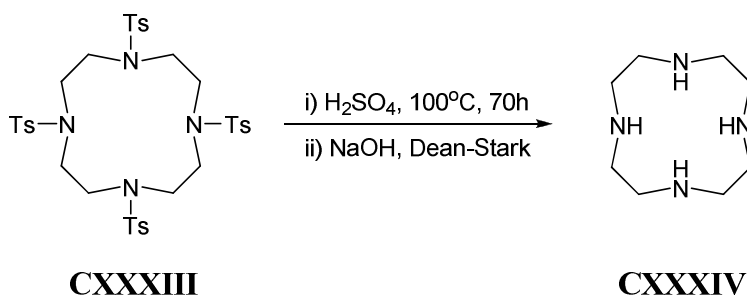
Scheme 76 – Cyclisation of macrocyclic amines in DMF. X = OTs, Cl, Br, I.



Step 3 – Removal of tosyl groups

The main method, used by Richman and Atkins, for the detosylation of cyclic amines, involves heating the tosylated macrocycle at 100°C in concentrated sulphuric acid for 70 hours, to isolate the sulphuric salt, which is converted to the neutral amine by treatment with sodium hydroxide and activated carbon.¹¹⁶ Dreissen and co-workers perform this reduction with the use of a Dean-Stark apparatus, to remove water from the solution to keep the product dry.¹²⁴

Scheme 77 – Detosylation of macrocyclic amines

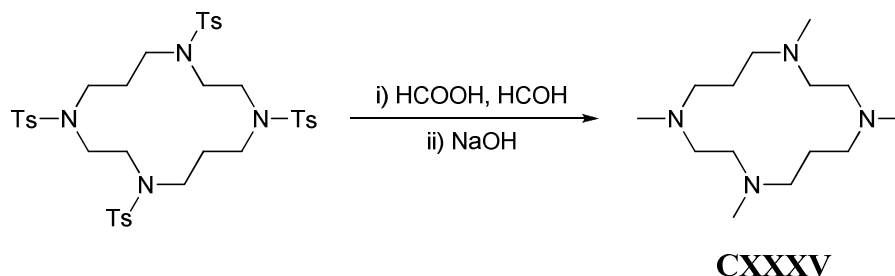


However, a problem that became apparent in our studies was that the sulphuric salt was unstable, and was not easily handleable. In addition to this, the neutralisation of the sulphuric salt by sodium hydroxide often did not yield a pure product in consistent amounts. The solution to these problems is discussed later (*vide infra*) in our synthetic section.

Further functionalisation of macrocycles

As stated previously, the nitrogen atom in macrocyclic amines can be substituted with various group that may influence the reactivity of steric bulk of the compound. Barefield and Wagner produced a method for methylating 1,4,8,11-tetraazacyclotetradecane (4N14ane), by treating the neutral macrocycle with a mixture of formic acid and formaldehyde.¹²⁵ After neutralisation of excess acid, the product 4N14ane-Me₄ (**CXXXV**) was formed in yields of up to 80%.

Scheme 78 – Methylation of 4N14ane.

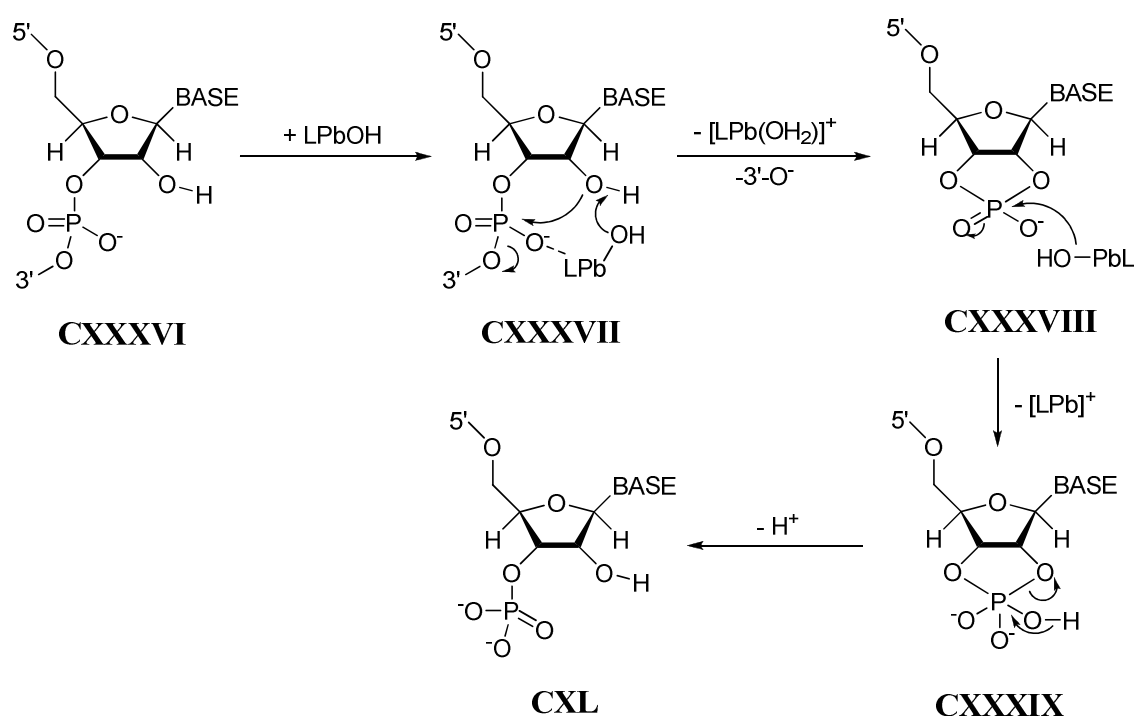


For larger functional groups, Halfen and co-workers partly detosylated a macrocyclic complex, and treated this with an alkyl halide to substitute larger alkyl groups at the detosylated nitrogen atoms.¹²⁶ Removal of the remaining tosyl groups gave a convenient route to unsymmetrically-substituted cyclic amine compounds.

4.1.3 Phosphate ester hydrolysis by metal centres

Within cells in the body, lead has been shown to associate with nucleic acids, and compete for cysteine-rich binding sites with zinc ions, due to its ability to form strong bonds with thiol units.¹²⁷ At concentrations higher than around 20 μM , lead has been shown to hydrolyse RNA units in a catalytic fashion, via a lead hydroxide intermediate.¹²⁸ The hydrolysis has been suggested to occur in a stepwise fashion from the lead hydrate, and cleaves the RNA polymer at a phosphate centre (scheme 79).

Scheme 79 – Accepted mechanism for the stepwise lead-induced hydrolysis of RNA. L = spectator ligand.



After initial coordination to the phosphate, the lead hydroxide deprotonates the 2'-OH (CXXXVII), which attacks the phosphate diester, causing cleavage of the P-O bond and the formation of a five-membered cyclic phosphate CXXXVIII. The second step involves attack at the phosphate centre by another lead hydroxide, which results in the *penta*-coordinate phosphate CXXXIX, which decomposes to monophosphate CXI. This mechanism is similar to the hydrolysis of carboxylic acid esters and phosphate diesters carried out with zinc, copper and cobalt hydroxides, and has highlighted that the coordination of the metal centre to the phosphate is an important factor in the hydrolysis reaction.¹²⁹ The hydrolysis reaction was studied in detail by Morrow and co-workers,

using the 4-nitrophenyl phosphate ester of propylene glycol (**21**) as a model system for the backbone strand of RNA.¹³⁰ Morrow notes that, although RNA itself can be used in mechanistic studies, many systems readily precipitate metal hydroxides or metal nucleotides in the course of the study. By using a model system, such as a phosphate diester, these unwanted precipitates are minimised or avoided entirely.

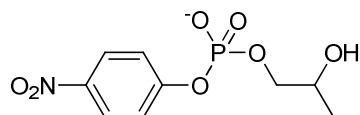
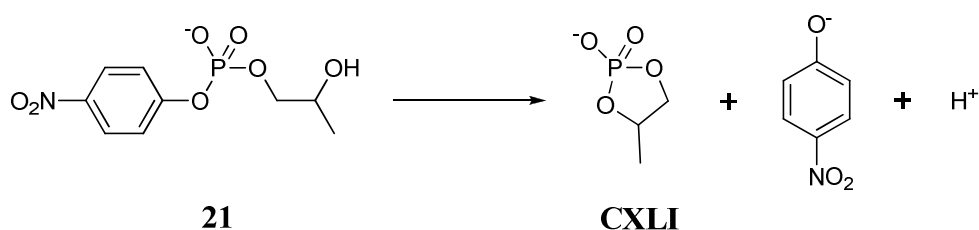


Figure 63 – 4-nitrophenyl phosphate diester of propylene glycol (**21**).

The hydrolysis of the phosphate ester (scheme 80) produces the cyclic phosphate **CXLI** and one equivalent of *para*-nitrophenolate, the latter of which has a distinct absorption at 400 nm. By monitoring the reaction with UV-visible spectrophotometry, the increase in absorption at 400 nm can be observed as the reaction progresses.^{113,130,131}

Scheme 80 – Hydrolysis of phosphate diester **21**.

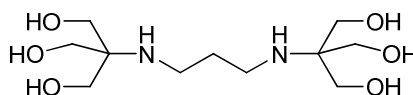


Morrow reports that hydrolysis of phosphate ester **21** was carried out in a combination of sodium nitrate and HEPES buffer solution (N-(2-hydroxyethyl)piperazine-N'-ethanesulphonic acid) at pH 6.85 at 37°C.¹³⁰ These conditions were chosen in order to mimic the physiological environment, albeit slightly acidified to prevent the precipitation of metal hydroxide species that occurred at more basic pHs. Hydrolysis with a range of di- and trivalent metal ions showed first-order kinetics with respect to the phosphate within the concentration ranges 1×10^{-4} to 1×10^{-3} M. The studies also showed first-order kinetics with respect to the metal ions, but over a broader concentration range (table 25).¹³⁰

Table 25 – Concentration ranges for metal ions showing first-order dependence.

Concentration range (M)	Metal ions
1.0×10^{-4} to 5.0×10^{-4}	Pb^{2+} , La^{3+} , Nd^{3+} , Eu^{3+} , Gd^{3+} , Tb^{3+} , Yb^{3+} , Lu^{3+}
6.0×10^{-4} to 1.4×10^{-3}	Zn^{2+}
1.0×10^{-3} to 4.0×10^{-3}	Co^{2+} , Ni^{2+} , Mn^{2+}
5.0×10^{-5} to 3.0×10^{-4}	Cu^{2+}
0.1 to 0.6	Ca^{2+} , Mg^{2+}

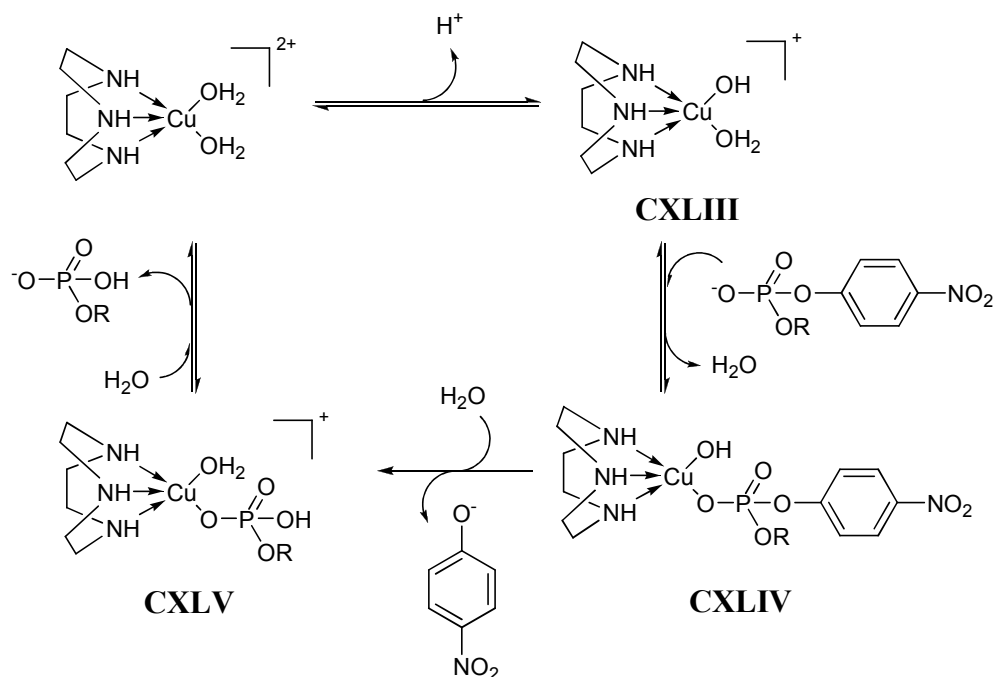
Performing the hydrolysis kinetics in the presence of the spectator ligand *bis*-(*tris*-(hydroxymethyl)aminomethane)propane **CXLII**, Yatsimirsky prepared reaction solutions by combination of metal and ligand stock solutions to the desired volume, effectively generating a metal-ligand complex *in situ*.¹³¹ For the hydrolysis of nitrophenyl phosphates by lanthanide complexes, first-order kinetics were observed with respect to the phosphate undergoing hydrolysis, in the presence of a high excess of metal complex, and the formation of metal hydroxide complexes was observed by potentiometric titrations.

**CXLII**Figure 64 – *Bis*-(*tris*-(hydroxymethyl)aminomethane)propane spectator ligand.

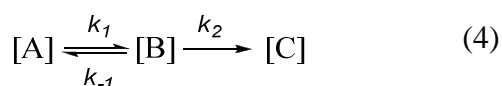
Synthesis of a metal-ligand complex can also be carried out prior to the kinetic study, as described by Burstyn and co-workers.¹¹³ A series of copper macrocyclic complexes were synthesised (*vide supra*) and shown to be active with respect to phosphate hydrolysis. The $\text{p}K_{\text{a}}$ of the coordinated water molecules was shown to be affected by the size of the coordinated macrocyclic ring; the $\text{p}K_{\text{a}}$ increased as the ring size increased. As the coordinated water molecules are the source of the hydroxide ions which hydrolyse the phosphate, the $\text{p}K_{\text{a}}$ of these water molecules directly affects the rate of hydrolysis.¹¹³ To study the reactivity of these different complexes in the hydrolysis of the phosphate ester, the concentrations of the metal-containing species and the phosphate were alternately varied, and studied using the method of initial rates – in this

case, the reaction was observed for no more than one hour. The proposed mechanism is shown in scheme 81, and shows equilibria between the free metal complex (**CXLIII**) and the metal complex bound to the phosphate (**CXLIV**).¹¹³

Scheme 81 – Proposed mechanism for copper-catalysed phosphate hydrolysis. R = *para*-nitrophenyl.

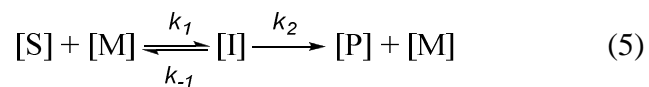


The hydrolysis of phosphate diester **21** can therefore be shown as a consecutive reaction, with the first step the coordination of the metal species to the phosphate diester, which then undergoes hydrolysis to form the product, and release *para*-nitrophenolate. McDaniel and Smoot developed a general approximation for the kinetics of a consecutive reaction of this type using the steady-state approximation (equation (4)).¹³²



Assuming the intermediate B is used up as soon as it is created (i.e. the concentration is negligible), the appearance of product C depends exclusively on the concentration of reagent A. However, if a catalytic compound is present, such as in the phosphate

hydrolysis reaction or enzyme kinetics, a secondary term must be introduced and the reaction becomes as shown in equation (5), following Michelis-Menten type kinetics.



(S = substrate, M = catalytic metal-containing species, I = coordinated intermediate, P = product).

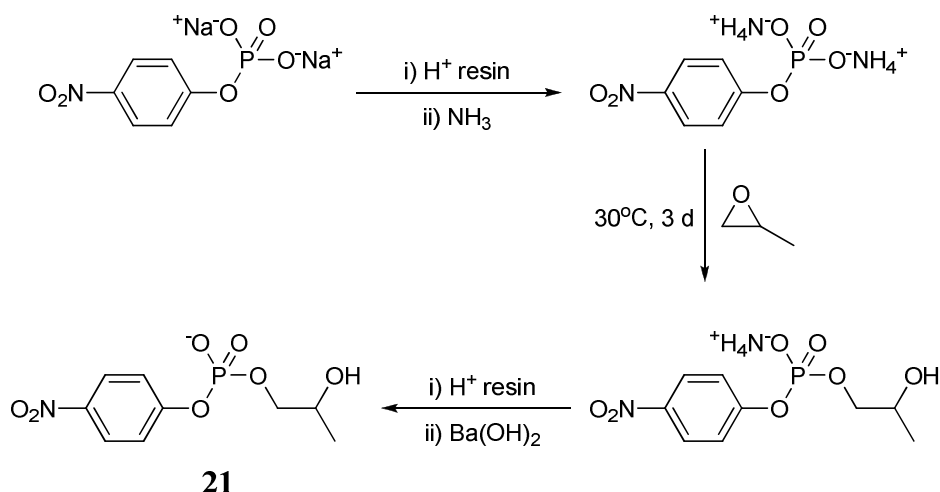
Flooding the reaction with excess substrate removes the dependence on it from the rate equation, effectively making the metal complex the rate-determining reagent, and therefore, the coordination of metal complex to substrate (k_1) the rate-determining step. This methodology is saturation kinetics, where there is an excess of substrate, and the reaction can proceed at its maximum rate. This is a feature of enzyme kinetics, where an excess of substrate allows all available enzyme binding sites to be filled, and the rate of reaction ceases to increase.

4.2 Results and discussion

4.2.1 Synthesis of barium 2-hydroxypropyl 4-nitrophenyl phosphate (**21**)

The synthesis of phosphate diester **21** used a slightly modified procedure based on the previously reported synthesis by Brown and co-workers.¹³³ A solution of disodium 4-nitrophenyl phosphate in water was passed down a column of IR-120 ion exchange resin to exchange the sodium ions for protons. The clear eluent was collected and made basic to pH 8 by the addition of aqueous ammonia. An excess of epoxyp propane was added, and the mixture refluxed at 30-35°C for three days, after which the solvent was removed under reduced pressure to yield a bright yellow oil. The oil was passed down the IR-120 ion exchange column, and the colourless eluent made almost neutral to pH 6.5 with aqueous barium hydroxide solution. Excess barium hydroxide was precipitated by addition of ethanol, and removed with a centrifuge. Removal of solvent under reduced pressure yielded a yellow oil, and acetone was added to precipitate the desired phosphate **21**, which was collected as a white powder and dried in 43% yield.

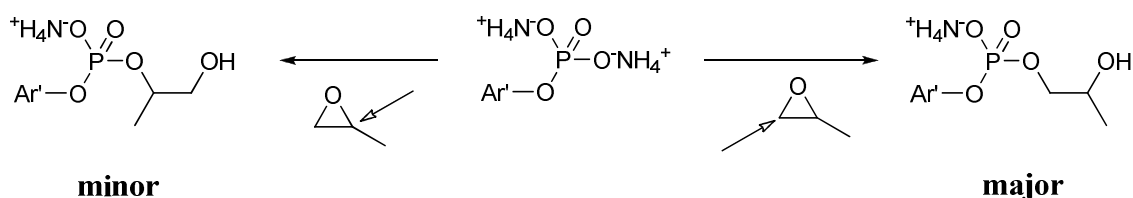
Scheme 82 – Synthesis of phosphate diester **21**



The ^1H NMR spectrum shows two doublet resonances at δ 8.27 and 7.48, corresponding to the aryl protons, as well as three signals at δ 3.98, 3.89 and 3.47, assigned to the alkyl protons in the propyl chain on the phosphate. However, two resonances are observed in

the $^{31}\text{P}\{^1\text{H}\}$ NMR spectrum, corresponding to the two possible isomers of diester **21** (scheme 83). The two isomers occur upon addition of the epoxyp propane. A resonance at δ -5.83 is assigned to the major isomer, which is formed when the epoxyp propane is attacked at the least hindered end. A much less intense resonance at δ -6.30 is assigned to the minor isomer, which is formed when the epoxyp propane is attacked from the more hindered end.

Scheme 83 – Generation of the isomers of phosphate diester **21**. Attack at least hindered end (right) gives the major product, attack at most hindered end (left) give the minor product. $\text{Ar}' = \textit{para}$ -nitrophenyl



Care was taken when refluxing the mixture, as a longer reaction time led to increased quantities of the more-hindered product, identified by the increase in intensity of the minor-product signal at δ -6.30. Optimum yields of the least-hindered (major) product were achieved with around 70 hours of refluxing.

4.2.2 Macrocyclic synthesis

Six starting materials were used to generate a large range of macrocyclic ligands, over a total of four synthetic steps with isolatable products at each stage. The methodology involved was broadly very similar, independent of the final product, however, each material was required to be treated slightly differently. No pattern was evident, and so the optimisation of reaction conditions was done by trial and error.

Starting materials containing primary or secondary amines were protected (or activated, in those materials containing alcohols) by the addition of a tosylate group under basic conditions. These tosylated compounds were then cyclised in N,N -dimethylformamide, after which the tosyl groups were removed by the addition of sulphuric and

hydrochloric acids to form the salts of the macrocycles. Addition of strong base to these salts, and the removal of water yielded the neutral ligands.

4.2.2.1 Tosylation of starting materials

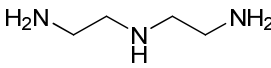
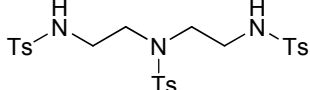
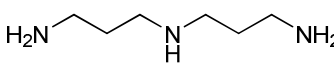
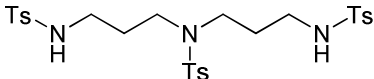
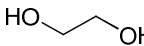
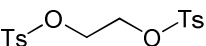
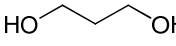
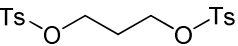
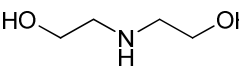
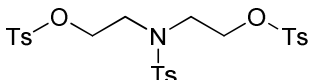
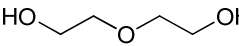
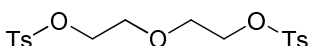
Three methods of protecting linear amines and alcohols were used, depending upon the individual compound. The presence of base was required to deprotonate the starting material to allow addition of the tosyl group. The three bases used were pyridine (method A), triethylamine (method B) and potassium hydroxide (method C), and each was used under slightly different conditions (See experimental section for further details).

Characterisation was carried out by ^1H and $^{13}\text{C}\{^1\text{H}\}$ NMR spectroscopy in deuterated chloroform and mass spectrometry. The NMR spectra produced a very clear spectrum for the tosylated compounds. Key resonances to observe were aromatic doublets and methyl group resonances on the tosylate groups, and CH_2 signals for the main backbone of the compound.

General Procedure – Tosylation

The compound to be tosylated was added slowly to a solution of tosyl chloride in the presence of the appropriate base. In all cases, the addition was observed to be greatly exothermic, and care was taken to maintain a constant reaction temperature by slowing the addition as necessary. Upon complete addition of the starting material, the reaction was allowed to stir overnight and come to room temperature. Ice and hydrochloric acid were used to remove excess base, and to wash the organic layer containing the tosylated product. Further washing with deionised water and subsequent drying of this organic layer *in vacuo* produced the product in good yield, which was collected and used in the next step without further purification. Starting materials and their respective products are shown in table 26, and all reported yields of ~ 80%.

Table 26 – Starting materials, respective methods and tosylated products.

Starting material	Methodology	Tosylated product
 N,N-diethylenetriamine	Method A (Pyridine, 60°C)	 22
 N,N-dipropylenetriamine	Method B (DCM, NEt ₃ , 0°C)	 23
 Ethane-1,2-diol	Method B (DCM, NEt ₃ , 0°C)	 24
 Propane-1,3-diol	Method C (DCM, KOH, -10°C)	 25
 N,N-diethanolamine	Method B (DCM, NEt ₃ , 0°C)	 26
 Diethylene glycol	Method C (DCM, KOH, -10°C)	 27

The ¹H NMR spectra of the tosylated products showed that these compounds were isolated cleanly, with signals corresponding to the tosyl groups (two sets of aryl protons and a methyl group) and the CH₂ groups clearly visible. In products **22**, **23** and **26**, where three tosyl groups are present, a second set of tosyl group signals are observed, corresponding to the tosyl group on the central nitrogen atom. A mass spectrum for each product was recorded, with a mass peak (*m/z*) corresponding to the sodiated ion of each respective compound observed.

4.2.2.2 Cyclisation of starting materials to protected macrocycles

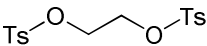
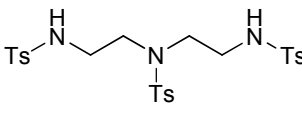
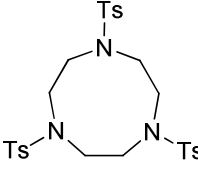
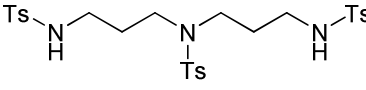
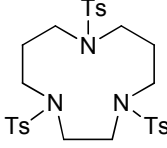
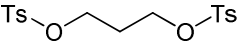
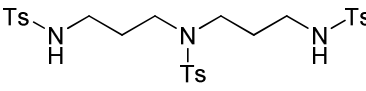
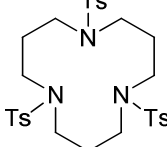
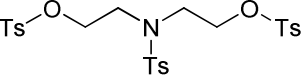
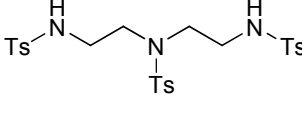
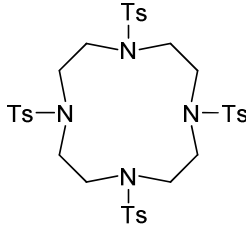
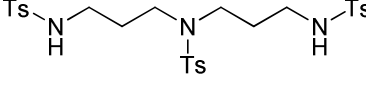
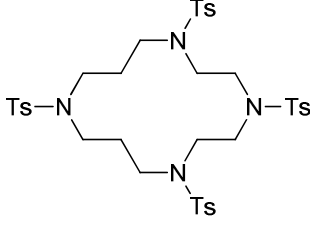
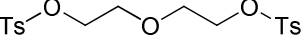
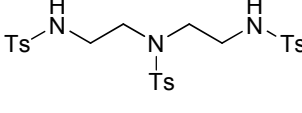
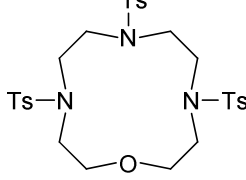
The protected amines **22** and **23** were combined with the activated alcohols **24**, **25**, **26** and **27** to generate six cyclised compounds containing nitrogen or oxygen heteroatoms within the ring structure. The method used was based on the cyclisation method described by Atkins and Richman.¹¹⁶ At this stage, all the nitrogen atoms still remained protected with tosyl groups, an indicator that could be used to observe the compound by ^1H and $^{13}\text{C}\{^1\text{H}\}$ NMR study.

General Procedure – Cyclisation

The tosylated macrocycles were generated by addition of one equivalent of one of the activated alcohols to a hot (100°C) dimethylformamide (DMF) solution containing one of the protected amines and an excess of potassium carbonate. After complete addition, and subsequently allowing the mixture to cool, water was added to dissolve the excess base, and the mixture left to stir overnight to allow precipitation of the product. The pale, sticky solid was then filtered from the mother liquor, washed with copious amounts of deionised water and dried at high temperature (~150°C) *in vacuo*. Yields of the cyclised products varied from ~ 30 – 80%. Residual DMF, observed in the ^1H NMR spectra of the cyclised products, did not appear to affect the subsequent deprotection step.

Table 27 shows the combinations of activated alcohol, protected amine and respective cyclised product. The experimental section provides further reaction details. Combinations of alcohol and amine that do not appear did not provide an isolatable product.

Table 27 – Combinations of protected amines and activated alcohols to form cyclised products **28** – **33**.

Activated alcohol	Protected amine	Cyclised product
 <p>24</p>	 <p>22</p>	 <p>28</p>
	 <p>23</p>	 <p>29</p>
 <p>25</p>	 <p>23</p>	 <p>30</p>
 <p>26</p>	 <p>22</p>	 <p>31</p>
	 <p>23</p>	 <p>32</p>
 <p>27</p>	 <p>22</p>	 <p>33</p>

The ^1H NMR spectra of the compounds all displayed distinct signals corresponding to the tosyl groups on the cyclised compounds. The 3- and 4-axis symmetric compounds 3N9ane-Ts₃ **28**, 3N12ane-Ts₃ **30** and 4N12ane-Ts₄ **31** displayed the two aromatic doublets and the methyl group singlet representative of only one tosyl group environment. The compounds 3N11ane-Ts₃ **29**, 4N14ane-Ts₄ **32** and O3N12ane-Ts₃ **33**, containing one axis of symmetry, displayed multiple tosyl group resonances, respective of the number of tosyl group environments present. Signals corresponding to the CH₂ units of the macrocycle backbone are identifiable on all complexes, and can be assigned to the appropriate protons. A mass spectrum was recorded for all compounds **28** – **33**, with a mass peak (m/z) corresponding to the sodiated or potassiated ion of each respective compound observed.

4.2.2.3 Removal of tosyl groups to form hydrochloride salts

The tosyl groups were removed by heating the protected macrocycle in sulphuric acid to produce the sulphate salt of the material, in a similar fashion to the method by Atkins and Richman.¹¹⁶ However, the sulphate salt was observed to be difficult to handle easily, and the method did not give consistently repeatable yields of the products. Removing the water from the compound in the final step also proved to be very difficult. An improvement to this method was suggested by Driessen and co-workers,¹²⁴ but was also found to have the same water-removal problem. Both methods also required prolonged heating of concentrated sulphuric acid at high temperatures. We carried out these procedures in an attempt to optimise them, but faced the same problems, in addition to the obvious safety concern of high-temperature concentrated sulphuric acid. Karsten Meyer and Oanh Lam provided us with a “fast-cracking” method, which only required short, vigorous heating in concentrated sulphuric acid, followed by hydrochloric acid workup.¹³⁴ The hydrochloride salt was stable enough to be isolated, and removal of water from this salt proved easier to accomplish than from the sulphate analogue.

General Procedure – Fast Cracking

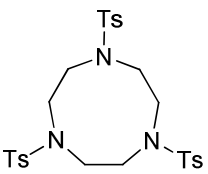
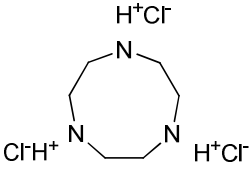
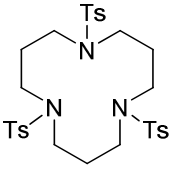
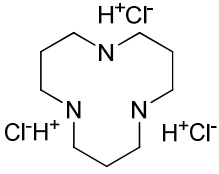
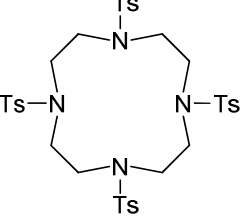
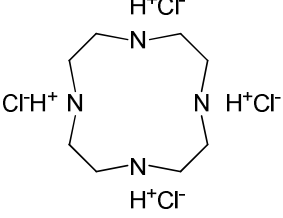
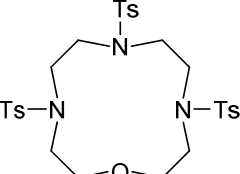
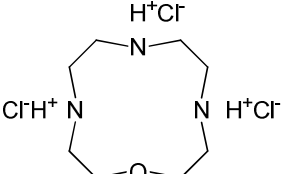
The macrocycle to be cracked was added to hot (150°C) concentrated sulphuric acid, which resulted in the solution darkening, and stirred at for 15-20 minutes. The brown-black mixture was then poured **very carefully** into ice-cooled ethanol, in a procedure that was observed to be very exothermic. Slow addition of the acid mixture and vigorous stirring of the ethanol was important in order to prevent clumping of the precipitated material. The beige-grey powder was collected by filtration, then dissolved in water and heated to near reflux. Concentrated hydrochloric acid was then added very slowly. After complete addition of the acid the heat was removed and the light brown solution was allowed to stand overnight, resulting in the precipitation of the hydrochloride salt of the macrocycle as a white, crystalline powder. Yields of this method of cracking were very high, resulting in almost complete conversion to the hydrochloride salt.

The hydrochloride salts were observed to be far more stable than their sulphate analogues, and could be stored indefinitely in a sealed vial on the bench. The hydrochloride salts were observed to be soluble in aqueous solvents, and insoluble in organic solvents. NMR spectra for all salts were recorded in D₂O, rather than deuterated chloroform. In all ¹H NMR spectra, no tosyl peaks were observed, which indicated their removal. Aside from the residual water peak, only signals corresponding to the CH₂ units on the macrocycle backbone were observed, and could be assigned accordingly. The hydrochloride units could not be observed, indicating these units are probably undergoing rapid proton exchange with the D₂O solvent.

Table 28 shows the hydrochloride salts **34 – 37**, obtained from their respective tosylated precursors 3N9ane-Ts₃ **28**, 3N12ane-Ts₃ **30**, 4N12ane-Ts₄ **31** and O3N12ane-Ts₃ **33**.

Attempts to crack 3N11ane-Ts₃ **29** and 4N14ane-Ts₄ **32** were not successful. These were the two more difficult macrocycles to cyclise, and so were omitted from the fast-cracking process.

Table 28 – Fast cracking of tosylated macrocycles **28**, **30**, **31** and **33** to produce hydrochloride salts **34** – **37**. Conditions: i) H₂SO₄, 150°C. ii) HCl, 100°C.

Tosylated macrocycle	Hydrochloride salt
 <p>28</p>	 <p>34</p>
 <p>30</p>	 <p>35</p>
 <p>31</p>	 <p>36</p>
 <p>33</p>	 <p>37</p>

4.2.2.4 Neutralisation to generate macrocyclic compounds

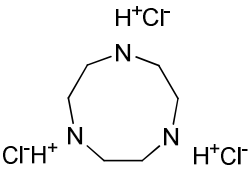
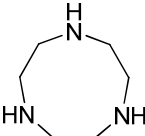
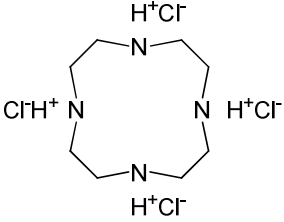
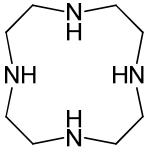
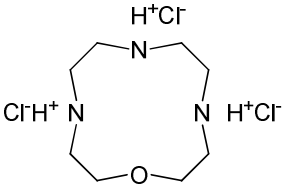
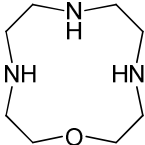
The method of neutralising the hydrochloride salts was a slight modification of the procedure by Driessen, and employed the use of sodium hydroxide and a Dean-Stark water eliminator. The neutral macrocyclic compounds were found to be very hygroscopic, and were observed to deliquesce if exposed to even small quantities of water. Removal of water from a neutral macrocycle was found to be a non-trivial procedure, with fairly strong conditions required. For example, exposure to activated

molecular sieves did not remove water associated with the macrocycles. The compounds were stored in an inert atmosphere glovebox to avoid exposure to moisture, after drying *in vacuo* overnight.

General Procedure – Neutralisation

The hydrochloride salt was dissolved in a mixture of water and toluene in a roughly 2:3 ratio. Sodium hydroxide was added to the mixture, which was then heated at reflux. Additional portions of sodium hydroxide were required to be added throughout the procedure, as the water was removed from the mixture *via* the Dean-Stark apparatus. When all the water had been distilled off, the toluene was removed under reduced pressure to yield the neutral macrocycle as a white powder in medium-low yields of around 20 – 40%.

Table 29 – Neutral macrocycles **38**, **39** and **40**, acquired from their corresponding salts.

Hydrochloride salt	Neutral macrocycle
 <p style="text-align: center;">34</p>	 <p style="text-align: center;">38</p>
 <p style="text-align: center;">36</p>	 <p style="text-align: center;">39</p>
 <p style="text-align: center;">37</p>	 <p style="text-align: center;">40</p>

The ^1H NMR spectrum of each of the neutral macrocycles shows resonances corresponding to the CH_2 units in the respective macrocycle backbone, which can be assigned accordingly. Although no amine protons can be detected in the ^1H NMR, probably due to exchange with the solvent, mass spectrum peaks (m/z) were recorded corresponding to the protonated forms of the neutral macrocycles.

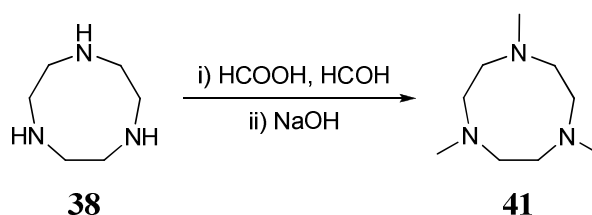
4.2.2.5 Further macrocycle functionalisation

A brief study was carried out to investigate the possibility of further functionalising the macrocyclic ligands in the series, with the intention of investigating the effect of functionalisation upon the phosphate hydrolysis reaction. The methylation of larger macrocyclic ligands was reported by Barefield and Wagner, and it was this procedure that was adopted for the generation of 3N9ane- Me_3 **41**.¹²⁵

1,4,7-trimethyl-1,4,7-triazacyclononane (**41**)

3N9ane **38** was dissolved in water with an excess of formic acid and formaldehyde. The mixture was heated to reflux for 24 hours, after which it was allowed to cool. Sodium hydroxide solution was added to create a strongly basic environment to neutralise excess acid. The methylated product, 3N9ane- Me_3 **41**, was extracted with chloroform, and isolated as a yellow oil in 82% yield.

Scheme 84 – Methylation of 3N9ane **38** to produce 3N9ane- Me_3 **41**.



The ^1H NMR spectrum shows an uncluttered spectrum, with two distinct resonances, of integration 3:4. The resonance at δ 2.60 is assigned to the CH_2 protons on the ring of the ligand, with a resonance at δ 2.31 corresponding to the methyl amine groups. The $^{13}\text{C}\{^1\text{H}\}$ NMR spectrum shows a similar set of resonances, with one at δ 57.1 assigned to the CH_2 units, and another resonance at δ 46.7 corresponding to the methyl groups. In

addition to this, a mass spectrum peak was present at m/z 172, representative of the protonated complex, $3N9ane-Me_3.H^+$.

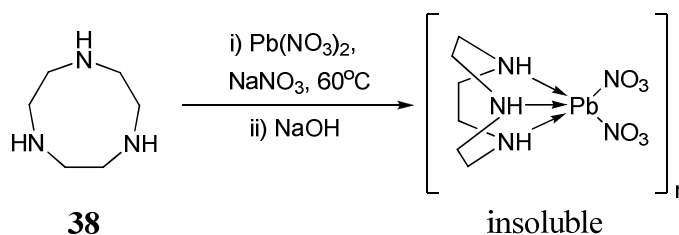
4.2.3 Macrocyclic complexes with metal centres

Metal complexes of macrocyclic ligands are well-known (*vide supra*), and it was attempted to synthesise a small number of metal-containing complexes to investigate the binding properties of the macrocycles. Following the procedures detailed earlier, complexes of lead, copper and zinc were attempted.

Lead(II) nitrate¹⁰⁹

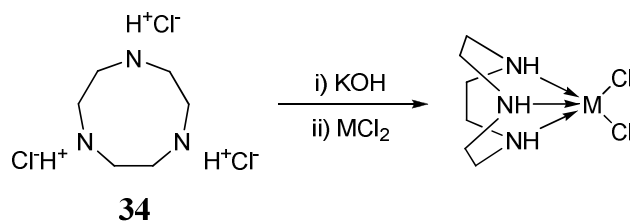
3N9ane **38** was mixed with aqueous $Pb(NO_3)_2$ in the presence of excess sodium nitrate at 60°C. Sodium hydroxide was added and storage at 4°C overnight yielded a fine white powder. However, this powder was completely insoluble, and resisted any attempts to characterise it. Further concentration of the solution did not produce any further material.

Scheme 85 – Attempted synthesis of $Pb(3N9ane)(NO_3)_2$



Copper(II) and zinc(II) chloride¹⁰⁵

3N9ane.3HCl **34** was mixed with an ethanol solution of excess potassium hydroxide, and a solution of either copper(II) or zinc(II) chloride was added. The solution was concentrated *in vacuo*, and cooled to 4°C to encourage crystallisation. No crystals were observed in the case of the zinc complex, but a large, blue plate was formed from the copper-containing solution. However, 1H NMR spectroscopy showed that this did not contain any macrocyclic proton resonances.

Scheme 86 – Attempted synthesis of $M(3N9ane)Cl_2$. ($M = Cu, Zn$.)

4.2.4 Studies on the hydrolysis of 2-hydroxypropyl 4-nitrophenyl phosphate

Kinetic studies were carried out to study the hydrolysis mechanism of *para*-nitrophenyl phosphate **21** as a model system for the lead-based cleavage of RNA. Our aim was to investigate the effect on reaction rate by the presence of different-sized macrocyclic ligands, and derive a quantitative correlation between the rate of hydrolysis of the phosphate diester and the pK_a of the lead-macrocyclic complex. This would provide us with further evidence for both the mechanism of RNA cleavage, and evidence for the rate-determining step for the cleavage reaction.

A buffer solution of 0.01 M HEPES (N-(2-hydroxyethyl)piperazine-N'-ethanesulphonic acid) and 0.1 M sodium nitrate was prepared in Milli-Q water, and the pH adjusted to 6.85 by dropwise addition of concentrated sodium hydroxide solution at 37°C. All quantities of phosphate and metal salts were freshly prepared in this buffer solution. Studies of reaction kinetics were carried out on a Varian Cary 50 UV-vis spectrophotometer equipped with a water-cooled Peltier chip set at 37°C. 2.00 ml of nitrophenylphosphate **21** in the buffer solution was placed in a quartz UV cell, and warmed to 37°C in the spectrophotometer housing by the Peltier system. 20 μ l of 1×10^{-5} M lead nitrate solution was added, and an automated method was begun immediately. For ten minutes, an absorbance reading was taken every thirty seconds, and then every four minutes for a subsequent ninety minutes at 405.1 nm to observe the increase in concentration of the *para*-nitrophenolate produced by the hydrolysis reaction.

The kinetic runs were duplicated a number of times to test for reproducibility, and then the procedure was then carried out for different concentrations of phosphate. The runs were found to be reproducible; however, there was some slight variation in the initial

absorbance of the solutions, but only within 0.05 – 0.1 absorbance units. Plots of concentration of *para*-nitrophenolate against time provided reaction rates for each of the studies at different starting concentrations of phosphate **21** (figure 65). The concentration of nitrophenolate was calculated using the extinction coefficient from Morrow's work, $\epsilon = 18\,500\text{ M cm}^{-1}$.¹³⁰

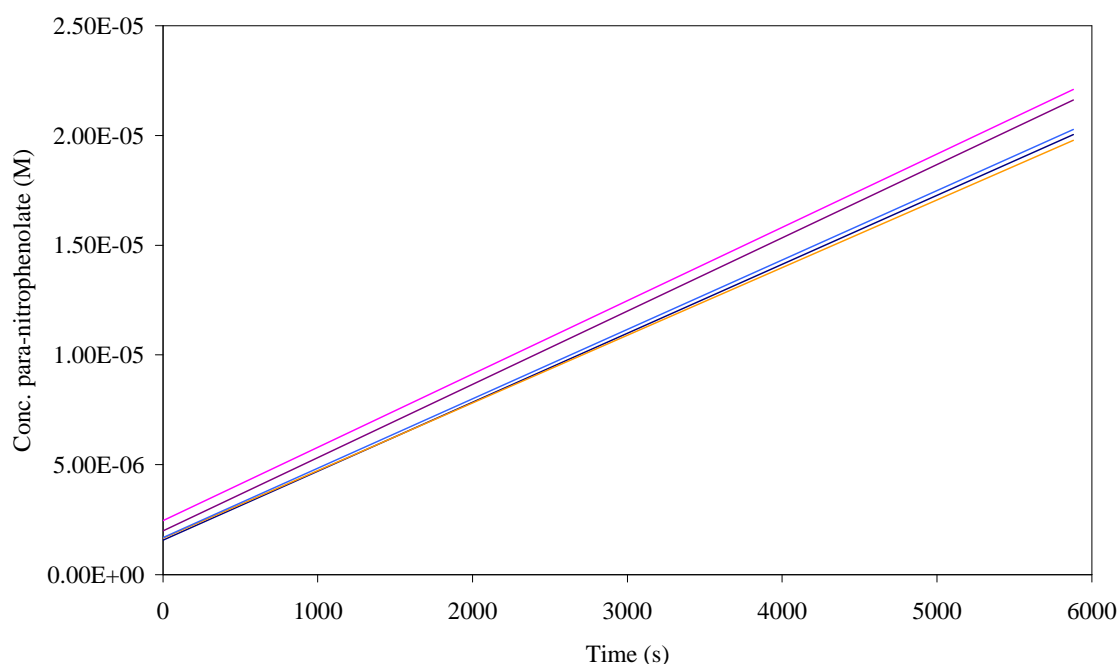
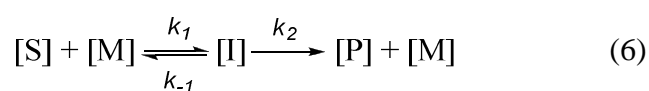


Figure 65 – Concentration of *para*-nitrophenolate against time (five repetitions).
Initial phosphate concentration = $2.0 \times 10^{-3}\text{ M}$.

The two-stage equation for the hydrolysis reaction is stated below, and the rate equation can be derived as follows:



(S = substrate, M = catalytic metal-containing species, I = coordinated intermediate, P = product).

The generation of product P depends upon the concentration of intermediate I and the rate constant k_2 .

$$\frac{d[\text{P}]}{dt} = k_2 [\text{I}] \quad (7)$$

Assuming the intermediate I is converted to product P as soon as it is formed, the generation of intermediate I depends as follows:

$$\frac{d[I]}{dt} = k_I [S][M] - k_2 [I] - k_{-I} [I] \quad (8)$$

Therefore, the concentration of intermediate I can be written as:

$$[I] = \frac{k_I [S][M]}{k_2 + k_{-I}} \quad (9)$$

Combining equations (7) and (9), the generation of product P – the observed rate of reaction – can be written as:

$$\frac{d[P]}{dt} = k_{obs} [M] \quad (10)$$

Where:

$$k_{obs} = \frac{k_2 k_I [S]}{k_2 + k_{-I}} \quad (11)$$

Hence, a graph of k_{obs} against substrate concentration [S], would yield a straight line with slope corresponding to the overall reaction rate constant k_{cat} , where:

$$k_{cat} = \frac{k_2 k_I}{k_2 + k_{-I}} \quad (12)$$

Table 30 – Observed reaction rates, k_{obs} (M s^{-1}) obtained from each run for differing initial concentrations of nitrophenyl phosphate **21**. Within the cell; 2.0 ml of 0.01 M HEPES, 0.1 M NaNO_3 (buffer), 2.0 μl of 1×10^{-5} $\text{Pb}(\text{NO}_3)_2$.

Initial phosphate concentration (M):	1.00×10^{-3}	2.00×10^{-3}	3.00×10^{-3}	5.00×10^{-3}
Run 1	1.75×10^{-9}	3.14×10^{-9}	4.83×10^{-9}	4.98×10^{-9}
Run 2	1.59×10^{-9}	3.34×10^{-9}	4.41×10^{-9}	4.64×10^{-9}
Run 3	1.58×10^{-9}	3.08×10^{-9}	4.60×10^{-9}	4.46×10^{-9}
Run 4	1.55×10^{-9}	3.16×10^{-9}	4.43×10^{-9}	4.21×10^{-9}
Run 5	1.59×10^{-9}	3.34×10^{-9}	4.69×10^{-9}	4.08×10^{-9}
Average rate (M s^{-1})	1.61×10^{-9}	3.21×10^{-9}	4.50×10^{-9}	4.47×10^{-9}
Standard Deviation	7.9×10^{-11}	1.2×10^{-10}	1.4×10^{-10}	3.6×10^{-10}

The reaction rates from the lower three phosphate concentrations appear consistent; as the initial concentration increases, the rate of reaction increases. However, the spread of results from the highest concentration (5.00×10^{-3} M) shows anomalies. The standard deviation is very large when compared to the average rate – at least 2.5 times larger than the standard deviation for the other phosphate concentrations. Therefore, we postulated that this concentration was not following the same profile as for the rest of the reactions. This is more easily seen on the reaction rate profile in figure 66, where the lower three phosphate concentrations form a trend, but the higher concentration lies off the trendline. This reveals the presence of saturation within the solution, which is that the reaction rate is proceeding as fast as it is able to. The overall rate constant, k_{cat} , derived from the three data points that lie on the straight line, is $1.45 \times 10^{-6} \text{ s}^{-1}$. However, comparing with Morrow's data, our results show little in the way of agreement, as the rate constant for the lead-based hydrolysis in her work is given as $2.7 \times 10^{-3} \text{ s}^{-1}$.¹³⁰

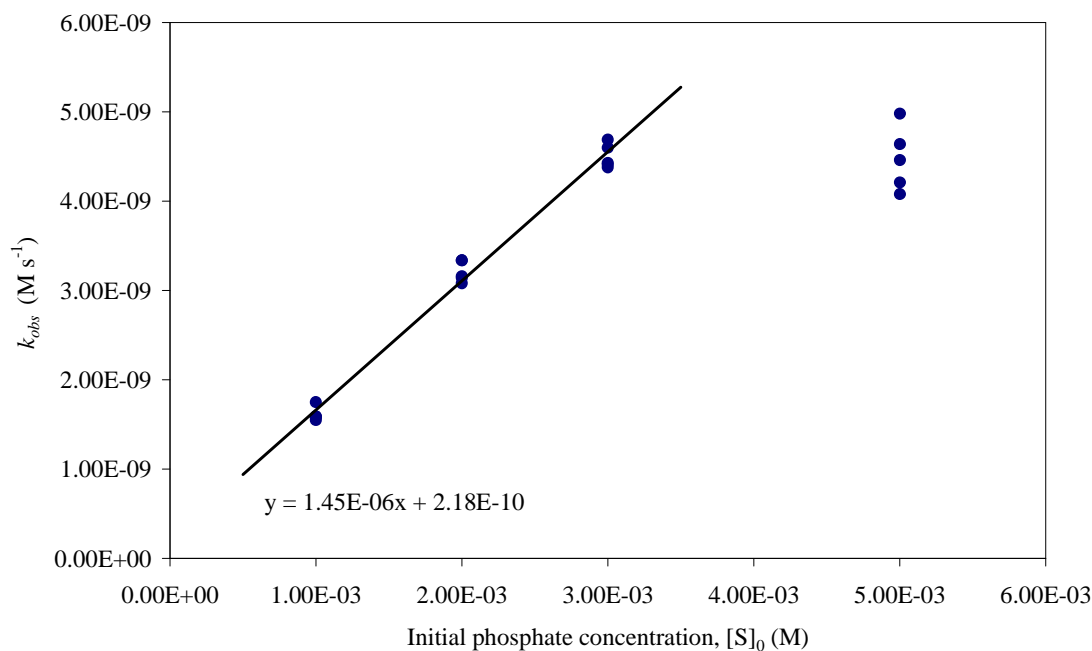


Figure 66 – Change in reaction rate, dependent upon initial phosphate concentration. Saturation kinetics are observed at $[S]_0 > \sim 4.00 \times 10^{-3} \text{ M}$.

Studies to investigate the effect of the presence of a macrocycle were carried out with the addition of one equivalent of 3N9ane **38** (*vide infra*) to the metal salt solution during preparation. The same methodology was carried out for the metal salt/macrocycle study that was carried out for the lone metal salt studies. However, an almost complete inhibition of reaction was observed, with a drop in reaction rates of an order of magnitude. For studies where the initial concentration of phosphate was low (1.0 or $2.0 \times 10^{-3} \text{ M}$), very low absorbances were observed of around $0.02 - 0.06$. The higher concentration ($5.0 \times 10^{-3} \text{ M}$) was already discounted for erroneous data in the metal salt study. Figure 67 shows the plot of concentration of nitrophenolate against time for the kinetic study of $3.0 \times 10^{-3} \text{ M}$ phosphate with $1.0 \times 10^{-5} \text{ M}$ lead nitrate, in the presence of $1.0 \times 10^{-5} \text{ M}$ of 3N9ane. The reaction rates for the repetitions are shown in table 31, and we can see that the rate has slowed greatly in the presence of a macrocycle. However, in the absence of other suitable conditions to study the hydrolysis reaction, there were few conclusions that we could draw from this.

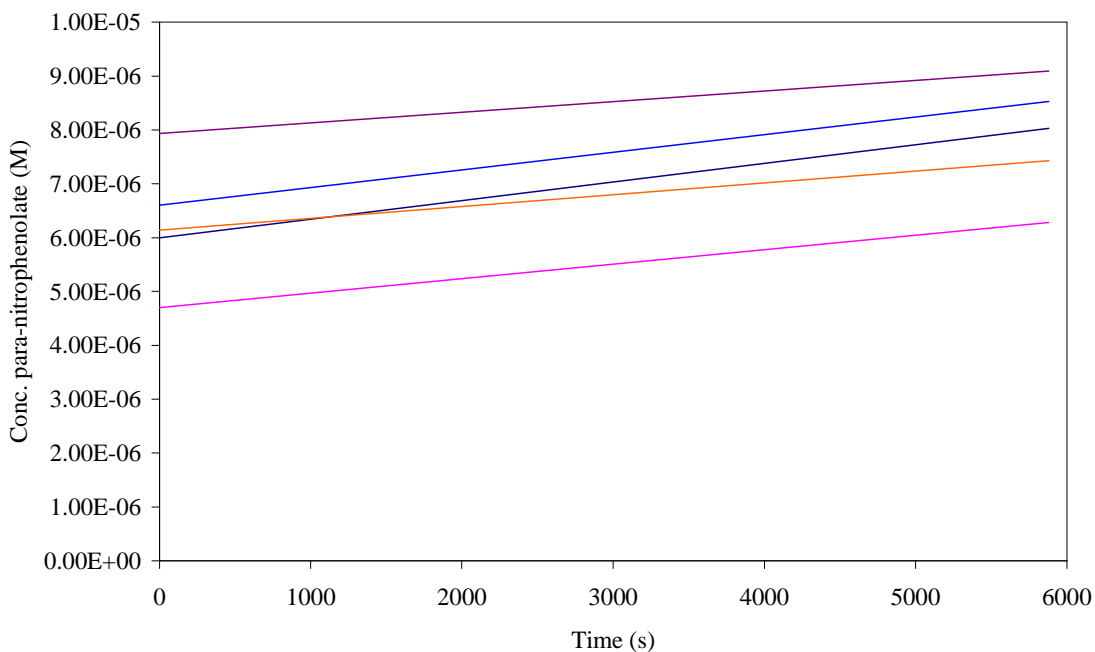


Figure 67 – Concentration of *para*-nitrophenolate against time (five repetitions).
Initial phosphate concentration = 2.0×10^{-3} M.

Table 31 - Reaction rates (M s^{-1}) obtained from each run in the presence of one equivalent of 3N9ane **38**.

Initial phosphate concentration (M):	3.00×10^{-3}
Run 1	3.45×10^{-10}
Run 2	2.69×10^{-10}
Run 3	3.27×10^{-10}
Run 4	2.19×10^{-10}
Run 5	1.96×10^{-10}
Average rate (M s^{-1})	2.71×10^{-10}
Standard Deviation	6.51×10^{-11}

We can see from these results that the rate has slowed significantly in the presence of a macrocycle, but the standard deviation – the spread of reaction rates – is now large in comparison to the average rate. This is potentially due to the coordination of the macrocycle to the metal centre. This coordination could provide steric hinderance to the hydrolysis reaction, physically preventing the lead centre coming close to the

phosphate, as well as modify the pK_a of the coordinated water molecules to the lead centre to slow the rate of hydrolysis.

In order to eliminate the possibility of inherent problems with the hydrolysis reaction under study, attempts were made to reproduce the results of Morrow, following her stated methodology exactly.¹³⁰ However, despite repeated attempts at duplication, we were unable to produce agreeable results. As a consequence of this, our study was set aside.

4.3 *Summary*

A range of macrocyclic amines and amine ethers have been synthesised and characterised at each stage of the synthetic process. In most cases, literature procedures were found to be sufficient; however, many omitted problems that could only be solved by trial and error. Three slightly different methods of tosylating amines and alcohols were used to prepare materials for cyclisation, which was found to produce better results when carried out on a larger scale. Removal of the tosyl groups from the cyclised products was carried out by a novel “fast-cracking” method, yielding the stable hydrochloride salts as an intermediate compound. Further functionalisation of the macrocycles was investigated, in addition to forming metal complexes. We also present a modified synthesis for barium 2-hydroxypropyl 4-nitrophenyl phosphate, to be used as a model system in studies of the hydrolysis of RNA.

Our hydrolysis studies followed a similar procedure to that carried out by Morrow and Burstyn,^{113,130} but with an excess of phosphate substrate to flood the reaction and make the metal complex the rate-determining reagent, but the data obtained from our kinetic studies were not consistent with any previous patterns. Attempts to duplicate the experimental work of Morrow, following her methodology exactly did not give the same results.¹³⁰ In case the lead species was causing unforeseen problems with the kinetic study, a similar repetition of existing work was carried out, following the experimental study by Mancin and co-workers, using zinc as the catalytic species.¹³⁵ However, this did also not produce the same, or even similar, results to those reported by the original authors. For these reasons, our kinetic study was postponed indefinitely.

4.4 Experimental details

Synthesis of barium 2-hydroxypropyl 4-nitrophenyl phosphate (21)

Disodium 4-nitrophenyl phosphate (1.94 g, 7.34 mmol) was dissolved in water (5 ml), and the yellow solution run through a column containing IR-120 ion exchange resin. The portions of the clear eluent visible under UV light were collected, combined and brought to pH 8 by addition of a few millilitres of ammonia solution, resulting in the appearance of a bright yellow colour. Epoxypropane (80 ml, excess.) was added, and the mixture refluxed at 30°C for three days. The solvent was removed *in vacuo*, giving a bright yellow oil. Diethyl ether was added until the mixture turned slightly cloudy, and the mixture was stored at -30°C overnight, after which the solvent was removed *in vacuo* once again. The oily yellow product was dissolved in water (12 ml) and passed through the IR-120 column, again giving a colourless eluent. The portions visible under UV light were collected, and made almost neutral (pH ~ 6.5) with aqueous saturated barium hydroxide solution. The mixture was concentrated to ~ 20 ml, and double the volume of ethanol (~ 40 ml) was added. A white precipitate was observed, and was removed by centrifuge. The solvent was then removed *in vacuo* to yield a pale yellow oil. Acetone (20 ml) was added, and the mixture centrifuged to separate the fine white precipitate from the solution layer. The solution was discarded, and the white powder carefully collected and dried. Yield: 0.77 g (42.8%).

^1H NMR (399.5 MHz, CD_3OD , 30°C): δ 8.27 (d, $J = 9.0$ Hz, 2H, H_{aryl}), 7.48 (d, $J = 9.0$ Hz, 2H, H_{aryl}), 3.98 (m, 1H, CH), 3.89 (m, 2H, CH_2), 3.83 (m, 1H, OH), 3.47 (d, $J = 5.4$ Hz, 3H, CH_3).

$^{31}\text{P}\{^1\text{H}\}$ NMR (161.7 MHz, CD_3OD , 30°C): δ -5.83 (major isomer), -6.30 (minor isomer).

Literature ^1H NMR (300 MHz, CD_3OD): δ 8.25 (d, $J = 9$ Hz, 2H, H_{aryl}), 7.43 (d, $J = 9$ Hz, 2H, H_{aryl}), 3.92 (m, 1H, CH), 3.83 (m, 2H, CH_2), 1.16 (d, $J = 6$ Hz, 3H, CH_3).¹³³

Synthesis of tritosyl-diethylenetriamine (22)

Tosyl chloride (380 g, 1.99 mol) was placed in a 3-neck round-bottomed flask equipped with a magnetic stirrer. Pyridine (1 litre) was added, and the flask warmed to 50°C to

dissolve the tosyl chloride. Upon cooling to $\sim 30^{\circ}\text{C}$, N,N-diethylenetriamine (69 g, 0.66 mol) was dissolved in a further 100 ml of pyridine, and was added dropwise to the TsCl solution. The addition was slow enough so as not to allow the reaction temperature to exceed 60°C . Upon complete addition, the mixture was stirred whilst heating at 60°C for another thirty minutes, and then allowed to cool to room temperature. The transparent orange solution was poured into a conical flask equipped with an overhead stirrer, and ~ 600 ml water was added. Upon addition, the solution was seen to turn a custard yellow colour. The mixture was allowed to stir overnight, and then was cooled in an ice bath for two hours. The beige-yellow solid precipitate was collected by filtration and washed with cold ethanol. After drying *in vacuo*, the total yield was 279 g (74.4%).

^1H NMR (499.91 MHz, CDCl_3 , 30°C): δ 7.74 (d, $J = 8.2$ Hz, 4H, H_{aryl}), 7.59 (d, $J = 8.2$ Hz, 2H, H_{aryl}), 7.29 (d, $J = 7.1$ Hz, 6H, H_{aryl}), 5.11 (t, $J = 5.8$ Hz, 2H, NH), 3.17 (t, $J = 5.6$ Hz, 4H, $\text{N}(\text{H})\text{CH}_2$), 3.12 (t, $J = 5.7$ Hz, 4H, $\text{H}_2\text{CN}(\text{Ts})\text{CH}_2$), 2.41 (s, 6H, $\text{CH}_3(\text{tosyl})$), 2.15 (s, 3H, $\text{CH}_3(\text{tosyl})$).

$^{13}\text{C}\{^1\text{H}\}$ NMR (125.7 MHz, CDCl_3 , 30°C): δ 143.6, 136.7, 134.7, 129.8, 129.7, 127.3 (C_{aryl}), 50.5 ($\text{N}(\text{H})\text{CH}_2$), 42.6 ($\text{H}_2\text{CN}(\text{Ts})\text{CH}_2$), 21.5 ($\text{CH}_3(\text{tosyl})$).

ESI-MS: m/z 588.13 [$\text{C}_{25}\text{H}_{31}\text{N}_3\text{O}_6\text{S}_3\text{Na}$] $^+$. Calculated 565.14 [$\text{C}_{25}\text{H}_{31}\text{N}_3\text{O}_6\text{S}_3$].

Synthesis of tritosyl-dipropylenetriamine (23)

Tosyl chloride (87.5 g, 0.459 mol) was placed in a round bottomed flask equipped with a magnetic stirrer. Dichloromethane (750 ml) was added, and the suspension cooled to -10°C . N,N-dipropylenetriamine (21.6 ml, 0.153 mol), triethylamine (50 ml, 0.36 mol) and dichloromethane (250 ml) were placed together in a dropping funnel, and added dropwise to the cold TsCl suspension over an hour, giving a pale yellow solution and a white gas. This was left to stir and warm to room temperature overnight, after which ice (~ 250 ml) and 3M hydrochloric acid (150 ml) were added. The mixture was stirred for thirty minutes until the ice melted. The organic layer was then separated and washed with 150 ml portions of water, hydrochloric acid, saturated sodium hydrogen carbonate solution and brine. The solution was dried over magnesium sulphate, and concentrated *in vacuo*, and cold ethanol added. This was then cooled to -30°C , and stored overnight, giving a beige solid mass and a layer of solvent. Once warmed to room temperature, the solvent was concentrated *in vacuo* once more, and hot ethanol was added, and the

solution stirred vigorously for twenty minutes. The beige precipitate was collected by filtration and washed with cold ethanol. After drying, the yield was 66.6 g (73.4%).

^1H NMR (499.91 MHz, CDCl_3 , 30°C): δ 7.70 (d, $J = 8.2$ Hz, 4H, H_{aryl}), 7.61 (d, $J = 8.2$ Hz, 2H, H_{aryl}), 7.27 (d, $J = 6.8$ Hz, 6H, H_{aryl}), 5.19 (br, 2H, NH), 3.08 (t, $J = 6.7$ Hz, 4H, $\text{N}(\text{H})\text{CH}_2$), 2.93 (t, $J = 6.2$ Hz, 4H, $\text{H}_2\text{CN}(\text{Ts})\text{CH}_2$), 2.40 (s, 3H, $\text{CH}_3(\text{tosyl})$), 2.39 (s, 6H, $\text{CH}_3(\text{tosyl})$), 1.69 (pent, 4H, $\text{CH}_2\text{CH}_2\text{CH}_2$).

$^{13}\text{C}\{^1\text{H}\}$ NMR (125.7 MHz, CDCl_3 , 30°C): δ 143.7, 136.8, 135.5, 129.9, 129.7, 127.0 (C_{aryl}), 46.8 ($\text{N}(\text{H})\text{CH}_2$), 40.1 ($\text{H}_2\text{CN}(\text{Ts})\text{CH}_2$), 29.2 ($\text{CH}_2\text{CH}_2\text{CH}_2$) 21.5 ($\text{CH}_3(\text{tosyl})$).

ESI-MS: m/z 616.16 [$\text{C}_{27}\text{H}_{35}\text{N}_3\text{O}_6\text{S}_3\text{Na}$] $^+$. Calculated 593.45 [$\text{C}_{27}\text{H}_{35}\text{N}_3\text{O}_6\text{S}_3$].

Synthesis of ditosyl-ethan-1,2-diol (24)

Tosyl chloride (58.4 g, 0.306 mol) was placed in a round bottom flask equipped with a magnetic stirrer. Dichloromethane (750 ml) was added, and the suspension cooled to -10°C . 1,2-ethandiol (8.5 ml, 0.153 mol), triethylamine (50 ml, 0.36 mol) and dichloromethane (250 ml) were placed together in a dropping funnel, and added dropwise to the cold TsCl suspension over twenty minutes, giving a pale yellow solution and a white gas. This was left to stir and warm to room temperature overnight, after which ice (250 ml) and 3M hydrochloric acid (150 ml) were added. The mixture was stirred for thirty minutes until the ice melted. The organic layer was then separated and washed with 150 ml portions of water and brine. The solution was dried over magnesium sulphate, and was evaporated to dryness *in vacuo*, leaving a pink-beige residue. The residue was washed with diethyl ether to remove excess tosyl chloride, and the precipitate filtered off and dried. Total yield: 37.1 g (65.5%).

^1H NMR (499.91 MHz, CDCl_3 , 30°C): δ 7.71 (d, $J = 8.2$ Hz, 4H, H_{aryl}), 7.32 (d, $J = 8.0$ Hz, 4H, H_{aryl}), 4.17 (s, 4H, CH_2), 2.44 (s, 6H, CH_3).

$^{13}\text{C}\{^1\text{H}\}$ NMR (125.7 MHz, CDCl_3 , 30°C): δ 145.2, 132.4, 129.9, 127.9 (C_{aryl}), 66.6 (OCH_2) 21.7 ($\text{CH}_3(\text{tosyl})$).

ESI-MS: m/z 393.04 [$\text{C}_{16}\text{H}_{18}\text{O}_6\text{S}_2\text{Na}$] $^+$. Calculated 370.37 [$\text{C}_{16}\text{H}_{18}\text{O}_6\text{S}_2$].

Synthesis of ditosyl-propan-1,3-diol (25)

1,3-propandiol (11.0 ml, 0.153 mol) and tosyl chloride (58.4 g, 0.306 mol) were dissolved in dichloromethane (500 ml) in a 3-necked round bottomed flask, which was

then cooled to 0°C. Powdered potassium hydroxide (68.7 g, 1.23 mol) was added slowly, giving an opaque white solution. The mixture was allowed to stir and warm to room temperature overnight, after which dichloromethane (500 ml) and ice (600 ml) was added, and the mixture was stirred until the ice had melted. The organic layer was separated, and the aqueous layer washed with a small portion of dichloromethane (100 ml). The dichloromethane washings were combined with the rest of the organic layer, which was then washed with 150 ml portions of water and brine, giving a clear solution. This solution was reduced to dryness *in vacuo*, giving a white solid. Total yield was 46.5 g (79.0%).

^1H NMR (499.91 MHz, CDCl_3 , 30°C): δ 7.72 (d, J = 8.3 Hz, 4H, H_{aryl}), 7.32 (d, J = 8.4 Hz, 4H, H_{aryl}), 4.04 (t, J = 6.0 Hz, 4H, OCH_2), 2.43 (s, 6H, $\text{CH}_3(\text{tosyl})$), 1.98 (pent, J = 6.0 Hz, 2H, $\text{CH}_2\text{CH}_2\text{CH}_2$).

$^{13}\text{C}\{^1\text{H}\}$ NMR (125.7 MHz, CDCl_3 , 30°C): δ 145.0, 132.7, 129.9, 127.9 (C_{aryl}), 65.8 (OCH_2), 28.7 ($\text{CH}_2\text{CH}_2\text{CH}_2$), 21.6 ($\text{CH}_3(\text{tosyl})$).

ESI-MS: m/z 407.06 [$\text{C}_{17}\text{H}_{20}\text{O}_6\text{S}_2\text{Na}$] $^+$. Calculated 384.30 [$\text{C}_{17}\text{H}_{20}\text{O}_6\text{S}_2$].

Synthesis of tritosyl-diethanolamine (26)

Tosyl chloride (87.5 g, 0.459 mol) was placed in a round bottom flask equipped with a magnetic stirrer. Dichloromethane (750 ml) was added, and the suspension cooled to -10°C. Diethanolamine (15 ml, 0.153 mol), triethylamine (50 ml, 0.36 mol) and dichloromethane (250 ml) were placed together in a dropping funnel, and added dropwise to the cold TsCl suspension over twenty minutes, giving a pale yellow solution and a white gas. This was left to stir and warm to room temperature overnight, after which ice (250 ml) and 3M hydrochloric acid (150 ml) were added. The mixture was stirred for thirty minutes until the ice melted. The organic layer was then separated and washed with 150 ml portions of water, hydrochloric acid, saturated sodium hydrogen carbonate solution and brine. The solution was dried over magnesium sulphate, and was concentrated *in vacuo*. Cold ethanol was added and the solution left at -30°C overnight, after which it was observed to have solidified. Upon warming slowly to room temperature, a white solid was observed, which was collected by filtration and washed with cold ethanol. After drying, the total yield obtained was: 28.1 g (32.3%).

^1H NMR (499.91 MHz, CDCl_3 , 30°C): δ 7.74 (d, J = 8.3 Hz, 4H, H_{aryl}), 7.59 (d, J = 8.3 Hz, 2H, H_{aryl}), 7.34 (d, J = 8.0 Hz, 4H, H_{aryl}), 7.27 (d, J = 8.0 Hz, 2H, H_{aryl}), 4.09 (t, J =

6.0 Hz, 4H, OCH_2), 3.36 (t, $J = 6.0$ Hz, 4H, NCH_2), 2.44 (s, 6H, $\text{CH}_3(\text{tosyl})$), 2.41 (s, 3H, $\text{CH}_3(\text{tosyl})$).

$^{13}\text{C}\{^1\text{H}\}$ NMR (125.7 MHz, CDCl_3 , 30°C): δ 145.2, 144.1, 135.3, 132.5, 130.0, 128.0, 127.3 (C_{aryl}), 68.3 (OCH_2), 48.5 (NCH_2), 21.6 ($\text{CH}_3(\text{tosyl})$).

ESI-MS: m/z 590.09 [$\text{C}_{25}\text{H}_{29}\text{NO}_8\text{S}_3\text{Na}$] $^+$. Calculated 567.59 [$\text{C}_{25}\text{H}_{29}\text{NO}_8\text{S}_3$].

Synthesis of ditosyl-diethylene glycol (27)

Diethylene glycol (14.5 ml, 0.153 mol) and tosyl chloride (58.4 g, 0.306 mol) were dissolved in dichloromethane (500 ml) in a 3-necked round bottomed flask, which was then cooled to 0°C . Powdered potassium hydroxide (68.7 g, 1.23 mol) was added slowly, giving an opaque white solution. The mixture was allowed to stir and warm to room temperature overnight, after which dichloromethane (500 ml) and ice (600 ml) was added, and the mixture was stirred until the ice had melted. The organic layer was separated, and the aqueous layer washed with a small portion of dichloromethane (100 ml). The dichloromethane washings were combined with the rest of the organic layer, which was then washed with 150 ml portions of water and brine, giving a very pale yellow solution. This solution was reduced to dryness *in vacuo*, giving a white solid. Total yield was 52.9 g (83.3%).

^1H NMR (499.91 MHz, CDCl_3 , 30°C): δ 7.75 (d, $J = 8.3$ Hz, 4H, H_{aryl}), 7.32 (d, $J = 8.4$ Hz, 4H, H_{aryl}), 4.07 (m, 4H, TsOCH_2), 3.58 (m, 4H, CH_2OCH_2), 2.42 (s, 6H, $\text{CH}_3(\text{tosyl})$).

$^{13}\text{C}\{^1\text{H}\}$ NMR (125.7 MHz, CDCl_3 , 30°C): δ 145.0, 132.9, 129.9, 127.9 (C_{aryl}), 69.0, 68.7 (OCH_2), 21.6 ($\text{CH}_3(\text{tosyl})$).

ESI-MS: m/z 437.07 [$\text{C}_{18}\text{H}_{22}\text{O}_7\text{S}_2\text{Na}$] $^+$. Calculated 414.42 [$\text{C}_{18}\text{H}_{22}\text{O}_7\text{S}_2$].

Synthesis of 1,4,7-triaza-1,4,7-tritosyl-cyclononane; 3N9ane-Ts₃ (28)

Tosylated diethylenetriamine **22** (47.1g, 83.3 mmol) and potassium carbonate (45 g, 0.33 mol, 4eq) were dissolved in dimethylformamide (700 ml) in a round bottomed flask equipped with a magnetic stirrer and condenser. The flask was heated to 100°C and allowed to stir for an hour. Tosylated ethandiol **24** (30.9 g, 83.3 mmol) was dissolved in dimethylformamide (275 ml), and this was added dropwise to the hot solution, forming a cloudy white suspension. The mixture was left to stir at 100°C for thirty minutes, after which the heat was removed and water (450 ml) was added. The

mixture was then allowed to stir overnight, after which a white solid had precipitated. The white solid was collected by filtration and washed with cold ethanol. After drying *in vacuo*, the yield was 37.5 g (76.0%).

^1H NMR (499.91 MHz, CDCl_3 , 30°C): δ 7.68 (d, $J = 8.2$ Hz, 6H, H_{aryl}), 7.30 (d, $J = 8.2$ Hz, 6H, H_{aryl}), 3.40 (s, 12H, CH_2), 2.41 (s, 9H, $\text{CH}_{3(\text{tosyl})}$).

$^{13}\text{C}\{^1\text{H}\}$ NMR (125.7 MHz, CDCl_3 , 30°C): δ 143.9, 134.7, 129.9, 127.5 (C_{aryl}), 51.9 (CH_2), 21.5 ($\text{CH}_{3(\text{tosyl})}$).

ESI-MS: m/z 630.12 [$\text{C}_{27}\text{H}_{33}\text{N}_3\text{O}_6\text{S}_3\text{K}$] $^+$. Calculated 591.60 [$\text{C}_{27}\text{H}_{33}\text{N}_3\text{O}_6\text{S}_3$].

Synthesis of 1,4,8-triaza-1,4,8-tritosyl-cycloundecane; 3N11ane-Ts₃ (29)

Tosylated dipropyleneetriamine **23** (40.0g, 67.5 mmol) and potassium carbonate (38 g, 0.27 mol, 4eq) were dissolved in dimethylformamide (350 ml) in a round bottomed flask equipped with a magnetic stirrer and condenser. The flask was heated to 100°C and allowed to stir for an hour. Tosylated ethandiol **24** (25.0 g, 67.5 mmol) was dissolved in dimethylformamide (100 ml), and this was added dropwise to the hot solution, forming a cloudy white suspension. The mixture was left to stir at 100°C for thirty minutes, after which the heat was removed and water (100 ml) was added, giving a clear solution. The mixture was then allowed to stir overnight, after which a thick, sticky white deposit had appeared. The white material was collected and stirred in dichloromethane overnight. The solvent was removing *in vacuo* to give a white powder, in 13.5 g (32.4%) yield.

^1H NMR (499.91 MHz, CDCl_3 , 30°C): δ 7.65 (m, 6H, H_{aryl}), 7.29 (m, 6H, H_{aryl}), 3.40 (m, 4H, NCH_2), 3.25 (m, 4H, NCH_2), 2.97 (br, 4H, NCH_2), 2.40 (s, br, 9H, $\text{CH}_{3(\text{tosyl})}$), 1.88 (br, 4H, $\text{CH}_2\text{CH}_2\text{CH}_2$).

$^{13}\text{C}\{^1\text{H}\}$ NMR (125.7 MHz, CDCl_3 , 30°C): δ 143.9, 133.8, 129.8, 129.7, 127.6, (C_{aryl}), 52.4, 48.9, 43.4 (NCH_2), 24.2 ($\text{CH}_2\text{CH}_2\text{CH}_2$), 21.5 ($\text{CH}_{3(\text{tosyl})}$).

ESI-MS: m/z 642.17 [$\text{C}_{29}\text{H}_{37}\text{N}_3\text{O}_6\text{S}_3\text{Na}$] $^+$. Calculated 619.45 [$\text{C}_{29}\text{H}_{37}\text{N}_3\text{O}_6\text{S}_3$].

Synthesis of 1,5,9-triaza-1,5,9-tritosyl-cyclododecane; 3N12ane-Ts₃ (30)

Tosylated dipropyleneetriamine **23** (23.9g, 40.3 mmol) and potassium carbonate (22 g, 0.16 mol, 4eq) were dissolved in dimethylformamide (380 ml) in a round bottomed flask equipped with a magnetic stirrer and condenser. The flask was heated to 100°C

and allowed to stir for an hour. Tosylated propandiol **25** (15.5 g, 40.3 mmol) was dissolved in dimethylformamide (150 ml), and this was added dropwise to the hot solution, forming a cloudy white suspension, which cleared after a few minutes. The mixture was left to stir at 100°C for one hour, after which the heat was removed and water (250 ml) was added slowly. The mixture was then allowed to stir overnight, after which a white solid had precipitated. The solid was collected by filtration, washed with cold ethanol and dried *in vacuo*, giving a yield of 19.3 g (75.7%).

^1H NMR (499.91 MHz, CDCl_3 , 30°C): δ 7.64 (d, J = 8.1 Hz, 6H, H_{aryl}), 7.30 (d, J = 7.9 Hz, 6H, H_{aryl}), 3.20 (t, J = 6.7 Hz, 6H, NCH_2), 3.12 (m, 6H, NCH_2), 2.42 (s, 9H, $\text{CH}_3(\text{tosyl})$), 1.91 (pent, J = 6.5 Hz, 6H, $\text{CH}_2\text{CH}_2\text{CH}_2$).

$^{13}\text{C}\{^1\text{H}\}$ NMR (125.7 MHz, CDCl_3 , 30°C): δ 143.6, 135.1, 129.8, 127.3, (C_{aryl}), 47.8, 45.5 (NCH_2), 26.3 ($\text{CH}_2\text{CH}_2\text{CH}_2$), 21.5 ($\text{CH}_3(\text{tosyl})$).

ESI-MS: m/z 672.16 [$\text{C}_{30}\text{H}_{39}\text{N}_3\text{O}_6\text{S}_3\text{K}$] $^+$. Calculated 633.45 [$\text{C}_{30}\text{H}_{39}\text{N}_3\text{O}_6\text{S}_3$].

Synthesis of 1,4,7,10-tetraaza-1,4,7,10-tetratosyl-cyclododecane; 4N12ane-Ts₄ (31)

Tosylated diethylenetriamine **22** (21.2g, 37.4 mmol) and potassium carbonate (21 g, 0.15 mol, 4eq) were dissolved in dimethylformamide (360 ml) in a round bottomed flask equipped with a magnetic stirrer and condenser. The flask was heated to 100°C and allowed to stir for an hour. Tosylated diethanolamine **26** (21.3 g, 37.4 mmol) was dissolved in dimethylformamide (120 ml), and this was added dropwise to the hot solution, forming a cloudy yellow suspension. The mixture was left to stir at 100°C for thirty minutes, after which the heat was removed and water (200 ml) was added. The mixture was then allowed to stir overnight, after which a white solid had precipitated. The white solid was collected by filtration and washed with water and cold ethanol. After drying *in vacuo*, the yield was 15.3 g (52.6%).

^1H NMR (499.91 MHz, CDCl_3 , 30°C): δ 7.66 (d, J = 8.2 Hz, 8H, H_{aryl}), 7.31 (d, J = 8.2 Hz, 8H, H_{aryl}), 3.41 (s, br, 16H, CH_2), 2.42 (s, 12H, $\text{CH}_3(\text{tosyl})$).

$^{13}\text{C}\{^1\text{H}\}$ NMR (125.7 MHz, CDCl_3 , 30°C): δ 143.9, 129.9, 127.7, (C_{aryl}), 52.3 (NCH_2), 21.5 ($\text{CH}_3(\text{tosyl})$).

ESI-MS: m/z 827.17 [$\text{C}_{36}\text{H}_{44}\text{N}_4\text{O}_8\text{S}_4\text{K}$] $^+$. Calculated 789.02 [$\text{C}_{36}\text{H}_{44}\text{N}_4\text{O}_8\text{S}_4$].

Synthesis of 1,4,7,11-tetraaza-1,4,7,11-tetratosyl-cyclotetradecane; 4N14ane-Ts₄ (32)

Tosylated dipropylenetriamine **23** (14.8g, 25.0 mmol) and potassium carbonate (14 g, 0.10 mol, 4eq) were dissolved in dimethylformamide (225 ml) in a round bottomed flask equipped with a magnetic stirrer and condenser. The flask was heated to 100°C and allowed to stir for an hour. Tosylated diethanolamine **26** (14.2 g, 25.0 mmol) was dissolved in dimethylformamide (75 ml), and this was added dropwise to the hot solution, forming a cloudy yellow mixture. The flask was left to stir at 100°C overnight, after which the heat was removed and water (250 ml) was added. The mixture was then allowed to stir overnight, after which a sticky beige material had precipitated. The solid was collected by filtration and washed with cold ethanol. After substantial drying *in vacuo*, the yield was 12.3 g (60.2%).

¹H NMR (499.91 MHz, CDCl₃, 30°C): δ 7.72 (d, J = 8.2 Hz, 2H, H_{aryl}), 7.66 (d, J = 8.2 Hz, 4H, H_{aryl}), 7.63 (d, J = 8.2 Hz, 2H, H_{aryl}), 7.33 (dd, J = 14.3, 6.6 Hz, 8H, H_{aryl}), 3.35 (m, 4H, NCH₂), 3.19 (m, 4H, NCH₂), 3.14 (m, 4H, NCH₂), 3.10 (t, J = 6.9 Hz, 4H, NCH₂), 2.45 (s, 3H, CH₃(tosyl)), 2.44 (s, 6H, CH₃(tosyl)), 2.43 (s, 3H, CH₃(tosyl)), 1.89 (m, 4H, CH₂CH₂CH₂).

¹³C{¹H} NMR (125.7 MHz, CDCl₃, 30°C): δ 143.8, 135.6, 135.0, 134.9, 129.9, 127.4, 127.3, 127.2, (C_{aryl}), 50.0, 48.4, 48.3, 48.0 (NCH₂), 29.7 (CH₂CH₂CH₂), 21.5 (CH₃(tosyl)).

ESI-MS: *m/z* 855.20 [C₃₈H₄₈N₄O₈S₄K]⁺. Calculated 817.07 [C₃₈H₄₈N₄O₈S₄].

Synthesis of 1-oxa-4,7,10-triaza-4,7,10-tritosyl-cyclododecane; O3N12ane-Ts₃ (33)

Tosylated diethylenetriamine **22** (39.6g, 70 mmol) and potassium carbonate (40 g, 0.29 mol, 4eq) were dissolved in dimethylformamide (500 ml) in a round bottomed flask equipped with a magnetic stirrer and condenser. The flask was heated to 100°C and allowed to stir for an hour. Tosylated diethylene glycol **27** (29.0 g, 70 mmol) was dissolved in dimethylformamide (200 ml), and this was added dropwise to the hot solution, forming a cloudy white suspension. The mixture was left to stir at 100°C overnight, after which the heat was removed and water (200 ml) was added. The mixture was then allowed to stir for two hours, after which a white solid had precipitated. The white solid was collected by filtration and washed with cold ethanol. After drying *in vacuo*, the yield was 37.39 g (84.0%).

^1H NMR (499.91 MHz, CDCl_3 , 30°C): δ 7.79 (d, $J = 8.3$ Hz, 2H, H_{aryl}), 7.61 (d, $J = 8.2$ Hz, 4H, H_{aryl}), 7.38 (d, $J = 8.1$ Hz, 2H, H_{aryl}), 7.29 (d, $J = 8.1$ Hz, 4H, H_{aryl}), 3.63 (m, 4H, OCH_2), 3.50 (t, $J = 6.4$ Hz, 4H, NCH_2), 3.18 (m, 8H, NCH_2), 2.44 (s, 3H, $\text{CH}_{3(\text{tosyl})}$), 2.41 (s, 6H, $\text{CH}_{3(\text{tosyl})}$).

$^{13}\text{C}\{^1\text{H}\}$ NMR (125.7 MHz, CDCl_3 , 30°C): δ 143.6, 143.3, 136.7, 135.1, 129.8, 127.5, 127.3, (C_{aryl}), 72.0 (OCH_2), 50.7, 50.6, 48.0 (NCH_2), 21.5 ($\text{CH}_{3(\text{tosyl})}$).

ESI-MS: m/z 658.17 [$\text{C}_{29}\text{H}_{37}\text{N}_3\text{O}_7\text{S}_3\text{Na}$] $^+$. Calculated 635.81 [$\text{C}_{29}\text{H}_{37}\text{N}_3\text{O}_7\text{S}_3$].

Synthesis of 1,4,7-trihydrochloro-1,4,7-triazacyclononane; 3N9ane.3HCl (34)

Concentrated sulphuric acid (~16 M, 33 ml) was placed in a 250ml round-bottomed flask fitted with a stirrer bar and condenser, and heated to 150°C . 3N9ane-Ts₃ **28** (30 g, 0.05 mol) was added with the evolution of a white gas. The black mixture was stirred for 15 minutes, after which the heat was removed and the mixture allowed to cool enough to be handled easily. The mixture was then poured **very slowly** in small portions into fast-stirring, ice-cooled ethanol (300 ml), resulting in an immediate brown-grey precipitate. The precipitate was filtered off and washed with cold ethanol.

The grey solid was then dissolved in water (25 ml) in a 250 ml round-bottomed flask equipped with a stirrer and condenser. This was heated to just below reflux temperature, and concentrated hydrochloric acid (~12M, 25 ml) was added **very slowly** via pipette, resulting in the evolution of white gas. Upon complete addition, the pale yellow-brown solution was stirred at reflux for 30 minutes. The heat was then removed, and the solution allowed to stand **without stirring** overnight, after which an off-white solid was observed. The solid was filtered off, washed with ethanol and diethyl ether, and dried via suction in air. Yield: 9.48 g (79.7%).

^1H NMR (499.91 MHz, D_2O , 30°C): δ 3.72 (s, 12H, CH_2).

$^{13}\text{C}\{^1\text{H}\}$ NMR (125.7 MHz, D_2O , 30°C): δ 41.8 (CH_2).

Synthesis of 1,5,9-trihydrochloro-1,5,9-triazacyclododecane; 3N12ane.3HCl (35)

Concentrated sulphuric acid (~16 M, 30 ml) was placed in a 2-necked, 250ml round-bottomed flask fitted with a stirrer bar and condenser, and heated to 150°C . 3N12ane-Ts₃ **30** (25.6 g, 0.04 mol) was added with the evolution of large amounts of white gas. The brown-black mixture was stirred for 15 minutes, after which the heat was removed

and the mixture allowed to cool enough to be handled easily. The mixture was then poured **very slowly** in small portions into fast-stirring, ice-cooled ethanol (300 ml), resulting in an immediate brown-grey precipitate and clouds of white gas. The precipitate was filtered off and washed with cold ethanol. The grey solid was then dissolved in water (30 ml) in a 250 ml round-bottomed flask equipped with a stirrer and condenser. This was heated to just below reflux temperature (95°C), and concentrated hydrochloric acid (~12M, 25 ml) was added **very slowly** via pipette, resulting in the evolution of more white gas. Upon complete addition, the pale brown solution was stirred at reflux for 30-45 minutes. The heat was then removed, and the solution allowed to stand **without stirring** overnight, after which a pale brown solid was observed. The solid was filtered off, washed with ethanol and diethyl ether, and dried via suction in air, in quantitative yield. Yield: 11.1 g (100%).

^1H NMR (499.91 MHz, D_2O , 30°C): δ 3.27 (s, 12H, NCH_2), 2.23 (s, 6H, $\text{CH}_2\text{CH}_2\text{CH}_2$).

$^{13}\text{C}\{^1\text{H}\}$ NMR (125.7 MHz, D_2O , 30°C): δ 44.6, 40.7, 36.6, 23.7, 22.6, 22.2, 18.9 (CH_2).

Synthesis of 1,4,7,10-tetrahydrochloro-1,4,7,10-tetraazacyclododecane; 4N12ane.4HCl (36)

Concentrated sulphuric acid (~16 M, 44 ml) was placed in a 2-necked, 250ml round-bottomed flask fitted with a stirrer bar and condenser, and heated to 150°C. 4N12ane-Ts₄ **32** (40 g, 0.05 mol) was added with the evolution of large amounts of white gas. The dark brown mixture was stirred for 15 minutes, after which the heat was removed and the mixture allowed to cool enough to be handled easily. The mixture was then poured **very slowly** in small portions into fast-stirring, ice-cooled ethanol (400 ml), resulting in an immediate white-grey precipitate and further evolution of white gas. The precipitate was filtered off and washed with cold ethanol. The grey solid was then dissolved in water (30 ml) in a 250 ml round-bottomed flask equipped with a stirrer and condenser. This was heated to just below reflux temperature (95°C), and concentrated hydrochloric acid (~12M, 30 ml) was added **very slowly** via pipette, resulting in the evolution of more white gas. Upon complete addition, the pale yellow solution was stirred at reflux for 30-45 minutes. The heat was then removed, and the solution allowed to stand **without stirring** overnight, after which ice-cooled ethanol was added, resulting

in the precipitation of a white solid. The solid was filtered off, washed with cold ethanol and diethyl ether, and dried via suction in air. Yield: 10.9 g (96.2%).

^1H NMR (499.91 MHz, D_2O , 30°C): δ 3.36 (s, br, 16H, CH_2)

$^{13}\text{C}\{^1\text{H}\}$ NMR (125.7 MHz, D_2O , 30°C): δ 47.8, 44.7, 43.8, 41.8 (CH_2)

Synthesis of 4,7,10-trihydrochloro-1-oxa-4,7,10-triazacyclododecane; O3N12ane.3HCl (37)

Concentrated sulphuric acid (~16 M, 35 ml) was placed in a 250ml round-bottomed flask fitted with a stirrer bar and condenser, and heated to 150°C . O3N12ane- Ts_3 **33** (31.8 g, 0.05 mol) was added, resulting in the evolution of a white gas. The black mixture was stirred for 15 minutes, after which the heat was removed and the mixture allowed to cool enough to be handled easily. The mixture was then poured **very slowly** in portions, into fast-stirring, ice-cooled ethanol (300 ml), resulting in an immediate white-grey precipitate. The precipitate was filtered off and washed with cold ethanol. The grey solid was then dissolved in water (25 ml) in a 250 ml round-bottomed flask equipped with a stirrer and condenser. This was heated to just below reflux temperature, and concentrated hydrochloric acid (~12M, 25 ml) was added **very slowly** via pipette, resulting in the evolution of white gas. Upon complete addition, the pale yellow-brown solution was stirred at reflux for 40 minutes. The heat was then removed, and the solution allowed to stand without stirring overnight, after which pale brown-yellow solid was observed. The solid was filtered off, washed with ethanol and diethyl ether, and dried via suction in air, giving quantitative yield. Yield: 14.03 g (100%).

^1H NMR (499.91 MHz, D_2O , 30°C): δ 3.72 (m, 8H, CH_2), 1.24 (t, $J = 7.0$ Hz, 8H, CH_2).

$^{13}\text{C}\{^1\text{H}\}$ NMR (125.7 MHz, D_2O , 30°C): δ 57.5 (OCH_2), 16.8 (NCH_2).

Synthesis of 1,4,7-triazacyclononane; 3N9ane (38)

3N9ane.3HCl **34** (9.5 g, 0.04 mol) was dissolved in water (17 ml) in a 250 ml round-bottomed flask equipped with a magnetic stirrer and a Dean-Stark water eliminator apparatus. Toluene (60 ml) and sodium hydroxide (3 g, 0.075 mol, 1.75 eq) was added to the flask and the mixture heated to reflux and the water distilled off. After approximately half the water (~ 9 ml) had been removed, more sodium hydroxide (3 g, 0.075 mol, 1.75 eq) was added and the mixture left to reflux overnight, until all the

water had been removed. The clear solution was removed from the white residue by filtration whilst hot, and the toluene was then removed *in vacuo* to give a white crystalline powder. Yield: 1.01 g (19.6%)

^1H NMR (499.91 MHz, D_2O , 30°C): δ 3.03 (s, 12H, CH_2).

$^{13}\text{C}\{^1\text{H}\}$ NMR (125.7 MHz, D_2O , 30°C): δ 43.4 (CH_2).

ESI-MS: m/z 130.13 [$\text{C}_6\text{H}_{16}\text{N}_3$] $^+$. Calculated 129.0 [$\text{C}_6\text{H}_{15}\text{N}_3$].

Synthesis of 1,4,7,10-tetraazacyclododecane; 4N12ane (39)

4N12ane.4HCl **36** (10.9 g, 0.035 mol) was dissolved in water (18 ml) in a 250 ml round-bottomed flask equipped with a magnetic stirrer and a Dean-Stark water separator apparatus. Toluene (60 ml) and sodium hydroxide (3.5 g, 0.086 mol, 2.5 eq) was added to the flask and the mixture heated to reflux and the water distilled off. After approximately half the water (~ 9 ml) had been removed, more sodium hydroxide (3.5 g, 0.086 mol, 2.5 eq) was added and the mixture left to reflux over three days, until all the water had been removed. The clear solution was removed from the white residue by filtration whilst hot, and the toluene was then removed *in vacuo* to give a white crystalline powder. Yield: 2.97 g (49.3%).

^1H NMR (499.91 MHz, CDCl_3 , 30°C): δ 2.73 (s, 16H, CH_2).

$^{13}\text{C}\{^1\text{H}\}$ NMR (125.7 MHz, CDCl_3 , 30°C): δ 44.7 (CH_2).

ESI-MS: m/z 173.18 [$\text{C}_8\text{H}_{20}\text{N}_4$] $^+$. Calculated 172.0 [$\text{C}_8\text{H}_{20}\text{N}_4$].

Synthesis of 1-oxa-4,7,10-triazacyclododecane; O3N12ane (40)

O3N12ane.3HCl **37** (14.0 g, 0.05 mol) was dissolved in water (20 ml) in a 250 ml round-bottomed flask equipped with a magnetic stirrer and a Dean-Stark water separator apparatus. Toluene (60 ml) and sodium hydroxide (3.75 g, 0.095 mol, 1.75 eq) was added to the flask and the mixture heated to reflux and the water distilled off. After approximately half the water (~ 9 ml) had been removed, more sodium hydroxide (3.75 g, 0.095 mol, 1.75 eq) was added and the mixture left to reflux overnight, until all the water had been removed. The clear solution was removed from the white residue by filtration whilst hot, and the toluene was then removed *in vacuo* to give a white crystalline powder. Yield: 1.04 g (12.0%)

^1H NMR (499.91 MHz, D_2O , 30°C): δ 3.72 (m, 4H, OCH_2), 2.85 (m, 4H, NCH_2), 2.80 (m, 4H, NCH_2), 2.73 (m, 4H, NCH_2).

$^{13}\text{C}\{^1\text{H}\}$ NMR (125.7 MHz, D_2O , 30°C): δ 66.6 (OCH_2), 45.1, 45.0, 44.7 (NCH_2).

ESI-MS: m/z 174.16 $[\text{C}_8\text{H}_{20}\text{N}_3\text{O}]^+$. Calculated 173.0 $[\text{C}_8\text{H}_{19}\text{N}_3\text{O}]$.

Synthesis of 1,4,7-trimethyl-1,4,7-triazacyclononane; 3N9ane-Me₃ (41)

3N9ane **38** (0.5 g, 3.88 mmol) was dissolved in water (0.5 ml) in a 25 ml round-bottomed flask equipped with a stirrer bar. Formic acid (98%, 4.5 ml) and formaldehyde (37% soln., 4.0 ml) were added, and the mixture set to reflux for 24 hours. The mixture was then allowed to cool to room temperature, and poured into water (5 ml), and cooled in an ice bath. A solution of sodium hydroxide (4 g) in water (10 ml) was added slowly via pipette, with the temperature kept below 10°C during the addition. The pH was observed to be >12 upon complete addition of the base. The mixture was extracted with portions of chloroform, the organic layer dried with MgSO_4 , and the solvent removed *in vacuo*, yielding a pale yellow oil in good yield. Yield: 545 mg (82.2 %)

^1H NMR (499.91 MHz, CDCl_3 , 30°C): δ 2.60 (s, 12H, CH_2), 2.31 (s, 9H, CH_3).

$^{13}\text{C}\{^1\text{H}\}$ NMR (125.7 MHz, CDCl_3 , 30°C): δ 57.1 (CH_2), 46.7 (CH_3).

ESI-MS: m/z 172.18 $[\text{C}_9\text{H}_{22}\text{N}_3]^+$. Calculated 171.0 $[\text{C}_9\text{H}_{21}\text{N}_3]$.

5. References

- (1) Bourget-Merle, L.; Lappert, M. F.; Severn, J. R. *Chem. Rev.* **2002**, *102*, 3031–3066.
- (2) Ferro, L.; Coles, M. P.; Day, I. J.; Fulton, J. R. *Organometallics* **2010**, *29*, 2911–2915.
- (3) Räke, B.; Zülch, F.; Ding, Y.; Prust, J.; Roesky, H. W.; Noltemeyer, M.; Schmidt, H.-G. *Z. Anorg. Allg. Chem.* **2001**, *627*, 836–840.
- (4) Hitchcock, P. B.; Lappert, M. F.; Liu, D.-S. *J. Chem. Soc., Chem. Commun.* **1994**, 1699–1700.
- (5) Eckert, N. A.; Bones, E. M.; Lachicotte, R. J.; Holland, P. L. *Inorg. Chem.* **2003**, *42*, 1720–1725.
- (6) Hill, M. S.; Hitchcock, P. B.; Pongtavornpinyo, R. *Science* **2006**, *311*, 1904 – 1907.
- (7) Smith, J. M.; Lachicotte, R. J.; Pittard, K. A.; Cundari, T. R.; Lukat-Rodgers, G.; Rodgers, K. R.; Holland, P. L. *J. Am. Chem. Soc.* **2001**, *123*, 9222–9223.
- (8) Smith, J. M.; Lachicotte, R. J.; Holland, P. L. *Organometallics* **2002**, *21*, 4808–4814.
- (9) Parks, J. E.; Holm, R. H. *Inorg. Chem.* **1968**, *7*, 1408–1416.
- (10) Everett, G. W.; Holm, R. H. *J. Am. Chem. Soc.* **1965**, *87*, 2117–2127.
- (11) McGeachin, S.G. *Can. J. Chem.* **1968**, *46*, 1903–1912.
- (12) Dorman, L. C. *Tetrahedron Lett.* **1966**, *7*, 459–464.
- (13) Stender, M.; Wright, R. J.; Eichler, B. E.; Prust, J.; Olmstead, M. M.; Roesky, H. W.; Power, P. P. *J. Chem. Soc., Dalton Trans.* **2001**, 3465–3469.
- (14) Hitchcock, P. B.; Lappert, M. F.; Liu, D.-S. *J. Chem. Soc., Chem. Commun.* **1994**, 2637–2638.
- (15) Huang, Y.-L.; Huang, B.-H.; Ko, B.-T.; Lin, C.-C. *J. Chem. Soc., Dalton Trans.* **2001**, 1359–1365.
- (16) M. Budzelaar, P. H.; van Oort, A. B.; Orpen, A. G. *Eur. J. Inorg. Chem.* **1998**, *1998*, 1485–1494.
- (17) Carey, D. T.; Cope-Eatough, E. K.; Vilaplana-Mafe, E.; Mair, F. S.; Pritchard, R. G.; Warren, J. E.; Woods, R. J. *Dalton Trans.* **2003**, 1083–1093.

- (18) Rahim, M.; Taylor, N. J.; Xin, S.; Collins, S. *Organometallics* **1998**, *17*, 1315–1323.
- (19) Venugopalt, A.; Ghosh, M. K.; Jorgens, H.; Tornroos, K., W.; Swang, O.; Tilset, M.; Heyn, R., H. *Organometallics* **2010**, *29*, 2248–2253.
- (20) Johnson, K. R. D.; Côté, A. P.; Hayes, P. G. *J. Organomet. Chem.* **2010**, *695*, 2747–2755.
- (21) Neculai, D.; Roesky, H. W.; Neculai, A. M.; Magull, J.; Herbst-Irmer, R.; Walfort, B.; Stalke, D. *Organometallics* **2003**, *22*, 2279–2283.
- (22) Dai, X.; Warren, T. H. *J. Am. Chem. Soc.* **2004**, *126*, 10085–10094.
- (23) Dai, X.; Warren, T. H. *Chem. Commun.* **2001**, 1998–1999.
- (24) Basuli, F.; Tomaszewski, J.; Huffman, J. C.; Mindiola, D. J. *Organometallics* **2003**, *22*, 4705–4714.
- (25) Willems, S. T. H.; Budzelaar, P. H. M.; Moonen, N. N. P.; de Gelder, R.; Smits, J. M. M.; Gal, A. W. *Chem. Eur. J.* **2002**, *8*, 1310–1320.
- (26) Yu, Y.; Brennessel, W. W.; Holland, P. L. *Organometallics* **2007**, *26*, 3217–3226.
- (27) Aboulkacem, S.; Tyrre, W.; Pantenburg, I. *Z. Anorg. Allg. Chem.* **2003**, *629*, 1569–1574.
- (28) Kuhn, N.; Kuhn, A.; Boese, R.; Augart, N. *J. Chem. Soc., Chem. Commun.* **1989**, 975–976.
- (29) Kuhn, N.; Kuhn, A.; Lewandoski, J.; Speis, M. *Chem. Ber.* **1991**, *124*, 2197.
- (30) Gornitzka, H.; Stalke, D. *Organometallics* **1994**, *13*, 4398–4405.
- (31) Qian, B.; Ward, D. L.; Smith, M. R. *Organometallics* **1998**, *17*, 3070–3076.
- (32) Stender, M.; Eichler, B. E.; Hardman, N. J.; Power, P. P.; Prust, J.; Noltemeyer, M.; Roesky, H. W. *Inorg. Chem.* **2001**, *40*, 2794–2799.
- (33) Hardman, N. J.; Eichler, B. E.; Power, P. P. *Chem. Commun.* **2000**, 1991–1992.
- (34) Ding, Y.; Roesky, H. W.; Noltemeyer, M.; Schmidt, H.-G.; Power, P. P. *Organometallics* **2001**, *20*, 1190–1194.
- (35) Harris, L. A.-M.; Coles, M. P.; Fulton, J. R. *Inorg. Chim. Acta.* **2011**, *369*, 97–102.
- (36) Jana, A.; Roesky, H. W.; Schulzke, C.; Döring, A.; Beck, T.; Pal, A.; Herbst-Irmer, R. *Inorg. Chem.* **2009**, *48*, 193–197.
- (37) Dove, A. P.; Gibson, V. C.; Marshall, E. L.; Rzepa, H. S.; White, A. J. P.; Williams, D. J. *J. Am. Chem. Soc.* **2006**, *128*, 9834–9843.

- (38) Ferro, L.; Hitchcock, P. B.; Coles, M. P.; Cox, H.; Fulton, J. R. *Inorg. Chem.* **2011**, *50*, 1879–1888.
- (39) Inoue, S.; Driess, M. *Organometallics* **2009**, *28*, 5032–5035.
- (40) Eichler, B. E.; Power, P. P. *J. Am. Chem. Soc.* **2000**, *122*, 8785–8786.
- (41) Pineda, L. W.; Jancik, V.; Starke, K.; Oswald, R. B.; Roesky, H. W. *Angew. Chem. Int. Ed.* **2006**, *45*, 2602–2605.
- (42) Ruff, J. K.; Hawthorne, M. F. *J. Am. Chem. Soc.* **1960**, *82*, 2141–2144.
- (43) Chen, M.; Fulton, J. R.; Hitchcock, P. B.; Johnstone, N. C.; Lappert, M. F.; Protchenko, A. V. *Dalton Trans.* **2007**, 2770–2778.
- (44) Fulton, J. R.; Hitchcock, P. B.; Johnstone, N. C.; Tam, E. C. Y. *Dalton Trans.* **2007**, 3360–3362.
- (45) Tam, E. C. Y.; Johnstone, N. C.; Ferro, L.; Hitchcock, P. B.; Fulton, J. R. *Inorg. Chem.* **2009**, *48*, 8971–8976.
- (46) Jana, A.; Sarish, S. P.; Roesky, H. W.; Schulzke, C.; Döring, A.; John, M. *Organometallics* **2009**, *28*, 2563–2567.
- (47) Yao, S.; Block, S.; Brym, M.; Driess, M. *Chem. Commun.* **2007**, 3844–3846.
- (48) Schiffer, M.; Scheer, M. *Angew. Chem. Int. Ed.* **2001**, *40*, 3413–3416.
- (49) Vidovic, D.; Lu, Z.; Reeske, G.; Moore, J. A.; Cowley, A. H. *Chem. Commun.* **2006**, 3501–3503.
- (50) Lesikar, L. A.; Richards, A. F. *J. Organomet. Chem.* **2006**, *691*, 4250–4256.
- (51) Pineda, L. W.; Jancik, V.; Nembenna, S.; Roesky, H. W. *Z. Anorg. Allg. Chem.* **2007**, *633*, 2205–2209.
- (52) Pu, L.; Twamley, B.; Power, P. P. *Organometallics* **2000**, *19*, 2874–2881.
- (53) B. Maksic, Z.; Kovacevic, B. *J. Chem. Soc., Perkin Trans. 2* **1999**, 2623–2629.
- (54) Datta, D.; Sharma, G. T. *J. Chem. Soc., Dalton Trans.* **1989**, 115–118.
- (55) Clayden, J.; Greeves, N.; Warren, S.; Wothers, P. *Organic Chemistry*; Oxford University Press, 2001.
- (56) Hansch, C.; Leo, A.; Taft, R. W. *Chem. Rev.* **1991**, *91*, 165–195.
- (57) Driess, M.; Janoschek, R.; Pritzkow, H.; Rell, S.; Winkler, U. *Angew. Chem. Int. Ed. Engl.* **1995**, *34*, 1614–1616.
- (58) Cox, H.; Stace, A. J. *Intl. Rev. Phys. Chem.* **2011**, *29*, 555–588.
- (59) Greer, B. J.; Michaelis, V. K.; Katz, M. J.; Leznoff, D. B.; Schreckenbach, G.; Kroeker, S. *Chem. Eur. J.* **2011**, *17*, 3609–3618.

- (60) Dmitrenko, O.; Bai, S.; Dybowski, C. *Solid State Nucl. Magn. Reson.* **2008**, *34*, 186–190.
- (61) Feldman, J.; McLain, S. J.; Parthasarathy, A.; Marshall, W. J.; Calabrese, J. C.; Arthur, S. D. *Organometallics* **1997**, *16*, 1514–1516.
- (62) Harris, D. H.; Lappert, M. F. *J. Chem. Soc., Chem. Commun.* **1974**, 895–896.
- (63) Goldberg, D. E.; Harris, D. H.; Lappert, M. F.; Thomas, K. M. *J. Chem. Soc., Chem. Commun.* **1976**, 261–262.
- (64) Cotton, J. D.; Cundy, C. S.; Harris, D. H.; Hudson, A.; Lappert, M. F.; Lednor, P. W. *J. Chem. Soc., Chem. Commun.* **1974**, 651–652.
- (65) Schaeffer, C. D.; Zuckerman, J. J. *J. Am. Chem. Soc.* **1974**, *96*, 7160–7162.
- (66) Klinkhammer, K. W.; Schwarz, W. *Angew. Chem. Int. Ed. Engl.* **1995**, *34*, 1334–1336.
- (67) Simons, R. S.; Power, P. P. *J. Am. Chem. Soc.* **1996**, *118*, 11966–11967.
- (68) Rivard, E.; Power, P. P. *Inorg. Chem.* **2007**, *46*, 10047–10064.
- (69) Hino, S.; Brynda, M.; Phillips, A. D.; Power, P. P. *Angew. Chem. Int. Ed.* **2004**, *43*, 2655–2658.
- (70) Taylor, M. J.; Saunders, A. J.; Coles, M. P.; Fulton, J. R. *Organometallics* **2011**, *30*, 1334–1339.
- (71) Ayers, A. E.; Dias, H. V. R. *Inorg. Chem.* **2002**, *41*, 3259–3268.
- (72) Stender, M.; Phillips, A. D.; Power, P. P. *Inorg. Chem.* **2001**, *40*, 5314–5315.
- (73) Pineda, L. W.; Jancik, V.; Roesky, H. W.; Neculai, D.; Neculai, A. M. *Angew. Chem. Int. Ed.* **2004**, *43*, 1419–1421.
- (74) Driess, M.; Yao, S.; Brym, M.; van Wüllen, C. *Angew. Chem. Int. Ed.* **2006**, *45*, 4349–4352.
- (75) Woodul, W. D.; Richards, A. F.; Stasch, A.; Driess, M.; Jones, C. *Organometallics* **2010**, *29*, 3655–3660.
- (76) Horton, A. D.; de With, J.; van der Linden, A. J.; van de Weg, H. *Organometallics* **1996**, *15*, 2672–2674.
- (77) Darensbourg, D. J.; Maynard, E. L.; Holtcamp, M. W.; Klausmeyer, K. K.; Reibenspies, J. H. *Inorg. Chem.* **1996**, *35*, 2682–2684.
- (78) Hitchcock, P. B.; Lappert, M. F.; Layh, M.; Liu, D.-S.; Sablong, R.; Shun, T. J. *J. Chem. Soc., Dalton Trans.* **2000**, 2301–2312.
- (79) Clegg, W.; Cope, E. K.; Edwards, A. J.; Mair, F. S. *Inorg. Chem.* **1998**, *37*, 2317–2319.

- (80) Gibson, V. C.; Segal, J. A.; White, A. J. P.; Williams, D. J. *J. Am. Chem. Soc.* **2000**, *122*, 7120–7121.
- (81) Bailey, P. J.; Dick, C. M. E.; Fabre, S.; Parsons, S. *J. Chem. Soc., Dalton Trans.* **2000**, 1655–1661.
- (82) Dove, A. P.; Gibson, V. C.; Hormnirun, P.; Marshall, E. L.; Segal, J. A.; White, A. J. P.; Williams, D. J. *Dalton Trans.* **2003**, 3088–3097.
- (83) Kuhn, N.; Speis, M. *Inorg. Chim. Acta.* **1988**, *145*, 5.
- (84) F. Caro, C.; B. Hitchcock, P.; F. Lappert, M. *Chem. Commun.* **1999**, 1433–1434.
- (85) Bonyhady, S. J.; Jones, C.; Nembenna, S.; Stasch, A.; Edwards, A. J.; McIntyre, G. J. *Chem. Eur. J.* **2010**, *16*, 938–955.
- (86) Green, S. P.; Jones, C.; Stasch, A. *Science* **2007**, *318*, 1754–1757.
- (87) Sidiropoulos, A.; Jones, C.; Stasch, A.; Klein, S.; Frenking, G. *Angew. Chem. Int. Ed.* **2009**, *48*, 9701–9704.
- (88) Crimmin, M. R.; Casely, I. J.; Hill, M. S. *J. Am. Chem. Soc.* **2005**, *127*, 2042–2043.
- (89) Chisholm, M. H.; Gallucci, J.; Phomphrai, K. *Chem. Commun.* **2003**, 48–49.
- (90) Crimmin, M. R.; Barrett, A. G. M.; Hill, M. S.; Hitchcock, P. B.; Procopiou, P. A. *Organometallics* **2007**, *26*, 2953–2956.
- (91) Sarish, S.; Nembenna, S.; Nagendran, S.; Roesky, H. W.; Pal, A.; Herbst-Irmer, R.; Ringe, A.; Magull, J. *Inorg. Chem.* **2008**, *47*, 5971–5977.
- (92) Sarish, S. P.; Roesky, H. W.; John, M.; Ringe, A.; Magull, J. *Chem. Commun.* **2009**, 2390–2392.
- (93) Clegg, W.; Coles, S. J.; Cope, E. K.; Mair, F. S. *Angew. Chem. Int. Ed.* **1998**, *37*, 796–798.
- (94) Avent, A. G.; Crimmin, M. R.; Hill, M. S.; Hitchcock, P. B. *Dalton Trans.* **2005**, 278–284.
- (95) Bailey, P. J.; Coxall, R. A.; Dick, C. M.; Fabre, S.; Henderson, L. C.; Herber, C.; Liddle, S. T.; Loroño-González, D.; Parkin, A.; Parsons, S. *Chem. Eur. J.* **2003**, *9*, 4820–4828.
- (96) Sadique, A. R.; Heeg, M. J.; Winter, C. H. *Inorg. Chem.* **2001**, *40*, 6349–6355.
- (97) Coles, M. P.; Swenson, D. C.; Jordan, R. F.; Young, V. G. *Organometallics* **1997**, *16*, 5183–5194.

- (98) Sánchez-Barba, L. F.; Garcés, A.; Fernández-Baeza, J.; Otero, A.; Alonso-Moreno, C.; Lara-Sánchez, A.; Rodríguez, A. M. *Organometallics* **2011**, *30*, 2775–2789.
- (99) E. Mulvey, R.; Wade, K.; R. Armstrong, D.; T. Walker, G.; Snaith, R.; Clegg, W.; Reed, D. *Polyhedron* **1987**, *6*, 987–993.
- (100) Hey, E.; Engelhardt, L. M.; Raston, C. L.; White, A. H. *Angew. Chem. Int. Ed. Engl.* **1987**, *26*, 81–82.
- (101) Day, B. M.; Coles, M. P. *Eur. J. Inorg. Chem.* **2010**, *2010*, 5471–5477.
- (102) Westerhausen, M.; Pfitzner, A. J. *Organomet. Chem.* **1995**, *487*, 187–195.
- (103) Pedersen, C. J. *J. Am. Chem. Soc.* **1967**, *89*, 7017–7036.
- (104) Curtis, N. F. *Coord. Chem. Rev.* **1968**, *3*, 3–47.
- (105) Yang, R.; Zompa, L. J. *Inorg. Chem.* **1976**, *15*, 1499–1502.
- (106) Zompa, L. J. *Inorg. Chem.* **1978**, *17*, 2531–2536.
- (107) Boeyens, J. C. A.; Forbes, A.; Hancock, R. D.; Wieghardt, K. *Inorg. Chem.* **1985**, *24*, 2926–2931.
- (108) Hart, S. M.; Boeyens, J. C. A.; Hancock, R. D. *Inorg. Chem.* **1983**, *22*, 982–986.
- (109) Wieghardt, K.; Kleine-Boymann, M.; Nuber, B.; Weiss, J.; Zsolnai, L.; Huttner, G. *Inorg. Chem.* **1986**, *25*, 1647–1650.
- (110) Castro-Rodriguez, I.; Nakai, H.; Zakharov, L. N.; Rheingold, A. L.; Meyer, K. *Science* **2004**, *305*, 1757–1759.
- (111) Wieghardt, K.; Hahn, M.; Swiridoff, W.; Weiss, J. *Inorg. Chem.* **1984**, *23*, 94–99.
- (112) Williams, N. H.; Cheung, W.; Chin, J. *J. Am. Chem. Soc.* **1998**, *120*, 8079–8087.
- (113) Hegg, E. L.; Mortimore, S. H.; Cheung, C. L.; Huyett, J. E.; Powell, D. R.; Burstyn, J. N. *Inorg. Chem.* **1999**, *38*, 2961–2968.
- (114) Wei, N.; Murthy, N. N.; Karlin, K. D. *Inorg. Chem.* **1994**, *33*, 6093–6100.
- (115) Richman, J. E.; Atkins, T. J. *J. Am. Chem. Soc.* **1974**, *96*, 2268–2270.
- (116) Atkins, T. J.; Richman, J. E.; Oettle, W. F. *Organic Syntheses* **1978**, *58*, 86–98.
- (117) Amorim, M. T. S.; Chaves, S.; Delgado, R.; da Silva, J. J. R. F. *J. Chem. Soc., Dalton Trans.* **1991**, 3065–3072.
- (118) Meunier, I.; Mishra, A. K.; Hanquet, B.; Guillard, R.; Cocolios, P. *Can. J. Chem.* **1995**, *73*, 685–695.
- (119) Sun, Y.; Martell, A. E.; Welch, M. J. *Tetrahedron* **1991**, *47*, 8863–8868.
- (120) Chavez, F.; Sherry, A. D. *J. Org. Chem.* **1989**, *54*, 2990–2992.

- (121) Bazzicalupi, C.; Bencini, A.; Fusi, V.; Micheloni, M.; Paoletti, P.; Valtancoli, B. *J. Org. Chem.* **1994**, *59*, 7508–7510.
- (122) Qian, L.; Sun, Z.; Mertes, M. P.; Mertes, K. B. *J. Org. Chem.* **1991**, *56*, 4904–4907.
- (123) Keegstra, E. M. D.; Zwikker, J. W.; Roest, M. R.; Jenneskens, L. W. *J. Org. Chem.* **1992**, *57*, 6678–6680.
- (124) Kramer, J.; Scholten, A.; Driessen, W. L.; Reedijk, J. *Eur. J. Inorg. Chem.* **2002**, *2002*, 1488–1494.
- (125) Barefield, E. K.; Wagner, F. *Inorg. Chem.* **1973**, *12*, 2435–2439.
- (126) Halfen, J. A.; Tolman, W. B.; Weighardt, K. *Inorg. Synth.* **2007**, 75–81.
- (127) Payne, J. C.; ter Horst, M. A.; Godwin, H. A. *J. Am. Chem. Soc.* **1999**, *121*, 6850–6855.
- (128) Barciszewska, M. Z.; Szymanski, M.; Wyszko, E.; Pas, J.; Rychlewski, L.; Barciszewski, J. *Mutat. Res.* **2005**, *589*, 103–110.
- (129) Yatsimirsky, A. K. *Coord. Chem. Rev.* **2005**, *249*, 1997–2011.
- (130) Morrow, J. R.; Buttrey, L. A.; Berback, K. A. *Inorg. Chem.* **1992**, *31*, 16–20.
- (131) Gómez-Tagle, P.; Yatsimirsky, A. K. *Inorg. Chem.* **2001**, *40*, 3786–3796.
- (132) McDaniel, D. H.; Smoot, C. R. *J. Phys. Chem.* **1956**, *60*, 966–969.
- (133) Tsang, J. S. W.; Neverov, A. A.; Brown, R. S. *J. Am. Chem. Soc.* **2003**, *125*, 1559–1566.
- (134) Lam, O.; Meyer, K. *Private Communication* **2009**.
- (135) Bonfá, L.; Gatos, M.; Mancin, F.; Tecilla, P.; Tonellato, U. *Inorg. Chem.* **2003**, *42*, 3943–3949.

Appendices

1. β -Diketiminato lead(II) alkyl complexes; computational details

1.1 β -Diketiminato lead(II) methyl, LPbMe (3)

1.1.1 Bond angles ($^{\circ}$) and distances (\AA)

	LANL2DZ		LANL2DZ & 6-31G*	
	<i>endo-</i>	<i>exo-</i>	<i>endo-</i>	<i>exo-</i>
N1-Pb-C30	91.93	97.42	91.64	96.75
N2-Pb-C30	91.93	97.36	91.64	96.88
N1-Pb-N2	84.82	83.89	84.52	83.18
C1-N1-C6	120.32	121.71	120.38	121.29
C1-N1-Pb	123.70	122.51	122.84	120.89
C6-N1-Pb	115.97	114.80	116.77	116.59
C3-N2-C18	120.32	122.07	120.38	122.30
C3-N2-Pb	123.70	122.52	122.84	120.99
C18-N2-Pb	115.97	114.45	116.77	115.49
N1-C1-C2	125.25	124.98	125.81	125.37
C1-C2-C3	131.01	131.08	131.79	131.58
C2-C3-N2	125.25	125.04	125.81	125.40
Pb-C30	2.283	2.270	2.287	2.275
N1-Pb	2.308	2.311	2.340	2.338
N2-Pb	2.308	2.316	2.340	2.351
N1-C1	1.350	1.349	1.333	1.335
C1-C2	1.421	1.419	1.413	1.409
C2-C3	1.421	1.422	1.413	1.415
C3-N2	1.350	1.347	1.333	1.328
Pb-plane	0.613	0.773	0.627	0.882
DOP (%)	101.47	90.37	102.44	92.43

1.1.2 Molecular orbital energy levels

	LANL2DZ		LANL2DZ & 6-31G*	
Energy level	<i>endo-</i>	<i>exo-</i>	<i>endo-</i>	<i>exo-</i>
HOMO -1	-146.4	-145.4	-143.5	-143.6
HOMO	-131.7	-132.1	-125.6	-125.3
LUMO	-2.470	-1.016	-0.063	2.702
LUMO +1	9.493	12.36	8.020	9.223
HOMO-LUMO gap	129.3	131.0	125.6	128.0
LP	-214.5	-213.6	-226.3	-225.7
LP level	HOMO -10	HOMO -10	HOMO -10	HOMO -10

1.2 β -Diketiminato lead(II) iso-propyl, LPb^iPr (4)

1.2.1 Bond angles ($^\circ$) and distances (\AA)

	LANL2DZ		LANL2DZ & 6-31G*	
	<i>endo-</i>	<i>exo-</i>	<i>endo-</i>	<i>exo-</i>
N1-Pb-C30	91.57	100.22	91.72	99.58
N2-Pb-C30	100.62	100.22	100.56	99.58
N1-Pb-N2	84.67	82.99	84.40	82.47
C1-N1-C6	121.65	121.22	121.52	120.88
C1-N1-Pb	123.52	120.74	122.56	118.96
C6-N1-Pb	114.82	116.91	115.89	118.65
C3-N2-C18	119.13	121.11	119.41	120.88
C3-N2-Pb	123.41	120.74	122.27	118.95
C18-N2-Pb	117.36	116.91	118.22	118.65
N1-C1-C2	125.28	124.85	125.70	125.24
C1-C2-C3	131.10	130.54	131.63	131.10
C2-C3-N2	125.19	124.85	125.77	125.24
Pb-C30	2.318	2.297	2.334	2.313
N1-Pb	2.341	2.323	2.371	2.351
N2-Pb	2.301	2.323	2.332	2.351
N1-C1	1.344	1.349	1.327	1.333
C1-C2	1.428	1.421	1.420	1.413
C2-C3	1.413	1.421	1.405	1.413
C3-N2	1.358	1.349	1.340	1.333
Pb-plane	0.618	0.953	0.652	1.048
DOP (%)	92.38	85.08	92.58	87.08

1.2.2 Molecular orbital energy levels

	LANL2DZ		LANL2DZ & 6-31G*	
Energy level	<i>endo-</i>	<i>exo-</i>	<i>endo-</i>	<i>exo-</i>
HOMO -1	-146.1	-131.8	-126.0	-126.2
HOMO	-64.61	-120.5	-124.7	-124.0
LUMO	-4.113	-64.16	-0.884	-61.12
LUMO +1	-1.862	17.95	8.220	9.035
HOMO - LUMO gap	60.50	56.38	123.8	62.92
LP	-213.3	-213.7	-277.3	-277.2
LP level	HOMO -10	HOMO -10	HOMO -10	HOMO -10

1.3 β -Diketiminato lead(II) *sec*-butyl, LPb^sBu (5)

1.3.1 Bond angles (°) and distances (Å)

	LANL2DZ		LANL2DZ & 6-31G*	
	<i>endo</i> -	<i>exo</i> -	<i>endo</i> -	<i>exo</i> -
N1-Pb-C30	99.95	100.48	100.10	100.18
N2-Pb-C30	91.61	101.15	91.39	100.85
N1-Pb-N2	84.99	82.98	84.63	82.26
C1-N1-C6	119.49	120.68	119.44	120.87
C1-N1-Pb	123.53	120.13	122.68	119.22
C6-N1-Pb	116.73	117.90	117.63	118.38
C3-N2-C18	121.43	120.79	121.29	120.97
C3-N2-Pb	123.78	120.08	122.29	119.14
C18-N2-Pb	114.75	117.84	115.68	118.38
N1-C1-C2	125.43	124.85	125.93	125.22
C1-C2-C3	131.41	130.41	131.92	131.08
C2-C3-N2	125.41	124.81	125.86	125.20
Pb-C30	2.330	2.308	2.346	2.323
N1-Pb	2.317	2.322	2.344	2.354
N2-Pb	2.334	2.321	2.367	2.352
N1-C1	1.355	1.350	1.338	1.333
C1-C2	1.416	1.421	1.407	1.413
C2-C3	1.425	1.421	1.418	1.412
C3-N2	1.346	1.350	1.328	1.333
Pb-plane	0.557	0.994	0.579	1.045
DOP (%)	92.72	83.77	93.20	85.23

1.3.2 Molecular orbital energy levels

	LANL2DZ		LANL2DZ & 6-31G*	
Energy level	<i>endo-</i>	<i>exo-</i>	<i>endo-</i>	<i>exo-</i>
HOMO -1	-146.1	-146.6	-144.8	-144.0
HOMO	-133.1	-132.1	-124.8	-126.4
LUMO	-3.474	-2.477	-2.583	8.339
LUMO +1	7.662	18.65	8.151	8.885
HOMO - LUMO gap	129.6	129.7	122.2	134.7
LP	-213.7	-213.5	-227.5	-227.1
LP level	HOMO -10	HOMO -10	HOMO -10	HOMO -10

1.4 β -Diketimate lead(II) neo-pentyl, LPbNp (6)

1.4.1 Bond angles (°) and distances (Å)

	LANL2DZ	LANL2DZ & 6-31G*
	<i>exo</i> -	<i>exo</i> -
N1-Pb-C30	96.71	95.28
N2-Pb-C30	97.07	97.24
N1-Pb-N2	82.90	82.49
C1-N1-C6	121.96	121.80
C1-N1-Pb	119.82	118.54
C6-N1-Pb	116.85	118.24
C3-N2-C18	122.02	121.95
C3-N2-Pb	119.84	118.40
C18-N2-Pb	116.71	117.99
N1-C1-C2	124.66	125.06
C1-C2-C3	130.40	131.07
C2-C3-N2	124.67	125.09
Pb-C30	2.290	2.305
N1-Pb	2.319	2.343
N2-Pb	2.320	2.348
N1-C1	1.349	1.333
C1-C2	1.421	1.412
C2-C3	1.421	1.413
C3-N2	1.348	1.332
Pb-plane	1.019	1.080
DOP (%)	92.58	94.43

1.4.2 Molecular orbital energy levels

	LANL2DZ	LANL2DZ & 6-31G*
Energy level	<i>exo-</i>	<i>exo-</i>
HOMO -1	-146.2	-143.8
HOMO	-131.9	-126.4
LUMO	-1.724	5.850
LUMO +1	15.23	8.741
HOMO - LUMO gap	130.1	132.2
LP	-213.7	-226.8
LP level	HOMO -10	HOMO -12

1.5 β -Diketiminato lead(II) benzyl, LPbBn (7)

1.5.1 Bond angles (°) and distances (Å)

	LANL2DZ	LANL2DZ & 6-31G*
	<i>exo</i> -	<i>exo</i> -
N1-Pb-C30	97.65	97.50
N2-Pb-C30	97.76	97.79
N1-Pb-N2	83.01	82.36
C1-N1-C6	121.94	122.10
C1-N1-Pb	120.56	119.26
C6-N1-Pb	116.30	117.25
C3-N2-C18	121.92	122.10
C3-N2-Pb	120.55	119.23
C18-N2-Pb	116.37	117.24
N1-C1-C2	124.67	125.02
C1-C2-C3	130.39	131.01
C2-C3-N2	124.67	125.04
Pb-C30	2.317	2.326
N1-Pb	2.313	2.343
N2-Pb	2.313	2.344
N1-C1	1.349	1.332
C1-C2	1.421	1.413
C2-C3	1.421	1.413
C3-N2	1.349	1.332
Pb-plane	0.973	1.045
DOP (%)	90.64	91.50

1.5.2 Molecular orbital energy levels

	LANL2DZ	LANL2DZ & 6-31G*
Energy level	<i>exo-</i>	<i>exo-</i>
HOMO -1	-136.3	-135.4
HOMO	-66.38	-128.9
LUMO	-4.834	1.367
LUMO +1	-4.815	6.396
HOMO - LUMO gap	61.55	130.2
LP	-220.9	-232.3
LP level	HOMO -13	HOMO -15

1.6 β -Diketiminato lead(II) *tert*-butyl, LPb^tBu (8)

1.6.1 Bond angles (°) and distances (Å)

	LANL2DZ	LANL2DZ & 6-31G*
	<i>exo</i> -	<i>exo</i> -
N1-Pb-C30	105.48	105.06
N2-Pb-C30	105.04	104.72
N1-Pb-N2	82.82	82.07
C1-N1-C6	121.34	121.29
C1-N1-Pb	116.35	115.46
C6-N1-Pb	119.93	120.57
C3-N2-C18	121.22	121.00
C3-N2-Pb	115.65	114.68
C18-N2-Pb	120.92	121.66
N1-C1-C2	124.79	125.16
C1-C2-C3	130.74	131.28
C2-C3-N2	124.76	125.13
Pb-C30	2.332	2.357
N1-Pb	2.314	2.371
N2-Pb	2.337	2.366
N1-C1	1.349	1.331
C1-C2	1.423	1.415
C2-C3	1.420	1.411
C3-N2	1.352	1.336
Pb-plane	1.202	1.251
DOP (%)	74.07	75.72

1.6.2 Molecular orbital energy levels

	LANL2DZ	LANL2DZ & 6-31G*
Energy level	<i>exo-</i>	<i>exo-</i>
HOMO -1	-146.1	-144.5
HOMO	-64.01	-126.6
LUMO	-2.119	6.916
LUMO +1	-1.950	8.308
HOMO - LUMO gap	61.9	133.5
LP	-213.8	-229.2
LP level	HOMO -10	HOMO -12

1.7 β -Diketimate lead(II) phenyl, LPbPh (9)

1.7.1 Bond angles (°) and distances (Å)

	LANL2DZ	LANL2DZ & 6-31G*
	<i>endo-</i>	<i>endo-</i>
N1-Pb-C30	94.64	94.96
N2-Pb-C30	94.89	94.97
N1-Pb-N2	84.59	84.42
C1-N1-C6	120.37	120.30
C1-N1-Pb	125.24	124.38
C6-N1-Pb	114.38	115.27
C3-N2-C18	120.17	120.29
C3-N2-Pb	125.21	124.37
C18-N2-Pb	114.60	115.29
N1-C1-C2	125.13	125.75
C1-C2-C3	130.86	131.67
C2-C3-N2	125.16	125.75
Pb-C30	2.288	2.296
N1-Pb	2.301	2.333
N2-Pb	2.300	2.332
N1-C1	1.350	1.333
C1-C2	1.421	1.413
C2-C3	1.420	1.412
C3-N2	1.351	1.333
Pb-plane	0.475	0.467
DOP (%)	95.42	95.17

1.7.2 Molecular orbital energy levels

	LANL2DZ	LANL2DZ & 6-31G*
Energy level	<i>endo-</i>	<i>endo-</i>
HOMO -1	-137.7	-135.9
HOMO	-66.75	-128.1
LUMO	-4.772	-3.355
LUMO +1	-4.471	5.800
HOMO-LUMO gap	62.0	124.8
LP	-216.1	-229.2
LP level	HOMO -13	HOMO -13

2. β -Diketimate plumbylene and stannylene complexes; computational details

2.1 β -Diketimate plumbyl-(II)-ene (solvated), $[LPb]^+.[CH_2Cl_2]$

2.1.1 Bond angles ($^\circ$) and distances (\AA)

	LANL2DZ	LANL2DZ & 6-31G*
N1-Pb-N2	86.83	85.76
N1-Pb-Cl1	68.34	131.51
N2-Pb-Cl1	68.46	129.03
C1-N1-C6	120.45	120.89
C1-N1-Pb	127.99	127.98
C6-N1-Pb	111.55	111.13
C3-N2-C18	120.58	120.86
C3-N2-Pb	128.06	127.95
C18-N2-Pb	111.36	111.19
N1-C1-C2	123.58	123.86
C1-C2-C3	129.99	130.55
C2-C3-N2	123.50	123.90
Pb-Cl1	5.573	4.141
C-Cl1	1.851	1.793
C-Cl2	1.861	1.795
N1-Pb	2.159	2.191
N2-Pb	2.159	2.191
N1-C1	1.364	1.345
C1-C2	1.413	1.406
C2-C3	1.414	1.406
C3-N2	1.363	1.345
Pb-plane	0.050	0.022

2.1.2 Molecular orbital energy levels

	LANL2DZ	LANL2DZ & 6-31G*
Energy level		
HOMO -1	-210.1	-209.0
HOMO	-209.9	-208.9
LUMO	-115.1	-113.8
LUMO +1	-89.51	-81.03
HOMO - LUMO gap	94.8	95.1
LP	-335.8	-343.6
LP level	HOMO -15	HOMO -15

2.2 *β -Diketimate plumbyl-(II)-ene (free cation), [LPb]⁺*

2.2.1 Bond angles (°) and distances (Å)

	LANL2DZ	LANL2DZ & 6-31G*
N1-Pb-N2	86.70	86.25
C1-N1-C6	120.36	120.84
C1-N1-Pb	128.18	127.72
C6-N1-Pb	111.45	111.45
C3-N2-C18	120.37	120.84
C3-N2-Pb	128.18	127.72
C18-N2-Pb	111.45	111.45
N1-C1-C2	123.52	123.88
C1-C2-C3	129.91	130.57
C2-C3-N2	123.51	123.88
N1-Pb	2.160	2.182
N2-Pb	2.160	2.182
N1-C1	1.363	1.346
C1-C2	1.415	1.406
C2-C3	1.415	1.406
C3-N2	1.363	1.346
Pb-plane	0.000	0.000

2.2.2 Molecular orbital energy levels

	LANL2DZ	LANL2DZ & 6-31G*
Energy level		
HOMO -1	-212.4	-211.4
HOMO	-212.4	-211.4
LUMO	-118.1	-117.2
LUMO +1	-93.61	-85.12
HOMO - LUMO gap	94.3	94.1
LP	-339.3	-347.5
LP level	HOMO -11	HOMO -11

2.3 β -Diketiminato stannyl-(II)-ene (solvated), $[LSn]^+.[Et_2O]$

2.3.1 Bond angles ($^\circ$) and distances (\AA)

	LANL2DZ	LANL2DZ & 6-31G*
N1-Sn-N2	88.19	88.55
N1-Sn-O	93.09	93.17
N2-Sn-O	94.29	93.61
C1-N1-C6	119.85	120.06
C1-N1-Sn	126.01	124.97
C6-N1-Sn	113.82	114.52
C3-N2-C18	118.99	119.22
C3-N2-Sn	125.86	124.77
C18-N2-Sn	114.90	115.76
N1-C1-C2	123.68	124.10
C1-C2-C3	129.25	129.92
C2-C3-N2	123.70	124.18
C30-O-Sn	123.35	122.55
C32-O-Sn	123.62	124.02
C30-O-C32	112.60	112.61
Sn-O	2.385	2.485
O-C30	1.501	1.458
O-C32	1.499	1.457
N1-Sn	2.147	2.159
N2-Sn	2.134	1.144
N1-C1	1.361	1.344
C1-C2	1.418	1.410
C2-C3	1.415	1.405
C3-N2	1.364	1.348
Sn-plane	0.371	0.376
DOP _{tin} (%)	93.8	94.1
DOP _{oxygen} (%)	0.48	0.91

2.3.2 Molecular orbital energy levels

	LANL2DZ	LANL2DZ & 6-31G*
Energy level		
HOMO -1	-206.9	-206.4
HOMO	-206.2	-205.3
LUMO	-142.3	-101.6
LUMO +1	-68.34	-95.02
HOMO - LUMO gap	63.9	103.6
LP	-267.7	-258.1
LP level	HOMO -9	HOMO -9

2.4 β -Diketimate stannyl-(II)-ene (free cation), $[LSn]^+$

2.4.1 Bond angles ($^\circ$) and distances (\AA)

	LANL2DZ	LANL2DZ & 6-31G*
N1-Sn-N2	88.20	87.99
C1-N1-C6	119.85	120.31
C1-N1-Sn	128.43	127.88
C6-N1-Sn	111.72	111.82
C3-N2-C18	119.85	120.30
C3-N2-Sn	128.43	127.88
C18-N2-Sn	111.72	111.82
N1-C1-C2	122.97	123.32
C1-C2-C3	129.00	129.62
C2-C3-N2	122.97	123.32
N1-Sn	2.088	2.104
N2-Sn	2.088	2.104
N1-C1	1.366	1.349
C1-C2	1.413	1.404
C2-C3	1.413	1.404
C3-N2	1.366	1.349
Sn-plane	0.000	0.000

2.4.2 Molecular orbital energy levels

	LANL2DZ	LANL2DZ & 6-31G*
Energy level		
HOMO -1	-213.1	-212.2
HOMO	-213.1	-212.2
LUMO	-119.6	-119.6
LUMO +1	-91.11	-91.11
HOMO - LUMO gap	93.5	92.5
LP	-298.7	-298.7
LP level	HOMO -9	HOMO -9

3. β -Diketimate magnesium phosphide complexes; computational details

3.1 β -Diketimate magnesium diphenylphosphide, $LMgPPh_2$ (19)

3.1.1 Bond angles ($^\circ$) and distances (\AA)

	Solvated	Free		Solvated	Free
N1-Mg-N2	94.50	94.97	Mg-P	2.552	2.504
N1-Mg-P	119.31	124.96	Mg-O	2.111	-
N2-Mg-P	123.58	139.43	N1-Mg	2.099	2.056
C1-N1-C6	118.23	119.86	N2-Mg	2.106	2.050
C1-N1-Mg	118.93	122.29	N1-C1	1.338	1.338
C6-N1-Mg	122.82	117.84	C1-C2	1.412	1.411
C3-N2-C18	119.09	119.55	C2-C3	1.414	1.408
C3-N2-Mg	119.19	118.07	C3-N2	1.336	1.340
C18-N2-Mg	121.71	122.39			
N1-C1-C2	125.06	124.51	DOP _{phos} (%)	41.13	44.54
C1-C2-C3	131.00	130.74	DOP _{Mg-THF} (%)	25.12	0.71
C2-C3-N2	104.21	124.61			
Mg-P-C36	106.76	106.69	Mg-plane	0.545	0.140
Mg-P-C30	112.01	108.49			
C30-P-C36	104.21	104.73	N1-Mg-P-C30	177.31	-159.54
N1-Mg-O	104.73	-	N1-Mg-P-C36	63.84	88.13
N2-Mg-O	102.81	-			
O-Mg-P	109.27	-			

3.1.2 Molecular orbital energy levels

	Solvated	Free
Energy level		
HOMO -1	-123.3	-136.2
HOMO	-116.2	-132.7
LUMO	6.979	-6.634
LUMO +1	20.49	0.834
HOMO - LUMO gap	123.2	126.1
LP _{phos}	-232.6	-232.0
LP _{phos} energy level	HOMO -17	HOMO -16

3.2 β -Diketiminato magnesium dicyclohexylphosphide, $LMgPCy_2$ (20)

3.2.1 Bond angles ($^\circ$) and distances (\AA)

	Solvated	Free		Solvated	Free
N1-Mg-N2	94.74	94.69	Mg-P	2.508	2.500
N1-Mg-P	120.42	143.60	Mg-O	2.168	-
N2-Mg-P	116.51	121.57	N1-Mg	2.110	2.071
C1-N1-C6	119.87	119.15	N2-Mg	2.102	2.070
C1-N1-Mg	118.86	121.53	N1-C1	1.334	1.341
C6-N1-Mg	121.22	119.24	C1-C2	1.417	1.408
C3-N2-C18	119.66	118.64	C2-C3	1.414	1.411
C3-N2-Mg	118.85	121.70	C3-N2	1.336	1.338
C18-N2-Mg	121.46	119.61			
N1-C1-C2	125.03	124.80	DOP _{phos} (%)	27.23	43.81
C1-C2-C3	131.03	130.76	DOP _{Mg-THF} (%)	31.48	0.16
C2-C3-N2	124.89	124.66			
Mg-P-C36	112.61	109.37	Mg-plane	0.547	0.286
Mg-P-C30	112.68	105.75			
C30-P-C36	110.20	105.45	N1-Mg-P-C30	176.14	-118.39
N1-Mg-O	99.91	-	N1-Mg-P-C36	58.44	128.50
N2-Mg-O	99.92	-			
O-Mg-P	120.97	-			

3.2.2 Molecular orbital energy levels

	Solvated	Free
Energy level		
HOMO -1	-141.3	-143.4
HOMO	-120.3	-130.4
LUMO	8.797	-3.593
LUMO +1	22.47	3.060
HOMO - LUMO gap	129.1	126.8
LP _{phos}	-175.6	-214.6
LP _{phos} energy level	HOMO-9	HOMO -10